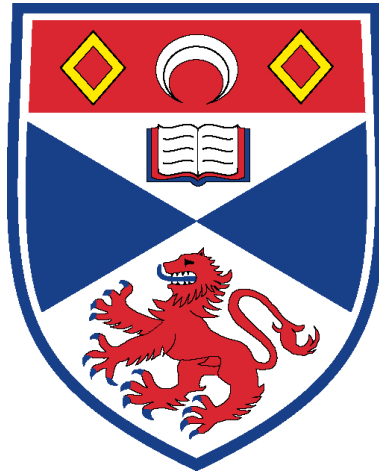


# Hawking Radiation in Dispersive Media

by

**Scott James Robertson**

School of Physics and Astronomy,  
University of St Andrews



Submitted for the degree of  
Doctor of Philosophy

May, 2011



### **I. Candidate's declarations**

I, Scott James Robertson, hereby certify that this thesis, which is approximately 40,000 words in length, has been written by me, that it is the record of work carried out by me and that it has not been submitted in any previous application for a higher degree.

I was admitted as a research student in September 2006 and as a candidate for the degree of PhD in September 2006; the higher study for which this is a record was carried out in the University of St Andrews between 2006 and 2010.

*Date*

*Signature of candidate*

### **II. Supervisor's declaration**

I hereby certify that the candidate has fulfilled the conditions of the Resolution and Regulations appropriate for the degree of PhD in the University of St Andrews and that the candidate is qualified to submit this thesis in application for that degree.

*Date*

*Signature of supervisor*

### **III. Permission for electronic publication**

In submitting this thesis to the University of St Andrews I understand that I am giving permission for it to be made available for use in accordance with the regulations of the University Library for the time being in force, subject to any copyright vested in the work not being affected thereby. I also understand that the title and the abstract will be published, and that a copy of the work may be made and supplied to any bona fide library or research worker, that my thesis will be electronically accessible for personal or research use unless exempt by award of an embargo as requested below, and that the library has the right to migrate my thesis into new electronic forms as required to ensure continued access to the thesis. I have obtained any third-party copyright permissions that may be required in order to allow such access and migration, or have requested the appropriate embargo below.

The following is an agreed request by candidate and supervisor regarding the electronic publication of this thesis:

*Access to printed copy and electronic publication of thesis through the University of St Andrews.*

*Date*

*Signature of candidate*

*Signature of supervisor*





## Abstract

Hawking radiation, despite its presence in theoretical physics for over thirty years, remains elusive and undetected. It also suffers, in its original context of gravitational black holes, from conceptual difficulties. Of particular note is the trans-Planckian problem, which is concerned with the apparent origin of the radiation in absurdly high frequencies. In order to gain better theoretical understanding and, it is hoped, experimental verification of Hawking radiation, much study is being devoted to systems which model the spacetime geometry of black holes, and which, by analogy, are also thought to emit Hawking radiation. These analogue systems typically exhibit dispersion, which regularizes the wave behaviour at the horizon but does not lend itself well to analytic treatment, thus rendering Hawking's prediction less secure. A general analytic method for dealing with Hawking radiation in dispersive systems has proved difficult to find.

This thesis presents new numerical and analytic results for Hawking emission spectra in dispersive systems. It examines two black-hole analogue systems: it begins by introducing the well-known acoustic model, presenting some original results in that context; then, through analogy with the acoustic model, goes on to develop the lesser-known fibre-optical model. The following original results are presented in the context of both of these models:

- an analytic expression for the low-frequency temperature is found for a hyperbolic tangent background profile, valid in the entire parameter space; it is well-known that the spectrum is approximately thermal at low frequencies, but a universally valid expression for the corresponding temperature is an original development;
- an analytic expression for the spectrum, valid over almost the entire frequency range, when the velocity profile parameters lie in the regime where the low-frequency temperature is given by the Hawking prediction; previous work has focused on the low-frequency thermal spectrum and the characterization of the deviations from thermality, rather than a single analytic expression; and
- a new unexplored regime where no group-velocity horizon exists is examined; the Hawking spectra are found to be non-zero here, but also highly non-thermal, and are found, in the limit of small deviations, to vary with the square of the maximum deviation; the analytic expression for the case with a horizon is found to carry over to this new regime, with appropriate modifications.

Furthermore, the thesis examines the results of a classical frequency-shifting experiment in the context of fibre-optical horizons. The theory of this process is presented for both a constant-velocity and a constantly-decelerating pulse, the latter case taking account of the Raman effect. The resulting spectra are at least qualitatively explained, but there is a discrepancy between theory and experiment that has not yet been accounted for.



# Contents

<b>I. Introduction</b>	<b>13</b>
<b>1. Hawking Radiation</b>	<b>15</b>
1.1. The Schwarzschild metric as a moving medium . . . . .	17
1.2. The acoustic field and its wave equation . . . . .	24
1.3. Stationary modes . . . . .	26
1.4. Quantization of the acoustic field . . . . .	28
1.5. Event horizon . . . . .	29
1.6. Out-modes and in-modes with an event horizon . . . . .	30
1.7. Spontaneous creation of phonons . . . . .	32
1.8. Conclusion and discussion . . . . .	34
<b>II. Hawking Radiation in Dispersive Fluids</b>	<b>37</b>
<b>2. The Acoustic Model</b>	<b>39</b>
2.1. The wave equation and its solutions . . . . .	39
2.2. Scalar product . . . . .	43
2.3. Decomposition into modes . . . . .	44
2.4. Transforming to the $\omega$ -representation . . . . .	46
2.4.1. Supersonic flow . . . . .	46
2.4.2. Subsonic flow . . . . .	49
2.4.3. Inhomogeneous flow . . . . .	51
2.5. Spontaneous creation of phonons . . . . .	56
2.6. Conclusion and discussion . . . . .	59
<b>3. Methods of Acoustic Model</b>	<b>61</b>
3.1. Wavepacket propagation . . . . .	61
3.2. Steady-state solution . . . . .	66
3.2.1. General velocity profile . . . . .	66
3.2.2. Discontinuous velocity profile . . . . .	70
3.3. Linearized velocity profile . . . . .	73
3.3.1. Solution in Fourier space . . . . .	74
3.3.2. Transforming back to position space . . . . .	76
3.3.3. Generalization to nonlinear velocity profiles . . . . .	77
3.4. Summary . . . . .	79

<b>4. Results for Acoustic Model</b>	<b>81</b>
4.1. Dispersion profile . . . . .	81
4.2. Velocity profile . . . . .	83
4.3. Normalizing the wave equation . . . . .	84
4.4. Thermal behaviour . . . . .	86
4.4.1. Validity of linearized velocity profile . . . . .	86
4.4.2. Validity of discontinuous velocity profile . . . . .	88
4.5. Nonthermal behaviour and critical frequencies . . . . .	89
4.6. Phase integral analysis . . . . .	90
4.7. Numerical results . . . . .	93
4.7.1. Central horizon . . . . .	93
4.7.2. Non-central horizon . . . . .	97
4.7.3. No low-frequency horizon . . . . .	100
4.8. Concluding remarks . . . . .	102
 <b>III. Hawking Radiation in Optical Fibres</b>	 <b>105</b>
<b>5. Nonlinear Fibre Optics</b>	<b>107</b>
5.1. Linear effects . . . . .	107
5.2. Nonlinear effects . . . . .	111
5.2.1. Nonlinear polarization . . . . .	111
5.2.2. Optical solitons . . . . .	113
5.2.3. Pulse and probe . . . . .	115
5.3. Co-moving frame . . . . .	117
5.3.1. Coordinate transformation . . . . .	117
5.3.2. Dispersion relation . . . . .	120
5.4. Conclusion and discussion . . . . .	121
 <b>6. Frequency Shifting in Optical Fibres</b>	 <b>123</b>
6.1. The fiber-optical analogy and geometrical optics . . . . .	123
6.2. Wave solutions of the pulse-probe interaction . . . . .	127
6.3. General solution . . . . .	131
6.4. Solution for a continuous wave . . . . .	133
6.5. The Raman effect . . . . .	135
6.6. Accelerated waves in the absence of a pulse . . . . .	138
6.7. Including the pulse-probe interaction . . . . .	140
6.8. Solution in the decelerating case . . . . .	143
6.9. Comparison with experimental results . . . . .	146
6.10. Conclusion and discussion . . . . .	148
 <b>7. The Fibre-Optical Model for Hawking Radiation</b>	 <b>149</b>
7.1. Action and scalar product . . . . .	149
7.2. Decomposition into modes . . . . .	151

7.3.	Transforming to the $\omega'$ -representation . . . . .	153
7.3.1.	Constant $\chi$ . . . . .	153
7.3.2.	Nonconstant $\chi$ . . . . .	157
7.4.	Spontaneous creation of photons . . . . .	160
7.5.	Concluding remarks . . . . .	161
<b>8.</b>	<b>Methods of Fibre-Optical Model</b>	<b>163</b>
8.1.	Wavepacket propagation . . . . .	163
8.2.	Steady-state solution . . . . .	165
8.2.1.	General nonlinearity profile . . . . .	165
8.2.2.	Discontinuous nonlinearity profile . . . . .	166
8.3.	Linearized intensity profile . . . . .	168
8.4.	Summary . . . . .	171
<b>9.</b>	<b>Results for the Fibre-Optical Model</b>	<b>173</b>
9.1.	Dispersion relation . . . . .	173
9.2.	Intensity profile . . . . .	175
9.3.	Normalizing the wave equation . . . . .	175
9.4.	Predicted behaviour for a low-frequency event horizon . . . . .	176
9.5.	Numerical results . . . . .	179
9.5.1.	With a low-frequency horizon . . . . .	179
9.5.2.	With realistic values of $\chi$ . . . . .	180
9.6.	Concluding remarks . . . . .	187
<b>10.</b>	<b>The Low-Frequency Problem</b>	<b>189</b>
10.1.	Frequency-dependent $\chi$ . . . . .	189
10.1.1.	Quadratic dependence on $\omega$ . . . . .	189
10.1.2.	Results . . . . .	190
10.2.	Reduction to two solutions . . . . .	192
10.2.1.	Analogy between acoustic and optical wave equations . . . . .	192
10.2.2.	“Half” wave equation . . . . .	193
10.2.3.	Dispersion relation . . . . .	193
10.2.4.	Numerical results . . . . .	197
10.3.	Concluding remarks . . . . .	201
<b>IV.</b>	<b>Appendices</b>	<b>203</b>
<b>A.</b>	<b>Low-Frequency Temperature in Acoustic Model</b>	<b>205</b>
<b>B.</b>	<b>Low-Frequency Temperature in Optical Model</b>	<b>211</b>



# List of Figures

1.1. BLACK HOLE SPACETIME . . . . .	18
1.2. RADIAL NULL CURVES NEAR A BLACK HOLE HORIZON . . . . .	20
1.3. BLACK HOLE HORIZON IN A RIVER . . . . .	22
1.4. WHITE HOLE HORIZON IN A RIVER . . . . .	23
2.1. DISPERSION PROFILES . . . . .	41
2.2. SOLUTIONS AT CONSTANT FLOW . . . . .	42
2.3. SOLUTIONS FOR SUPERSONIC FLOW AND SUBLUMINAL DISPERSION . . . . .	47
2.4. SOLUTIONS FOR SUBSONIC FLOW AND SUBLUMINAL DISPERSION . . . . .	50
2.5. VARIATION OF SOLUTIONS WITH FLOW VELOCITY . . . . .	52
2.6. SPACE-TIME DIAGRAM OF IN- AND OUT-MODES . . . . .	54
2.7. ORTHOGONALITY OF IN- OR OUT-MODES . . . . .	54
3.1. WAVEPACKET PROPAGATION . . . . .	65
3.2. INTEGRATION OF STATIONARY SOLUTION . . . . .	67
3.3. SOLUTIONS AND THEIR GROUP VELOCITIES . . . . .	69
3.4. CONSTRUCTING A DISCONTINUOUS VELOCITY PROFILE . . . . .	71
3.5. LINEARIZING THE VELOCITY PROFILE . . . . .	74
4.1. QUARTIC DISPERSION . . . . .	82
4.2. HYPERBOLIC TANGENT VELOCITY PROFILE . . . . .	83
4.3. THE THERMAL SPECTRUM . . . . .	87
4.4. CRITICAL FREQUENCIES . . . . .	89
4.5. PHASE INTEGRALS WITH A GROUP-VELOCITY HORIZON . . . . .	91
4.6. PHASE INTEGRALS WITH NO GROUP-VELOCITY HORIZON . . . . .	92
4.7. HAWKING SPECTRA WITH A CENTRAL HORIZON, 1 . . . . .	94
4.8. HAWKING SPECTRA WITH A CENTRAL HORIZON, 2 . . . . .	95
4.9. LOW-FREQUENCY TEMPERATURE . . . . .	98
4.10. HAWKING SPECTRA WITH NON-CENTRAL HORIZON . . . . .	99
4.11. HAWKING SPECTRUM WITH NO LOW-FREQUENCY HORIZON, 1 . . . . .	101
4.12. HAWKING SPECTRA WITH NO LOW-FREQUENCY HORIZON, 2 . . . . .	103
5.1. OPTICAL SOLITONS . . . . .	116
5.2. CO-MOVING FRAME . . . . .	119
6.1. FREQUENCY SHIFTING BY A PULSE . . . . .	125
6.2. FREQUENCY SHIFTING CONTOURS . . . . .	126

## List of Figures

6.3. REFLECTION AND TRANSMISSION AMPLITUDES . . . . .	130
6.4. FREQUENCY SHIFTING SPECTRA FOR A CONSTANT-VELOCITY PULSE . .	135
6.5. THE AIRY FUNCTION . . . . .	139
6.6. FREQUENCY SHIFTING SPECTRA INCLUDING RAMAN DECELERATION . .	147
7.1. SOLUTIONS OF FIBRE-OPTICAL DISPERSION RELATION . . . . .	154
7.2. EFFECT OF NONLINEARITY ON SOLUTIONS OF DISPERSION RELATION . .	157
9.1. LOW-FREQUENCY TEMPERATURE . . . . .	179
9.2. HAWKING SPECTRA WITH A LOW-FREQUENCY HORIZON . . . . .	181
9.3. SELF-STEEPENING OF A PULSE . . . . .	182
9.4. HAWKING SPECTRA FOR REALISTIC VALUES OF $\chi$ , 1 . . . . .	184
9.5. HAWKING SPECTRA FOR REALISTIC VALUES OF $\chi$ , 2 . . . . .	185
9.6. HAWKING SPECTRA AND THE PHASE-INTEGRAL APPROXIMATION . . . .	186
10.1. HAWKING SPECTRA WITH FREQUENCY-DEPENDENT $\chi$ . . . . .	191
10.2. HAWKING SPECTRA AND PHASE-INTEGRAL APPROXIMATION . . . . .	191
10.3. TWO-SOLUTION DISPERSION WITH POSITIVE $\xi$ . . . . .	195
10.4. TWO-SOLUTION DISPERSION WITH NEGATIVE $\xi$ . . . . .	196
10.5. HAWKING SPECTRA WITH TWO-SOLUTION DISPERSION . . . . .	198
10.6. COMPARING TWO-SOLUTION WITH QUARTIC DISPERSION . . . . .	199
10.7. TWO-SOLUTION DISPERSION AND PHASE-INTEGRAL APPROXIMATION . .	200
A.1. SPACE-TIME DIAGRAM OF THE $K^{ur}$ -OUT MODE . . . . .	206
B.1. SPACE-TIME DIAGRAM OF THE $\Omega^{ul}$ -OUT MODE . . . . .	212



Part I.

Introduction



# 1. Hawking Radiation

Black holes - so-called because of the apparent impossibility of escape from them - are not entirely black. That was the surprising claim made by Hawking [1, 2] over thirty years ago. Examining the behaviour of quantum fields in the vicinity of a black hole, he showed that, far from being emission-free, it should emit a steady flux of thermal radiation, with a temperature proportional to  $\kappa$ , the gravitational field strength at the event horizon:

$$k_B T = \frac{\hbar \kappa}{2\pi c} = \frac{\hbar c^3}{8\pi G M}. \quad (1.0.1)$$

With this remarkable result, Hawking completed a thermodynamic treatment of black holes that had been developed previously by Bekenstein [3, 4], who had concluded that the temperature of a Schwarzschild black hole should be proportional to  $\kappa$  [3] (though his analysis is based mainly on entropy, and he did not consider the possibility of thermal emission). The work of Bekenstein and Hawking - and of others [5, 6, 7, 8, 9, 10], rederiving Hawking's result in various ways - brings together the normally disparate areas of gravity, quantum theory and thermodynamics; a glance at the various fundamental constants appearing in Eq. (1.0.1) makes this fusion clear. Thirst for understanding of the underlying connections between these mighty realms of physics provides ample motivation for the study of what has come to be known as Hawking radiation.

A pre-requisite for any such study must be the acknowledgement that Hawking radiation is not without its own problems, both practical and conceptual. On the practical side, the predicted temperature - at least in the gravitational context in which it was first derived - is virtually untestable. A solar mass black hole would, according to Eq. (1.0.1), have a temperature of about  $10^{-6}$  K - six orders of magnitude smaller than the temperature of the cosmic microwave background (CMB). Any radiation from the black hole would be drowned out by the CMB. Therefore, experimental verification of black hole radiation would seem to require an unusually light black hole, orders of magnitude lighter than the Sun - a very unlikely object.

Conceptually, there is the trans-Planckian problem [11, 12, 13], which has to do with the validity of the derivation of Hawking radiation. Let us briefly explain the problem; it is discussed further in §1.5. In most derivations, the spacetime is assumed to collapse, as in a star collapsing to form a black hole. Modes of the quantum vacuum are incident from infinity, propagating through the collapsing spacetime and out to infinity again, experiencing a gravitational redshift as they climb out of the ever-deepening gravitational well. The steady thermal flux seen at late times can be traced back to those vacuum modes which just manage to escape the event horizon, slowed and redshifted to greater and greater degrees. Thus, any low-frequency mode seen in the late-time thermal spectrum can be traced back to an incident vacuum mode of ever-increasing frequency;

## 1. Hawking Radiation

indeed, to an *exponentially* increasing frequency! The frequencies of these incident modes very quickly exceed the Planck scale [13], widely believed to be a fundamental quantum limit. We cannot justify the use of quantum field theory at such scales, yet it appears that Hawking radiation is dependent on the existence of these initial trans-Planckian frequencies. Whatever is the correct physics, can we be sure that it will preserve Hawking radiation?

These difficulties can be tackled by appealing to artificial event horizons, or physical systems possessing horizons analogous to those of gravitational black holes [14, 15]. This idea was first proposed by Unruh [16], who found that perturbations of a stationary background fluid flow behave just as a scalar field in Lorentzian spacetime [16, 17]. In particular, if the flow velocity crosses the speed of sound, the surface where it does so is entirely analogous to a black-hole event horizon, and on quantizing the perturbation field, one predicts analog Hawking radiation in such a system. Of course, this model is subject to the same trans-Planckian problem as the gravitational case. In reality, however, the trans-Planckian problem tends not to arise, because sound waves in fluids - or, indeed, propagating waves in any of the experimentally-realizable analog systems - exhibit *dispersion*. That is, the behaviour of waves changes at different scales by mechanisms which are better-understood than quantum gravity; for example, the sizes of atoms or molecules places a fundamental limit on the wavelengths of sound waves. Unruh showed numerically that even after taking high-frequency dispersion into account (and assuming that the dispersion is not too strong), Hawking radiation is still predicted, with the same temperature as in the dispersionless model [18]. The conclusion is that the trans-Planckian problem is a mathematical artifact, while the Hawking radiation exists regardless of the physics at the high-energy scale. This discovery has prompted a great deal of interest in a range of black-hole analogue systems: in Bose-Einstein condensates [19, 20, 21, 22, 23], in ultracold fermions [24], in superfluid Helium-3 [25, 26, 27, 28, 29], in water [30, 31, 32], and in optics [33, 34, 35, 36]. These black-hole analogies might not teach us about quantum gravity directly, but they can give insight into the particle creation process, hopefully pointing towards the real origin of Hawking radiation [37].

As we shall see, Hawking radiation derives from the conversion of incident *positive*-norm vacuum fluctuations into outgoing modes with *negative* norm. Determination of the resultant spectrum is achieved through the calculation of the relevant coefficients (known as *Bogoliubov coefficients*). In the absence of dispersion, Hawking's original result is obtained. Unsurprisingly, the introduction of dispersion complicates the derivation, and its general effects on the Hawking radiation are not yet clear. It has been shown that, in the limit of a low velocity gradient or weak dispersion (the *adiabatic* limit), Hawking's prediction is preserved in the low-frequency regime. This was first demonstrated numerically by Unruh [18], using a finite-difference time-domain (FDTD) algorithm for wavepacket propagation and introducing a high-frequency truncation to the dispersion relation. The result was explained analytically by Brout *et al.* [38] by solving the wave equation in momentum space, where, in the vicinity of the horizon, the equations become more tractable. Corley and Jacobson considered stationary modes of a single frequency, reducing the wave equation to an ordinary differential equation. Thus, they were able to calculate entire spectra numerically [39, 40], and to characterise their

### 1.1. The Schwarzschild metric as a moving medium

deviations from thermality. Corley used equations in momentum space to solve for the stationary modes analytically [41], using a different dispersion relation from that used by Unruh but coming to the same conclusion that the Hawking prediction remains valid for low frequencies in the adiabatic limit. He also found that the spectrum remains thermal in the non-adiabatic limit, i.e., in the limit of very large velocity gradient, but that this can still be solved for analytically [40]; a similar result has been demonstrated more recently in the context of Bose-Einstein condensates [42]. Further numerical [43, 44, 45] and analytic [46, 47, 48, 49] works have extended the context in various directions, but all are agreed that, in the adiabatic limit and low-frequency regime, Hawking radiation behaves as it does in the dispersionless case. While deviations and lowest-order approximations for the high-frequency regime have been studied [47, 44], a general expression for the spectrum valid over the entire frequency range has never been found; nor has such an expression for the low-frequency temperature, connecting the adiabatic limit with the step-discontinuous limit. Furthermore, the regime which contains no horizon in the dispersionless limit has not yet been explored.

In this thesis, we shall examine two analogue systems. In Part II we discuss Unruh's original model of acoustic waves in a moving fluid; in Part III, we focus on the lesser-known analogy of light in optical fibres. We shall see that Hawking radiation is robust, remaining when high-frequency modes are suppressed, and even when there is no event horizon (in the usual sense); that said, thermality is not so robust, for only in the dispersionless case is the Hawking spectrum strictly thermal. We shall see that, in the cases examined, we can find general analytic expressions for the Hawking spectrum and for the low-frequency temperature. For the rest of this introduction, we shall use the acoustic model to examine how black hole analogies arise in theory and how, in the strictly dispersionless case, Hawking radiation derives from trans-Planckian vacuum modes.

### 1.1. The Schwarzschild metric as a moving medium

General Relativity identifies gravity with curvature of spacetime, described by the space-time metric  $ds^2$ . It has a unique spherically symmetric vacuum metric: the Schwarzschild metric [50], which in coordinates  $(t_S, r, \theta, \phi)$  takes the form

$$ds^2 = \left(1 - \frac{r_S}{r}\right) c^2 dt_S^2 - \left(1 - \frac{r_S}{r}\right)^{-1} dr^2 - r^2 d\Omega^2, \quad (1.1.1)$$

where  $d\Omega^2 = d\theta^2 + \sin^2 \theta d\phi^2$  is the angular line element,  $t_S$  is the Schwarzschild time coordinate and  $r_S = 2GM/c^2$  is the Schwarzschild radius. This describes, for example, the spacetime around a star or planet with relatively low rotation rate. As  $r_S/r \rightarrow 0$ , the Schwarzschild metric approaches the flat Minkowski metric, so the coordinates  $(t_S, r, \theta, \phi)$  correspond to the usual spherical coordinates of flat spacetime for an observer at infinity. However, Eq. (1.1.1) contains two singularities, at  $r = 0$  and  $r = r_S$ . The singularity at  $r = 0$  is a genuine singularity of Schwarzschild spacetime [50]; we shall not be concerned with it here. It is the surface  $r = r_S$  - the event horizon - that is of interest to us.

Let us briefly review the effects of the event horizon by examining light trajectories, or null curves, with  $ds^2 = 0$ . Since the spacetime is spherically symmetric, we shall not

## 1. Hawking Radiation

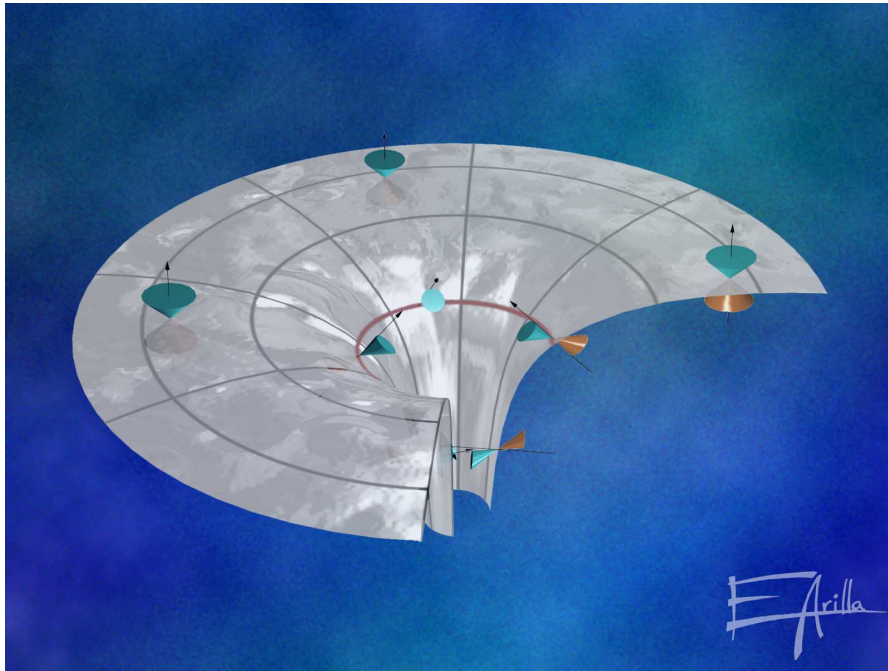


Figure 1.1.: BLACK HOLE SPACETIME: The curvature of spacetime near a black hole is such that all future-directed paths are ingoing within the event horizon.  
[Credit: Enrique Arilla]

### 1.1. The Schwarzschild metric as a moving medium

concern ourselves with angular trajectories, so we also set  $d\Omega^2 = 0$ . This leaves us with a differential equation for the null curves:

$$\frac{dt_S}{dr} = \pm \frac{1}{c} \left(1 - \frac{r_S}{r}\right)^{-1}. \quad (1.1.2)$$

Far from the Schwarzschild radius, where  $r \gg r_S$ ,  $|dt_S/dr| \rightarrow 1/c$ , so that light behaves just as it does in flat spacetime. However, as we approach the Schwarzschild radius,  $|dt_S/dr|$  diverges: light takes longer and longer to travel any distance, and, if travelling towards the event horizon, can never reach it in a finite time  $t_S$ . The time  $t_S$  comes to a standstill at the event horizon.

Despite this peculiar behaviour, the event horizon is not a genuine singularity of Schwarzschild spacetime; it simply appears as such in the coordinates  $(t_S, r)$ , which are unsuited to the region  $r \leq r_S$ . The Schwarzschild time  $t_S$  is the main culprit, for we may follow in the footsteps of Painlevé [51], Gullstrand [52] and Lemaître [53] by defining a new time,

$$t = t_S + 2\frac{\sqrt{r_S r}}{c} + \frac{r_S}{c} \ln \left( \frac{\sqrt{r/r_S} - 1}{\sqrt{r/r_S} + 1} \right); \quad (1.1.3)$$

this has the differential

$$dt = dt_S + \frac{1}{c} \sqrt{\frac{r_S}{r}} \left(1 - \frac{r_S}{r}\right)^{-1} dr, \quad (1.1.4)$$

which, when substituted in Eq. (1.1.1), yields the metric

$$ds^2 = c^2 dt^2 - \left( dr + \sqrt{\frac{r_S}{r}} c dt \right)^2 + r^2 d\Omega^2. \quad (1.1.5)$$

In the coordinates  $(t, r, \theta, \phi)$ , the metric clearly has no singularity at  $r = r_S$ . (It is true that the coefficient of  $dt^2$  vanishes there, but this is easily remedied by considering a new position coordinate  $q$  such that  $dq = c dt + \sqrt{r/r_S} dr$ , so that  $ds^2 = c^2 dt^2 - (r/r_S) dq^2 + r^2 d\Omega^2$ . This is not too important, however, and we can gain a more intuitive understanding of the metric by keeping  $r$  as our position coordinate.) Notice that, while the definition of  $t$ , Eq. (1.1.3), is applicable only when  $r > r_S$ , the metric of Eq. (1.1.5) is easily extendable to all values of  $r$  greater than zero. The new coordinate  $t$  has opened up a previously inaccessible region of the spacetime. Keeping  $t$  fixed while decreasing  $r$ , we see from Eq. (1.1.3) that, as we approach the Schwarzschild radius, we must have  $t_S \rightarrow \infty$  to compensate for the divergence of the logarithm. Thus, with respect to our original coordinates, the transformation to the coordinates  $(t, r)$  is accompanied by an extension of the spacetime into the infinite future. Our discussion of light trajectories anticipated this: since an ingoing light ray approaches the horizon at an infinitely slower rate (with respect to  $t_S$ ), crossing the horizon requires  $t_S \rightarrow \infty$ .

Let us take a moment to interpret the metric (1.1.5). Again, we shall consider only radial trajectories, setting  $d\Omega^2 = 0$ . The key point to note is that, if  $dr/dt = -c\sqrt{r_S/r}$ , the metric reduces to  $ds^2 = c^2 dt^2$ .  $t$ , then, is the proper time measured by an observer

## 1. Hawking Radiation

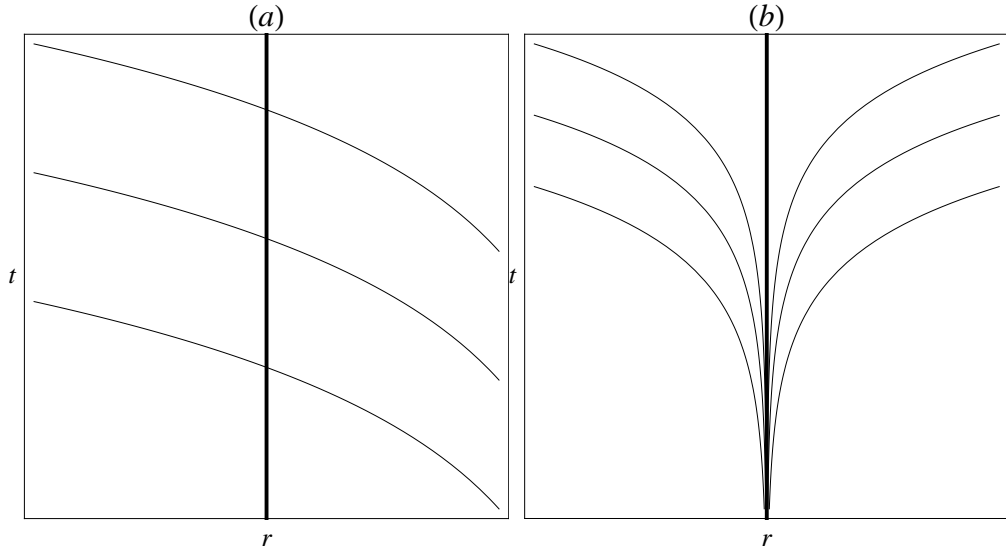


Figure 1.2.: RADIAL NULL CURVES NEAR A BLACK HOLE HORIZON: Spacetime diagrams of light trajectories in the metric of Eq. (1.1.5), where the thick centre line represents the horizon  $r = r_S$ . Figure (a) shows the trajectories which are left-moving with respect to the imagined fluid, obeying the first equation of (1.1.6); these experience nothing unusual at the horizon. Figure (b) shows the trajectories which are right-moving with respect to the imagined fluid, obeying the second equation of (1.1.6); as these are propagated further back in time, they come to a standstill at the horizon.



### 1.1. The Schwarzschild metric as a moving medium

on the trajectory  $dr/dt = -c\sqrt{r_S/r}$ . Since this condition clearly maximises  $ds^2$ , these trajectories are geodesics, and  $t$  measures proper time along them. It is as though space consists of a fluid [54, 55], flowing inwards with velocity  $-c\sqrt{r_S/r}$  to converge on the point  $r = 0$ . The geodesics just defined are those which are stationary with respect to this fluid. The coordinate  $q$ , defined above, is constant on such a geodesic, and can be thought of as the proper spatial coordinate; its differential, combining  $dr$  and  $dt$ , is derived from simple addition of velocities (which can be done in the Galilean fashion since all velocities are measured with respect to the proper time  $t$ ). The fluid should be thought of as the fabric of space itself, for the speed of light is measured with respect to it. At the Schwarzschild radius, the fluid flows inward with speed  $c$ ; anything that falls beneath this radius will inexorably be dragged towards the centre,  $r = 0$ . This view is reinforced by looking at the radial null curves in the coordinates  $(t, r)$ . Setting  $ds^2 = 0$  and  $d\Omega^2 = 0$ , we find two possible trajectories for light:

$$\frac{dt}{dr} = -\frac{1}{c} \left(1 + \sqrt{\frac{r_S}{r}}\right)^{-1}, \quad \text{or} \quad \frac{dt}{dr} = \frac{1}{c} \left(1 - \sqrt{\frac{r_S}{r}}\right)^{-1}. \quad (1.1.6)$$

The forms of these trajectories near the point  $r = r_S$  are shown in Figure 1.2. The first possibility represents rays which are ingoing with respect to the fluid; the total velocity is  $-c - c\sqrt{r_S/r}$ , the sum of the light's velocity and the fluid's velocity. It is perfectly regular at the horizon, and tilts over as it propagates, travelling faster and faster as it moves to ever smaller radii. The second possibility represent rays which are outgoing with respect to the fluid, having a total velocity of  $c - c\sqrt{r_S/r}$ . This is not regular at the horizon, nor should it be: there, the competing velocities of the fluid and the light exactly cancel, giving a total velocity of zero. Rays at higher radii will have a positive total velocity, and will eventually escape to infinity; rays at smaller radii will have a negative total velocity, unable to overcome the fluid flow, and will propagate inwards to  $r = 0$ .

This analogy with a moving medium forms the basis of artificial black holes and event horizon analogies. We may simply replace  $-c\sqrt{r_S/r}$  in Eq. (1.1.5) with the more general velocity profile  $V(x)$  to obtain, in 1 + 1-dimensional spacetime, the metric

$$ds^2 = c^2 dt^2 - (dx - V(x) dt)^2, \quad (1.1.7)$$

where now  $c$  is to be interpreted as the velocity with respect to the medium in question (not necessarily the speed of light). For example, this generalized metric may be applied to a system so far removed from astrophysics as a river flowing towards a waterfall, so that the flow speed increases in the direction of flow, as illustrated in Figure 1.3. Imagine this river is populated by fish who can swim only up to a maximum speed  $c$ ; this speed is, of course, with respect to the water, not the coordinate  $x$ . Then the above metric suffices to describe the trajectories of fish in this river. Fish who are far from the waterfall, where the current is low, are free to swim around as they please, experiencing no significant resistance in either direction. However, as the current increases, there may be a point at which  $|V| = c$ . As the fish approach this point, they will find it increasingly difficult to swim back upstream; passing this point, motion upstream is impossible, for the current is

## 1. Hawking Radiation

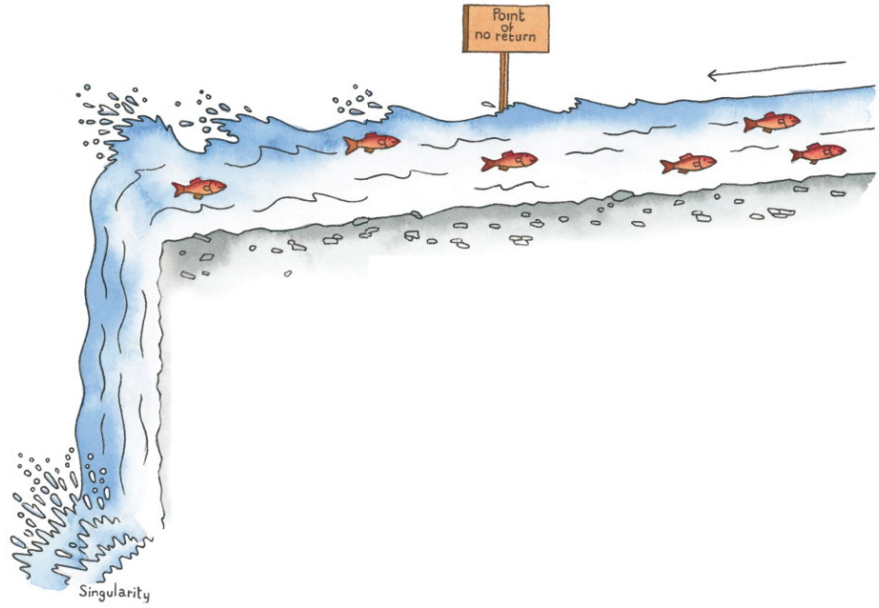


Figure 1.3.: BLACK HOLE HORIZON IN A RIVER: At the “Point of no return”, the flow speed of the water is exactly equal to the maximum speed of the fish. Any fish that travel further downstream than this point will be dragged inexorably towards the waterfall. [Credit: Yan Nascimbene]

so strong that the fish, no matter how hard or in which direction they swim with respect to the water, are doomed to be swept over the waterfall. The point where  $|V| = c$  is the event horizon, and the trajectories of fish swimming at exactly the speed  $c$  are analogous to the trajectories of light near a black hole horizon (see Eqs. (1.1.6) and Fig. 1.2).

It is important to note that the existence of a point at which  $|V| = c$  does not necessarily imply that the metric (1.1.7) is equivalent to a black hole spacetime. Nothing can escape from a black hole once the horizon is crossed; more precisely, the region where the flow is superluminal ( $|V| > c$ ) flows *away* from the horizon. But the opposite is also possible: starting with a black hole-like spacetime and performing the transformation  $V \rightarrow -V$  - or, equivalently,  $t \rightarrow -t$  - we find that the superluminal region flows *towards* the horizon. This is a white hole spacetime, the time-reverse of a black hole spacetime, and white hole trajectories are simply time-reversed black hole trajectories. Therefore, all light rays initially in the superluminal region are dragged towards the horizon. Those moving counter to the flow will come to a standstill there: whether on the superluminal or subluminal side, they will approach the horizon asymptotically, never actually reaching it. In the river analogy, this is equivalent to water flowing *from* a waterfall, so that its flow is initially very fast but slows as it travels; this is shown in Figure 1.4. The horizon is again where  $|V| = c$ . Fish far from the waterfall, where the current is low, may come and go as they please; but as they travel upstream, they will find it increasingly difficult to continue, and must come to a standstill at the horizon.

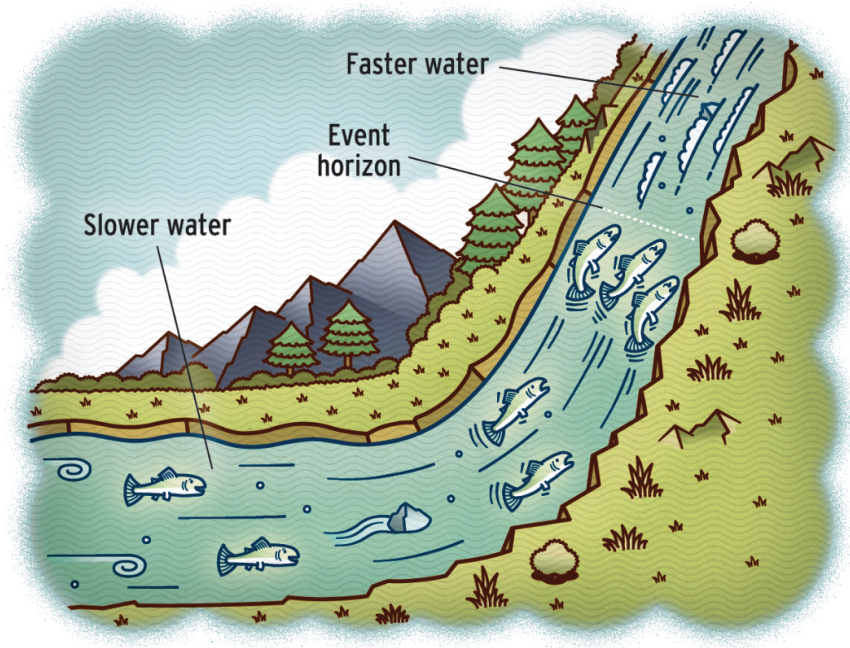


Figure 1.4.: WHITE HOLE HORIZON IN A RIVER: As in Figure 1.3, the event horizon is the point at which the flow speed is exactly equal to the maximum speed of the fish. Here, however, the flow speed *decreases* in the direction of flow, so that the fish may swim arbitrarily close to the event horizon, but may never cross it. [Credit: A. Cho, Science **319**, 1321 (2008)]

## 1. Hawking Radiation

The white hole is of limited use in astrophysics. It *is* encoded in Schwarzschild spacetime, from which it is derived by changing the sign of the  $r$ -dependent terms in Eqs. (1.1.3)-(1.1.5), but it extends the spacetime into the infinite past. Therefore, its validity requires that the Schwarzschild metric is valid for  $t_S \rightarrow -\infty$ , which is seldom the case, for black holes are believed to form from gravitational collapse. However, turning away from gravity to the more general case of moving media, white holes are just as realisable as black holes, and we shall make use of them in Part III when we discuss light in optical fibres.

## 1.2. The acoustic field and its wave equation

Having now shown the spacetime metric (1.1.7) of a moving medium to be analogous to that of a Schwarzschild black hole, let us study the behaviour of fields in such a spacetime. For simplicity, we shall assume a massless scalar field; in the context of a fluid, such a field may arise from small perturbations in the background flow [16, 14]. If the fluid is irrotational (as it must be in one spatial dimension), the flow velocity may be expressed as the derivative of a potential:  $V(x) = -\partial\Phi/\partial x$ . Variations in pressure and density (i.e., sound waves) give rise to small deviations  $\phi = \delta\Phi$ . We shall treat the background flow as constant in time, and the small variations as the independent field  $\phi$ , which will be referred to as the acoustic field. Being massless, the acoustic field has speed  $c$  with respect to the medium; since this holds for all frequencies, this implies that the fluid is dispersionless. (Dispersion is introduced in Part II.)

Let us begin with the Principle of Least action: the acoustic field  $\phi(t, x)$  varies from one configuration to another in such a way that the action integral is an extremum (usually a minimum). The action is the integral of the Lagrangian:

$$S = \int \int dx dt L(\phi, \partial_t \phi, \partial_x \phi), \quad (1.2.1)$$

so all the physics of the model is contained in the Lagrangian,  $L$ . An extremum of the action is found by infinitesimally varying the field  $\phi$  and its derivatives,  $\partial_t \phi$  and  $\partial_x \phi$ , then setting the resulting variation in  $S$  to zero. This yields the Euler-Lagrange equation:

$$\frac{\partial L}{\partial \phi^*} - \frac{\partial}{\partial t} \left( \frac{\partial L}{\partial (\partial_t \phi^*)} \right) - \frac{\partial}{\partial x} \left( \frac{\partial L}{\partial (\partial_x \phi^*)} \right) = 0. \quad (1.2.2)$$

Being scalar and massless, the Lagrangian for the acoustic field is [56]

$$L = \frac{1}{2} \sqrt{-g} g^{\mu\nu} \partial_\mu \phi^* \partial_\nu \phi. \quad (1.2.3)$$

$g^{\mu\nu}$  is the inverse metric tensor, and  $g$  is the determinant of the metric tensor  $g_{\mu\nu}$ . Using the metric (1.1.7), the Lagrangian becomes

$$L = \frac{1}{2c} \left( |(\partial_t + V(x) \partial_x) \phi|^2 - c^2 |\partial_x \phi|^2 \right), \quad (1.2.4)$$

## 1.2. The acoustic field and its wave equation

and plugging this into the Euler-Lagrange equation yields the wave equation

$$(\partial_t + \partial_x V)(\partial_t + V\partial_x)\phi - c^2\partial_x^2\phi = 0. \quad (1.2.5)$$

Solutions of the wave equation are more easily derived once its conservation laws have been identified. These are directly related to symmetries of the Lagrangian. There are two nontrivial symmetries of the Lagrangian (1.2.4). One is time translation:  $L$  is invariant under the transformation  $t \rightarrow t + \Delta t$ . This leads to conservation of frequency; more precisely, it implies the existence of stationary modes of the form  $\phi_\omega(x) e^{-i\omega t}$ , which are examined in §1.3 below. The other symmetry is phase rotation:  $L$  is invariant under the transformation  $\phi \rightarrow \phi e^{i\alpha}$ , where  $\alpha$  is a real constant. This implies conservation of the scalar product, defined as

$$\begin{aligned} (\phi_1, \phi_2) &= i \int_{-\infty}^{+\infty} dx \{ \phi_1^* (\partial_t + V\partial_x) \phi_2 - \phi_2 (\partial_t + V\partial_x) \phi_1^* \} \\ &= i \int_{-\infty}^{+\infty} dx \{ \phi_1^* \pi_2 - \phi_2 \pi_1^* \}, \end{aligned} \quad (1.2.6)$$

where  $\phi_1$  and  $\phi_2$  are both solutions of the wave equation (1.2.5), and the canonical momentum

$$\pi = \frac{\partial L}{\partial(\partial_t \phi^*)} = (\partial_t + V(x)\partial_x)\phi. \quad (1.2.7)$$

The scalar product of a solution with itself is of particular importance, and is called the *norm*.

A general solution to the acoustic wave equation (1.2.5) is easily found. We define new variables  $u$  and  $v$  as follows:

$$u = t - \int^x \frac{dx'}{c + V(x')}, \quad v = t + \int^x \frac{dx'}{c - V(x')}. \quad (1.2.8)$$

Then, after some algebra, we find that the wave equation in the coordinates  $(u, v)$  is simply

$$\partial_u \partial_v \phi = 0. \quad (1.2.9)$$

So, in the absence of horizons where  $|V| = c$ ,  $\phi$  is simply a sum of two arbitrary functions, one a function of  $u$  only, the other a function of  $v$  only:

$$\begin{aligned} \phi &= \phi_u(u) + \phi_v(v) \\ &= \phi_u \left( t - \int^x \frac{dx'}{c + V(x')} \right) + \phi_v \left( t + \int^x \frac{dx'}{c - V(x')} \right). \end{aligned} \quad (1.2.10)$$

With respect to the fluid,  $\phi_u$  is right-moving while  $\phi_v$  is left-moving. The fact that the two functional forms maintain their shapes is a consequence of the absence of dispersion: all wave components have the same velocity,  $c$ , with respect to the fluid, and so does the waveform as a whole. The only ambiguity is in the direction of travel; thus the solution splits into a right-moving and a left-moving part.

If horizons are present, the coordinates  $u$  and  $v$  defined in Eqs. (1.2.8) do not cover the entire spacetime, so that extra coordinates - and hence extra functions in the general solution (1.2.10) - must be added. This is examined in greater detail in §1.5.

### 1.3. Stationary modes

The general solution (1.2.10) ceases to apply when dispersion is introduced (although the labels  $u$  and  $v$ , representing waves which are right- and left-moving with respect to the fluid, continue to be useful). However, even with dispersion, the symmetries of the Lagrangian described above remain valid, as do their corresponding conservation laws. We shall present here a more comprehensive form for the general solution: a linear superposition of stationary modes.

As previously mentioned, the invariance of the Lagrangian under time translation implies the existence of solutions of the form

$$\phi(t, x) = e^{-i\omega t} \phi_\omega(x), \quad (1.3.1)$$

called *stationary modes*. In the present case of no dispersion, Eq. (1.2.10) implies that the spatial part of the solution takes the form

$$\begin{aligned} \phi_\omega(x) &= C_u \exp\left(i\omega \int^x \frac{dx'}{c + V(x')}\right) + C_v \exp\left(-i\omega \int^x \frac{dx'}{c - V(x')}\right) \\ &= C_u \phi_\omega^u(x) + C_v \phi_\omega^v(x). \end{aligned} \quad (1.3.2)$$

It thus splits into two independent parts, one right-moving and one left-moving with respect to the fluid. Defining the local wavevector  $k(x)$  such that  $\phi_\omega^{u/v}(x) = \exp\left(i \int^x dx' k_\omega^{u/v}(x')\right)$ , we see that

$$k_\omega^u(x) = \frac{\omega}{c + V(x)}, \quad k_\omega^v(x) = -\frac{\omega}{c - V(x)}, \quad (1.3.3)$$

which are summarized by the relation

$$(\omega - Vk)^2 = c^2 k^2. \quad (1.3.4)$$

This formula is very intuitive once we recognise that  $\omega$  is related to the free-fall frequency  $\omega_{\text{ff}}$  (i.e., the frequency measured in the frame in which the medium is at rest) via the Doppler formula:  $\omega = \omega_{\text{ff}} + Vk$ . Equation (1.3.4), then, is simply  $\omega_{\text{ff}}^2 = c^2 k^2$  - the dispersion relation in the free-fall frame. Comparing with Eqs. (1.3.3), we see that

$$\omega_{\text{ff}} = \omega - Vk = \begin{cases} ck & \text{for } u\text{-modes} \\ -ck & \text{for } v\text{-modes} \end{cases}. \quad (1.3.5)$$

Consider the stationary modes

$$\phi_\omega^{u/v}(t, x) = \exp\left(-i\omega t \pm i\omega \int^x \frac{dx'}{c \pm V(x')}\right), \quad (1.3.6)$$

with canonical momenta

$$\pi_\omega^{u/v}(t, x) = -i \frac{\omega c}{c \pm V} \phi_\omega^{u/v}(t, x). \quad (1.3.7)$$

The scalar product between  $u$ -modes is

$$\begin{aligned}
(\phi_{\omega_1}^u, \phi_{\omega_2}^u) &= i \int dx \{ \phi_{\omega_1}^{u*} \pi_{\omega_2}^u - \phi_{\omega_2}^u \pi_{\omega_1}^{u*} \} \\
&= (\omega_1 + \omega_2) e^{i(\omega_1 - \omega_2)t} \int dx \frac{c}{c + V(x)} \exp \left( -i(\omega_1 - \omega_2) \int^x \frac{dx'}{c + V(x')} \right) \\
&= 4\pi c \omega_1 \operatorname{sgn}(c + V) \delta(\omega_1 - \omega_2) , \tag{1.3.8}
\end{aligned}$$

where the last line is found by making the substitution  $z = \operatorname{sgn}(c + V) \int^x dx' / (c + V(x'))$ , and the integration is taken over the whole real line of  $z$ . If  $c + V$  is nowhere zero, there is a one-to-one correspondence between the  $z$ - and  $x$ -axes, and the integration thus extends over all  $x$ . (When  $c + V = 0$  for some  $x$ , the mode must be split between separate regions; this is dealt with in §1.5.) Similarly, the scalar product between  $v$ -modes is

$$\begin{aligned}
(\phi_{\omega_1}^v, \phi_{\omega_2}^v) &= i \int dx \{ \phi_{\omega_1}^{v*} \pi_{\omega_2}^v - \phi_{\omega_2}^v \pi_{\omega_1}^{v*} \} \\
&= (\omega_1 + \omega_2) e^{i(\omega_1 - \omega_2)t} \int dx \frac{c}{c - V(x)} \exp \left( i(\omega_1 - \omega_2) \int^x \frac{dx'}{c - V(x')} \right) \\
&= 4\pi c \omega_1 \operatorname{sgn}(c - V) \delta(\omega_1 - \omega_2) , \tag{1.3.9}
\end{aligned}$$

where the last line is found via the substitution  $z = \operatorname{sgn}(c - V) \int^x dx' / (c - V(x'))$ , and the integration is taken over the entire  $z$ -axis. (Again, if  $c - V = 0$  for some  $x$ , the mode must be split into regions; see §1.5.) Finally, we remark that the  $u$ - and  $v$ -modes are orthogonal to each other, as are modes and their conjugates:

$$(\phi_{\omega_1}^u, \phi_{\omega_2}^v) = (\phi_{\omega_1}^u, \phi_{\omega_2}^{u*}) = (\phi_{\omega_1}^v, \phi_{\omega_2}^{v*}) = 0 . \tag{1.3.10}$$

Notice, from Eqs. (1.3.8) and (1.3.9), that the sign of the norm is equal to the sign of the wavevector  $k$  for  $u$ -modes, but to minus the sign of  $k$  for  $v$ -modes. More succinctly, with the use of Eq. (1.3.5), the sign of the norm is equal to the sign of the free-fall frequency:

$$\operatorname{sgn} \left[ (\phi_{\omega}^{u/v}, \phi_{\omega}^{u/v}) \right] = \operatorname{sgn} [\omega_{\text{ff}}] . \tag{1.3.11}$$

This correspondence continues to hold in dispersive systems.

We may redefine the stationary modes so that they are normalized: for  $\omega > 0$ ,

$$\phi_{\omega}^u(t, x) = \frac{e^{-\operatorname{sgn}(c+V) i \omega t}}{\sqrt{4\pi c \omega}} = \frac{1}{\sqrt{4\pi c \omega}} \exp \left( -\operatorname{sgn}(c + V) i \omega \left[ t - \int^x \frac{dx'}{c + V(x')} \right] \right) , \tag{1.3.12}$$

$$\phi_{\omega}^v(t, x) = \frac{e^{-\operatorname{sgn}(c-V) i \omega t}}{\sqrt{4\pi c \omega}} = \frac{1}{\sqrt{4\pi c \omega}} \exp \left( -\operatorname{sgn}(c - V) i \omega \left[ t + \int^x \frac{dx'}{c - V(x')} \right] \right) , \tag{1.3.13}$$

so that

$$(\phi_{\omega_1}^u, \phi_{\omega_2}^u) = (\phi_{\omega_1}^v, \phi_{\omega_2}^v) = \delta(\omega_1 - \omega_2) . \tag{1.3.14}$$

### 1. Hawking Radiation

A complete set of modes must include the complex conjugates of these. According to Eq. (1.2.6), complex conjugation changes the sign of the scalar product:

$$(\phi_{\omega_1}^{u*}, \phi_{\omega_2}^{u*}) = (\phi_{\omega_1}^{v*}, \phi_{\omega_2}^{v*}) = -\delta(\omega_1 - \omega_2) . \quad (1.3.15)$$

Finally, then, any solution of the wave equation (1.2.5) can be written as a linear superposition of modes:

$$\phi(t, x) = \int_0^\infty d\omega \{ a_\omega^u \phi_\omega^u(t, x) + b_\omega^u \phi_\omega^{u*}(t, x) + a_\omega^v \phi_\omega^v(t, x) + b_\omega^v \phi_\omega^{v*}(t, x) \} , \quad (1.3.16)$$

where

$$\begin{aligned} a_\omega^u &= (\phi_\omega^u, \phi) , & b_\omega^u &= -(\phi_\omega^{u*}, \phi) , \\ a_\omega^v &= (\phi_\omega^v, \phi) , & b_\omega^v &= -(\phi_\omega^{v*}, \phi) . \end{aligned} \quad (1.3.17)$$

### 1.4. Quantization of the acoustic field

Having expressed the acoustic field in terms of orthonormal modes, it is readily quantized via the usual methods of Quantum Field Theory [56]. Firstly, however, we note that the physical acoustic field is a real-valued quantity, so that we may write Eq. (1.3.16) in the form

$$\begin{aligned} \phi(t, x) &= \int_0^\infty d\omega \{ a_\omega^u \phi_\omega^u(t, x) + a_\omega^{u*} \phi_\omega^{u*}(t, x) + a_\omega^v \phi_\omega^v(t, x) + a_\omega^{v*} \phi_\omega^{v*}(t, x) \} \\ &= \int_0^\infty d\omega \{ a_\omega^u \phi_\omega^u(t, x) + a_\omega^v \phi_\omega^v(t, x) + \text{c.c.} \} , \end{aligned} \quad (1.4.1)$$

where c.c. stands for complex conjugate. We may now promote the real-valued field variable  $\phi$  to the Hermitian operator  $\hat{\phi}$ , the coefficient variables  $a_\omega^{u/v}$  to annihilation operators  $\hat{a}_\omega^{u/v}$  and the complex conjugate coefficient variables  $(a_\omega^{u/v})^*$  to creation operators  $(\hat{a}_\omega^{u/v})^\dagger$ :

$$\begin{aligned} \hat{\phi}(t, x) &= \int_0^\infty d\omega \{ \hat{a}_\omega^u \phi_\omega^u(t, x) + \hat{a}_\omega^{u\dagger} \phi_\omega^{u*}(t, x) + \hat{a}_\omega^v \phi_\omega^v(t, x) + \hat{a}_\omega^{v\dagger} \phi_\omega^{v*}(t, x) \} \\ &\quad \int_0^\infty d\omega \{ \hat{a}_\omega^u \phi_\omega^u(t, x) + \hat{a}_\omega^v \phi_\omega^v(t, x) + \text{h.c.} \} , \end{aligned} \quad (1.4.2)$$

where h.c. stands for Hermitian conjugate. We also have a Hermitian operator for the canonical momentum:

$$\hat{\pi}(t, x) = \int_0^\infty d\omega \{ \hat{a}_\omega^u \pi_\omega^u(t, x) + \hat{a}_\omega^v \pi_\omega^v(t, x) + \text{h.c.} \} . \quad (1.4.3)$$

These may be inverted, as in (1.3.17), to find expressions for the annihilation and creation operators:

$$\hat{a}_\omega^u = i \int_{-\infty}^{+\infty} dx \left\{ \phi_\omega^{u*}(t, x) \hat{\pi}(t, x) - \pi_\omega^{u*}(t, x) \hat{\phi}(t, x) \right\} , \quad (1.4.4)$$



where the Hermitian conjugate gives the operator  $\hat{a}_\omega^{u\dagger}$  and a similar expression holds for the  $v$ -mode operators.

To complete the quantization, the commutators of the various operators must be specified. This is done for  $\hat{\phi}$  and  $\hat{\pi}$ , the other operators following suit. We define

$$\left[ \hat{\phi}(\tau, x), \hat{\pi}(\tau, x') \right] = i \delta(x - x'), \quad \left[ \hat{\phi}(\tau, x), \hat{\phi}(\tau, x') \right] = \left[ \hat{\pi}(\tau, x), \hat{\pi}(\tau, x') \right] = 0. \quad (1.4.5)$$

Then the annihilation and creation operators obey the Bose commutation relations

$$\left[ \hat{a}_{\omega_1}^u, \hat{a}_{\omega_2}^{u\dagger} \right] = \left[ \hat{a}_{\omega_1}^v, \hat{a}_{\omega_2}^{v\dagger} \right] = \delta(\omega_1 - \omega_2), \quad (1.4.6)$$

all other commutators being zero.

## 1.5. Event horizon

Suppose there exists a point at which  $V = -c$ . Since the flow is to the left at precisely the wave speed with respect to the flow, the total speed of right-moving waves here is zero. This is an event horizon for right-moving waves.

Let us suppose that the event horizon is situated at the origin,  $x = 0$ ; and, moreover, that the derivative of  $V$  is non-zero there. Then we may approximate the flow velocity to first-order in  $x$  as follows:

$$V(x) \approx -c + \alpha x. \quad (1.5.1)$$

If  $\alpha > 0$ , the magnitude of the velocity increases in the direction of flow; this is equivalent to a black hole horizon. However, if  $\alpha < 0$ , the speed decreases in the direction of flow, and we have a white hole horizon. We shall assume in what follows that  $\alpha > 0$ , so that we have a black hole. It should be borne in mind that the white hole is entirely analogous, and behaves as the time reverse of a black hole.

Equation (1.2.10) states that waves which are right-moving with respect to the fluid are described by the arbitrary function  $\phi_u(u)$ , where  $u$  is given by

$$u = t - \int^x \frac{dx'}{c + V(x')} = t - \frac{1}{\alpha} \log \left( \frac{\alpha}{c} |x| \right); \quad (1.5.2)$$

the second equality holds in the vicinity of the horizon. It is evident from Eq. (1.5.2) that a horizon is located at  $x = 0$ , for the space is divided into two separate regions, with  $x = 0$  marking the boundary between them. To see this, imagine first that we have a wavepacket centred at a certain value of  $u$ , and that this is located, at a certain time, at a positive value of  $x$ . If  $t$  increases, then  $\log(\alpha|x|/c)/\alpha$  must increase by exactly the same amount, and so  $|x|$  increases. Since  $x$  is positive,  $x$  itself increases, and the wavepacket moves to the right. Similarly, if we trace the wavepacket back in time by decreasing  $t$ ,  $\log(\alpha|x|/c)/\alpha$  must also decrease by the same amount, and  $x$  decreases; the wavepacket has come from the left. But the logarithm diverges to  $-\infty$  at the origin; this means that, no matter how far back in time we look,  $\log(\alpha|x|/c)/\alpha$  can be decreased by a

## 1. Hawking Radiation

corresponding amount *without  $x$  ever becoming negative*. The wavepacket must have originated arbitrarily close to the event horizon, moving very slowly forwards at first, picking up speed the further it travels. (The trajectories are precisely those plotted on the right-hand side of Fig. 1.2(b).) If the horizon has existed since the infinite past, then the wavepacket could never have been in the left-hand region (where  $x$  is negative). Since this applies to the entire wavepacket, it also implies that the wavepacket must initially have been arbitrarily thin; or, equivalently, that it must have originated from arbitrarily short wavelengths. This is precisely the trans-Planckian problem.

Exactly the same analysis holds in the left-hand region, but in the opposite direction. Any wavepacket that exists there moves to the left, and must have originated arbitrarily close to the left-hand side of the horizon. If the horizon has existed since the infinite past, then at no point in the past could the wavepacket have been located at a positive value of  $x$ . Moreover, the further back in time the wavepacket is traced, the thinner it becomes. (This corresponds to the left-hand side of Fig. 1.2(b).)

Since a complete set of modes must be able to account for the existence of waves throughout all space, there must be two separate  $u$ -modes for each frequency, one for each of the regions separated by the horizon:

$$\phi_{\omega,R}^u(t,x) = \theta(x) \frac{1}{\sqrt{4\pi c\omega}} \exp(-i\omega u), \quad (1.5.3)$$

$$\phi_{\omega,L}^u(t,x) = \theta(-x) \frac{1}{\sqrt{4\pi c\omega}} \exp(i\omega u). \quad (1.5.4)$$

The modes of Eqs. (1.5.3) and (1.5.4) are normalized according to Eq. (1.3.14). The change in sign of the exponent between the right-hand and left-hand regions comes about because of the change in sign of  $c + V$  (see Eq. (1.3.12)); it ensures that both  $\phi_{\omega,R}^u$  and  $\phi_{\omega,L}^u$  have positive norm.

## 1.6. Out-modes and in-modes with an event horizon

The modes  $\phi_{\omega,R}^u$  and  $\phi_{\omega,L}^u$  - defined above for the case of an event horizon for  $u$ -modes - are not unique. Each has the same frequency (in the observer's frame) as the complex conjugate of the other. Therefore, any linear combination of one with the complex conjugate of the other is itself a stationary mode. In order to normalize such a linear combination, we simply employ the linearity of the scalar product:

$$\begin{aligned} & (\alpha\phi_{\omega_1,R}^u + \beta\phi_{\omega_1,L}^{u*}, \alpha\phi_{\omega_2,R}^u + \beta\phi_{\omega_2,L}^{u*}) \\ &= \alpha^*\alpha (\phi_{\omega_1,R}^u, \phi_{\omega_2,R}^u) + \alpha^*\beta (\phi_{\omega_1,R}^u, \phi_{\omega_2,L}^{u*}) + \beta^*\alpha (\phi_{\omega_1,L}^{u*}, \phi_{\omega_2,R}^u) + \beta^*\beta (\phi_{\omega_1,L}^{u*}, \phi_{\omega_2,L}^{u*}) \\ &= (|\alpha|^2 - |\beta|^2) \delta(\omega_1 - \omega_2). \end{aligned}$$

So, if  $|\alpha|^2 - |\beta|^2 = 1$ , the linear combination  $\alpha\phi_{\omega,R}^u + \beta\phi_{\omega,L}^{u*}$  is normalized with positive norm; it is also automatically orthogonal to any such combination involving a different

### 1.6. Out-modes and in-modes with an event horizon

frequency or the modes  $\phi_{\omega,L}^u$  and  $\phi_{\omega,R}^{u\star}$ , since the individual modes are orthogonal to these. Therefore, any set of modes

$$\phi_{\omega,1}^u = \alpha_{\omega,1}\phi_{\omega,R}^u + \beta_{\omega,1}\phi_{\omega,L}^{u\star}, \quad \phi_{\omega,2}^u = \alpha_{\omega,2}\phi_{\omega,L}^u + \beta_{\omega,2}\phi_{\omega,R}^{u\star}, \quad (1.6.1)$$

where

$$|\alpha_{\omega,j}|^2 - |\beta_{\omega,j}|^2 = 1, \quad (1.6.2)$$

form a complete set of orthonormal, positive-norm  $u$ -modes. A transformation between different sets of modes is called a *Bogoliubov transformation*.

Despite the limitless possibilities, very few of these sets of modes are useful. We should deal only with those sets of modes which correspond to possible measurements. Consider the simplest example:  $\alpha_{\omega,j} = 1$ ,  $\beta_{\omega,j} = 0$ . This, of course, is simply the set of localized modes given in Eqs. (1.5.3) and (1.5.4). As we have seen, these modes correspond to single outgoing wavepackets. An outgoing phonon travelling to the right with frequency  $\omega$  is precisely an excitation of the mode  $\phi_{\omega,R}^u$ ; similarly, a phonon travelling to the left with frequency  $\omega$  is an excitation of  $\phi_{\omega,L}^u$ . They differ in this respect from the other linear combinations, which correspond to two outgoing wavepackets rather than just one. In light of this property, the set of modes  $\phi_{\omega,R}^u$  and  $\phi_{\omega,L}^u$  are termed *out-modes*: they correspond to a single outgoing wave.

We expect that there should also exist a set of modes that correspond to a single ingoing wave. However, the behaviour of the modes already found would seem to belie this expectation. As noted in §1.5 above, all  $u$ -modes drift away from the horizon; how can we possibly form an ingoing wavepacket from these? We cannot, of course; not while there is a horizon. There is a trick, however, due to Unruh and others, which we borrow from the gravitational case [6, 7, 57]. There, the analysis normally begins by assuming that a horizon has not always existed, but forms at some finite time from a collapsing spacetime. The in-modes, then, are well-defined, for they are constructed in a spacetime where a horizon has not yet formed. It is found that the results of this analysis, in which in-modes are defined as positive-norm with respect to the initial time coordinate, are identical to the results obtained by ignoring the formation process and defining the in-modes as positive-norm with respect to the Kruskal coordinate. Now, near  $x = 0$ , the unit vector defined by the Kruskal coordinate is proportional, but opposite in direction, to the unit vector defined by the  $x$ -coordinate. Therefore, purely positive-norm modes with respect to the Kruskal coordinate must be analytic in the upper-half  $x$ -plane near  $x = 0$ . This completely defines the in-modes:  $x$ , on traversing the upper-half complex plane to  $-x$ , simply picks up a phase factor of  $e^{i\pi}$ , so that the relative amplitude of the left-hand mode compared to the right-hand mode is  $e^{-\pi\omega/\alpha}$ . After normalizing, we have

$$\begin{aligned} \phi_{\omega,R}^{u,\text{in}} &= \frac{1}{\sqrt{2 \sinh\left(\frac{\pi\omega}{\alpha}\right)}} \left( e^{\frac{\pi\omega}{2\alpha}} \phi_{\omega,R}^{u,\text{out}} + e^{-\frac{\pi\omega}{2\alpha}} \phi_{\omega,L}^{u,\text{out}\star} \right), \\ \phi_{\omega,L}^{u,\text{in}} &= \frac{1}{\sqrt{2 \sinh\left(\frac{\pi\omega}{\alpha}\right)}} \left( e^{\frac{\pi\omega}{2\alpha}} \phi_{\omega,L}^{u,\text{out}} + e^{-\frac{\pi\omega}{2\alpha}} \phi_{\omega,R}^{u,\text{out}\star} \right). \end{aligned} \quad (1.6.3)$$

## 1. Hawking Radiation

The in-modes and out-modes - together with their complex conjugates - are distinct sets of orthonormal  $u$ -modes. Taken together with the  $v$ -modes, they form a complete set of orthonormal modes which are solutions of the wave equation (1.2.5). Therefore, we have two natural ways of decomposing the  $u$  part of the field operator in Eq. (1.4.2) when a horizon is present:

$$\hat{\phi}(t, x) = \int_0^\infty d\omega \left\{ \hat{a}_{\omega, R}^{u, \text{in}} \phi_{\omega, R}^{u, \text{in}}(t, x) + \hat{a}_{\omega, L}^{u, \text{in}} \phi_{\omega, L}^{u, \text{in}}(t, x) + \hat{a}_{\omega}^v \phi_{\omega}^v(t, x) + \text{h.c.} \right\} \quad (1.6.4)$$

$$= \int_0^\infty d\omega \left\{ \hat{a}_{\omega, R}^{u, \text{out}} \phi_{\omega, R}^{u, \text{out}}(t, x) + \hat{a}_{\omega, L}^{u, \text{out}} \phi_{\omega, L}^{u, \text{out}}(t, x) + \hat{a}_{\omega}^v \phi_{\omega}^v(t, x) + \text{h.c.} \right\} \quad (1.6.5)$$

Given that these two representations are equivalent, and that we know the Bogoliubov transformation that relates the in- and out-modes, we also find that an analogous transformation exists between the quantum amplitude operators. Plugging the transformation into Eq. (1.6.4) and comparing with Eq. (1.6.5), we find:

$$\begin{aligned} \hat{a}_{\omega, R}^{u, \text{out}} &= \frac{1}{\sqrt{2 \sinh\left(\frac{\pi\omega}{\alpha}\right)}} \left( e^{\frac{\pi\omega}{2\alpha}} \hat{a}_{\omega, R}^{u, \text{in}} + e^{-\frac{\pi\omega}{2\alpha}} \hat{a}_{\omega, L}^{u, \text{in}\dagger} \right), \\ \hat{a}_{\omega, L}^{u, \text{out}} &= \frac{1}{\sqrt{2 \sinh\left(\frac{\pi\omega}{\alpha}\right)}} \left( e^{\frac{\pi\omega}{2\alpha}} \hat{a}_{\omega, L}^{u, \text{in}} + e^{-\frac{\pi\omega}{2\alpha}} \hat{a}_{\omega, R}^{u, \text{in}\dagger} \right). \end{aligned} \quad (1.6.6)$$

## 1.7. Spontaneous creation of phonons

The quantum amplitudes  $\hat{a}$  and  $\hat{a}^\dagger$  are to be interpreted as annihilation and creation operators, respectively. That is, the operator  $\hat{a}^\dagger$  has the effect of exciting its corresponding mode by a single quantum, while the operator  $\hat{a}$  has the opposite effect. The *vacuum state* is that in which no modes are excited: it is the absence of “particles”. Since one cannot annihilate an excitation from the vacuum state, it must vanish when acted on by any annihilation operator. Mathematically speaking, then, the vacuum state is uniquely defined as the eigenstate of all annihilation operators with eigenvalue zero:

$$\hat{a} |0\rangle = 0 \quad \forall \hat{a}, \quad (1.7.1)$$

where  $|0\rangle$  denotes the vacuum state.

The vacuum state would seem to depend on the specific set of annihilation operators - and, hence, on the specific set of orthonormal modes - used to define it. However, if the positive-norm modes of one set are formed from linear combinations of positive-norm modes of the other set - and, equivalently, one set’s negative-norm modes are linear combinations of the other set’s negative-norm modes - then the annihilation operators of each set are also linear combinations of each other. In this case, the vacuum states defined by the two sets of modes are identical, for all annihilation operators, of either set, give zero when acting on  $|0\rangle$ . Thus, the vacuum state is uniquely defined by the space spanned by the positive-norm modes, and is not so sensitive to the individual modes themselves.

### 1.7. Spontaneous creation of phonons

The corollary of the previous statement is perhaps more interesting: two sets of modes, whose positive-norm elements span different spaces, define different vacuum states. Although the entire space, combining both positive- and negative-norm modes (that is, the field operator  $\hat{\phi}$ ), is exactly the same, a state which is empty with respect to one set of modes can look non-empty with respect to another, provided the elements of one set combine positive- *and* negative-norm modes of the other.

This is precisely the situation with the in- and out-modes of Eq. (1.6.3). We conclude that the vacua defined by these two sets of modes - called, respectively, the *in-vacuum* and the *out-vacuum* - are different. The in-vacuum is that state which contains no phonons in the infinite past; since all wavepackets are incoming (travelling towards the horizon) in the infinite past, this is the same as saying that there are no incoming phonons. Conversely, the out-vacuum contains no phonons in the infinite future, and since all wavepackets are outgoing there, this is equivalent to there being no outgoing phonons. The inequality of the two vacua means that, if there are no incoming phonons - the in-vacuum  $|0_{\text{in}}\rangle$  being the usual, and most natural, assumption for the state - then there *will* be outgoing phonons. The event horizon leads to spontaneous particle creation.

We may show this explicitly using Eq. (1.6.6). The expectation value of right-moving outgoing phonons in the in-vacuum is

$$\begin{aligned}
\langle n_{\omega,R}^{u,\text{out}} \rangle &= \langle 0_{\text{in}} | \hat{a}_{\omega,R}^{u,\text{out}\dagger} \hat{a}_{\omega',R}^{u,\text{out}} | 0_{\text{in}} \rangle \\
&= \langle 0_{\text{in}} | \frac{1}{\sqrt{2 \sinh(\frac{\pi\omega}{\alpha})}} \left( e^{\frac{\pi\omega}{2\alpha}} \hat{a}_{\omega,R}^{u,\text{in}\dagger} + e^{-\frac{\pi\omega}{2\alpha}} \hat{a}_{\omega,L}^{u,\text{in}} \right) \frac{1}{\sqrt{2 \sinh(\frac{\pi\omega'}{\alpha})}} \left( e^{\frac{\pi\omega'}{2\alpha}} \hat{a}_{\omega',R}^{u,\text{in}} + e^{-\frac{\pi\omega'}{2\alpha}} \hat{a}_{\omega',L}^{u,\text{in}\dagger} \right) | 0_{\text{in}} \rangle \\
&= \frac{1}{\sqrt{4 \sinh(\frac{\pi\omega}{\alpha}) \sinh(\frac{\pi\omega'}{\alpha})}} e^{-\frac{\pi(\omega+\omega')}{2\alpha}} \langle 0_{\text{in}} | \hat{a}_{\omega,L}^{u,\text{in}} \hat{a}_{\omega',L}^{u,\text{in}\dagger} | 0_{\text{in}} \rangle \\
&= \frac{1}{\sqrt{4 \sinh(\frac{\pi\omega}{\alpha}) \sinh(\frac{\pi\omega'}{\alpha})}} e^{-\frac{\pi(\omega+\omega')}{2\alpha}} \langle 0_{\text{in}} | \hat{a}_{\omega',L}^{u,\text{in}\dagger} \hat{a}_{\omega,L}^{u,\text{in}} + \delta(\omega - \omega') | 0_{\text{in}} \rangle \\
&= \frac{1}{2 \sinh(\frac{\pi\omega}{\alpha})} e^{-\frac{\pi\omega}{\alpha}} \delta(\omega - \omega') \\
&= \frac{1}{e^{\frac{2\pi\omega}{\alpha}} - 1} \delta(\omega - \omega') .
\end{aligned} \tag{1.7.2}$$

Remarkably, the spectrum of phonons emitted is precisely a bosonic thermal distribution with temperature  $\alpha/(2\pi)$ ; replacing fundamental constants,

$$k_B T = \frac{\hbar\alpha}{2\pi} . \tag{1.7.3}$$

Although the result in Eq. (1.7.2) has been derived as a number expectation value, the appearance of the delta function shows that it is really a density. In §2.5 (and Ref. [39]), it is shown that this is proportional to the spectral flux density,

$$\frac{d^2 N}{d\omega dt} = \frac{1}{2\pi} \frac{1}{e^{\frac{2\pi\omega}{\alpha}} - 1} , \tag{1.7.4}$$

## 1. Hawking Radiation

the number of phonons emitted per unit frequency interval per unit time.

Due to the symmetry of the transformation (1.6.6), the expectation value of left-moving outgoing phonons is exactly equal to the thermal spectrum of (1.7.2). There is a deeper significance to this than just symmetry, however. The transformation of the in- and out-operators allows us to write the in-vacuum explicitly in terms of the out-vacuum. Using the Fock basis, in which the annihilation and creation operators behave in the standard way:

$$\hat{a}_\omega |n\rangle_\omega = \sqrt{n} |n-1\rangle_\omega, \quad \hat{a}_\omega^\dagger |n\rangle_\omega = \sqrt{n+1} |n+1\rangle_\omega, \quad (1.7.5)$$

the in-vacuum state is given by

$$\begin{aligned} |0_{\text{in}}\rangle &= Z^{-\frac{1}{2}} \prod_\omega \sum_{n=0}^{\infty} \frac{1}{n!} \left( e^{-\frac{\pi\omega}{a}} \hat{a}_{\omega,R}^{u,\text{out}\dagger} \hat{a}_{\omega,L}^{u,\text{out}\dagger} \right)^n |0_{\text{out}}\rangle \\ &= Z^{-\frac{1}{2}} \prod_\omega \sum_{n=0}^{\infty} e^{-\frac{n\pi\omega}{a}} |n\rangle_{\omega,R}^{u,\text{out}} |n\rangle_{\omega,L}^{u,\text{out}}, \end{aligned} \quad (1.7.6)$$

where  $Z$  is a normalizing prefactor defined such that  $\langle 0_{\text{in}} | 0_{\text{in}} \rangle = 1$ . The fact that the out-creation operators appear only in  $R$ - $L$  pairs shows that the radiation, though it looks thermal in the right and left sides separately, is strongly correlated *between* the two sides. Phonons are emitted in pairs, one in the subsonic, the other in the supersonic region; and a measurement of the number of phonons in any state on one side of the horizon infers that there are equally many phonons in the corresponding state on the other side. The left and right systems, separated by the horizon, are *entangled*.

## 1.8. Conclusion and discussion

The above derivation is quite general, in that it applies to any spacetime that can be described by the metric (1.1.7). Of course, this includes gravitational black holes (see Eq. (1.1.5)): using  $V(r) = -c\sqrt{r_S/r}$ , we find that, at the Schwarzschild radius,  $V'(r_S) = c/(2r_S) = c^3/(4GM)$ , and plugging into Eq. (1.7.3), we have  $k_B T = \hbar c^3/(8\pi GM)$  - exactly Hawking's original formula, Eq. (1.0.1).

In the absence of dispersion, the event horizon is a well-defined point; for there is only one wave speed,  $c$ , and it is precisely where  $|V| = c$  that a horizon is established. Hawking radiation is derived by linearizing  $V$  around this point; and since, as discussed in §1.5, any wavepacket can be traced back in time to arbitrary thinness and arbitrary closeness to the horizon, it does not matter how small is the region over which this linearized velocity profile is valid. Thus, the Hawking temperature can depend only on the first derivative,  $\alpha$ , of  $V$  at the horizon.

This is no longer true once dispersion is taken into account. In that case, the wave velocity with respect to the medium is not constant but varies with frequency. The horizon, then, is no longer so well-defined, and it is impossible to pick out a single parameter which determines the Hawking spectrum. Moreover, as has been demonstrated by Unruh [18] and as will be shown in Chapter 3, an outgoing wavepacket does not originate from

an arbitrarily thin wavepacket squeezed up against its own horizon. Instead, dispersive effects cause a change in the speed of the wavepacket as its wavelength is reduced, and the wavepacket turns around at a shifted frequency, originating from infinity. Thus, with the introduction of dispersion, we are inclined to ask: does the Hawking spectrum survive? And if so, what is its shape, and on what parameters does it depend?

In the next chapter, we formulate the theoretical framework for a quantized acoustic field, much as in the present chapter, but with dispersion taken into account. Chapter 3 examines some ways of finding the spectrum in specific circumstances, and Chapter 4 presents some numerical results. Later chapters extend the analogy to the case of optical fibres.





Part II.

# Hawking Radiation in Dispersive Fluids



## 2. The Acoustic Model

In Chapter 1, we examined the acoustic model in the absence of dispersion. We shall now deal with the generalization of this model to a dispersive fluid. Much of the following treatment is directly analogous to the analysis of Chapter 1. However, the solutions are more complicated: dispersion leads to the new phenomenon of frequency shifting, whereby a wavepacket is reflected from a group-velocity horizon at a different frequency. The trans-Planckian problem is in this manner avoided, but the solutions are not so tractable as Eq. (1.2.10), nor is the Bogoliubov transformation of Eqs. (1.6.3) and (1.6.6) so simple. The present chapter describes the theoretical model; the methods used to determine its solutions, and some numerical results of these methods, are left to Chapters 3 and 4.

### 2.1. The wave equation and its solutions

Dispersion - which describes a frequency-dependent wave velocity - manifests itself as a breakdown of Lorentz invariance. The wave behaviour can no longer be described by a spacetime metric, and we must instead take the Lagrangian as the starting point. Dispersion is modelled by the appearance of higher-order derivatives in the Lagrangian, so we must now write the action integral as

$$S = \int \int dx dt L(\phi, \partial_t \phi, \partial_x \phi, \dots). \quad (2.1.1)$$

The Lagrangian, given in the absence of dispersion by Eq. (1.2.4), is now generalized to [18, 39]

$$L = \frac{1}{2} |(\partial_t + V \partial_x) \phi|^2 - \frac{1}{2} |F(-i \partial_x) \phi|^2. \quad (2.1.2)$$

$F(k)$  describes the dispersive properties of the fluid; as a function of an operator, we consider it as a Taylor series in that operator. We require that  $F(k)$  is an odd function, so that  $F(-i \partial_x) \phi$  contains only odd-degree derivatives of  $\phi$ .

An extremum of the action is found by infinitesimally varying the field  $\phi$  and its derivatives  $\partial_t \phi$ ,  $\partial_x \phi$ ,  $\partial_x^2 \phi$ , etc., then setting the resulting variation in  $S$  to zero. The result is the following Euler-Lagrange equation:

$$\frac{\partial L}{\partial \phi^*} - \frac{\partial}{\partial t} \left( \frac{\partial L}{\partial (\partial_t \phi^*)} \right) - \frac{\partial}{\partial x} \left( \frac{\partial L}{\partial (\partial_x \phi^*)} \right) + \frac{\partial^2}{\partial x^2} \left( \frac{\partial L}{\partial (\partial_x^2 \phi^*)} \right) - \frac{\partial^3}{\partial x^3} \left( \frac{\partial L}{\partial (\partial_x^3 \phi^*)} \right) + \dots = 0. \quad (2.1.3)$$

## 2. The Acoustic Model

Substituting  $L$  from Eq. (2.1.2) - and using the fact that  $F(k)$  is odd when performing integration by parts - we find the acoustic wave equation [18]:

$$(\partial_t + \partial_x V)(\partial_t + V\partial_x)\phi + F^2(-i\partial_x)\phi = 0. \quad (2.1.4)$$

If  $F^2(k)$  is a polynomial of finite degree, this is a partial differential equation that can be solved numerically. However,  $F^2(k)$  need not be of finite degree, and it is useful to express its operation on  $\phi$  in terms of its Fourier transform [18]: by definition, we have

$$\phi(t, x) = \frac{1}{2\pi} \int_{-\infty}^{+\infty} dk \tilde{\phi}(t, k) e^{ikx}, \quad (2.1.5)$$

so that

$$\begin{aligned} F^2(-i\partial_x)\phi(t, x) &= \frac{1}{2\pi} \int_{-\infty}^{+\infty} dk F^2(k) \tilde{\phi}(t, k) e^{ikx} \\ &= \frac{1}{2\pi} \int_{-\infty}^{+\infty} dk \int_{-\infty}^{+\infty} dx' F^2(k) \phi(t, x') e^{ik(x-x')}. \end{aligned} \quad (2.1.6)$$

Let us assume for now that the flow velocity  $V$  is constant in space. Then, taking the Fourier transform of Eq. (2.1.4) by making the substitutions  $\phi(t, x) \rightarrow \tilde{\phi}(\omega, k)$ ,  $\partial_t \rightarrow -i\omega$  and  $\partial_x \rightarrow ik$ , we find

$$\left[ -(\omega - Vk)^2 + F^2(k) \right] \tilde{\phi}(\omega, k) = 0, \quad (2.1.7)$$

so that  $\tilde{\phi}(\omega, k)$  can only be non-zero when  $\omega$  and  $k$  satisfy

$$(\omega - Vk)^2 = F^2(k). \quad (2.1.8)$$

This is the generalization to dispersive media of Eq. (1.3.4). We see that the function  $\pm F(k)$  simply gives the free-fall frequency,  $\omega_{\text{ff}}$ , as a function of the wavevector  $k$ . (The sign is determined as in Eq. (1.3.5).) In the absence of dispersion, the relation is one of direct proportionality:  $F(k) = ck$ . Typically, waves exhibit very little dispersion for low values of  $k$ , so that  $F(k) \rightarrow ck$  as  $k \rightarrow 0$ . For higher values of  $k$ , the dispersion can take two basic forms: superluminal and subluminal. These are defined according to whether the magnitude of the phase velocity,  $|\omega/k|$ , becomes higher or lower than  $c$  as  $k$  increases; examples are shown in Figure 2.1. Our specification that  $F(k)$  be an odd function means that the fluid (in its rest frame) is isotropic, for  $-k$  is simply a spatial inversion of  $k$ .

For a given frequency, the possible (real) values of  $k$  can be found by plotting  $\pm |F(k)|$  and the line  $\omega - Vk$ , then reading off their points of intersection; examples are shown in Figure 2.2. (The sign now determines the sign of the free-fall frequency, and not whether the mode is on the  $u$ - or  $v$ -branch.) When the fluid is static, the possible wavevectors always occur in pairs of opposite sign and velocity: the  $u$ - and  $v$ -branches, familiar from the dispersionless case. When the fluid is flowing, the possible wavevectors still split into  $u$ - and  $v$ -branches. But now, as in Fig. 2.2(d), something else can occur: a given  $\omega$  can

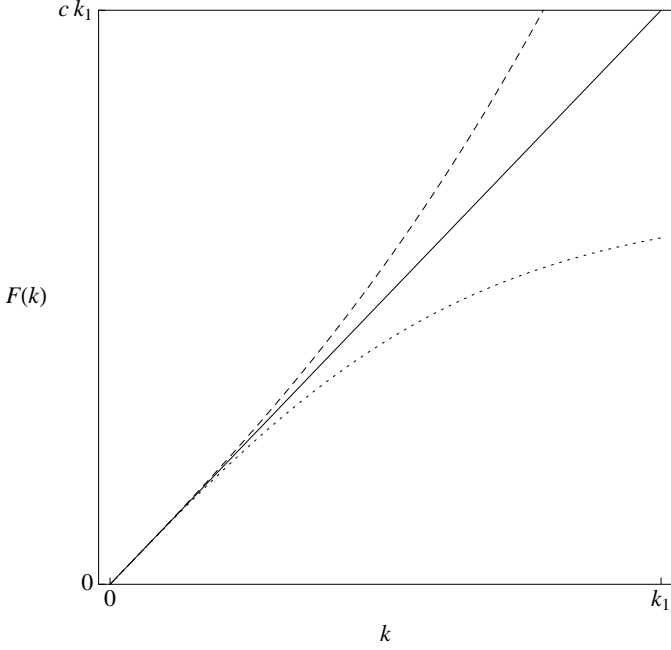


Figure 2.1.: DISPERSION PROFILES: The solid line shows the dispersionless curve, the dashed curve corresponds to superluminal dispersion, and the dotted curve corresponds to subluminal dispersion.

have several different wavevectors on the same branch. It can even have wavevectors with different signs of the free-fall frequency, and given remarks made in §1.3, this suggests that a given  $\omega$  may have solutions of oppositely-signed norm. We should bear this possibility in mind, for it lies at the heart of the Hawking effect. While the route may not be obvious at this stage, the fact that mixing of modes of oppositely-signed norm leads to Hawking radiation in the dispersionless case (see §1.7) would suggest that the same is true here.

The case of a constant fluid flow is not particularly interesting, for any wavepacket, centred around any of the possible solutions of the dispersion relation (2.1.8), simply propagates from one infinity to the other. The analysis can be performed in any Galilean frame, for the fluid flow velocity will always be constant. The fact that certain values of  $k$  share the same value of  $\omega$  in a certain reference frame is of no consequence, because this will not be so in another reference frame; this mathematical relationship is purely incidental. In particular, the relationship between  $k$ -values with different signs of the free-fall frequency is physically meaningless and purely a matter of definition; for, we can always transform to the free-fall frame, where such a relationship cannot (by definition) occur.

This picture changes radically when the fluid flow velocity is not constant, but has some spatial dependence. In this situation, we cannot transform into any Galilean frame without forcing the fluid velocity profile to take on a time dependence as well as a spatial one. There is now a naturally preferred reference frame: that in which the fluid velocity

## 2. The Acoustic Model

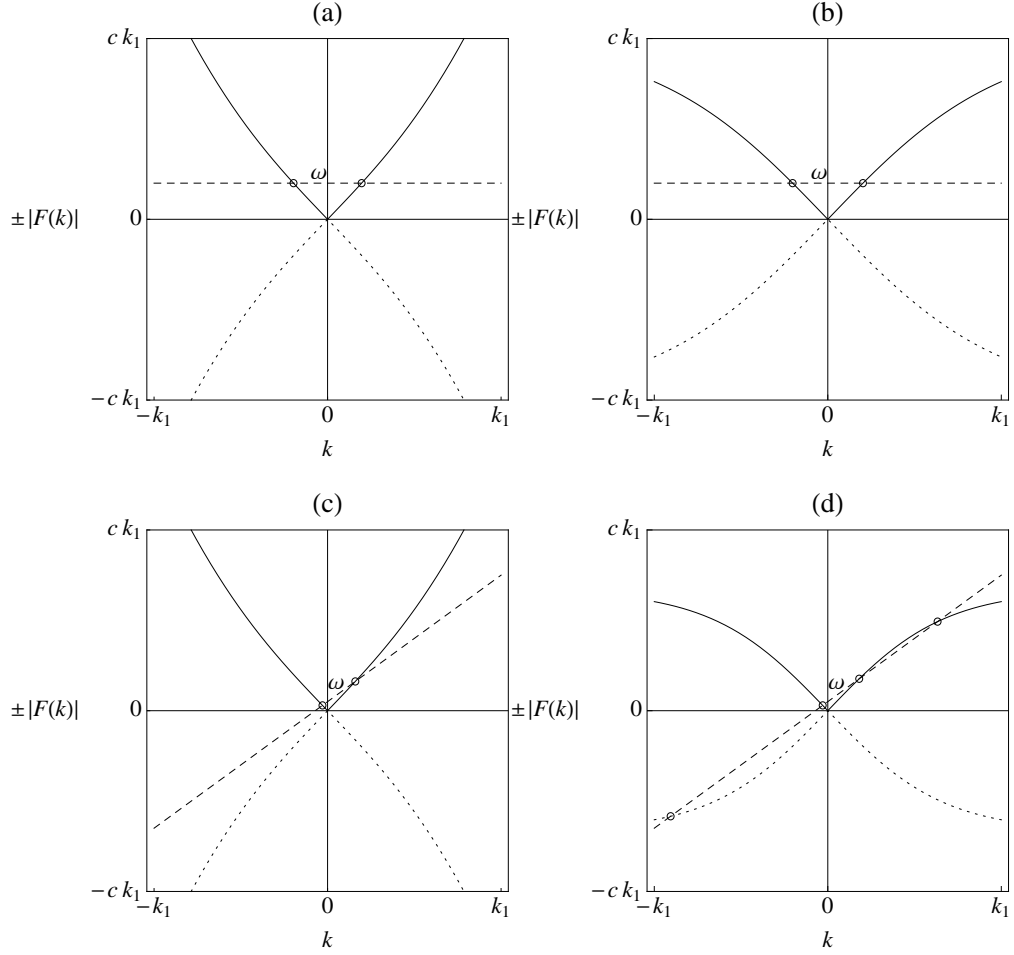


Figure 2.2.: SOLUTIONS AT CONSTANT FLOW: For a given  $\omega$  and  $V$ , the possible values of  $k$  are solutions of  $\omega - Vk = \pm |F(k)|$ . Figures (a) and (b) show the solutions when the fluid is static ( $V = 0$ ) for superluminal and subluminal dispersion, respectively; each frequency has one  $u$ -mode and one  $v$ -mode, as in the dispersionless case. Figures (c) and (d) show the solutions when  $-c < V < 0$ ; superluminal dispersion still gives one  $u$ -mode and one  $v$ -mode, but subluminal dispersion gives three possible  $u$ -modes, one of which has negative free-fall frequency.

profile is dependent only on position and not on time. The *Killing frequency* - that which is conserved - is the value of  $\omega$  measured in this preferred reference frame. During the propagation of a wavepacket,  $k$  may be forced to change, but it can only change to a value of  $k$  with the same value of  $\omega$ . It is in this frame that such relationships - including that between different signs of the free-fall frequency - are physically meaningful.

## 2.2. Scalar product

As discussed in §1.2, invariance of the Lagrangian under phase rotation,  $\phi \rightarrow \phi e^{i\alpha}$ , leads to conservation of the scalar product:

$$\begin{aligned} (\phi_1, \phi_2) &= i \int_{-\infty}^{+\infty} \{ \phi_1^* (\partial_t + V \partial_x) \phi_2 - \phi_2 (\partial_t + V \partial_x) \phi_1^* \} dx \\ &= i \int_{-\infty}^{+\infty} \{ \phi_1^* \pi_2 - \phi_2 \pi_1^* \} dx, \end{aligned} \quad (2.2.1)$$

where the canonical momentum is given by

$$\pi = \frac{\partial L}{\partial (\partial_t \phi^*)} = (\partial_t + V \partial_x) \phi. \quad (2.2.2)$$

As before, the norm is defined as the scalar product of a wave with itself.

If  $V$  is constant, or if two wavepackets are localised in a region where  $V$  is constant, the scalar product takes a simple form. Here,  $\omega$  and  $k$  are related via the dispersion relation in Eq. (2.1.8), so that  $\omega = V k \pm |F(k)|$ , where, as has already been mentioned, the plus or minus sign refers to a positive or negative free-fall frequency. Rather than splitting the dispersion relation into  $u$ - and  $v$ -branches, then, we may split it into branches of positive and negative free-fall frequency. A general solution of the wave equation can be expressed as a sum of two Fourier integrals, one over each branch:

$$\phi(x, t) = \frac{1}{2\pi} \int_{-\infty}^{+\infty} \tilde{\phi}^{(+)}(k) e^{ikx - i(Vk + |F(k)|)t} dk + \frac{1}{2\pi} \int_{-\infty}^{+\infty} \tilde{\phi}^{(-)}(k) e^{ikx - i(Vk - |F(k)|)t} dk. \quad (2.2.3)$$

The canonical momentum is given by Eq. (2.2.2):

$$\begin{aligned} \pi(x, t) &= \frac{-i}{2\pi} \int_{-\infty}^{+\infty} |F(k)| \tilde{\phi}^{(+)}(k) e^{ikx - i(Vk + |F(k)|)t} dk \\ &\quad + \frac{i}{2\pi} \int_{-\infty}^{+\infty} |F(k)| \tilde{\phi}^{(-)}(k) e^{ikx - i(Vk - |F(k)|)t} dk. \end{aligned} \quad (2.2.4)$$

Then, applying Eq. (2.2.1), we find that the scalar product is

$$(\phi_1, \phi_2) = \frac{1}{\pi} \int_{-\infty}^{+\infty} |F(k)| \left\{ \tilde{\phi}_1^{(+)*}(k) \tilde{\phi}_2^{(+)}(k) - \tilde{\phi}_1^{(-)*}(k) \tilde{\phi}_2^{(-)}(k) \right\} dk. \quad (2.2.5)$$

## 2. The Acoustic Model

That is, the two branches of the dispersion relation are decoupled, contributing separately to the scalar product, and the integrand is simply the product of the Fourier transforms multiplied by the free-fall frequency. This formula is particularly useful when calculating the norm of a wave, in which case it becomes

$$(\phi, \phi) = \frac{1}{\pi} \int_{-\infty}^{+\infty} |F(k)| \left\{ \left| \tilde{\phi}^{(+)}(k) \right|^2 - \left| \tilde{\phi}^{(-)}(k) \right|^2 \right\} dk. \quad (2.2.6)$$

Conservation of the scalar product, and the norm in particular, is a very important characteristic of the acoustic wave equation. Much like conservation of energy and momentum in mechanics, it places a restriction on the types of evolution that can occur. On quantizing the acoustic field, normalized modes are multiplied by quantum amplitudes, and the norm corresponds to the excitation or “particle” number. Taking this into account, Eq. (2.2.6) makes the importance of mixing positive and negative free-fall frequencies more apparent: these different spectral components contribute to the norm *with different signs* (thus confirming that Eq. (1.3.11) continues to hold once dispersion is introduced). If a positive-norm mode is partly converted into a negative-norm mode, this must be accompanied by an increase in the norm from purely positive-norm modes; the positive-norm modes are amplified. Thus, a positive-norm particle is not converted into a negative-frequency particle; rather, two particles, one with positive and one with negative norm, are created, so that the total particle number increases. If the original state is vacuum, then these pairs of particles are created out of vacuum fluctuations. This is the process that gives rise to Hawking radiation.

## 2.3. Decomposition into modes

The following analysis is inspired by, and closely follows, that of Macher and Parentani [44].

Let us continue to assume that  $V$  is constant. We saw in Eq. (2.2.3) that we can write  $\phi$  as a sum over the plane waves  $e^{ikx-i\omega t}$ , where  $\omega = Vk \pm |F(k)|$ . These two branches of the dispersion relation have a very simple correspondence - a plane wave on one branch is the complex conjugate of a plane wave on the other:

$$e^{ikx-i(Vk+|F(k)|)t} = \left[ e^{i(-k)x-i(V(-k)-|F(-k)|)t} \right]^*.$$

Thus, we needn’t worry about there being two branches to the dispersion relation. For every value of  $k$ , we uniquely define  $\omega = Vk + |F(k)|$ , and then we include the complex conjugates of the resulting plane waves. This exhausts the possible modes; that is, they form a complete set of solutions. (Note that we are presently working in the  $k$ -representation, since we may write an exact expression for  $\omega$  as a function of  $k$ , but not vice versa.)

Before making use of the completeness of this set, we should first normalise them with respect to the scalar product. Applying Eq. (2.2.1), we find, for two positive-norm plane waves,

$$\left( e^{ik_1x-i(Vk_1+|F(k_1)|)t}, e^{ik_2x-i(Vk_2+|F(k_2)|)t} \right) = 4\pi |F(k_1)| \delta(k_1 - k_2),$$



### 2.3. Decomposition into modes

while, for two plane waves of oppositely-signed norm,

$$\left( e^{ik_1 x - i(Vk_1 + |F(k_1)|)t}, e^{ik_2 x - i(Vk_2 - |F(k_2)|)t} \right) = 0.$$

This agrees with the corresponding result in the dispersionless case (see §1.3), where an extra factor of  $c$  appears because the delta function has its argument in  $\omega$  rather than  $k$ .

An inspection of Eq. (2.2.1) reveals the identities

$$(\phi_1^*, \phi_2^*) = -(\phi_1, \phi_2)^*, \quad (2.3.1)$$

$$(\phi_2, \phi_1) = (\phi_1, \phi_2)^*. \quad (2.3.2)$$

Defining the mode  $\phi_k$  as follows:

$$\phi_k(x, t) = \frac{1}{\sqrt{4\pi |F(k)|}} e^{ikx - i(Vk + |F(k)|)t}, \quad (2.3.3)$$

then the  $\phi_k$  and their complex conjugates  $\phi_k^*$  form a complete orthonormal set, with

$$(\phi_{k_1}, \phi_{k_2}) = -(\phi_{k_1}^*, \phi_{k_2}^*) = \delta(k_1 - k_2), \quad (\phi_{k_1}, \phi_{k_2}^*) = -(\phi_{k_1}^*, \phi_{k_2}) = 0. \quad (2.3.4)$$

We refer to the  $\phi_k$  as *positive-norm modes* and to the  $\phi_k^*$  as *negative-norm modes*. In the free-fall frame, positive-norm modes are those that:

- if  $k > 0$ , are right-moving (i.e.,  $u$ -modes);
- if  $k < 0$ , are left-moving (i.e.,  $v$ -modes).

For negative-norm modes, this correspondence is reversed.

We may now write  $\phi$  in terms of the modes defined in Eq. (2.3.3). As before, we note that  $\phi$  represents a real-valued quantity, so that the coefficients of complex conjugate modes must themselves be complex conjugates; we have

$$\phi(x, t) = \int_{-\infty}^{+\infty} \{A(k) \phi_k(x, t) + A^*(k) \phi_k^*(x, t)\} dk, \quad (2.3.5)$$

with canonical momentum given by

$$\pi(x, t) = -i \int_{-\infty}^{+\infty} |F(k)| \{A(k) \phi_k(x, t) - A^*(k) \phi_k^*(x, t)\} dk. \quad (2.3.6)$$

The orthonormality of the modes, characterised by Eq. (2.3.4), allows us to express the coefficients very simply:

$$A(k) = (\phi_k, \phi), \quad A^*(k) = -(\phi_k^*, \phi). \quad (2.3.7)$$

The mode decomposition of the field in Eq. (2.3.5) is readily quantized as before (see §1.4). We promote the real-valued quantities  $\phi$  and  $\pi$  to Hermitian operators  $\hat{\phi}$  and  $\hat{\pi}$ ; the coefficient of the positive-norm modes,  $A(k)$ , to an annihilation operator,  $\hat{a}_k$ ; and the

## 2. The Acoustic Model

coefficient of the negative-norm modes,  $A^*(k)$ , to a creation operator,  $\hat{a}_k^\dagger$ , the Hermitian conjugate of  $\hat{a}_k$ :

$$\hat{\phi}(x, t) = \int_{-\infty}^{+\infty} \left\{ \hat{a}_k \phi_k(x, t) + \hat{a}_k^\dagger \phi_k^*(x, t) \right\} dk, \quad (2.3.8)$$

$$\hat{\pi}(x, t) = -i \int_{-\infty}^{+\infty} |F(k)| \left\{ \hat{a}_k \phi_k(x, t) - \hat{a}_k^\dagger \phi_k^*(x, t) \right\} dk. \quad (2.3.9)$$

Imposing the equal time commutation relation

$$\left[ \hat{\phi}(t, x), \hat{\pi}(t, x') \right] = i \delta(x - x'), \quad (2.3.10)$$

the annihilation and creation operators are found to satisfy the Bose commutation relations,

$$\left[ \hat{a}_{k_1}, \hat{a}_{k_2}^\dagger \right] = \delta(k_1 - k_2), \quad \left[ \hat{a}_{k_1}, \hat{a}_{k_2} \right] = \left[ \hat{a}_{k_1}^\dagger, \hat{a}_{k_2}^\dagger \right] = 0. \quad (2.3.11)$$

## 2.4. Transforming to the $\omega$ -representation

Eq. (2.3.8) describes the field operator  $\hat{\phi}$  as an integral over modes characterised by the wavenumber  $k$ . However, since in the general case of an inhomogeneous velocity profile it is the frequency  $\omega$  which is conserved rather than  $k$ , we would like to change this to an integral over  $\omega$ , so that each mode is separately conserved. In the dispersionless case,  $\omega$  and  $k$  are directly proportional, and the transformation is straightforward. In the presence of dispersion, however, the transformation depends on the dispersion profile, and one must be careful to include all possible solutions corresponding to each value of  $\omega$ .

For the sake of example, let us suppose that the dispersion is subluminal. We need only deal with the integral over the positive-norm modes, i.e., those modes with  $\omega = Vk + |F(k)|$ , keeping in mind that this does not necessarily mean that  $\omega$  is positive (although the free-fall frequency  $\omega_{\text{ff}}$  certainly is). The cases of supersonic and subsonic flow are qualitatively different, so let us examine them separately. (Note that, although the following analysis has been kept fairly general, it may require some modification given specific examples.)

### 2.4.1. Supersonic flow

It is easily seen that, if  $V < -c$  and the dispersion is subluminal, then each value of  $\omega$  corresponds to a single positive-norm mode. (See Figure 2.3.) If  $\omega$  is positive, the positive-norm mode has a negative value of  $k$ , and is therefore left-moving in the free-fall frame; these are the  $v$ -modes. On the other hand, a negative  $\omega$  has a positive-norm mode with a positive value of  $k$ , which is right-moving in the free-fall frame; these are

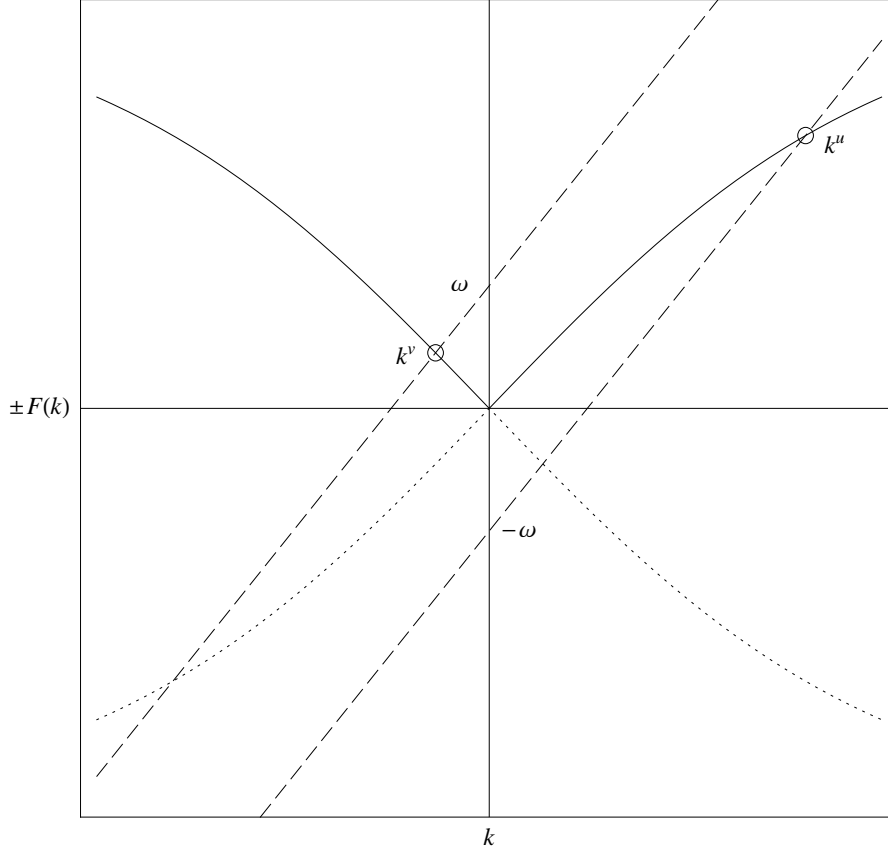


Figure 2.3.: SOLUTIONS FOR SUPERSONIC FLOW AND SUBLUMINAL DISPERSION: Each value of  $\omega$  corresponds to a single positive-norm mode. If  $\omega > 0$ , this is a  $v$ -mode; if  $\omega < 0$ , it is a  $u$ -mode. Each value of  $\omega$  also corresponds to a single negative-norm mode, which is the complex conjugate of the positive-norm mode corresponding to  $-\omega$ .

## 2. The Acoustic Model

the  $u$ -modes. Denoting the corresponding  $k$ -values by  $k^v$  and  $k^u$ , we have

$$\int_{-\infty}^0 \left\{ \hat{a}_k \phi_k(x, t) + \hat{a}_k^\dagger \phi_k^*(x, t) \right\} dk = \int_0^\infty \left\{ \hat{a}_{k^v(\omega)} \phi_{k^v(\omega)}(x, t) + \hat{a}_{k^v(\omega)}^\dagger \phi_{k^v(\omega)}^*(x, t) \right\} \left| \frac{dk^v}{d\omega} \right| d\omega, \quad (2.4.1)$$

$$\int_0^{+\infty} \left\{ \hat{a}_k \phi_k(x, t) + \hat{a}_k^\dagger \phi_k^*(x, t) \right\} dk = \int_{-\infty}^0 \left\{ \hat{a}_{k^u(\omega)} \phi_{k^u(\omega)}(x, t) + \hat{a}_{k^u(\omega)}^\dagger \phi_{k^u(\omega)}^*(x, t) \right\} \left| \frac{dk^u}{d\omega} \right| d\omega. \quad (2.4.2)$$

We want to have integrals similar to those on the left-hand side, parameterised by  $\omega$  rather than  $k$ , without the extra factor in the integrand:

$$\int_{-\infty}^0 \left\{ \hat{a}_k \phi_k(x, t) + \hat{a}_k^\dagger \phi_k^*(x, t) \right\} dk = \int_0^\infty \left\{ \hat{a}_\omega^v \phi_\omega^v(x, t) + \hat{a}_\omega^{v\dagger} \phi_\omega^{v*}(x, t) \right\} d\omega, \quad (2.4.3)$$

$$\int_0^{+\infty} \left\{ \hat{a}_k \phi_k(x, t) + \hat{a}_k^\dagger \phi_k^*(x, t) \right\} dk = \int_{-\infty}^0 \left\{ \hat{a}_\omega^u \phi_\omega^u(x, t) + \hat{a}_\omega^{u\dagger} \phi_\omega^{u*}(x, t) \right\} d\omega. \quad (2.4.4)$$

We would also like the modes and operators which appear in the integrand of the right-hand side to obey the usual normalisation and commutation relations:

$$(\phi_{\omega_1}^u, \phi_{\omega_2}^u) = \delta(\omega_1 - \omega_2) = \left| \frac{dk^u}{d\omega} \right| \delta(k_1^u - k_2^u), \quad (2.4.5)$$

$$[\hat{a}_{\omega_1}^u, \hat{a}_{\omega_2}^{u\dagger}] = \delta(\omega_1 - \omega_2) = \left| \frac{dk^u}{d\omega} \right| \delta(k_1^u - k_2^u), \quad (2.4.6)$$

with analogous relations for the  $v$ -branch. The conditions in Eqs. (2.4.3)-(2.4.6) are all satisfied if the modes and operators in the  $\omega$ -representation are defined as follows:

$$\phi_\omega^u = \sqrt{\left| \frac{dk^u}{d\omega} \right|} \phi_{k^u}, \quad \phi_\omega^v = \sqrt{\left| \frac{dk^v}{d\omega} \right|} \phi_{k^v}, \quad (2.4.7)$$

$$\hat{a}_\omega^u = \sqrt{\left| \frac{dk^u}{d\omega} \right|} \hat{a}_{k^u}, \quad \hat{a}_\omega^v = \sqrt{\left| \frac{dk^v}{d\omega} \right|} \hat{a}_{k^v}. \quad (2.4.8)$$

Then, writing explicitly the exponential time dependence of the modes, the operator  $\hat{\phi}$  is given by

$$\begin{aligned} \hat{\phi}(x, t) = & \int_0^\infty \left\{ \hat{a}_\omega^v \phi_\omega^v(x) e^{-i\omega t} + \hat{a}_\omega^{v\dagger} \phi_\omega^{v*}(x) e^{i\omega t} \right\} d\omega \\ & + \int_{-\infty}^0 \left\{ \hat{a}_\omega^u \phi_\omega^u(x) e^{-i\omega t} + \hat{a}_\omega^{u\dagger} \phi_\omega^{u*}(x) e^{i\omega t} \right\} d\omega, \end{aligned} \quad (2.4.9)$$

where, substituting Eq. (2.3.3) in Eq. (2.4.7) and recognising  $d\omega/dk$  as the group velocity  $v_g(k)$ , we have defined

$$\phi_\omega^u(x) = \frac{1}{\sqrt{4\pi |F(k^u(\omega))| |v_g(k^u(\omega))|}} \exp(ik^u(\omega)x), \quad (2.4.10)$$

with an analogous identity for the  $v$ -branch.

Although Eq. (2.4.9) is correct, it is not yet in its most useful form. Since  $\omega$  is a conserved quantity, any modes with the same value of  $\omega$  can be scattered into each other by an inhomogenous flow. What we have tried to do by writing  $\hat{\phi}$  as an integral over  $\omega$  rather than  $k$  is split the modes into groups according to their frequency. Eq. (2.4.9) does not quite achieve this, because while we have separated the modes into the complex conjugate pairs of positive and negative norm, we have also included negative values of  $\omega$  in the range of integration. Each value of  $\omega$ , then, actually applies to *two* different terms of the integrand; this can be seen in Figure 2.3, where each value of  $\omega$  clearly corresponds to one positive-norm *and* one negative-norm mode. These terms should be grouped together, because mixing between them is possible. To do this, we note simply that the integration over  $\omega$  should be over positive values only if the complex conjugate modes are included explicitly in the integrand. Therefore, we need to rewrite the second integral as follows:

$$\int_{-\infty}^0 \left\{ \hat{a}_{\omega}^u \phi_{\omega}^u(x) e^{-i\omega t} + \hat{a}_{\omega}^{u\dagger} \phi_{\omega}^{u*}(x) e^{i\omega t} \right\} d\omega = \int_0^{\infty} \left\{ \hat{a}_{-\omega}^u \phi_{-\omega}^u(x) e^{i\omega t} + \hat{a}_{-\omega}^{u\dagger} \phi_{-\omega}^{u*}(x) e^{-i\omega t} \right\} d\omega,$$

so that Eq. (2.4.9) can be rewritten as

$$\begin{aligned} \hat{\phi}(x, t) &= \int_0^{\infty} \left\{ \left[ \hat{a}_{\omega}^v \phi_{\omega}^v(x) + \hat{a}_{-\omega}^{u\dagger} \phi_{-\omega}^{u*}(x) \right] e^{-i\omega t} + \left[ \hat{a}_{\omega}^{v\dagger} \phi_{\omega}^{v*}(x) + \hat{a}_{-\omega}^u \phi_{-\omega}^u(x) \right] e^{i\omega t} \right\} d\omega \\ &= \int_0^{\infty} \left\{ \hat{\phi}_{\omega}(x) e^{-i\omega t} + \hat{\phi}_{\omega}^{\dagger}(x) e^{i\omega t} \right\} d\omega, \end{aligned} \quad (2.4.11)$$

where we have defined

$$\hat{\phi}_{\omega}(x) = \hat{a}_{\omega}^v \phi_{\omega}^v(x) + \hat{a}_{-\omega}^{u\dagger} \phi_{-\omega}^{u*}(x). \quad (2.4.12)$$

Eq. (2.4.12) shows that mixing between positive- and negative-norm modes corresponds to mixing of annihilation and creation operators. However, it must again be emphasised that, given the present physical situation of a background flow which is both temporally and spatially constant, such mixing cannot occur because  $\omega$  and  $k$  are independently conserved. The grouping of  $\phi_{-\omega}^{u*}(x)$  with  $\phi_{\omega}^v(x)$  in Eq. (2.4.12) is, at present, merely a mathematical convenience with no physical significance.

### 2.4.2. Subsonic flow

If  $-c < V < 0$  so that the slope of the line  $\omega - Vk$  is less than  $c$ , then, as was remarked previously, there are some frequencies with more than two possible values of  $k$ . The analysis performed for supersonic flow is also applicable here. The transformation of the  $v$ -branch carries over exactly, and the only change that occurs for the  $u$ -branch is that it begins at some  $k_0 > 0$  such that  $Vk_0 + |F(k_0)| = 0$ , so that the lower limit of the left-hand integral in Eqs. (2.4.2) and (2.4.4) is  $k_0$  rather than zero. Of course, this means that the operator  $\hat{\phi}$  in Eq. (2.4.9) is not equal to the operator  $\hat{\phi}$  in Eq. (2.3.8), since we have not yet included those values of  $k$  in the interval from zero to  $k_0$ . This region also splits into two branches, separated by a value  $k_m$  for which the line  $\omega - Vk$  is tangent

## 2. The Acoustic Model

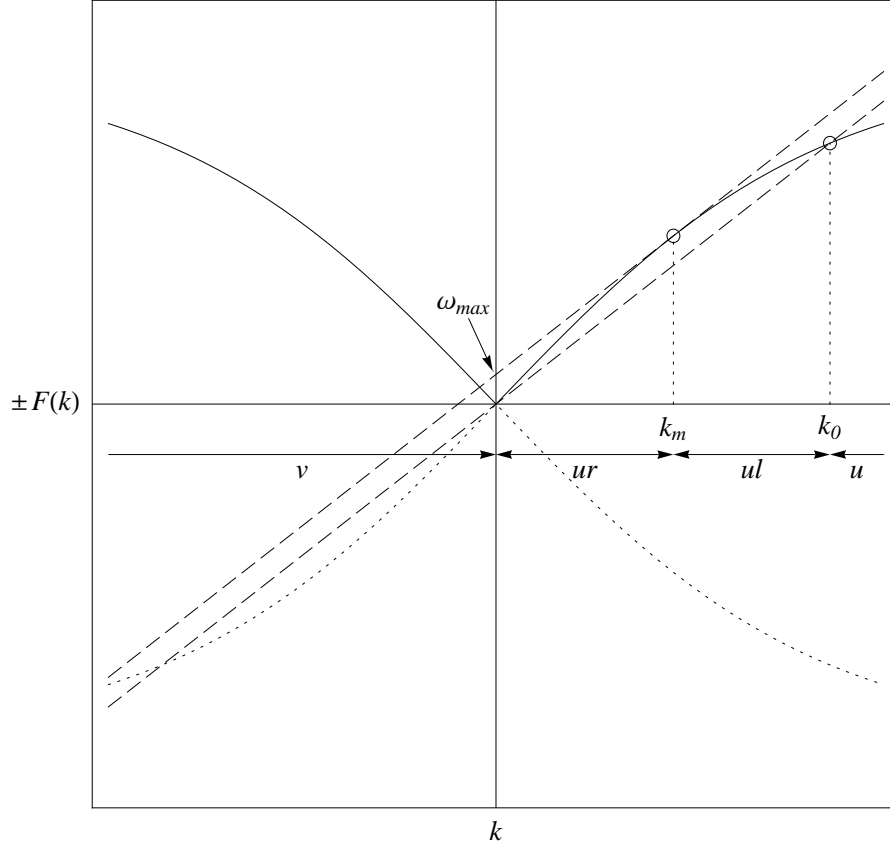


Figure 2.4.: SOLUTIONS FOR SUBSONIC FLOW AND SUBLUMINAL DISPERSION: For  $0 < \omega < \omega_{max}$ , each frequency corresponds to three positive-norm modes - a  $v$ -mode, a  $ur$ -mode and a  $ul$ -mode - and one negative-norm  $u$ -mode. For  $\omega > \omega_{max}$ , the situation is the same as for supersonic flow in Fig. 2.3, with one positive-norm  $v$ -mode and one negative-norm  $u$ -mode.

## 2.4. Transforming to the $\omega$ -representation

to  $F(k)$ . The frequency of this mode is the maximum frequency with more than two solutions, and we denote it by  $\omega_{max} = V k_m + |F(k_m)|$ . This wavevector therefore has zero group velocity, since  $d\omega/dk = 0$  there. Let us call the region from zero to  $k_m$  the *ur*-branch, and that from  $k_m$  to  $k_0$  the *ul*-branch; these are illustrated in Figure 2.4. These labels are chosen to indicate that, while all these modes are right-moving in the free-fall frame and therefore on the *u*-branch, those in the interval  $(0, k_m)$  are right-moving in the observer's frame while those in the interval  $(k_m, k_0)$  are left-moving in the observer's frame. The remainder of the analysis proceeds exactly as before, and relations analogous to those in Eqs. (2.4.7) and (2.4.8), with an additional two relations for the *ur*- and *ul*-branches, are found to implement the transformation to the  $\omega$ -representation. The contribution to the field from the *ur*- and *ul*-branches is

$$\begin{aligned} & \int_0^{k_0} \left\{ \hat{a}_k \phi_k(x, t) + \hat{a}_k^\dagger \phi_k^*(x, t) \right\} dk \\ &= \int_0^{\omega_{max}} \left\{ \left( \hat{a}_\omega^{ur} \phi_\omega^{ur} + \hat{a}_\omega^{ul} \phi_\omega^{ul} \right) e^{-i\omega t} + \left( \hat{a}_\omega^{ur\dagger} \phi_\omega^{ur*} + \hat{a}_\omega^{ul\dagger} \phi_\omega^{ul*} \right) e^{i\omega t} \right\} d\omega. \end{aligned} \quad (2.4.13)$$

The complete operator  $\hat{\phi}$  of Eq. (2.3.8) becomes

$$\hat{\phi}(x, t) = \int_0^\infty \left\{ \hat{\phi}_\omega(x) e^{-i\omega t} + \hat{\phi}_\omega^\dagger(x) e^{i\omega t} \right\} d\omega \quad (2.4.14)$$

where

$$\hat{\phi}_\omega(x) = \begin{cases} \hat{a}_\omega^v \phi_\omega^v(x) + \hat{a}_\omega^{ur} \phi_\omega^{ur}(x) + \hat{a}_\omega^{ul} \phi_\omega^{ul}(x) + \hat{a}_{-\omega}^{u\dagger} \phi_{-\omega}^{u*}(x) & \text{for } 0 < \omega < \omega_{max} \\ \hat{a}_\omega^v \phi_\omega^v(x) + \hat{a}_{-\omega}^{u\dagger} \phi_{-\omega}^{u*}(x) & \text{for } \omega > \omega_{max} \end{cases}. \quad (2.4.15)$$

### 2.4.3. Inhomogeneous flow

Let us now allow  $V$  to be spatially dependent, although we shall always assume that  $V$  approaches constant limiting values as  $x \rightarrow \pm\infty$ . The Lagrangian of Eq. (2.1.2) is no longer invariant under spatial translations, and  $k$  is no longer conserved. However, since  $V$  is time-independent, the Lagrangian is still invariant under time translations, and frequency remains a conserved quantity. In Figure 2.5, we represent pictorially the  $x$ -dependence of  $k$  simply by varying the slope of the line  $\omega - V k$  in Figs. 2.3 and 2.4, while its  $y$ -intercept, being equal to  $\omega$ , is kept fixed.

Firstly, let us remark that, in the context of an inhomogeneous flow, the existence of the *ur*- and *ul*-branches in subsonic regions, coupled with their absence in supersonic regions, is of very special importance. If the flow varies from subsonic to supersonic, these wavevectors experience a horizon: we see from Figure 2.5 that, as the flow speed increases, the two solutions vary continuously towards each other, until they merge into a single value; as the flow speed increases further, there are no real wavevectors corresponding to these branches. Instead, the wavevector becomes complex, in such a way that the solution is exponentially decreasing in the supersonic region. The point at which the

## 2. The Acoustic Model

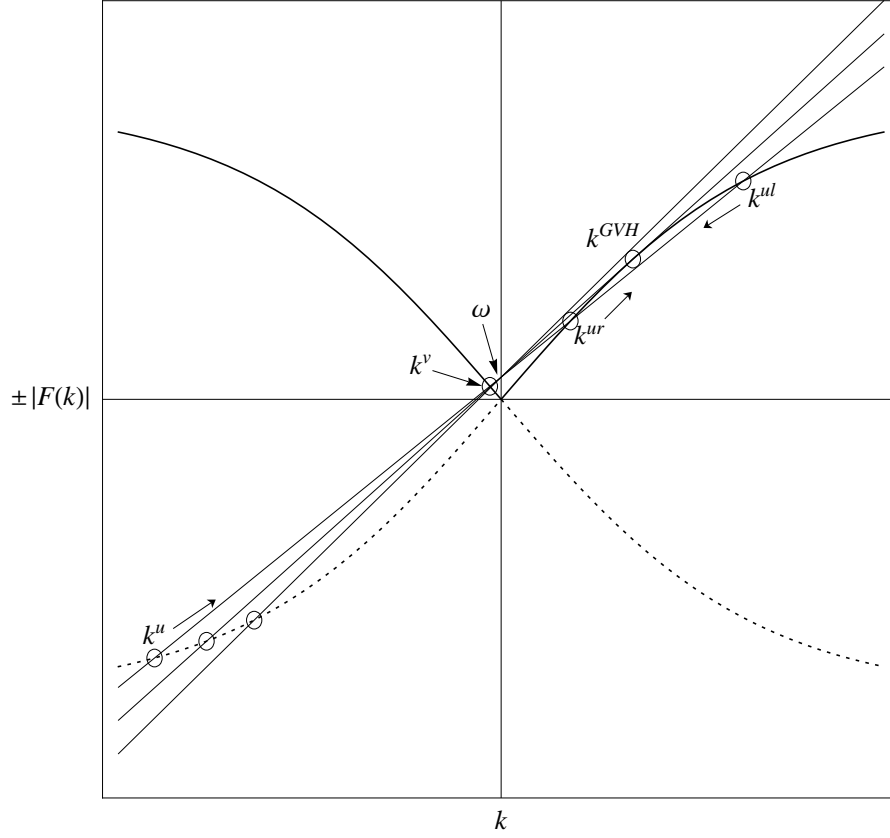


Figure 2.5.: VARIATION OF SOLUTIONS WITH FLOW VELOCITY: When  $V$  varies in space but not in time,  $\omega$  is conserved but  $k$  is not. The variation in  $k$  is seen by changing the slope of the line  $\omega - Vk$  while  $\omega$  is fixed. Thus, as  $V$  becomes more negative,  $k^u$  becomes less negative while  $k^v$  remains almost fixed.  $k^{ur}$  and  $k^{ul}$ , however, undergo a more significant change. These vary smoothly towards each other, eventually merging at some value of  $V$ , where a group-velocity horizon is established. As  $V$  changes further, there are no real solutions corresponding to the  $ur$ - and  $ul$ -branches, and they have become complex.



wavevectors merge is a *group-velocity horizon*: the line  $\omega - V k$  is tangent to  $F(k)$  there, so that the group velocity  $d\omega/dk$  vanishes. Since the *ur*- and *ul*-branches have oppositely-directed group velocities, reflection of a wavepacket from a group-velocity horizon is possible if its wavevector varies smoothly from one branch to the other. Numerical simulations of wavepacket propagation - discussed in §3.1 - show that this is indeed what happens. In particular, there is no shifting to arbitrarily short wavelengths as the horizon is approached, as in the dispersionless case (compare the out-modes of Fig. 1.2(b) with those of Fig. 2.6(b)). Dispersion regularizes the wave behaviour at the horizon such that wavevectors remain always finite; that is, there is no trans-Planckian problem.

Since  $k$  is no longer a conserved quantity, the  $\omega$ -representation of  $\hat{\phi}$  developed above is now the only natural description of the field. However, in this representation, we still have to assign a different mode to each value of  $k$ , indicated by which branch (*u*, *v*, *ur* or *ul*) it lies on. There arises an ambiguity: if  $k$  is not conserved, what do these separate modes mean? If a wavepacket centred at  $k^u(\omega)$  is scattered by the inhomogeneous flow into other wavepackets with wavenumbers  $k^v(\omega)$ ,  $k^{ul}(\omega)$  and  $k^{ur}(\omega)$ , on what basis can we still designate this the  $\phi_\omega^u$  mode? There are two natural ways of assigning labels to the various modes:

- Modes may be determined by a single *incoming* wavenumber, which is then scattered into several *outgoing* wavenumbers; these are known as *in-modes*;
- Modes may be determined by a single *outgoing* wavenumber, which results from the scattering of several *ingoing* wavenumbers; these are known as *out-modes*.

This is the same way in which we categorized the modes in the dispersionless case (see §1.6).

Although the modes have a purely exponential time dependence,  $e^{-i\omega t}$ , and therefore represent stationary solutions, their designation as in- or out-modes is made more intuitive if we consider them as wavepackets strongly peaked at the corresponding values of  $\omega$  and  $k$ . In that case, we can visualise the time evolution of the modes by the scattering of wavepackets, and the in- and out-modes are determined by whether we have a single incoming wavepacket at early times or a single outgoing wavepacket at late times. (See Figure 2.6 for an illustration.) *Wavepackets* offer an intuitive way of determining whether a particular *wavenumber* is incoming or outgoing, for this is clearly determined by the direction of the group velocity  $d\omega/dk$ , rather than the phase velocity  $\omega/k$ . (For an illustration of how the group velocity is determined, see Figure 3.3.)

The wavepacket picture also provides a simple way of seeing that the set of in-modes and the set of out-modes form complete orthonormal sets of solutions to the wave equation. Consider, for example, a pair of in-modes with different values of the initial incoming wavenumber. At early times, each of these lives entirely in one of the asymptotic constant velocity regions, and can be considered as wavepackets strongly peaked around their respective values of  $k$ . Their scalar product, as given in Eq. (2.2.5), will nearly vanish, and can be made arbitrarily close to zero by lengthening the wavepackets or, equivalently, narrowing their Fourier transforms; this is illustrated in Figure 2.7. Since the scalar product is conserved, this will also be true at late times, when the modes have scattered

## 2. The Acoustic Model

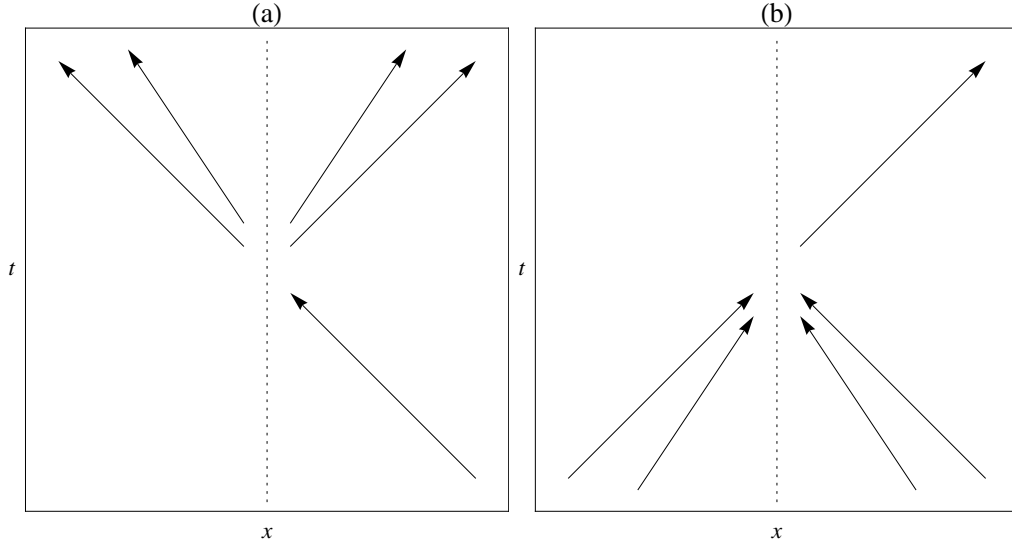


Figure 2.6.: SPACE-TIME DIAGRAM OF IN- AND OUT-MODES: Figure (a) represents an in-mode, containing a single ingoing wavepacket or wavenumber. Figure (b) is an out-mode, containing a single outgoing wavepacket or wavenumber. The correspondence between wavepackets and wavenumbers shows that the description of a wavenumber as ingoing or outgoing depends on the direction of the group velocity.

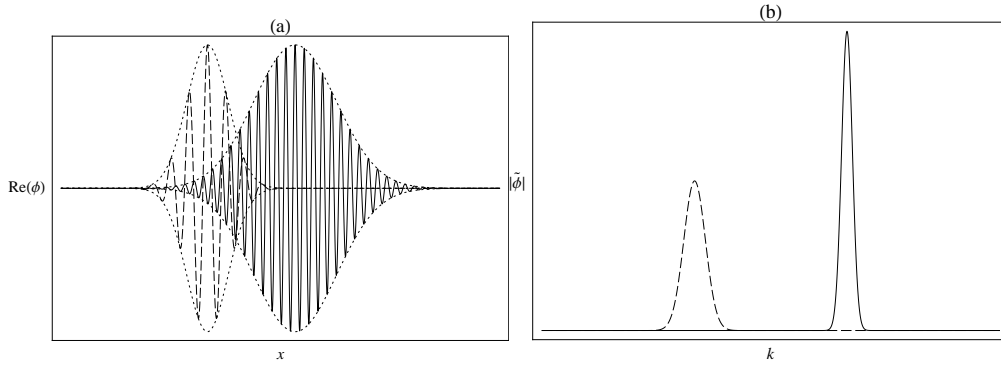


Figure 2.7.: ORTHOGONALITY OF IN- OR OUT-MODES: Although two early- or late-time wavepackets may have a significant overlap in real space (Fig. (a)), they are well separated in Fourier space (Fig. (b)), and their scalar product is vanishingly small. In the limit of a stationary solution, the Fourier transforms approach zero thickness and the scalar product vanishes completely.

into several outgoing wavepackets. In the limit of infinitely long initial wavepackets, corresponding to the stationary modes, the scalar product vanishes. Thus, the in-modes are orthogonal to each other. Moreover, they must be complete, for they span all possible values of  $k$ , which form a complete set. Therefore, Eqs. (2.4.14) and (2.4.15) are valid when the modes are interpreted as in-modes. Exactly the same argument applies to the out-modes, the only difference being that the scalar product between different modes is considered at late times, where it is found to vanish in the same manner as the in-modes. So, we may equally well interpret the modes as out-modes, which also form a complete orthonormal set.

Henceforward, we shall assume that the asymptotic constant velocity regions comprise one subsonic and one supersonic region. (This need not be true, of course. In §7.3, we perform a similar analysis for light in an optical fibre, analogous to the present case but with both asymptotic velocities subsonic.) The existence of a group-velocity horizon for *ur*- and *ul*-modes, discussed above, causes a slight change in the mode decomposition: since the solution must be exponentially decreasing in the supersonic region, only one linear combination of the *ur*- and *ul*-modes is allowed, and they degenerate into a single mode. This is the mathematical expression of the fact that one of these modes is ingoing while the other is outgoing, and there is no sense in which these roles can be swapped. The resulting mode shall be labelled the *url*-mode. For  $0 < \omega < \omega_{\max}$ , Eq. (2.4.15) becomes

$$\begin{aligned}\hat{\phi}_\omega(x) &= \hat{a}_\omega^{v,\text{in}} \phi_\omega^{v,\text{in}}(x) + \hat{a}_\omega^{url,\text{in}} \phi_\omega^{url,\text{in}}(x) + \left(\hat{a}_{-\omega}^{u,\text{in}}\right)^\dagger \left[\phi_{-\omega}^{u,\text{in}}(x)\right]^\star \\ &= \hat{a}_\omega^{v,\text{out}} \phi_\omega^{v,\text{out}}(x) + \hat{a}_\omega^{url,\text{out}} \phi_\omega^{url,\text{out}}(x) + \left(\hat{a}_{-\omega}^{u,\text{out}}\right)^\dagger \left[\phi_{-\omega}^{u,\text{out}}(x)\right]^\star.\end{aligned}\quad (2.4.16)$$

In the case, considered previously, of a velocity profile which is constant in  $x$ , it still makes sense to define in- and out-modes by considering the evolution of wavepackets. However, this case is special in that the in-mode and out-mode corresponding to a certain wavenumber are identical: an incoming wavepacket is not scattered, and emerges as a single outgoing wavepacket with the same value of  $k$ . So the modes and operators in each line of Eq. (2.4.16) are identical, and the superscripts *in* and *out* superfluous. Inhomogeneity of  $V$  breaks this degeneracy.

Completeness of each set of modes ensures that we can express one set as a linear transformation of the other. That is, we can write

$$\begin{aligned}\phi_\omega^{v,\text{in}}(x) &= C_\omega^{v,v} \phi_\omega^{v,\text{out}}(x) + C_\omega^{v,url} \phi_\omega^{url,\text{out}}(x) + C_\omega^{v,u} \left[\phi_{-\omega}^{u,\text{out}}(x)\right]^\star, \\ \phi_\omega^{url,\text{in}}(x) &= C_\omega^{url,v} \phi_\omega^{v,\text{out}}(x) + C_\omega^{url,url} \phi_\omega^{url,\text{out}}(x) + C_\omega^{url,u} \left[\phi_{-\omega}^{u,\text{out}}(x)\right]^\star, \\ \left[\phi_{-\omega}^{u,\text{in}}(x)\right]^\star &= C_\omega^{u,v} \phi_\omega^{v,\text{out}}(x) + C_\omega^{u,url} \phi_\omega^{url,\text{out}}(x) + C_\omega^{u,u} \left[\phi_{-\omega}^{u,\text{out}}(x)\right]^\star.\end{aligned}\quad (2.4.17)$$

The normalization of the modes, as expressed in Eq. (2.4.5), allows the Bogoliubov coefficients to be written as scalar products between in-modes and out-modes, e.g.  $C_\omega^{v,v} \delta(\omega_1 - \omega_2) = \left(\phi_{\omega_1}^{v,\text{out}}, \phi_{\omega_2}^{v,\text{in}}\right)$  or  $C_\omega^{v,u} \delta(\omega_1 - \omega_2) = -\left(\left(\phi_{-\omega_1}^{u,\text{out}}\right)^\star, \phi_{\omega_2}^{v,\text{in}}\right)$ . Using the

## 2. The Acoustic Model

identity in Eq. (2.3.2), we can then express the out-modes in terms of in-modes, using the same coefficients of Eqs. (2.4.17). The result is:

$$\begin{aligned}\phi_{\omega}^{v,\text{out}}(x) &= (C_{\omega}^{v,v})^{\star} \phi_{\omega}^{v,\text{in}}(x) + (C_{\omega}^{url,v})^{\star} \phi_{\omega}^{url,\text{in}}(x) - (C_{\omega}^{u,v})^{\star} [\phi_{-\omega}^{u,\text{in}}(x)]^{\star}, \\ \phi_{\omega}^{url,\text{out}}(x) &= (C_{\omega}^{v,url})^{\star} \phi_{\omega}^{v,\text{in}}(x) + (C_{\omega}^{url,url})^{\star} \phi_{\omega}^{url,\text{in}}(x) - (C_{\omega}^{u,url})^{\star} [\phi_{-\omega}^{u,\text{in}}(x)]^{\star}, \\ [\phi_{-\omega}^{u,\text{out}}(x)]^{\star} &= -(C_{\omega}^{v,u})^{\star} \phi_{\omega}^{v,\text{in}}(x) - (C_{\omega}^{url,u})^{\star} \phi_{\omega}^{url,\text{in}}(x) + (C_{\omega}^{u,u})^{\star} [\phi_{-\omega}^{u,\text{in}}(x)]^{\star}\end{aligned}\quad (2.4.18)$$

Substitution of Eqs. (2.4.17) in Eq. (2.4.16) yields the transformation for the operators:

$$\begin{aligned}\hat{a}_{\omega}^{v,\text{out}} &= C_{\omega}^{v,v} \hat{a}_{\omega}^{v,\text{in}} + C_{\omega}^{url,v} \hat{a}_{\omega}^{url,\text{in}} + C_{\omega}^{u,v} (\hat{a}_{-\omega}^{u,\text{in}})^{\dagger}, \\ \hat{a}_{\omega}^{url,\text{out}} &= C_{\omega}^{v,url} \hat{a}_{\omega}^{v,\text{in}} + C_{\omega}^{url,url} \hat{a}_{\omega}^{url,\text{in}} + C_{\omega}^{u,url} (\hat{a}_{-\omega}^{u,\text{in}})^{\dagger}, \\ (\hat{a}_{-\omega}^{u,\text{out}})^{\dagger} &= C_{\omega}^{v,u} \hat{a}_{\omega}^{v,\text{in}} + C_{\omega}^{url,u} \hat{a}_{\omega}^{url,\text{in}} + C_{\omega}^{u,u} (\hat{a}_{-\omega}^{u,\text{in}})^{\dagger}.\end{aligned}\quad (2.4.19)$$

Performing the same substitution with Eqs. (2.4.18) yields the inverse transformation:

$$\begin{aligned}\hat{a}_{\omega}^{v,\text{in}} &= (C_{\omega}^{v,v})^{\star} \hat{a}_{\omega}^{v,\text{out}} + (C_{\omega}^{v,url})^{\star} \hat{a}_{\omega}^{url,\text{out}} - (C_{\omega}^{u,v})^{\star} (\hat{a}_{-\omega}^{u,\text{out}})^{\dagger}, \\ \hat{a}_{\omega}^{url,\text{in}} &= (C_{\omega}^{url,v})^{\star} \hat{a}_{\omega}^{v,\text{out}} + (C_{\omega}^{url,url})^{\star} \hat{a}_{\omega}^{url,\text{out}} - (C_{\omega}^{url,u})^{\star} (\hat{a}_{-\omega}^{u,\text{out}})^{\dagger}, \\ (\hat{a}_{-\omega}^{u,\text{in}})^{\dagger} &= -(C_{\omega}^{u,v})^{\star} \hat{a}_{\omega}^{v,\text{out}} - (C_{\omega}^{u,url})^{\star} \hat{a}_{\omega}^{url,\text{out}} + (C_{\omega}^{u,u})^{\star} (\hat{a}_{-\omega}^{u,\text{out}})^{\dagger}.\end{aligned}\quad (2.4.20)$$

The mixing of creation and annihilation operators is here made explicit: a single annihilation or creation operator corresponding to an outgoing particle can be equivalent to a sum of both annihilation and creation operators for several incoming particles (and vice versa). We have seen this before, in the dispersionless case (see §1.6); and, as there, it leads to inequivalence of the in- and out-vacua.

## 2.5. Spontaneous creation of phonons

Making the reasonable assumption that the field is in the in-vacuum,  $|0_{\text{in}}\rangle$  - that is, that there are no incoming particles, and the quantum state is annihilated by all in-mode annihilation operators:

$$\hat{a}_{\omega}^{v,\text{in}} |0_{\text{in}}\rangle = \hat{a}_{\omega}^{url,\text{in}} |0_{\text{in}}\rangle = \hat{a}_{-\omega}^{u,\text{in}} |0_{\text{in}}\rangle = 0 \quad \forall \omega \quad (2.5.1)$$

## 2.5. Spontaneous creation of phonons

- we find that the number expectation value of outgoing particles is non-zero. For example, in the outgoing  $v$ -mode, the number expectation value is

$$\begin{aligned}
\langle 0_{\text{in}} | (\hat{a}_{\omega_1}^{v,\text{out}})^\dagger \hat{a}_{\omega_2}^{v,\text{out}} | 0_{\text{in}} \rangle &= \langle 0_{\text{in}} | \left\{ (C_{\omega_1}^{v,v})^* (\hat{a}_{\omega_1}^{v,\text{in}})^\dagger + (C_{\omega_1}^{url,v})^* (\hat{a}_{\omega_1}^{url,\text{in}})^\dagger + (C_{\omega_1}^{u,v})^* \hat{a}_{-\omega_1}^{u,\text{in}} \right\} \\
&\quad \times \left\{ C_{\omega_2}^{v,v} \hat{a}_{\omega_2}^{v,\text{in}} + C_{\omega_2}^{url,v} \hat{a}_{\omega_2}^{url,\text{in}} + C_{\omega_2}^{u,v} (\hat{a}_{-\omega_2}^{u,\text{in}})^\dagger \right\} | 0_{\text{in}} \rangle \\
&= \langle 0_{\text{in}} | \left\{ (C_{\omega_1}^{u,v})^* \hat{a}_{-\omega_1}^{u,\text{in}} \right\} \left\{ C_{\omega_2}^{u,v} (\hat{a}_{-\omega_2}^{u,\text{in}})^\dagger \right\} | 0_{\text{in}} \rangle \\
&= (C_{\omega_1}^{u,v})^* C_{\omega_2}^{u,v} \langle 0_{\text{in}} | \left\{ (\hat{a}_{-\omega_1}^{u,\text{in}})^\dagger \hat{a}_{-\omega_2}^{u,\text{in}} + \delta(\omega_1 - \omega_2) \right\} | 0_{\text{in}} \rangle \\
&= |C_{\omega_1}^{u,v}|^2 \delta(\omega_1 - \omega_2) , \tag{2.5.2}
\end{aligned}$$

where we used the commutator in Eq. (2.4.6) and the normalization of the state  $|0_{\text{in}}\rangle$ . Similar calculations give the number expectation values for the other outgoing modes:

$$\langle 0_{\text{in}} | (\hat{a}_{\omega_1}^{url,\text{out}})^\dagger \hat{a}_{\omega_2}^{url,\text{out}} | 0_{\text{in}} \rangle = |C_{\omega_1}^{u,url}|^2 \delta(\omega_1 - \omega_2) , \tag{2.5.3}$$

$$\langle 0_{\text{in}} | (\hat{a}_{-\omega_1}^{u,\text{out}})^\dagger \hat{a}_{-\omega_2}^{u,\text{out}} | 0_{\text{in}} \rangle = \left( |C_{\omega_1}^{v,u}|^2 + |C_{\omega_1}^{url,u}|^2 \right) \delta(\omega_1 - \omega_2) . \tag{2.5.4}$$

Before moving on, let us determine how these values are to be interpreted; for this we follow an argument made in §IV B of Ref. [39]. The appearance of the  $\delta$  functions shows that the results of Eqs. (2.5.2)-(2.5.4) are densities rather than numbers. This is because the orthonormal modes form a continuous spectrum, and are not normalized to unity but to a delta function, as in Eq. (2.4.5). We can overcome this problem by again turning to wavepackets. If  $V$  is constant - as in the asymptotic regions where phonons are detected - then the wavepackets

$$p_{jn} = \mathcal{N} \int_{j\epsilon}^{(j+1)\epsilon} dk e^{-i\omega(k)t + ikx + i2\pi nk/\epsilon} \tag{2.5.5}$$

form a complete orthonormal set. This splits the entire space of modes into wavepackets of reasonably well-defined wavevector (labelled by  $j$ ) and position (labelled by  $n$ ). The wavepacket  $p_{jn}$  is localised at the point where the derivative of the phase in the integrand vanishes, i.e., at the point

$$-v_g(k) t + x + \frac{2\pi n}{\epsilon} = 0 , \tag{2.5.6}$$

and, at a fixed position  $x$ , the time between one wavepacket and the next - or equivalently, the temporal width of a single wavepacket - is  $\Delta t = 2\pi / (v_g(k) \epsilon)$ . The frequency width of a single wavepacket is related to its wavevector width - and from the limits of the integral in Eq. (2.5.5) we see that  $\Delta k = \epsilon$  - by the formula  $\Delta\omega = (d\omega/dk) \Delta k = v_g(k) \epsilon$ . Thus,

$$\Delta t \Delta\omega = 2\pi . \tag{2.5.7}$$

## 2. The Acoustic Model

The number expectation value  $N(\omega)$  of a single wavepacket at frequency  $\omega$  contains no  $\delta$  function, and does indeed describe the particle content of the wavepacket. In a time  $\delta t \ll \Delta t$ , then, the rate of particles of frequency  $\omega$  is approximately

$$\frac{\delta N(\omega)}{\delta t} \approx \frac{N(\omega)}{\Delta t} = \frac{\Delta \omega}{2\pi} N(\omega) . \quad (2.5.8)$$

In the limit  $\epsilon \rightarrow 0$ , the first equality of Eq. (2.5.8) becomes exact, and since  $\Delta \omega$  becomes infinitesimal, we find

$$\frac{d^2 N}{dt d\omega} = \frac{1}{2\pi} N(\omega) . \quad (2.5.9)$$

The wavepackets themselves become plane waves in this limit, and  $N(\omega)$  is simply the factor multiplying the  $\delta$  functions in Eqs. (2.5.2)-(2.5.4). So, upon division by  $2\pi$ , these expressions give the *spectral flux density* of phonons: the number of phonons emitted per unit frequency interval per unit time.

Particle creation arises from pairings of oppositely-signed modes - in this case, the  $v$ -mode with the  $u$ -mode and the  $url$ -mode with the  $u$ -mode. Indeed, as was earlier remarked, conservation of the norm in the form of Eq. (2.2.6) suggests that particles are created in precisely such pairs, and never singly. We can show this to be true from the expectation values above: calculating the norms of the modes  $[\phi_{-\omega}^{u,\text{in}}]^*$  and  $[\phi_{-\omega}^{u,\text{out}}]^*$  in Eqs. (2.4.17) and (2.4.18), we find

$$|C_{\omega}^{u,v}|^2 + |C_{\omega}^{u,url}|^2 - |C_{\omega}^{u,u}|^2 = |C_{\omega}^{v,u}|^2 + |C_{\omega}^{url,u}|^2 - |C_{\omega}^{u,u}|^2 = -1 ,$$

and, therefore,

$$|C_{\omega}^{u,v}|^2 + |C_{\omega}^{u,url}|^2 = |C_{\omega}^{v,u}|^2 + |C_{\omega}^{url,u}|^2 = |C_{\omega}^{u,u}|^2 - 1 . \quad (2.5.10)$$

Comparing with Eqs. (2.5.2)-(2.5.4), we see that the expectation value for the  $u$ -out mode is equal to the sum of the expectation values for the  $v$ -out and  $url$ -out modes, consistent with their being produced in pairs of oppositely-signed norm.

That spontaneous creation occurs in such pairs can be shown explicitly by writing the in-vacuum  $|0_{\text{in}}\rangle$  in terms of out-modes, similar to Eq. (1.7.6). We define the outgoing Fock state  $|n\rangle_{\omega}^{v,\text{out}}$  as that state with  $n_{\omega}^v$  quanta in the state  $\phi_{\omega}^{v,\text{out}}$ , and similarly for other modes. The out-mode creation and annihilation operators act on these states according to the standard relations

$$\hat{a}_{\omega}^{v,\text{out}} |n\rangle_{\omega}^v = \sqrt{n} |n-1\rangle_{\omega}^{v,\text{out}} , \quad (2.5.11)$$

$$(\hat{a}_{\omega}^{v,\text{out}})^{\dagger} |n\rangle_{\omega}^v = \sqrt{n+1} |n+1\rangle_{\omega}^{v,\text{out}} , \quad (2.5.12)$$

with analogous relations for the other modes. Then

$$|0_{\text{in}}\rangle = \prod_{\omega} \frac{1}{|C_{\omega}^{u,u}|} \sum_{m=0}^{\infty} \sum_{n=0}^{\infty} \left( \frac{C_{\omega}^{u,v}}{C_{\omega}^{u,u}} \right)^m \left( \frac{C_{\omega}^{u,url}}{C_{\omega}^{u,u}} \right)^n \sqrt{\frac{(m+n)!}{m!n!}} |m\rangle_{\omega}^{v,\text{out}} |n\rangle_{\omega}^{url,\text{out}} |m+n\rangle_{\omega}^{u,\text{out}} , \quad (2.5.13)$$

for this is the quantum state which is annihilated by all the in-mode annihilation operators of Eqs. (2.4.20). Note that the only states appearing in the expansion are those with pairs of oppositely-signed norm -  $v$  with  $u$ , or  $url$  with  $u$ . Phonons must be created only in such pairs.

Eq. (2.5.13) is a generalization to a dispersive fluid of the dispersionless in-vacuum of Eq. (1.7.6). One noticeable difference is that it is now possible for  $u$ - and  $v$ -modes to couple to each other, but in practice this is unimportant since the strength of this coupling is typically very small. In what follows, we shall normally neglect the Bogoliubov coefficients  $C_{\omega}^{u,v}$  and  $C_{\omega}^{v,u}$ , so that Eq. (2.5.10) becomes

$$\left|C_{\omega}^{u,url}\right|^2 \approx \left|C_{\omega}^{url,u}\right|^2 \approx |C_{\omega}^{u,u}|^2 - 1, \quad (2.5.14)$$

and the creation rates of the  $u$ - and  $url$ -modes are approximately equal. Eq. (2.5.13) becomes

$$|0_{\text{in}}\rangle = \prod_{\omega} \frac{1}{|C_{\omega}^{u,u}|} \sum_{n=0}^{\infty} \left( \frac{C_{\omega}^{u,url}}{C_{\omega}^{u,u}} \right)^n |n\rangle_{\omega}^{url,\text{out}} |n\rangle_{\omega}^{u,\text{out}}. \quad (2.5.15)$$

There are two remaining differences with Eq. (1.7.6). One is that, while the two out-modes of the dispersionless case are definitely localized on opposite sides of the horizon, this is not necessarily true in the dispersive case. The main part of the  $url$ -mode is certainly localized in this way, but the  $u$ -mode is not, for, as seen in Fig. 2.5, it behaves perfectly regularly and experiences no group-velocity horizon. Thus it can happen that, for a black hole horizon, the two modes are emitted on opposite sides of the horizon, whilst for a white hole, they are emitted on the *same* side. The final difference is that, in the dispersionless case, the coefficients in the expansion (2.5.15) are generally unknown, depending on the dispersion profile and the flow velocity profile. However, their occurrence as Bogoliubov coefficients in Eqs. (2.4.18) provides a way of calculating them numerically; the methods for this are described in Chapter 3, with some results given in Chapter 4.

## 2.6. Conclusion and discussion

This chapter has shown how an acoustic field in a dispersive fluid can be quantized via the usual methods of quantum field theory. The process is very similar to that for a dispersionless fluid: a complete set of orthonormal modes is found, into which the field is decomposed; and the amplitudes of these modes are promoted to creation and annihilation operators. If the fluid flow is not constant in space, there are two natural sets of modes: those of a single ingoing wavevector, and those of a single outgoing wavevector. Either of these sets can be used to define a vacuum state, whose expectation value for any of the corresponding “particles” is zero. Under certain conditions - the mixing of modes with norms of opposite sign - these two vacua are not equal: the in-vacuum contains outgoing particles, and vice versa.

Dispersion *does* alter the picture, however. The correspondence between in- and out-modes is now one of scattering, and the Bogoliubov coefficients are simply the elements

## 2. The Acoustic Model

of a scattering matrix, as seen in Eqs. (2.4.17) or Eqs. (2.4.18). In this sense, the origin of mixing of positive- and negative-norm modes is simpler to understand than in the dispersionless case. There is no need to rely on there having been a formation, sometime in the past, of an event horizon; whereas, in the dispersionless case, the assumption of a past with no horizon allows us to determine how the in-modes should be defined. This poses a problem for an eternal horizon; but in the presence of dispersion, there is no such problem. This is closely related to the trans-Planckian problem, which is also swept away by dispersion. Tracing any outgoing wavepacket back into the past, we no longer find it having arisen from arbitrarily short wavelengths; rather, it scatters into several well-defined - and certainly finite - ingoing wavevectors.

Of course, there are drawbacks. Although the Bogoliubov coefficients have an intuitive interpretation as scattering amplitudes, they are not so easy to calculate, and in general must be found numerically. In Chapter 3 we shall attempt an analytic treatment by linearizing the velocity profile; but, as remarked in §1.8, since the wavepackets cannot now be traced back in time arbitrarily close to the horizon, this linearized profile can only give an approximate amplitude at best.

But perhaps the most surprising consequence of dispersion is that there is no need to talk of an event horizon in the derivation of spontaneous creation. Beginning with Eq. (2.4.16), we did assume the existence of one; but this only has the effect of reducing the dimensionality of the modes because of the degeneracy of the *ur*- and *ul*-modes, as discussed previously. We could have assumed that both asymptotic regions are subsonic, so that Eq. (2.4.15) continues to be valid, and it would have made no significant difference to the conclusions. Only the scattering between positive- and negative-norm modes is required for spontaneous creation to be possible. It may be that the existence of an event horizon has a significant effect on the calculated rate; we have yet to examine this. But even the smallest of velocity changes, which comes nowhere near to establishing an event horizon, can, in principle, induce particle creation.



### 3. Methods of Acoustic Model

Having derived the existence of Hawking radiation and a formula for the radiation rate, we come now to the problem of how to calculate this rate. Comparing Eqs. (2.4.18) with Eqs. (2.5.2)-(2.5.4), we see that finding the rate is equivalent to finding the coefficients of scattering into negative-norm modes. Neglecting the coupling into  $v$ -modes so that Eqs. (2.5.14) and (2.5.15) are valid, and assuming that  $V$  varies between a subsonic and a supersonic region so that the merging of the  $ul$ - and  $ur$ -modes into a single  $url$ -mode occurs, the only coefficient of interest is that for scattering between the  $u$ - and  $url$ -modes:  $|C_{\omega}^{u,url}|^2 \approx |C_{\omega}^{url,u}|^2 \equiv |\beta_{\omega}|^2$ . (We also use the standard notation for the elastic scattering,  $|C_{\omega}^{u,u}|^2 \equiv |\alpha_{\omega}|^2 = 1 - |\beta_{\omega}|^2$ .) We may examine one of several different modes to find this coefficient.

In this chapter, we shall examine two numerical methods for finding  $|\beta_{\omega}|^2$ : in §3.1, an FDTD (Finite Difference Time Domain) algorithm, which solves for wavepacket propagation; and in §3.2, an ordinary differential equation solver, for calculating steady-state solutions. Steady-state solutions can be found algebraically for velocity profiles constant everywhere except for step discontinuities, and this is also examined. Finally, in §3.3, we examine the linearized velocity profile, in imitation of §1.5 for the dispersionless case, to try to find an approximate analytic expression for  $|\beta_{\omega}|^2$ .

#### 3.1. Wavepacket propagation

Here, we present an FDTD algorithm (due to Unruh [18]) that solves directly for the propagation of a wavepacket. This is not so useful for calculating  $|\beta_{\omega}|^2$ : since a wavepacket is a linear superposition of solutions, the negative-norm contribution is likewise such a superposition and will not be exactly equal to  $|\beta_{\omega}|^2$ . Furthermore,  $|\beta_{\omega}|^2$  is a spectral density, required to be integrated over a broad frequency range, and the FDTD algorithm is too time-consuming to be practical for repetition over a range of frequencies. However, it is useful in visualising the solutions as scattering processes, as illustrated in Figure 2.6; it shows clearly that the  $ur$ - and  $ul$ -branches are shifted into each other by a group-velocity horizon, and that the wavepacket does not simply come to a standstill.

We begin by expressing the second-order wave equation (2.1.4) as two coupled first-order equations. This can be done using the canonical momentum,  $\pi$ , as defined in Eq. (1.2.7). We have:

$$\partial_t \phi + V(x) \partial_x \phi = \pi, \quad (3.1.1)$$

$$\partial_t \pi + \partial_x (V(x) \pi) = -F^2 (-i \partial_x) \phi. \quad (3.1.2)$$

### 3. Methods of Acoustic Model

Recall (see Eq. (2.1.6)) that the action of the operator  $F^2(-i\partial_x)$  on  $\phi$  can be expressed more explicitly using the Fourier transform  $\tilde{\phi}$ :

$$F^2(-i\partial_x)\phi = \frac{1}{2\pi} \int_{-\infty}^{+\infty} F^2(k) e^{ikx} \tilde{\phi}(k) dk. \quad (3.1.3)$$

The action of  $F^2(-i\partial_x)$  may be calculated by repeated application of a Fast Fourier Transform algorithm. (See, for example, Ref. [58] for a description.)

We now imagine a spatial grid, with separation  $\Delta_x$  between neighbouring points, on which we specify the values of  $V$  and keep track of the values of  $\phi$  and  $\pi$ . Since  $x$  is now replaced by a discrete variable, which we label  $i$ , the continuous function  $V(x)$ ,  $\phi(x)$  and  $\pi(x)$  are replaced by their discretized versions  $V_i = V(x_i)$ ,  $\phi_i = \phi(x_i)$  and  $\pi_i = \pi(x_i)$ . The  $x$ -derivative at a point is approximated by the formula

$$\partial_x \phi(x_i) = \frac{\phi_{i+1} - \phi_{i-1}}{2\Delta_x}. \quad (3.1.4)$$

A time grid is also introduced, with separation  $\Delta_t$  between neighbouring times. However, it is convenient to let the times on which we specify  $\phi$  and those on which we specify  $\pi$  to be offset by  $\Delta_t/2$ . Replacing  $t$  by the discrete variable  $m$ , the continuous functions  $\phi(t, x)$  and  $\pi(t, x)$  are replaced by their discretized versions  $\phi_{m,i} = \phi(t_m, x_i)$  and  $\pi_{m,i} = \pi(t_m + \Delta_t/2, x_i)$ . Since we have to relate values of one to derivatives of the other, we form time derivatives using the formula

$$\partial_t \phi(t_m + \Delta_t/2, x_i) = \frac{\phi_{m+1,i} - \phi_{m,i}}{\Delta_t}, \quad (3.1.5)$$

while spatial derivatives are taken to be the average of the spatial derivatives at times  $t_m$  and  $t_{m+1}$ :

$$\begin{aligned} \partial_x \phi(t_m + \Delta_t/2, x_i) &= \frac{1}{2} (\partial_x \phi(t_m, x_i) + \partial_x \phi(t_{m+1}, x_i)) \\ &= \frac{1}{2} \left( \frac{\phi_{m,i+1} - \phi_{m,i-1}}{2\Delta_x} + \frac{\phi_{m+1,i+1} - \phi_{m+1,i-1}}{2\Delta_x} \right). \end{aligned} \quad (3.1.6)$$

Applying Eqs. (3.1.5) and (3.1.6) to Eqs. (3.1.1) and (3.1.2), we find the finite-difference equations

$$\begin{aligned} \pi_{m,i} &= \frac{\phi_{m+1,i} - \phi_{m,i}}{\Delta_t} + V_i \frac{1}{2} \left( \frac{\phi_{m,i+1} - \phi_{m,i-1}}{2\Delta_x} + \frac{\phi_{m+1,i+1} - \phi_{m+1,i-1}}{2\Delta_x} \right), \\ -[F^2(-i\partial_x)\phi]_{m+1,i} &= \frac{\pi_{m+1,i} - \pi_{m,i}}{\Delta_t} \\ &\quad + \frac{1}{2} \left( \frac{V_{i+1}\pi_{m,i+1} - V_{i-1}\pi_{m,i-1}}{2\Delta_x} + \frac{V_{i+1}\pi_{m+1,i+1} - V_{i-1}\pi_{m+1,i-1}}{2\Delta_x} \right), \end{aligned}$$

### 3.1. Wavepacket propagation

which can be written in the more suggestive form

$$\phi_{m+1,i} + \frac{\Delta_t}{4\Delta_x} V_i (\phi_{m+1,i+1} - \phi_{m+1,i-1}) = \phi_{m,i} - \frac{\Delta_t}{4\Delta_x} V_i (\phi_{m,i+1} - \phi_{m,i-1}) + \Delta_t \pi_{m,i}, \quad (3.1.7)$$

$$\pi_{m+1,i} + \frac{\Delta_t}{4\Delta_x} (V_{i+1} \pi_{m+1,i+1} - V_{i-1} \pi_{m+1,i-1}) = \pi_{m,i} - \frac{\Delta_t}{4\Delta_x} (V_{i+1} \pi_{m,i+1} - V_{i-1} \pi_{m,i-1}) - \Delta_t [F^2 (-i\partial_x) \phi]_{m+1,i} \quad (3.1.8)$$

Equations (3.1.7) and (3.1.8) are almost closed, except at the boundaries, where the values of  $\phi$  or  $\pi$  at  $i = 1$  or  $n$  depends on their values at  $i = 0$  or  $n + 1$ . The latter are not included in the grid, but this problem can be overcome by imposing periodic boundary conditions; that is, we identify  $i = 0$  with  $i = n$  and  $i = n + 1$  with  $i = 1$ .

There remains the problem of specifying the initial profile for the momentum  $\pi$ , once the initial form of  $\phi$  has been specified. In principle, there are no limitations on  $\pi$ , for there are two possible dispersion branches and a general solution of the wave equation can contain an arbitrary mixture of the two. However, we wish to have a wavepacket centred at well-defined values of  $k$  and  $\omega$ ; this selects a single dispersion branch, and the momentum is uniquely specified. Given that we use wavepackets which are right-moving in the free-fall frame, and which are initially in a region of constant flow velocity, we have  $\omega = Vk + F(k)$  and the momentum is given by

$$\pi(x, t) = -\frac{i}{2\pi} \int_{-\infty}^{+\infty} F(k) \tilde{\phi}(k) e^{ikx - i(Vk + F(k))t} dk. \quad (3.1.9)$$

Thus, the momentum at time  $t = 0$  - which shall be labelled  $\pi_{1/2,i}$ , since it comes half a timestep before  $\pi_{1,i}$  - is easily calculated using the Fast Fourier Transform algorithm.  $\pi_{1,i}$  is then found by propagating forward  $\Delta_t/2$  using the modified difference equation

$$\pi_{1,i} = \pi_{1/2,i} - \frac{\Delta_t}{4\Delta_x} (V_{i+1} \pi_{1/2,i+1} - V_{i-1} \pi_{1/2,i-1}) - \frac{\Delta_t}{2} [F^2 (-i\partial_x) \phi]_{1,i}. \quad (3.1.10)$$

With these conditions, Eqs. (3.1.7) and (3.1.8) form a closed linear system for each value of  $m$ : given  $\phi_m$  and  $\pi_m$ , we can use Eq. (3.1.7) to find  $\phi_{m+1}$ , and this in turn allows us to use Eq. (3.1.8) to find  $\pi_{m+1}$ . At each stage, the right-hand side is known. The term  $[F^2 (-i\partial_x) \phi]_{m+1,i}$  is found via Eq. (3.1.3), using a Fast Fourier Transform algorithm first to find  $\tilde{\phi}$ , and then again to take the inverse Fourier transform after multiplying by  $F^2(k)$ . The knowns of the right-hand side form an  $n$ -dimensional vector; the left-hand side contains  $n$  unknowns in total. The whole linear system can be written in matrix

### 3. Methods of Acoustic Model

form as follows:

$$\begin{bmatrix}
 1 & aV_1 & & & & & & -aV_1 \\
 & \ddots & & & & & & \\
 & & \ddots & & & & & \\
 & & & -aV_{i-1} & 1 & aV_{i-1} & & \\
 & & & -aV_i & 1 & aV_i & & \\
 & & & & -aV_{i+1} & 1 & aV_{i+1} & \\
 & & & & & \ddots & & \\
 & & & & & & \ddots & \\
 & & & & & & & -aV_n & 1 \\
 aV_n & & & & & & & & -aV_n
 \end{bmatrix}
 \begin{bmatrix}
 \phi_{m+1,1} \\
 \vdots \\
 \vdots \\
 \phi_{m+1,i-1} \\
 \phi_{m+1,i} \\
 \phi_{m+1,i+1} \\
 \vdots \\
 \vdots \\
 \phi_{m+1,n}
 \end{bmatrix}
 =
 \begin{bmatrix}
 b_{m,1} \\
 \vdots \\
 \vdots \\
 b_{m,i-1} \\
 b_{m,i} \\
 b_{m,i+1} \\
 \vdots \\
 \vdots \\
 b_{m,n}
 \end{bmatrix}$$

$$\begin{bmatrix}
 1 & aV_2 & & & & & & -aV_n \\
 & \ddots & & & & & & \\
 & & \ddots & & & & & \\
 & & & -aV_{i-2} & 1 & aV_i & & \\
 & & & -aV_{i-1} & 1 & aV_{i+1} & & \\
 & & & & -aV_i & 1 & aV_{i+2} & \\
 & & & & & \ddots & & \\
 & & & & & & \ddots & \\
 & & & & & & & -aV_{n-1} & 1 \\
 aV_1 & & & & & & & & -aV_{n-1} & 1
 \end{bmatrix}
 \begin{bmatrix}
 \pi_{m+1,1} \\
 \vdots \\
 \vdots \\
 \pi_{m+1,i-1} \\
 \pi_{m+1,i} \\
 \pi_{m+1,i+1} \\
 \vdots \\
 \vdots \\
 \pi_{m+1,n}
 \end{bmatrix}
 =
 \begin{bmatrix}
 c_{m,1} \\
 \vdots \\
 \vdots \\
 c_{m,i-1} \\
 c_{m,i} \\
 c_{m,i+1} \\
 \vdots \\
 \vdots \\
 c_{m,n}
 \end{bmatrix}$$

where we have defined

$$a = \frac{\Delta_t}{4\Delta_x}, \quad (3.1.11)$$

$$b_{m,i} = \phi_{m,i} - \frac{\Delta_t}{4\Delta_x} V_i (\phi_{m,i+1} - \phi_{m,i-1}) + \Delta_t \pi_{m,i}, \quad (3.1.12)$$

$$c_{m,i} = \pi_{m,i} - \frac{\Delta_t}{4\Delta_x} (V_{i+1} \pi_{m,i+1} - V_{i-1} \pi_{m,i-1}) - \Delta_t [F^2 (-i\partial_x) \phi]_{m+1,i} \quad (3.1.13)$$

The linear systems above are known as *cyclic* equations, given their periodic nature, and are easily solved using an appropriate algorithm. (See Ref. [58], §2.4.)

Calculation of the norm of the solution before and after the propagation provides a check on the accuracy of the numerical procedure. Recall (see Eqs. (1.2.6) and (2.2.6)) that the norm is given by Eq. (2.2.1) or, in regions where  $V$  is constant, by Eq. (2.2.6). The negative-norm contribution, equivalent to the radiation rate, is

$$|\beta_\omega|^2 = \frac{1}{\pi} \int |F(k)| \left| \tilde{\phi}^{(-)}(k) \right|^2 dk, \quad (3.1.14)$$

where  $\tilde{\phi}^{(-)}(k)$  is the Fourier transform of the negative-norm branch. Therefore, if we begin with a positive-norm *url*-mode wavepacket and allow it to scatter completely into

### 3.1. Wavepacket propagation

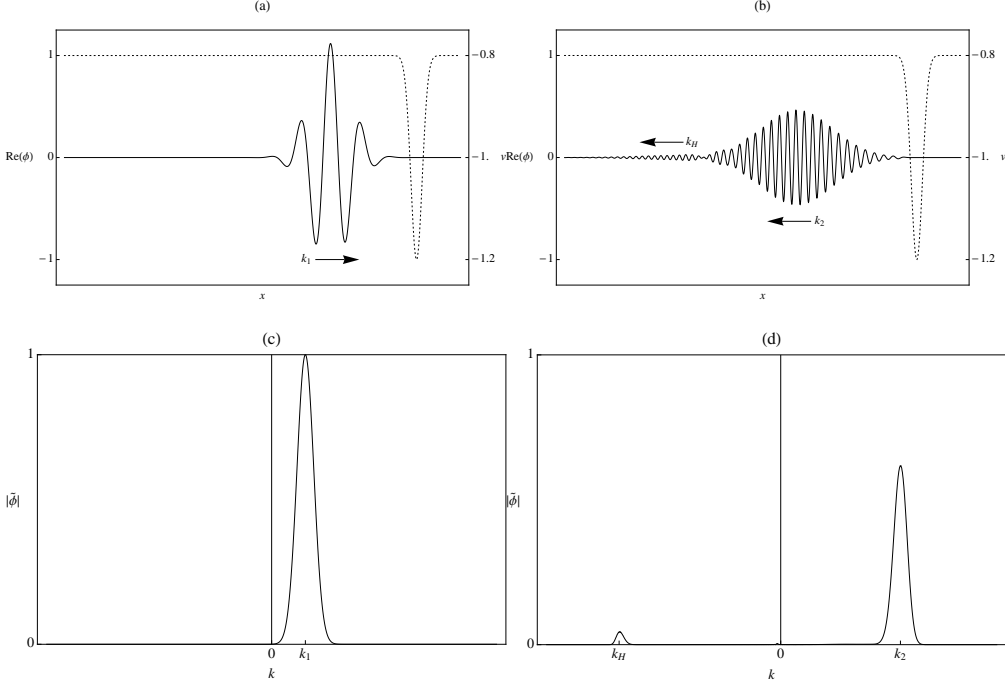


Figure 3.1.: WAVEPACKET PROPAGATION: These are results for the scattering of a *ur*-mode wavepacket incident on a white-hole horizon. Figure (a) shows the incident wavepacket and velocity profile. Figure (b) shows the resulting outgoing wavepackets: the *ur*-mode has been blueshifted into the *ul*-mode by the horizon, and a negative-norm *u*-mode wavepacket has also been produced. Figures (c) and (d) show the Fourier transforms of the waveforms in Figs. (a) and (b), respectively.

### 3. Methods of Acoustic Model

outgoing wavepackets,  $|\beta_\omega|^2$  is found by integrating Eq. (3.1.14) over the  $u$ -mode part of the resulting Fourier transform.

See Figure 3.1 for an example which shows frequency shifting between the  $ur$ - and  $ul$ -modes.

## 3.2. Steady-state solution

The creation rate  $|\beta_\omega|^2$  is exact only for a stationary solution, the wavepackets of §3.1 being superpositions of stationary solutions peaked at a certain value of  $\omega$ . Solving for the stationary solutions directly is also faster than performing the FDTD algorithm of §3.1, which makes it the more practical method for calculating a spectrum which extends over many frequencies. Here, we determine how to find the stationary solutions. We begin with a general velocity profile, which must be solved by numerical integration and linear algebra; such a method is also described and used in Refs. [39, 40, 44]. We then examine the special case of a velocity profile that is constant except for step discontinuities, which is solvable by linear algebra only; see also Refs. [40, 42].

### 3.2.1. General velocity profile

The time-independent acoustic wave equation is the ordinary differential equation satisfied by  $\phi_\omega(x)$ , where

$$\phi(x, t) = \phi_\omega(x) e^{-i\omega t}. \quad (3.2.1)$$

This is a stationary solution, whose time-dependence is purely oscillatory. Plugging it into Eq. (2.1.4), we find

$$i\omega(i\omega - V'(x))\phi_\omega - 2V(x)(i\omega - V'(x))\partial_x\phi_\omega + V^2(x)\partial_x^2\phi_\omega + F^2(-i\partial_x)\phi_\omega = 0. \quad (3.2.2)$$

If  $V$  is constant for all  $x$ , we may take the Fourier transform of this equation to obtain Eq. (2.1.7), with  $\omega$  now interpreted as a fixed parameter. The general solution is simply a linear combination of plane waves,

$$\phi_\omega(x) = \sum_j c_j \exp(ik_j x), \quad (3.2.3)$$

where the index  $j$  enumerates all possible solutions of the dispersion relation (2.1.8), and the  $c_j$  are complex constants. Note that some of the  $k_j$  might be complex (and if so, they will occur in complex conjugate pairs, since the dispersion relation is real); however, given that they will increase exponentially in one direction, these do not represent physical solutions and can be discarded. Also note that there may be infinitely many such plane waves, so that Eq. (3.2.3) is an infinite series; we shall, however, assume  $F^2(k)$  to be a finite polynomial, so that  $j$  has a maximum value.

Now let  $V$  be spatially varying, yet still asymptotically constant:  $V(x) \rightarrow V_\pm$  as  $x \rightarrow \pm\infty$ . Then, in the asymptotic regions,  $\phi_\omega$  can still be represented by the sum in Eq. (3.2.3). In general, the sums that correspond to the negative and positive asymptotic

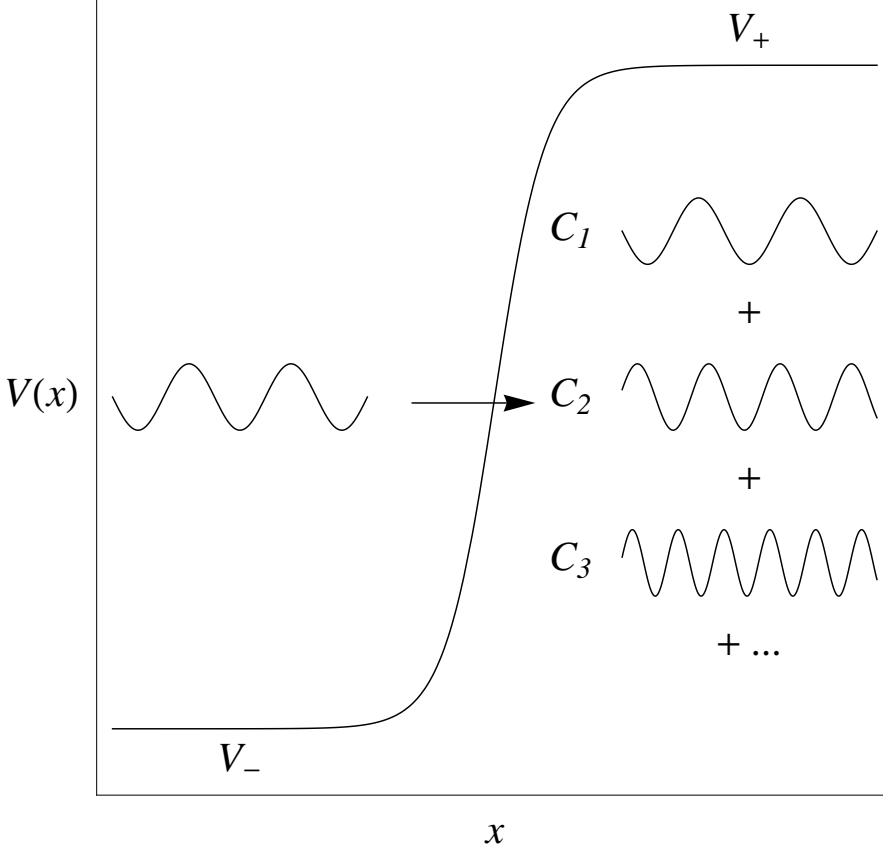


Figure 3.2.: INTEGRATION OF STATIONARY SOLUTION: In one asymptotic region, the solution is chosen to be a particular plane wave. Eq. (3.2.2) is then integrated through to the other region, where the solution is a linear combination of plane waves. This is done for all possible plane wave solutions in the initial region. The general solution is a linear combination of these, thus giving rise to the linear transformation of Eq. (3.2.4).

regions will not agree, even if  $V_+ = V_-$ . This allows the appearance of complex values of  $k$  which are exponentially decreasing towards infinity, for such a value of  $k$  need not (indeed, *will* not, for physical solutions) appear in the opposite asymptotic region.

The sums in the asymptotic regions are not arbitrary, but related to each other via Eq. (3.2.2). Suppose we specify that, in the negative asymptotic region,  $\phi_\omega(x)$  should be given by the plane wave  $\exp(ik_1^- x)$ . This is a boundary condition, and in a differential equation solver - such as the Mathematica function `NDSolve`, used for this thesis - we can set  $\phi_\omega$  and the necessary number of derivatives of  $\phi_\omega$  equal to those of  $\exp(ik_1^- x)$  in the negative asymptotic region, and solve Eq. (3.2.2) through to the positive asymptotic region; this is illustrated in Figure 3.2. Here,  $\phi_\omega$  is again expressible as a sum of exponentials:  $\phi_\omega(x) \rightarrow \sum_j C_{1j} \exp(ik_j^+ x)$ . This solution is wholly determined

### 3. Methods of Acoustic Model

by the constants  $C_{1j}$ , which form a vector:  $(C_{11}, C_{12}, \dots, C_{1n})$ . The same integration can be performed for all other  $k_i^-$  in the negative asymptotic region, whose solutions in the positive asymptotic region are wholly determined by vectors  $(C_{i1}, C_{i2}, \dots, C_{in})$ . Moreover, since Eq. (3.2.2) is linear in  $\phi_\omega$ , a linear superposition of solutions is itself a solution. Thus, if we form a solution in the negative asymptotic region of the form  $\phi_\omega \rightarrow \sum_i a_i \exp(ik_i^- x)$  - which can be represented as the vector  $(a_1, a_2, \dots, a_n)$  - the solution in the positive asymptotic region,  $\phi_\omega \rightarrow \sum_j b_j \exp(ik_j^+ x)$ , will be represented by the vector  $a_1 (C_{1j}) + a_2 (C_{2j}) + \dots + a_n (C_{nj})$ . It is clear that the vectors which specify the solutions in each of the asymptotic regions are related via a linear transformation, which can be written in matrix form:

$$\begin{pmatrix} b_1 \\ b_2 \\ \vdots \\ b_n \end{pmatrix} = \begin{pmatrix} C_{11} & C_{21} & \cdots & C_{n1} \\ C_{12} & C_{22} & \cdots & C_{n2} \\ \vdots & \vdots & \ddots & \vdots \\ C_{1n} & C_{2n} & \cdots & C_{nn} \end{pmatrix} \begin{pmatrix} a_1 \\ a_2 \\ \vdots \\ a_n \end{pmatrix}. \quad (3.2.4)$$

The importance of Eq. (3.2.4) is that it makes clear that there are only  $n$  values which need be specified to pick out a particular solution of  $\phi_\omega$ ; and, moreover, one of these is simply an overall multiplicative constant, which is unimportant. The  $n - 1$  values remaining need not refer to coefficients in a single asymptotic region. Indeed, when we solve for in- and out-modes, it will be found that some of the coefficients on either side must be set to zero, depending on whether they are ingoing or outgoing. The remaining coefficients are found by solving Eq. (3.2.4), with one of them set to an arbitrary constant which determines the overall multiplicative factor; in practice, we usually set the coefficient of the single ingoing or outgoing wave to unity.

If solving for an in- or out-mode, the  $a_i$  and  $b_j$  which should be set to zero are determined by the direction of propagation of the corresponding wavevectors. For example, if we are solving for an in-mode as in Fig. 2.6(a), then only the initial wavevector can propagate *towards* the horizon, whilst any wavevectors propagating away from the horizon are allowed; any ingoing wavevectors other than the initial one must have a coefficient of zero. Whether a wave is ingoing or outgoing depends on the sign of the group velocity,

$$v_g(k) = \frac{\partial \omega}{\partial k} = V \pm F'(k) = -(-V) \pm F'(k). \quad (3.2.5)$$

Therefore, if the slope of  $\pm F(k)$  is greater than the slope of  $\omega - Vk$ , the group velocity is positive and a wavepacket centred at the corresponding value of  $k$  travels to the right; whereas, if the slope of  $\pm F(k)$  is less than the slope of  $\omega - Vk$ , the group velocity is negative and such a wavepacket travels to the left. In Fig. 3.3,  $k^u$ ,  $k^v$  and  $k^{ul}$  have negative group velocities and travel to the left, while  $k^{ur}$  has a positive group velocity and travels to the right. Therefore, for a given value of  $V$ , we can easily determine the possible real values of  $k$  and the direction of travel of their wavepackets.

The Bogoliubov coefficients describe transformations between *normalized* solutions, which are given by Eq. (2.4.10). Having calculated the coefficient  $C_{\omega,k}$  of the plane wave



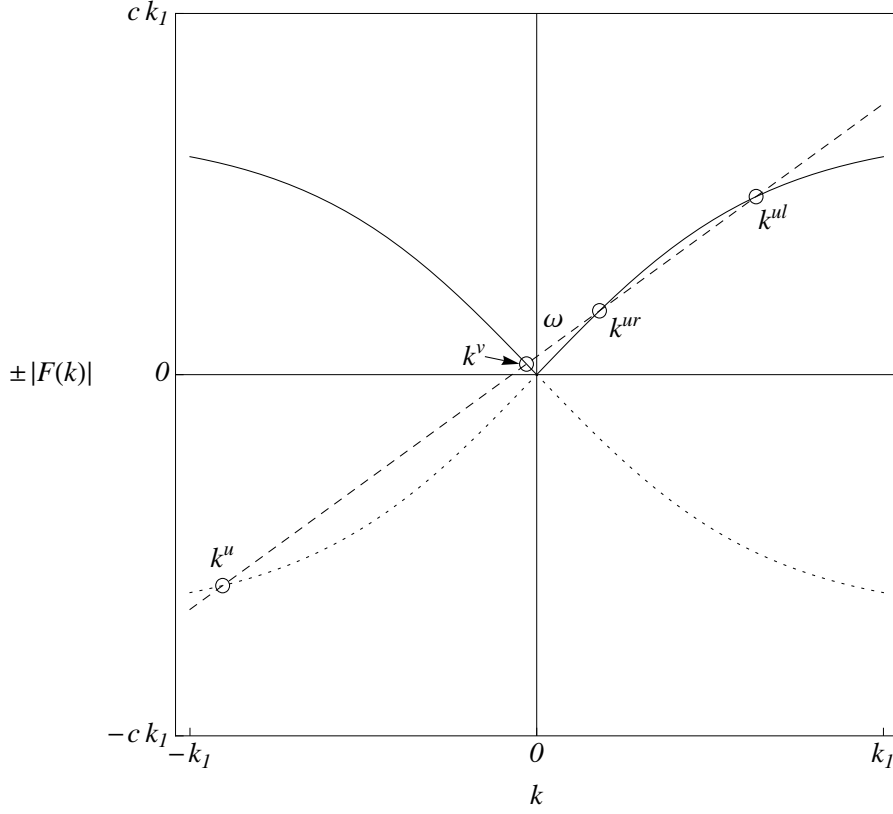


Figure 3.3.: SOLUTIONS AND THEIR GROUP VELOCITIES: The group velocity is  $v_g = -(-V) \pm F'(k)$ . Therefore, the direction of travel of a wave is determined by whether the slope of  $\pm F(k)$  is greater or less than the slope of  $\omega - Vk$ . In this figure,  $k^u$ ,  $k^v$  and  $k^{ul}$  all have a slope  $\pm F'(k)$  which is less than the slope of  $\omega - Vk$ , and are thus left-travelling wavepackets. However,  $k^{ur}$  has a slope  $F'(k)$  greater than that of  $\omega - Vk$ , and is therefore a right-travelling wavepacket.

### 3. Methods of Acoustic Model

$\exp(ikx - i\omega t)$ , the norm of this wave - relative to the norm of the incoming or outgoing wave - is given by [40]

$$\frac{(\phi_{\omega,k}, \phi_{\omega,k})}{(\phi_{\omega,k_{\text{in/out}}}, \phi_{\omega,k_{\text{in/out}}})} = \frac{\text{sgn}(\omega - Vk) |F(k)| |v_g(k)| |C_{\omega,k}|^2}{\text{sgn}(\omega - V k_{\text{in/out}}) |F(k_{\text{in/out}})| |v_g(k_{\text{in/out}})| |C_{\omega,k_{\text{in/out}}}|^2}, \quad (3.2.6)$$

This equation allows us to determine the accuracy of the solution by checking that the norm is conserved, i.e., that the sum of the norms of all incoming waves is equal to the sum of the norms of all outgoing waves. We can also find the creation rate  $|\beta_\omega|^2$ , which is simply the relative norm between wavevectors of oppositely-signed norm.

#### 3.2.2. Discontinuous velocity profile

Given the complexity of Eq. (3.2.2), purely analytic solutions are often impossible to obtain. An exception to this, however, occurs when  $V$  is constant everywhere except at discrete points, where any changes are marked by a sudden discontinuity. Such discontinuous velocity profiles form limiting cases, where the derivative of  $V$  has been allowed to increase without bound. Similar step-discontinuous profiles have been examined in References [39] and [42].

We have already observed that, in regions where the flow velocity is constant,  $\phi_\omega$  is simply a linear combination of plane waves. Suppose that  $F^2(k)$  is of order  $2n$ , giving  $2n$  solutions to the dispersion relation; then, in any such constant-velocity region, the general solution is characterised by the  $2n$  coefficients corresponding to the different possible plane waves. Suppose also that the velocity profile  $V(x)$  has  $r$  constant velocity regions (and therefore  $r - 1$  points of discontinuity). Then there are  $2nr$  coefficients in total, and all must be specified to completely characterise the solution. Of course, we still have only  $2n$  in- or out-modes, so the  $2nr$  coefficients are not all independent: they are restricted by  $2n(r - 1)$  conditions to be imposed at the points of discontinuity, or  $2n$  conditions at each such point. These conditions relate the function  $\phi_\omega$  and its first  $2n - 1$  derivatives on either side of the point of discontinuity, and are derived such that, as the velocity profile is gradually altered towards the formation of the discontinuity, Eq. (3.2.2) is always satisfied.

Firstly, note that Eq. (3.2.2) contains  $V$  and its first derivative  $V'$  only. A step discontinuity in  $V$  results in  $V'$  being infinite (i.e. proportional to the delta function) at the point of discontinuity. These must be compensated for by corresponding discontinuities and delta functions appearing in the derivatives of  $\phi$ . We can immediately conclude that, since the highest derivative of  $\phi$  appearing in Eq. (3.2.2) is of order  $2n$ ,  $\phi$  and its first  $2n - 2$  derivatives are continuous everywhere; for, if this were not the case,  $\partial_x^{2n}\phi$  would contain derivatives of the delta function, which would not be compensated for by similar infinities in another quantity. Therefore, at any point of discontinuity, the first  $2n - 1$  conditions imposed are that  $\phi, \partial_x\phi, \dots, \partial_x^{2n-2}\phi$  be continuous, their values on either side of the point being equal. This leaves one condition remaining, which relates  $\partial_x^{2n-1}\phi$  on either side of the point. There must be a discontinuity in  $\partial_x^{2n-1}\phi$  in order to generate a delta function in  $\partial_x^{2n}\phi$  to cancel that in  $V'$ ; but what is this discontinuity?

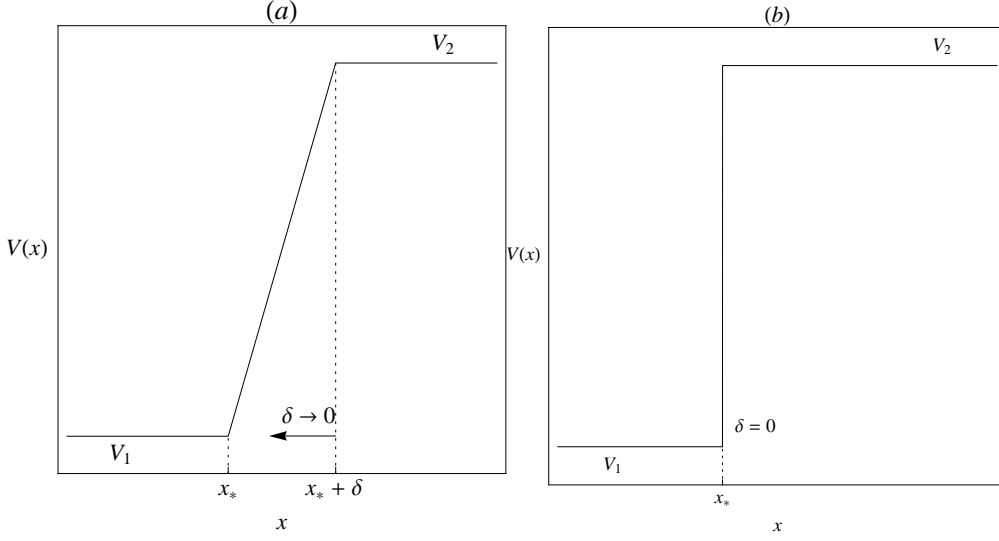


Figure 3.4.: CONSTRUCTING A DISCONTINUOUS VELOCITY PROFILE: In Figure (a),  $V$  is continuous while  $V'$  is not. As we let the length of the region of change go to zero, we obtain Figure (b), where  $V$  is discontinuous.

Let us proceed along lines suggested by Figure 3.4. We consider a velocity profile which varies between two velocities, which are constant in their respective regions. The variation between them is assumed to be linear. We therefore have a discontinuity not in  $V$ , but  $V'$ , which is zero for  $x < x_*$  and  $x > x_* + \delta$ , and equal to  $(V_2 - V_1)/\delta$  for  $x_* < x < x_* + \delta$ . Our task is to calculate the change in  $\partial_x^{2n-1}\phi$  between  $x = x_*$  and  $x = x_* + \delta$ , and then to take the limit as  $\delta \rightarrow 0$ .

With the velocity profile of Fig. 3.4(a), in order that Eq. (3.2.2) be satisfied on either side of the point  $x = x_*$  there must be a corresponding discontinuity in another quantity to cancel that from  $V'$ . For reasons similar to those given above, only the highest-order derivative of  $\phi$  that appears in Eq. (3.2.2) can be discontinuous; for, if a lower-order derivative were discontinuous, all higher-order derivatives would be infinite at  $x = x_*$ , and these infinities would not be cancelled. So, the discontinuity in  $V'$  is compensated for by a corresponding discontinuity in  $\partial_x^{2n}\phi$ . Writing  $F^2(k)$  explicitly as a finite polynomial,

$$F^2(k) = \sum_{j=1}^n f_j k^{2j}, \quad (3.2.7)$$

Eq. (3.2.2) becomes

$$-\omega^2\phi - 2i\omega V\partial_x\phi - i\omega V'\phi + 2VV'\partial_x\phi + V^2\partial_x^2\phi + \sum_{j=1}^n (-1)^j f_j \partial_x^{2j}\phi = 0. \quad (3.2.8)$$

### 3. Methods of Acoustic Model

In the limit as we approach the point of discontinuity - which we label  $x_*$  - we must have

$$\lim_{x \rightarrow x_*^-} [(-i\omega\phi + 2V\partial_x\phi)V' + (-1)^n f_n \partial_x^{2n}\phi] = \lim_{x \rightarrow x_*^+} [(-i\omega\phi + 2V\partial_x\phi)V' + (-1)^n f_n \partial_x^{2n}\phi]. \quad (3.2.9)$$

Therefore, defining  $\Delta V' = \lim_{x \rightarrow x_*^+} V' - \lim_{x \rightarrow x_*^-} V'$ , and similarly for  $\Delta(\partial_x^{2n}\phi)$ , we have

$$\begin{aligned} \Delta(\partial_x^{2n}\phi) &= \frac{(-1)^n}{f_n} (i\omega\phi - 2V\partial_x\phi) \Delta V' \\ &= \frac{(-1)^n}{f_n} (i\omega\phi - 2V_1\partial_x\phi) \frac{(V_2 - V_1)}{\delta}, \end{aligned} \quad (3.2.10)$$

where it is understood that  $\phi$  and  $\partial_x\phi$  are evaluated at  $x = x_*$  (since they are continuous, there is no ambiguity). Although this step discontinuity in  $\partial_x^{2n}\phi$  will cause  $\partial_x^{2n+1}\phi$  to become infinite (i.e. proportional to the delta function) precisely at the point of discontinuity, there may also be a discontinuity in the limiting values of  $\partial_x^{2n+1}\phi$ . This can be found exactly as above, but to find the differential equation containing  $\partial_x^{2n+1}\phi$ , we must differentiate Eq. (3.2.8). The result is

$$\begin{aligned} -\omega^2\partial_x\phi - 3i\omega V'\partial_x\phi - 2i\omega V\partial_x^2\phi - i\omega V''\phi + 2(V')^2\partial_x\phi + 2VV''\partial_x\phi + 4VV'\partial_x^2\phi + V^2\partial_x^3\phi \\ + \sum_{j=1}^n (-1)^j f_j \partial_x^{2j+1}\phi = 0. \end{aligned} \quad (3.2.11)$$

We have already argued that all derivatives up to and including  $\partial_x^{2n-1}\phi$  must be continuous at  $x_*$ ; therefore, the only possible discontinuous derivative appearing in Eq. (3.2.11) is  $\partial_x^{2n+1}\phi$ . Moreover, note that  $V''$ , though infinite precisely at  $x = x_*$  (as is  $\partial_x^{2n+1}\phi$ ), is zero on either side of this point. The discontinuity in  $V'$  must be balanced by a corresponding discontinuity (or, rather, a difference in limiting values) in  $\partial_x^{2n+1}\phi$ ; indeed, we have

$$\begin{aligned} \lim_{x \rightarrow x_*^-} [(-3i\omega\partial_x\phi + 4V\partial_x^2\phi)v' + 2(\partial_x\phi)(V')^2 + (-1)^n f_n \partial_x^{2n+1}\phi] \\ = \lim_{x \rightarrow x_*^+} [(-3i\omega\partial_x\phi + 4V\partial_x^2\phi)v' + 2(\partial_x\phi)(V')^2 + (-1)^n f_n \partial_x^{2n+1}\phi] \end{aligned} \quad (3.2.12)$$

which implies

$$\begin{aligned} \Delta(\partial_x^{2n+1}\phi) &= \frac{(-1)^n}{f_n} \left[ (3i\omega\partial_x\phi - 4V\partial_x^2\phi) \Delta V' - 2(\partial_x\phi) \Delta(V')^2 \right] \\ &= \frac{(-1)^n}{f_n} \left[ (3i\omega\partial_x\phi - 4V_1\partial_x^2\phi) \frac{(V_2 - V_1)}{\delta} - 2(\partial_x\phi) \frac{(V_2 - V_1)^2}{\delta^2} \right], \end{aligned} \quad (3.2.13)$$

where, again,  $\partial_x\phi$  and  $\partial_x^2\phi$  are understood to be evaluated at  $x = x_*$ .

Note that higher derivatives of  $\phi$  will also have discontinuities, which can be found by differentiating Eq. (3.2.11) further. In the resulting differential equations, however, this

### 3.3. Linearized velocity profile

will never yield a higher power of  $V'$  than  $(V')^2$ . Therefore, the discontinuities in higher derivatives can, at most, vary as  $1/\delta^2$ .

The change in  $\partial_x^{2n-1}\phi$  over the region of change in  $V$  can be found using a Taylor expansion:

$$\begin{aligned}\partial_x^{2n-1}\phi|_{x=x_*+\delta} - \partial_x^{2n-1}\phi|_{x=x_*} &= \partial_x^{2n}\phi|_{x \rightarrow x_*^+} \delta + \frac{1}{2} \partial_x^{2n+1}\phi|_{x \rightarrow x_*^+} \delta^2 + \frac{1}{6} \partial_x^{2n+2}\phi|_{x \rightarrow x_*^+} \delta^3 \dots \\ &= \partial_x^{2n}\phi|_{x \rightarrow x_*^-} \delta + \frac{1}{2} \partial_x^{2n+1}\phi|_{x \rightarrow x_*^-} \delta^2 + \frac{1}{6} \partial_x^{2n+2}\phi|_{x \rightarrow x_*^-} \delta^3 \\ &\quad + \Delta(\partial_x^{2n}\phi) \delta + \frac{1}{2} \Delta(\partial_x^{2n+1}\phi) \delta^2 + \frac{1}{6} \Delta(\partial_x^{2n+2}\phi) \delta^3 + \dots\end{aligned}$$

Letting  $\delta \rightarrow 0$ , we find that the first three terms of the second line vanish, since they are unaffected by the discontinuity. Moreover, since the discontinuities can have at most a  $1/\delta^2$  dependence, only the terms in  $\Delta(\partial_x^{2n}\phi)$  and  $\Delta(\partial_x^{2n+1}\phi)$  can yield terms that are independent of  $\delta$ . Consequently, we find that there is a discontinuity in  $\partial_x^{2n-1}\phi$  which is given by

$$\begin{aligned}\Delta(\partial_x^{2n-1}\phi) &= \frac{(-1)^n}{f_n} \left[ (i\omega\phi - 2V_1\partial_x\phi)(V_2 - V_1) - \partial_x\phi(V_2 - V_1)^2 \right] \\ &= \frac{(-1)^n}{f_n} [i\omega\phi - (V_1 + V_2)\partial_x\phi](V_2 - V_1) .\end{aligned}\tag{3.2.14}$$

Eq. (3.2.14) is the final condition to be imposed at each point of discontinuity. (To the author's knowledge, this general expression for the discontinuity in  $\partial_x^{2n-1}\phi$  has not been presented previously in the literature.) Having begun with  $2nr$  coefficients, we have seen that the differential equation imposes  $2n(r-1)$  linear conditions on them, which leaves only  $2n$  degrees of freedom: precisely the number required to uniquely specify a solution of the  $2n$ -order differential equation (3.2.2).

### 3.3. Linearized velocity profile

In our quest to find  $|\beta_\omega|^2$ , the amount of mode conversion into negative-frequency modes, we would like to have even an approximate analytic formula for the process. This allows us to see which parameters are important, and the derivation of such a formula can offer insight into the fundamental nature of the process.

Let us continue to deal with stationary solutions of the form (3.2.1), and which satisfy the differential equation (3.2.2). Dispersion adds higher derivatives to this equation through the operator  $F^2(-i\partial_x)$ , making it difficult to solve in position space and generally requiring numerical integration to do so, as in §3.2. However, in Fourier space, the operator simply becomes a multiplicative function  $F^2(k)$ , and does not determine the order of the differential equation. Instead, the velocity profile  $V(x)$  is replaced by the operator  $V(i\partial_k)$ , so it is  $V(x)$  which determines the order of the differential equation. Generally, the resulting equation is also very complicated; but, if we make the simplifying

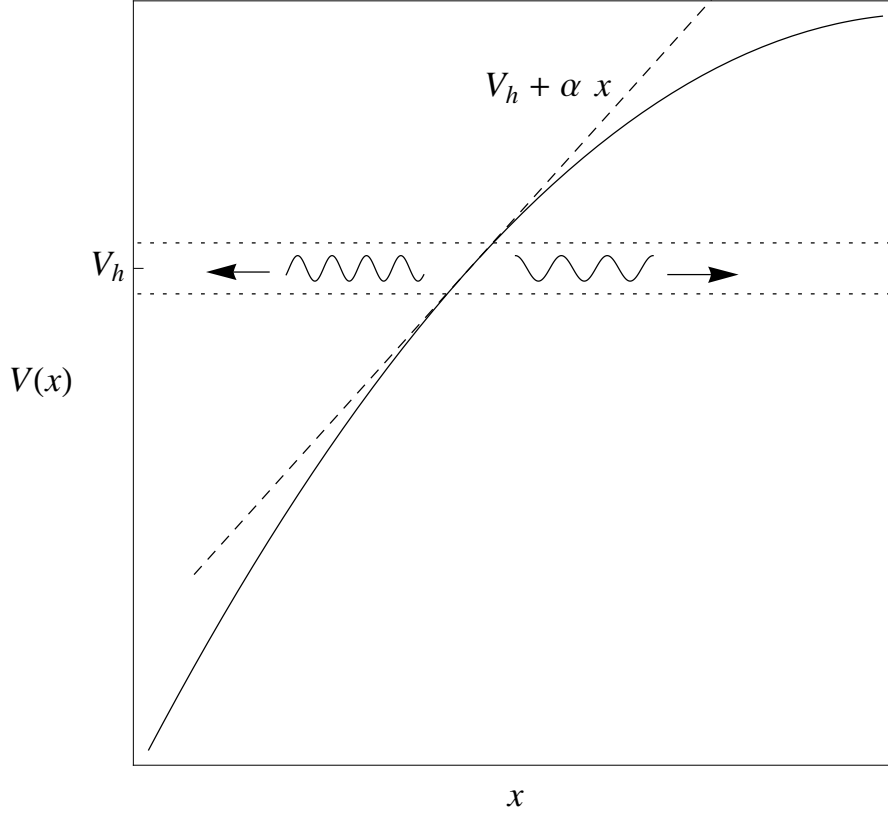


Figure 3.5.: LINEARIZING THE VELOCITY PROFILE: Assuming that mode conversion originates primarily in a small region around the horizon, where  $V = V_h$ , we may develop an approximate analytic description of the process by using a linearized form of the velocity profile,  $V_h + \alpha x$ .

assumption that the origins of mode conversion are mainly in the vicinity of the horizon, we may approximate  $V(x)$  by its linearized form

$$V(x) \approx V_h + \alpha x \quad (3.3.1)$$

(having taken the zero of  $x$  to be at the horizon, and assuming that  $V'$  is non-zero there). This is illustrated pictorially in Figure 3.5. The mathematical result is the reduction of Eq. (3.2.2) to a second-order differential equation, making it much more tractable. (Such a transformation is also performed in Refs. [41] and [48].)

### 3.3.1. Solution in Fourier space

Performing the transformation just described - that is, replacing  $V(x)$  with the approximation in Eq. (3.3.1), then transforming to the Fourier representation via the substitutions  $\phi_\omega(x) \rightarrow \tilde{\phi}_\omega(k)$ ,  $x \rightarrow i\partial_k$  and  $\partial_x \rightarrow ik$  - the differential equation (3.2.2)

becomes

$$\alpha^2 k^2 \partial_k^2 \tilde{\phi}_\omega + (2\alpha^2 k + 2i\alpha k (\omega - V_h k)) \partial_k \tilde{\phi}_\omega + \left( F^2(k) - (\omega - V_h k)^2 + i\alpha (\omega - 2V_h k) \right) \tilde{\phi}_\omega = 0. \quad (3.3.2)$$

This can be reduced to a standard form second-order differential equation by defining another field  $\tilde{\psi}_\omega$  such that

$$\begin{aligned} \tilde{\phi}_\omega &= \tilde{\psi}_\omega \exp \left( -\frac{1}{2} \int \frac{2\alpha^2 k + 2i\alpha k (\omega - V_h k)}{\alpha^2 k^2} dk \right) \\ &= \tilde{\psi}_\omega \exp \left( \left( -1 - i\frac{\omega}{\alpha} \right) \ln k + i\frac{V_h}{\alpha} k \right), \end{aligned} \quad (3.3.3)$$

for Eq. (3.3.2) then becomes the remarkably simple equation

$$\partial_k^2 \tilde{\psi}_\omega + \frac{F^2(k)}{\alpha^2 k^2} \tilde{\psi}_\omega = 0. \quad (3.3.4)$$

This is identical in form to the time-independent Schrödinger equation. By direct analogy, we can apply the WKB method [59] (see also [38, 41, 48] for applications to Hawking radiation) to find the approximate solution

$$\tilde{\psi}_\omega(k) \approx C^u \sqrt{\frac{k}{F(k)}} \exp \left( \frac{i}{\alpha} \int^k \frac{F(k')}{k'} dk' \right) + C^v \sqrt{\frac{k}{F(k)}} \exp \left( -\frac{i}{\alpha} \int^k \frac{F(k')}{k'} dk' \right), \quad (3.3.5)$$

where  $C^u$  and  $C^v$  are arbitrary constants. (The meaning of the labels shall soon become clear.) Eq. (3.3.5) is valid so long as the “de Broglie wavelength”,  $\lambda(k) = 2\pi |\alpha| k/F(k)$ , varies negligibly over a single cycle; more precisely [59],

$$\left| \frac{\lambda'(k)}{2\pi} \right| = \frac{|\alpha|}{F^2(k)} |F(k) - kF'(k)| \ll 1. \quad (3.3.6)$$

The full Fourier transform  $\tilde{\phi}_\omega(k)$  is found via substitution in Eq. (3.3.3):

$$\begin{aligned} \tilde{\phi}_\omega(k) &\approx C^u \sqrt{\frac{k}{F(k)}} \exp \left( \frac{i}{\alpha} \int^k \frac{F(k')}{k'} dk' + \left( -1 - i\frac{\omega}{\alpha} \right) \ln k + i\frac{V_h}{\alpha} k \right) \\ &\quad + C^v \sqrt{\frac{k}{F(k)}} \exp \left( -\frac{i}{\alpha} \int^k \frac{F(k')}{k'} dk' + \left( -1 - i\frac{\omega}{\alpha} \right) \ln k + i\frac{V_h}{\alpha} k \right) \\ &= \frac{C^u}{k} \sqrt{\frac{k}{F(k)}} \exp \left( -\frac{i}{\alpha} \int^k \left( \frac{\omega - F(k')}{k'} - V_h \right) dk' \right) \\ &\quad + \frac{C^v}{k} \sqrt{\frac{k}{F(k)}} \exp \left( -\frac{i}{\alpha} \int^k \left( \frac{\omega + F(k')}{k'} - V_h \right) dk' \right). \end{aligned} \quad (3.3.7)$$

### 3.3.2. Transforming back to position space

$\phi_\omega(x)$  is, of course, the inverse Fourier transform of  $\tilde{\phi}_\omega(k)$ :

$$\begin{aligned}\phi_\omega(x) &= \int_{-\infty}^{+\infty} \tilde{\phi}_\omega(k) \exp(ikx) dk \\ &\approx \int_{-\infty}^{+\infty} \frac{1}{k} \sqrt{\frac{k}{F(k)}} [C^u \exp(i\varphi^u(k)) + C^v \exp(i\varphi^v(k))] dk, \quad (3.3.8)\end{aligned}$$

where we have defined

$$\begin{aligned}\varphi^u(k) &= -\frac{1}{\alpha} \int^k \left( \frac{\omega - F(k')}{k'} - V_h - \alpha x \right) dk', \\ \varphi^v(k) &= -\frac{1}{\alpha} \int^k \left( \frac{\omega + F(k')}{k'} - V_h - \alpha x \right) dk' .\end{aligned}$$

We can find an approximate solution to Eq. (3.3.8) using the saddle-point approximation. This states that the main contribution to the integral in this equation comes from those points where the first derivatives of the phases  $\varphi^u(k)$  and  $\varphi^v(k)$  vanish. Then, to lowest order, the contribution from each of these points behaves like an overall constant multiplied by a Gaussian integral, so long as the integration contour may be taken along the direction of steepest descent. Given that the phases are integrals themselves, the saddle points are those where the integrands vanish, i.e.,

$$\begin{aligned}\frac{d\varphi^u}{dk} = 0 &\Rightarrow -\frac{1}{\alpha} \left( \frac{\omega - F(k)}{k} - V_h - \alpha x \right) = 0, \\ \frac{d\varphi^v}{dk} = 0 &\Rightarrow -\frac{1}{\alpha} \left( \frac{\omega + F(k)}{k} - V_h - \alpha x \right) = 0.\end{aligned}$$

Recall that, since we have linearized the velocity around the horizon,  $V_h + \alpha x$  is simply the flow velocity  $V(x)$ . Therefore, we can rewrite the above conditions in the form

$$\frac{d\varphi^u}{dk} = 0 \Rightarrow \omega = V(x)k + F(k), \quad (3.3.9)$$

$$\frac{d\varphi^v}{dk} = 0 \Rightarrow \omega = V(x)k - F(k). \quad (3.3.10)$$

At any position  $x$ , the saddle points of the phases in Eq. (3.3.8) are simply those values of  $k$  that solve the dispersion relation with the local value of the flow velocity. The phase  $\varphi^u(k)$  has saddle points at those solutions which are right-moving with respect to the fluid, and therefore lie on the  $u$ -branch; the saddle points of the phase  $\varphi^v(k)$  are solutions that are left-moving with respect to the fluid, and lie on the  $v$ -branch. For the sake of simplicity, we shall continue to assume that there is negligible coupling between the  $u$ - and  $v$ -branches, dealing exclusively with the  $u$ -branch; that is, we set  $C^v = 0$ .

In order to perform the integration by approximation with Gaussian integrals, we also need the second derivative of the phase at its saddle points:

$$\frac{d^2\varphi^u}{dk^2} = \frac{1}{\alpha} \frac{(\omega - F(k) + kF'(k))}{k^2} = \frac{1}{\alpha} \frac{(V(x) + F'(k))}{k}, \quad (3.3.11)$$



### 3.3. Linearized velocity profile

where, in the second equality, we have evaluated  $\omega - F(k)$  at the saddle points using Eq. (3.3.9). Therefore, in the vicinity of a solution  $k_j$  of Eq. (3.3.9), the phase  $\varphi^u(k)$  is approximately given by

$$\begin{aligned}\varphi^u(k) &\approx \varphi^u(k_j) + \frac{1}{2\alpha} \frac{(V(x) + F'(k_j))}{k_j} (k - k_j)^2 \\ &= \varphi^u(k_j) + \frac{v_g(k_j)}{2\alpha k_j} (k - k_j)^2,\end{aligned}\quad (3.3.12)$$

where from Eq. (3.3.9) we have identified  $V(x) + F'(k_j) = d\omega/dk(k_j) = v_g(k_j)$ , the local group velocity. (Note that, as a solution of Eq. (3.3.9),  $k_j$  is itself  $x$ -dependent.)

We may now perform the integral in Eq. (3.3.8). Firstly, note that the integral is properly Gaussian if  $\varphi^u(k)$  increases in the  $+i$  direction; therefore, the direction of steepest descent is proportional to  $\exp(i\frac{\pi}{4}\text{sgn}(v_g(k_j)/\alpha k_j))$ . Assuming that the integration contour may be deformed so as to pass through each saddle point in its direction of steepest descent, the position-space solution becomes

$$\phi_\omega(x) \approx C^u \sqrt{2\pi|\alpha|} \sum_j \frac{\text{sgn}(k_j)}{\sqrt{|v_g(k_j)| |F(k_j)|}} \exp\left(i\frac{\pi}{4}\text{sgn}\left[\frac{v_g(k_j)}{\alpha k_j}\right] + i\varphi^u(k_j)\right). \quad (3.3.13)$$

Notice that the factors of  $|v_g(k_j) F(k_j)|^{-1/2}$  are exactly those required to normalize the various plane waves in the  $\omega$ -representation according to Eq. (2.4.10). Therefore, the relative norms of the modes themselves are entirely determined by the phases  $\varphi^u(k_j)$ .

#### 3.3.3. Generalization to nonlinear velocity profiles

Within the limits of the saddle-point approximation, Eq. (3.3.13) is strictly valid only in the case of the linear velocity profile (3.3.1). However, this fact has been made implicit by writing the solution in its present form, and it is easy to extrapolate the solution to nonlinear velocity profiles. To see this, note that the prefactor is unimportant, and its dependence on  $\alpha$  can be removed simply by making  $C^u$  proportional to  $|\alpha|^{-1/2}$ .  $\alpha$  appears in the sign of the  $\frac{\pi}{4}$  part of the phase; however, it is only the sign of  $\alpha$  that matters here, and so long as  $V$  is monotonic in  $x$ , this sign is uniquely determined. We thus restrict our attention to monotonic velocity profiles. Now the only part of Eq. (3.3.13) still dependent on the linear form of Eq. (3.3.1) is the phase  $\varphi^u(k_j)$ :

$$\begin{aligned}\varphi^u(k_j) &= -\frac{1}{\alpha} \int^{k_j} \left( \frac{\omega - F(k')}{k'} - V_h - \alpha x \right) dk' \\ &= \int^{k_j} (x - x(k')) dk',\end{aligned}\quad (3.3.14)$$

where the function  $x(k)$  is defined according to Eq. (3.3.9) with the linearized velocity profile (3.3.1) substituted for  $V(x)$ .  $x(k)$ , then, is the position  $x$  at which the wavevector  $k$  is a solution of (the  $u$ -branch of) the dispersion relation. Although this has been derived

### 3. Methods of Acoustic Model

for the special case of a linear velocity profile, it is easily extendable to any monotonic velocity profile. When expressed in this general form, we also note that  $\alpha$ , the derivative of  $V$  at the horizon, no longer has a privileged status. We may not interpret Eq. (3.3.13) as being applicable to any monotonic velocity profile, and we may write

$$\phi_\omega(x) \approx C' \sum_j \frac{\text{sgn}(k_j)}{\sqrt{|v_g(k_j)| |F(k_j)|}} \exp \left( i \frac{\pi}{4} \text{sgn} \left[ \frac{v_g(k_j)}{V' k_j} \right] + i \int^{k_j} (x - x(k')) dk' \right). \quad (3.3.15)$$

Note that, while Eq. (3.3.15) is not an original result, its application to the entire velocity profile - not just the linearized form - is a novel approach, and leads to original results.

Not only are the velocity profiles we are interested in monotonic, but they also approach asymptotic limiting values as  $x \rightarrow \pm\infty$ . Thus, at those values of  $k$  which solve the dispersion relation in the asymptotic regions,  $x(k)$  rapidly diverges. The  $x$ -dependence of the phase is not obvious in the form of Eq. (3.3.14); however, differentiating with respect to  $x$ , and recalling that  $k_j$  is itself a function of  $x$ , we find  $d\varphi^u/dx = k_j$ , and so

$$\varphi^u(k_j) = \int^{k_j} (x - x(k')) dk' = \int^x k_j(x') dx' \quad (3.3.16)$$

up to an unimportant additive constant. (This is simply the formula for integration by parts.) The right side of Eq. (3.3.16) is the more usual form of the phase generated by the WKB approximation in position space, and it clearly shows that the individual components become plane waves in the asymptotic regions.

The first equality of Eq. (3.3.16) is the most useful for relating different *wavevectors* (as opposed to different *positions*) to each other. Their relative phase is simply the integral of  $x - x(k)$  between them; their relative norm, or squared amplitude, is determined by the imaginary part of this integral. Since  $x$  is always real, it is the imaginary part of the function  $x(k)$  which is important. Thus the norm of one wavevector  $k_1$  relative to that of another wavevector  $k_2$  is given by

$$\frac{(\phi_{\omega,k_1}, \phi_{\omega,k_1})}{(\phi_{\omega,k_2}, \phi_{\omega,k_2})} \approx \frac{\text{sgn}(\omega - V k_1)}{\text{sgn}(\omega - V k_2)} \exp(2 \text{Im}[J]), \quad J = \int_{k_2}^{k_1} x(k') dk'. \quad (3.3.17)$$

In particular, for particle creation, the relative weight between the Bogoliubov coefficients is given by

$$\left| \frac{\beta}{\alpha} \right|^2 = \exp \left( 2 \text{Im} \left[ \int_{k_\alpha}^{k_\beta} x(k') dk' \right] \right). \quad (3.3.18)$$

Eqs. (3.3.17) and (3.3.18) are new results, derived simply from the extension of the applicability of Eq. (3.3.15) to the entire velocity profile. Thus the validity of the former depends on the validity of the latter. Certainly, they cannot be applied when the WKB approximation breaks down and the condition (3.3.6) is not satisfied - that is, in the non-adiabatic limit of large  $|\alpha|$ . The question of when Eqs. (3.3.17) and (3.3.18) are applicable is rather more difficult to address, for, strictly speaking, Eq. (3.3.15) is *invalid* for any nonlinear velocity profile! Since the limits of the integrals in Eqs. (3.3.17) and (3.3.18) correspond to asymptotic regions where  $V$  approaches constant values, they

implicitly imply that  $V$  is nonlinear, and we cannot expect *a priori* that are valid in any regime. That they do possess a regime of validity will be shown in the following chapter by comparison with numerical results, but the reason for the existence of this regime remains a mystery.

It is important to note that, apart from the considerations just discussed, Eqs. (3.3.17) and (3.3.18) are valid only for a wave solution which can be expressed in terms of a single contour integral of the form in Eq. (3.3.8). In general, owing to the multivaluedness of the imaginary part of  $x(k)$ , there are several possible such integrals, with different results. This is to be expected: there are generally several solutions to the dispersion relation, each one giving rise to an independent solution of the wave equation. It is also generally true that, as described in §3.2, a particular in- or out-mode is formed via linear combination of these solutions. In this case, the relative norm of a particular wavevector will be given by some linear combination of its various norms of the form (3.3.17).

### 3.4. Summary

This chapter has demonstrated three ways of determining the amount of mode conversion induced by a given velocity profile:

- an FDTD algorithm to solve for the evolution of a wavepacket directly;
- numerical integration of an ordinary differential equation to find the steady-state solution for a given Killing frequency; this is done both generally and for the case of a profile with step discontinuities; and
- an analytic treatment involving linearizing the velocity profile around the horizon and extrapolating the result to more general profiles.



## 4. Results for Acoustic Model

In chapters 1 and 2, we demonstrated, from a purely theoretical standpoint, that mode conversion between positive- and negative-norm modes in both nondispersive and dispersive fluids leads to spontaneous creation of phonons. Chapter 3 turned to the practicalities of calculating the amount of mode conversion, and consequently the phonon creation rate. The descriptions and derivations of these chapters have been kept as general as possible, so as to be applicable to many different velocity and dispersion profiles.

In the present chapter, we turn our attention to specific examples, so as to provide a quantitative account of the Hawking phonon radiation expected in fluids. The velocity and dispersion profiles used are kept as simple as possible, and we expect many of the qualitative features of the results still to be applicable in the general case.

### 4.1. Dispersion profile

Firstly, let us define the dispersion relation to be used. Recall that the dispersionless case (see Eqs. (1.3.4) and (2.1.8)) has  $F^2(k) = c^2 k^2$ ; and that, since the fluid is isotropic in its rest frame,  $F^2(k)$  should contain only even powers of  $k$ . Since the complexities of dispersion arise through the introduction of higher-order derivatives in the wave equation, the simplest deviation from the dispersionless model is through the inclusion of a quartic term in  $F^2(k)$ :

$$F^2(k) = c^2 k^2 \left( 1 - \frac{k^2}{k_d^2} \right). \quad (4.1.1)$$

It is usually found that  $F^2(k)$  approaches a dispersionless form for low values of  $k$ , and this feature has been incorporated in Eq. (4.1.1);  $c$ , then, is the limiting wave velocity (both phase and group velocity) for small wavevectors. These are quantitatively defined as being much smaller than the parameter  $k_d$ , i.e., there is no or little dispersion for wavevectors  $k$  such that  $k^2/k_d^2 \ll 1$ . The parameter  $k_d$ , then, determines the point at which significant deviations from nondispersive behaviour first appear, and can be said to signify the strength of the dispersion: the larger is  $k_d$ , the larger is the value of  $k$  at which dispersive effects begin to take hold, and so the weaker is the dispersion. Finally, the minus attached to the deviation  $k^2/k_d^2$  corresponds to subluminal dispersion (phase velocity becoming less than  $c$ ); had this been a plus sign, it would describe superluminal dispersion (phase velocity becoming greater than  $c$ ). We have restricted ourselves to subluminal dispersion, since superluminal dispersion gives results which are qualitatively very similar, the main difference occurring in the coupling to  $v$ -modes [44] which is neglected here. Both Eq. (4.1.1) and its superluminal counterpart are plotted in Figure 4.1.

#### 4. Results for Acoustic Model

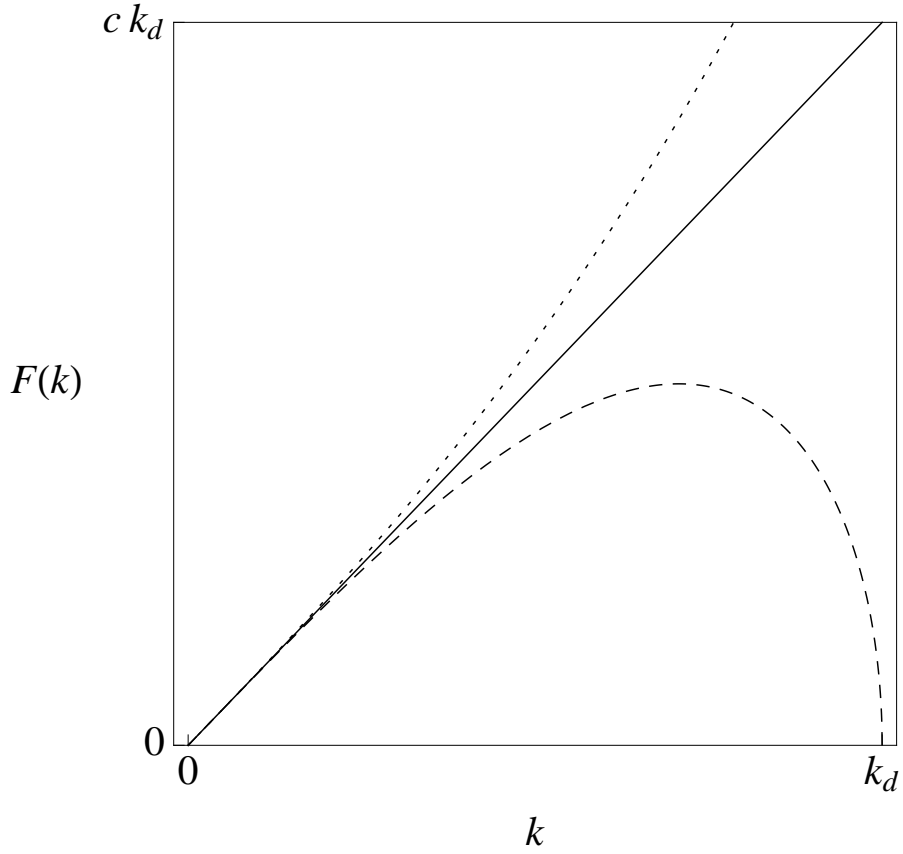


Figure 4.1.: QUARTIC DISPERSION: The dashed line plots Eq. (4.1.1), which describes subluminal dispersion; the dotted line corresponds to superluminal dispersion, where the minus sign in Eq. (4.1.1) is replaced with a plus sign.

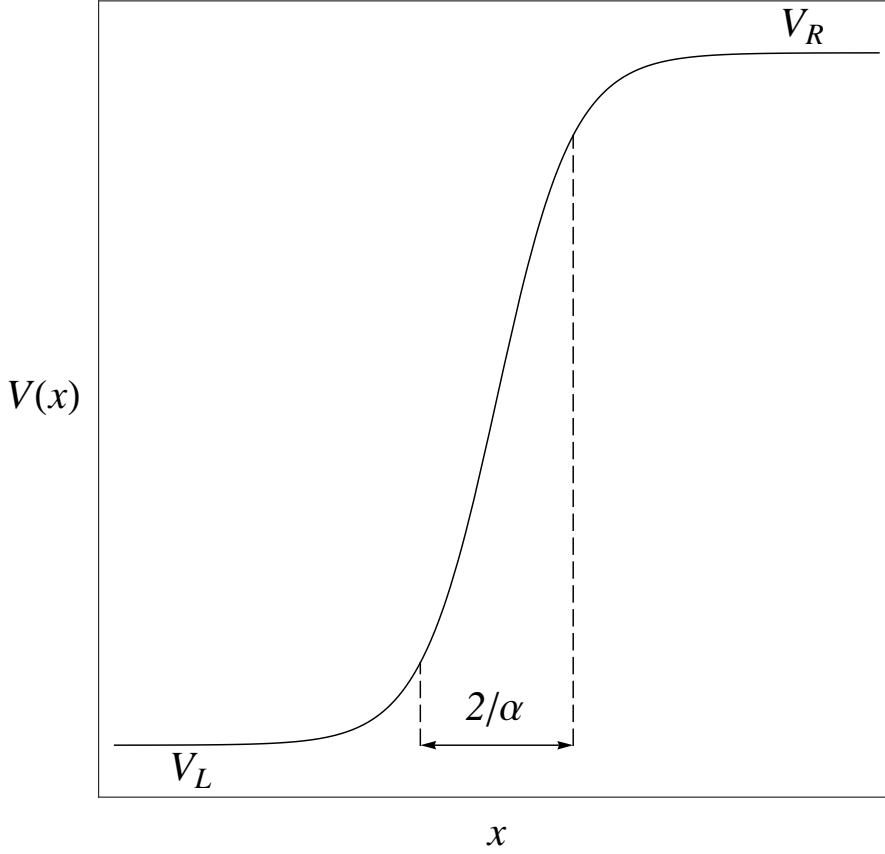


Figure 4.2.: HYPERBOLIC TANGENT VELOCITY PROFILE: This is the simplest monotonic profile with asymptotically constant values, and is expressed by Eq. (4.2.1).  $\alpha$  is inversely related to the length of the transition region.

## 4.2. Velocity profile

Endeavouring to keep the physical system as simple as possible, we shall use a velocity profile that varies monotonically between two asymptotic values; such a profile shall then be invertible, which is useful for application of the analytic results in Eqs. (3.3.15) and (3.3.17). The simplest candidate is the hyperbolic tangent function, and accordingly we restrict ourselves to velocity profiles of the form

$$V(x) = \frac{1}{2}(V_R + V_L) + \frac{1}{2}(V_R - V_L) \tanh(\alpha x) . \quad (4.2.1)$$

$V_R$  and  $V_L$  are the asymptotic values of  $V(x)$  as  $x$  tends to  $+\infty$  or  $-\infty$ , respectively. The parameter  $\alpha$  characterizes the steepness of the velocity profile, but this also depends on the difference  $V_R - V_L$ ; a more direct interpretation of  $\alpha$  is that it governs the length of the region of transition between  $V_L$  and  $V_R$ , which is of order  $2/\alpha$  as shown in Figure 4.2.

#### 4. Results for Acoustic Model

It may be argued that a velocity profile with equal asymptotic velocities would be a more desirable option. Certainly, such a profile would have greater practical applicability: the change in flow velocity is normally caused by a local disturbance, such as an obstacle that alters the depth of fluid and hence the speed of its flow, or an intense pulse of light that alters the refractive index of an optical fibre. In these practical scenarios, the change is local, and the physical conditions in a region far from the change are the same whether we are ahead of the change or behind it. But the corresponding velocity profile is not invertible, so that the analytic treatment of §3.3 is inapplicable; and a horizon, should one occur, must be accompanied by a partner horizon on the other side of the change. Since the derivatives of the flow velocity at these horizons must have opposite signs, one of them will be a black hole horizon, the other a white hole horizon. The Hawking spectrum emitted by such a system will be some superposition of the spectra of each horizon, and might exhibit interference. Given these complications, it is wise to limit ourselves to the investigation of a single horizon, or at least a monotonic variation, for which we must pay the reasonable price of physical equivalence of the asymptotic regions.

### 4.3. Normalizing the wave equation

With the dispersion and velocity profiles given by Eqs. (4.1.1) and (4.2.1), the acoustic wave equation (2.1.4) becomes

$$\partial_t^2 \phi + V'(x) \partial_t \phi + 2V(x) \partial_t \partial_x \phi + 2V(x) V'(x) \partial_x \phi + V^2(x) \partial_x^2 \phi - c^2 \partial_x^2 \phi - \frac{c^2}{k_d^2} \partial_x^4 \phi = 0. \quad (4.3.1)$$

This equation contains five parameters:  $c$  and  $k_d$  from the dispersion profile; and  $V_L$ ,  $V_R$  and  $\alpha$  from the velocity profile. However, two of these correspond to the scaling of space and time; in normalizing the variables to make them dimensionless, we can reduce the number of independent parameters to three.

Firstly, let us normalize the velocity profile with respect to  $c$ , the low- $k$  limit of the wave velocity. We define the dimensionless velocity  $U(x) = V(x)/c$ , and rewrite the wave equation in the form

$$\frac{1}{c^2} \partial_t^2 \phi + \frac{1}{c} U'(x) \partial_t \phi + 2 \frac{1}{c} U(x) \partial_t \partial_x \phi + 2U(x) U'(x) \partial_x \phi + U^2(x) \partial_x^2 \phi - \partial_x^2 \phi - \frac{1}{k_d^2} \partial_x^4 \phi = 0.$$

Next, let us normalize the position variable  $x$  (and, consequently, the wavenumber  $k$ ) by requiring that the dispersion parameter  $k_d$  be normalized to unity. This is done by defining the dimensionless position variable  $X = k_d x$ ; then the partial derivative  $\partial_x = k_d \partial_X$ , and the dimensionless wavenumber  $K = k/k_d$ . With this substitution, the



### 4.3. Normalizing the wave equation

wave equation becomes

$$\begin{aligned} \frac{1}{c^2 k_d^2} \partial_t^2 \phi + \frac{1}{ck_d} U'(X) \partial_t \phi + 2 \frac{1}{ck_d} U(X) \partial_t \partial_X \phi + 2U(X) U'(X) \partial_X \phi \\ + U^2(X) \partial_X^2 \phi - \partial_X^2 \phi - \partial_X^4 \phi = 0, \end{aligned}$$

where

$$U(X) = \frac{1}{2} (U_R + U_L) + \frac{1}{2} (U_R - U_L) \tanh(aX) \quad (4.3.2)$$

and  $a = \alpha/k_d$ . Finally, we shall normalize the time variable  $t$  (and the frequency  $\omega$ ). The present form of the wave equation shows that the tidiest way to do this is to define the dimensionless time variable  $T = ck_d t$ ; consequently, the partial derivative  $\partial_t = ck_d \partial_T$ , the dimensionless frequency  $\Omega$  is given by the relation  $\Omega = \omega / (ck_d)$ , and the wave equation takes the form

$$\begin{aligned} \partial_T^2 \phi + U'(X) \partial_T \phi + 2U(X) \partial_T \partial_X \phi + 2U(X) U'(X) \partial_X \phi + U^2(X) \partial_X^2 \phi \\ - \partial_X^2 \phi - \partial_X^4 \phi = 0. \end{aligned} \quad (4.3.3)$$

This can be factorized to give

$$(\partial_T + \partial_X U) (\partial_T + U \partial_X) \phi + f^2 (-i \partial_X) \phi = 0, \quad (4.3.4)$$

where the rescaled dispersion relation is

$$f^2(K) = K^2 (1 - K^2). \quad (4.3.5)$$

The wave equation now contains only three parameters:

- $U_R$  and  $U_L$ , the asymptotic values of the flow velocity relative to the low-frequency wave speed; and
- $a$ , a parameter that combines steepness of the flow velocity profile with dispersion strength. A higher value of  $a$  indicates greater steepness / stronger dispersion.

Often, the central value of the velocity is taken to be  $-1$ , so that this point would be the event horizon in the dispersionless case. Then,  $U_R + U_L$  is fixed (at  $-2$ ), and the number of parameters is reduced to two: one is still  $a$ ; the other is taken to be  $h = (U_R - U_L) / 2$ , the “height” of the velocity profile, where  $U_R = -1 + h$  and  $U_L = -1 - h$ . We shall examine this case; but we will also go on to examine more general velocity profiles where  $-1$  is not the central value, including those where  $V$  is nowhere equal to  $-1$ . Although, in the latter case, there is no horizon for low wavevectors, the discussion in §2.6 suggests that spontaneous phonon creation is still a possibility.

#### 4.4. Thermal behaviour

Purely thermal behaviour, as in Eq. (1.7.2), is characterized by the Planck spectrum

$$|\beta_\Omega|_T^2 = \frac{1}{\exp(\Omega/T) - 1}. \quad (4.4.1)$$

Clearly,  $|\beta_\Omega|_T^2 \rightarrow T/\Omega$  as  $\Omega \rightarrow 0$ , and the low-frequency temperature of any spectrum which behaves in a similar way can be defined accordingly; that is, we say that the spectrum has low-frequency temperature  $T$  if

$$|\beta_\Omega|^2 \rightarrow \frac{T}{\Omega} \quad \text{as} \quad \Omega \rightarrow 0. \quad (4.4.2)$$

In order to regularize the spectrum, it is useful to define a new quantity [44]

$$f_\Omega = \frac{\Omega}{T_{\text{pred}}} |\beta_\Omega|^2. \quad (4.4.3)$$

where  $T_{\text{pred}}$  is some predicted value for the temperature. Since  $|\beta_\Omega|^2$  is a number spectrum,  $f_\Omega$  is proportional to the energy spectrum. Its behaviour as  $\Omega \rightarrow 0$  is very instructive, for if  $|\beta_\Omega|^2$  has a low-frequency temperature  $T$  in the sense defined above, we have

$$f_\Omega \rightarrow \frac{T}{T_{\text{pred}}} \quad \text{as} \quad \Omega \rightarrow 0. \quad (4.4.4)$$

$f_\Omega$ , then, measures the low-frequency temperature relative to  $T_{\text{pred}}$ ; and in the special case when  $T_{\text{pred}} = T$ , the spectral form of  $f_\Omega$  provides a reference thermal curve (shown in Figure 4.3) against which other spectra may be compared.

Thermal effects, then, are dominant at low frequencies. Generally, the Hawking spectra are not purely thermal (see §4.5 for further discussion). However, when there is a point at which  $U = -1$ , there is an event horizon for all wavevectors in the limit  $K \rightarrow 0$ , since the dispersion profile approaches the dispersionless limit in this regime. We might reasonably expect that low-frequency thermal behaviour is preserved when  $U = -1$  at some point; the numerical results of §4.7 show that this is the case. To determine the value of the low-frequency temperature, we must look at two separate regimes.

##### 4.4.1. Validity of linearized velocity profile

If the linearized velocity profile of Eq. (3.3.1) is valid over some length scale, we expect the phase integral form of the creation rate in Eq. (3.3.17) to hold; and, moreover, it should agree with Eq. (1.7.3) for the temperature in the dispersionless case,

$$T = \frac{1}{2\pi} \left| \frac{dU}{dX} \right|_{U=-1}. \quad (4.4.5)$$

With the velocity profile given in Eq. (4.3.2), the event horizon occurs at the point  $X_h$  that satisfies

$$-1 = \frac{1}{2} (U_R + U_L) + \frac{1}{2} (U_R - U_L) \tanh(aX_h),$$

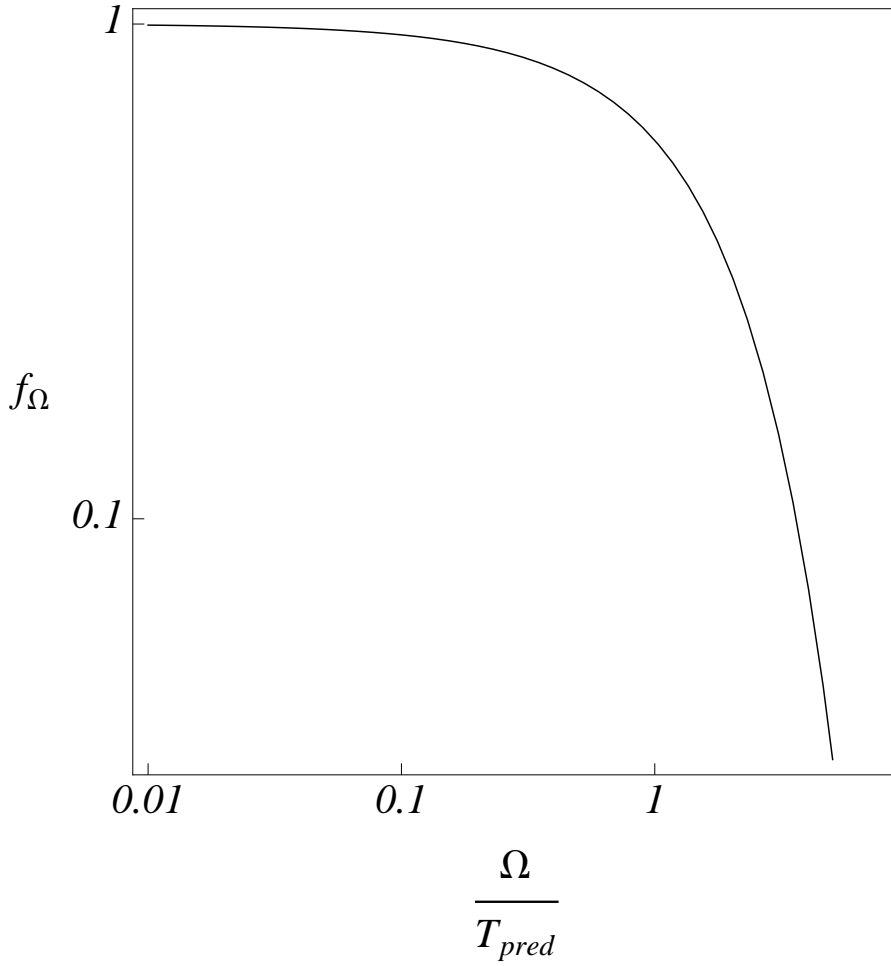


Figure 4.3.: THE THERMAL SPECTRUM: This shows the rescaled energy spectrum (4.4.3) which is purely thermal. Both axes use a logarithmic scale.

#### 4. Results for Acoustic Model

or

$$\tanh(aX_h) = -\frac{(2 + U_R + U_L)}{(U_R - U_L)}.$$

The derivative of the velocity profile at the event horizon is

$$\begin{aligned} U'(X_h) &= \frac{1}{2}(U_R - U_L)a \operatorname{sech}^2(aX_h) \\ &= \frac{1}{2}(U_R - U_L)a (1 - \tanh^2(aX_h)) \\ &= \frac{1}{2}(U_R - U_L)a \left( \frac{(U_R - U_L)^2 - (2 + U_R + U_L)^2}{(U_R - U_L)^2} \right) \\ &= -2a \frac{(1 + U_L)(1 + U_R)}{(U_R - U_L)}. \end{aligned}$$

Thus, the temperature predicted by the dispersionless model is

$$T_{\text{pred}} = \frac{a}{\pi} \left| \frac{(1 + U_L)(1 + U_R)}{(U_R - U_L)} \right|, \quad (4.4.6)$$

which reduces to  $T_{\text{pred}} = \hbar a / (2\pi)$  when  $-1$  is the central value of  $U$ , i.e. when  $U_R = -1 + h$  and  $U_L = -1 - h$ .

For the purpose of consistency, when we form the scaled energy spectrum of Eq. (4.4.3) it is the predicted temperature of Eq. (4.4.6) that shall be used.

##### 4.4.2. Validity of discontinuous velocity profile

If the change in velocity occurs over a much shorter length than some characteristic length scale, the linearized velocity profile is invalid and the system is better approximated by a step-discontinuous profile. Here, the method and analysis of §3.2 come into play. It was seen there that the mode conversion - and, consequently, the temperature - approaches a finite limiting value as the slope  $a$  increases without bound. The prediction of Eq. (4.4.6) cannot hold; the temperature should approach some limiting value,  $T_\infty$ , which is independent of  $a$ .

The calculation of  $T_\infty$  is not conceptually difficult, but it is quite lengthy, and has been relegated to Appendix A. The result is

$$T_\infty = (1 - U_R^2)^{1/2} \left| \frac{(1 + U_R)(1 + U_L)(U_R + U_L)}{(1 - U_R)(1 - U_L)(U_R - U_L)} \right|. \quad (4.4.7)$$

(This was presented previously in Ref. [40] and is very similar to a result given more recently in Ref. [42].) Note that Eq. (4.4.6) predicts a temperature of exactly  $T_\infty$  when  $a$  is given by

$$a = \pi (1 - U_R^2)^{1/2} \left| \frac{(U_R + U_L)}{(1 - U_R)(1 - U_L)} \right|.$$

It is when  $a$  is on the order of this value that the transition between the limiting forms of the temperature, given by Eqs. (4.4.6) and (4.4.7), takes place.

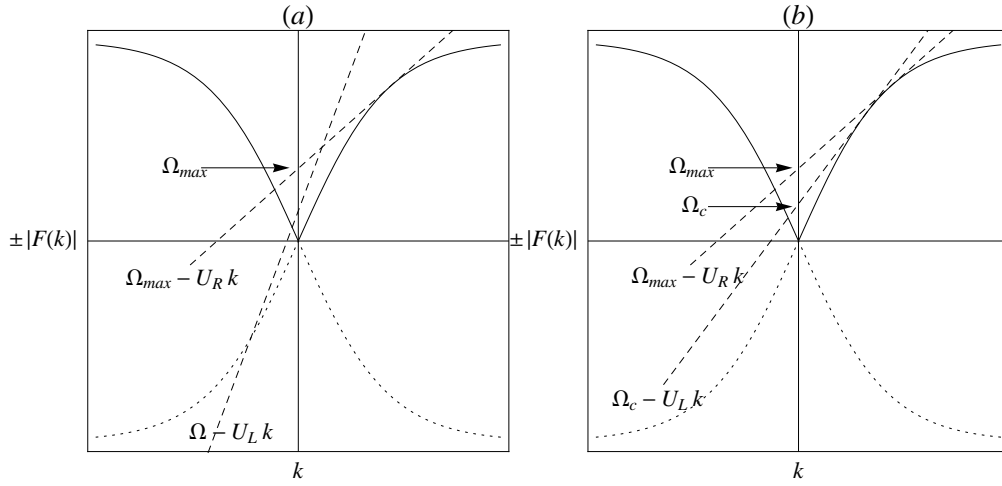


Figure 4.4.: CRITICAL FREQUENCIES: In (a), there is a point at which  $U = -1$ , so that there is a region of subsonic flow and one of supersonic flow. The dispersion relation in the region of supersonic flow has a maximum frequency at which  $ur$ - and  $ul$ -modes appear; but in the supersonic region, there is no such cut-off point. Figure (b) shows the altered picture when  $U$  is nowhere equal to  $-1$  and the flow is everywhere subsonic. Then both regions have a cut-off frequency; frequencies between the two cut-offs experience a group-velocity horizon, while those below both cut-offs, including very low frequencies, do not.

## 4.5. Nonthermal behaviour and critical frequencies

When  $U = -1$  at some point, it might be expected that the phonon spectrum is thermal at low frequencies, as discussed in §4.4. However, this spectrum cannot be purely thermal, for an examination of the dispersion relation (see Figure 4.4(a)) shows that there is a cut-off frequency above which mixing of positive- and negative-norm modes cannot occur. (It may occur between  $u$ - and  $v$ -modes, but this coupling is typically negligibly small.)

However, nonthermality must also come into play for low frequencies when  $U$  is nowhere equal to  $-1$ . Since group velocity is frequency-dependent, there may still be group-velocity horizons for certain frequencies, provided the velocity profile conforms to the relations given above. There will still be a cut-off frequency  $\Omega_{\max}$ , above which no group-velocity horizons exist and no mixing between positive and negative norms occurs. But there will also be no group-velocity horizons for very low frequencies, since, as  $\Omega \rightarrow 0$ , the group velocity approaches unity. Therefore, there exists a frequency,  $\Omega_c$ , which is the minimum frequency for which there exists a group-velocity horizon (see Figure 4.4(b)). The horizon begins, when  $\Omega = \Omega_c$ , at one infinity (in one of the asymptotic regions), and as  $\Omega$  increases to  $\Omega_{\max}$ , it moves smoothly to the other infinity (the other asymptotic region).

#### 4. Results for Acoustic Model

What happens for  $\Omega < \Omega_c$ ? Although there is no group-velocity horizon, mixing between positive and negative norms *is* possible; this is discussed in §2.6. What is more, the dimension of the space of solutions is greater than when a group-velocity horizon exists, because there is no merging of the *ur*- and *ul*-modes into a single *url*-mode. Therefore,  $\Omega_c$ , far from being a minimum frequency at which norm-mixing can occur, simply marks a boundary between two different types of behaviour, which must be treated separately in calculations. It may be noticed that, taking the thermal prediction at face value, it is to be concluded that virtually no radiation should be present since  $U$  is never equal to  $-1$ ; or, at the very least, radiation should only be omitted in the frequency range  $\Omega_c < \Omega < \Omega_{\max}$ , when there is a group-velocity horizon. As we shall see, these predictions are very far from the truth, and such horizons are unnecessary for the emission of radiation.

### 4.6. Phase integral analysis

Before we explore the results of numerical calculations, let us pause to examine the results of the one analytic tool at our disposal: the phase integral approximation of Eq. (3.3.18). Substituting the appropriate wavevectors, this predicts a Hawking emission rate given by

$$\left| \frac{\beta_\Omega}{\alpha_\Omega} \right|^2 = \exp(2 \operatorname{Im} \{J\}) \quad (4.6.1)$$

where

$$J = \int_{K_R^{ur}}^{K_R^u} X(K) dK \quad (4.6.2)$$

and  $X(K)$  is defined implicitly by the conservation of  $\Omega$  according to the dispersion relation  $\Omega = U(X)K + f(K)$ . Beginning with the  $X$ -dependent dispersion relation

$$\Omega = \left[ \frac{1}{2}(U_R + U_L) + \frac{1}{2}(U_R - U_L) \tanh(aX) \right] K + f(K),$$

we can find  $X$  as a function of  $K$ :

$$\tanh(aX) = \frac{2}{U_R - U_L} \left( \frac{\Omega - f(K)}{K} - \frac{1}{2}(U_R + U_L) \right),$$

or

$$X(K) = \frac{1}{a} \operatorname{arctanh} \left[ \frac{2}{U_R - U_L} \left( \frac{\Omega - f(K)}{K} - \frac{1}{2}(U_R + U_L) \right) \right]. \quad (4.6.3)$$

The only ambiguity is that  $\tanh(x + i\pi) = \tanh(x)$ , i.e., the hyperbolic tangent is periodic in the imaginary part of its argument, with period  $\pi$ .  $X(K)$ , therefore, is uniquely defined up to an integer multiple of  $i\pi/a$ . We restrict  $0 \leq \operatorname{Im} \{X(K)\} < \pi/a$ . A typical contour plot of the imaginary part of  $X(K)$  is shown in Fig. 4.5.

The branch cuts of Fig. 4.5 show clearly those values of  $K$  where  $\operatorname{Im} \{X(K)\} = 0$ , or where  $X(K)$  is real. These lines trace out the instantaneous values of  $K$  (for a particular

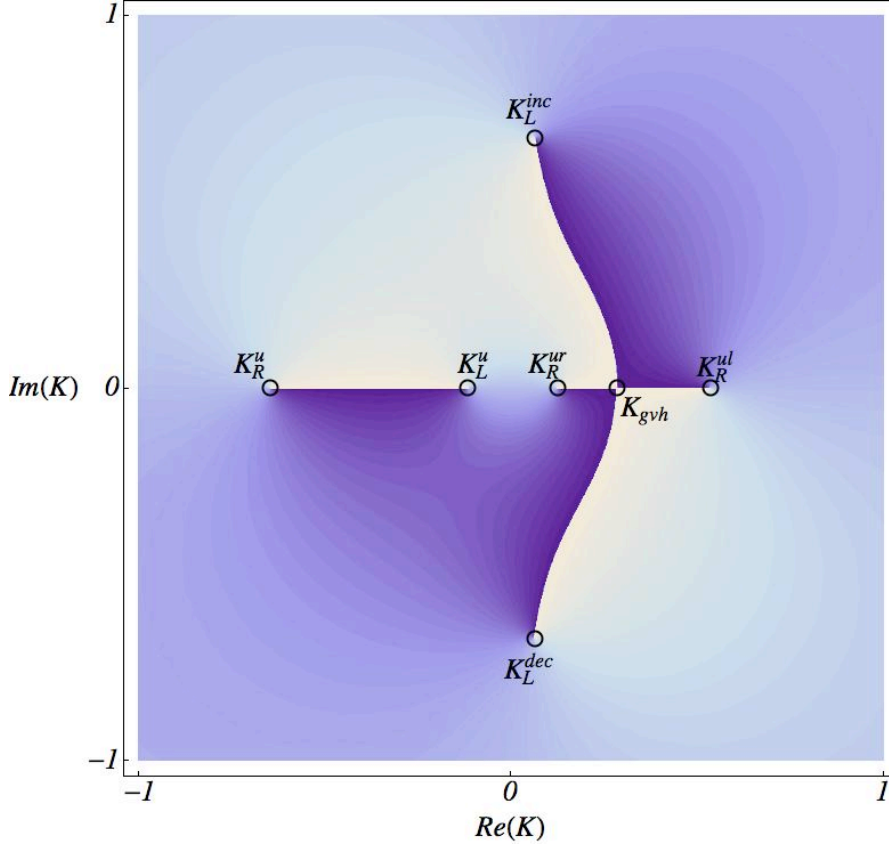


Figure 4.5.: PHASE INTEGRALS WITH A GROUP-VELOCITY HORIZON: The degree of shading shows the imaginary part of  $X(K)$ , which is restricted to the interval between 0 and  $\pi/a$ . The branch cuts show where it is equal to these boundary values; thus they show where  $X(K)$  is real, tracing out the values of  $K$  that are realised somewhere in the velocity profile.

#### 4. Results for Acoustic Model

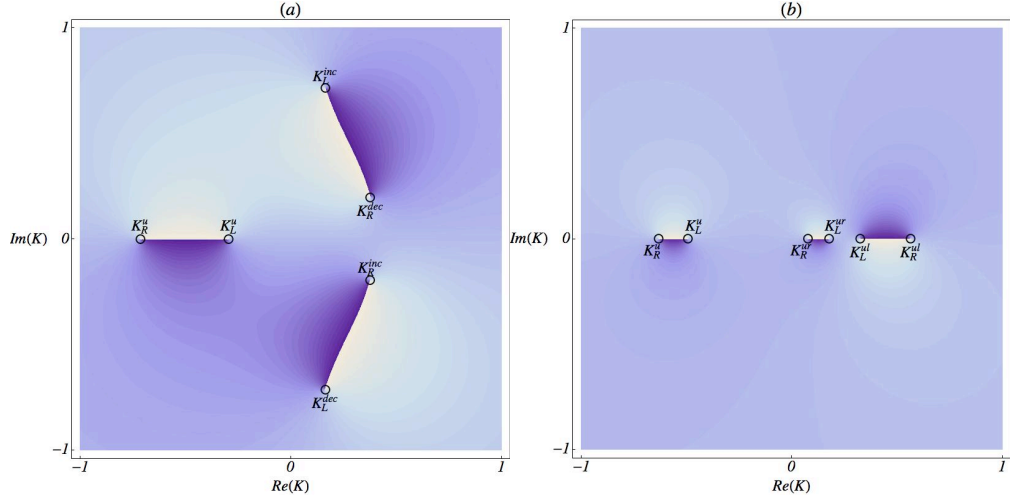


Figure 4.6.: PHASE INTEGRALS WITH NO GROUP-VELOCITY HORIZON: The degree of shading shows the imaginary part of  $X(K)$ , restricted to the interval between 0 and  $\pi/a$ . The branch cuts show where  $X(K)$  is real. In (a),  $\Omega > \Omega_{\max}$ ; in (b),  $\Omega < \Omega_c$ .

value of  $\Omega$ ) as one varies from one asymptotic region to the other. Their endpoints, which are labelled in the diagram, are those values of  $K$  which correspond to plane waves in the asymptotic regions themselves, i.e., they are solutions of either  $\Omega - U_R K = f(K)$  or  $\Omega - U_L K = f(K)$ . The cross-bow shaped feature, which joins together four different values of  $K$  - two of them real, two of them complex conjugates - is indicative of the presence of a group-velocity horizon. The solutions merge at the horizon itself, where they are equal to  $K_{\text{gvh}}$ ; moving in one direction, they split into two real values, reaching  $K_1$  and  $K_2$  in the asymptotic region; moving in the other direction, they split into two complex conjugate values, one of which is exponentially increasing while the other is decreasing. The other feature corresponds to the Hawking wave, which experiences no group-velocity horizon and simply varies from one real value to another.

Figure 4.6 shows the other possibilities mentioned in §4.5. Figure 4.6(a) shows the imaginary part of  $X(K)$  in the case where  $\Omega > \Omega_{\max}$ . The cross-bow pattern has disappeared, in accordance with the fact that there is no longer a group-velocity horizon. Instead, only the complex branches remain, so that the only real solution, for all values of  $X$ , is the negative value of  $K$ . No positive-norm modes exist, and hence no mode mixing is possible. Figure 4.6(b) corresponds to the case where  $\Omega < \Omega_c$ . (This requires that  $U$  is nowhere equal to  $-1$ .) We again have no group-velocity horizon, but this time it is the real branches that remain, so that we have three real solutions everywhere. Mixing of positive and negative norms is therefore possible in both asymptotic regions.

According to Eqs. (4.6.1) and (4.6.2), we can find an approximation to the Hawking radiation rate by taking the imaginary part of the integral of  $X(K)$  from the initial value of  $K$  to the Hawking value. If we restrict the integration to real values of  $K$ , this is simply



the integral of the imaginary part of  $X(K)$ . Fig (4.5) shows that we need integrate only between  $K_R^{ur}$  and  $K_L^u$ , since beyond these points,  $X(K)$  is real. What is more, for any real value of  $K$ , the argument of the inverse hyperbolic tangent in Eq. (4.6.3) is real; if the imaginary part of  $X(K)$  is not zero, then it must be equal to  $\pi/(2a)$ . Thus we have

$$\text{Im}\{J\} = \frac{\pi}{2a} (K_R^{ur} - K_L^u),$$

so that

$$\left|\frac{\beta}{\alpha}\right|^2 = \exp\left(-\frac{\pi}{a} (K_R^{ur} - K_L^u)\right). \quad (4.6.4)$$

Using the relation  $|\alpha|^2 - |\beta|^2 = 1$ , which corresponds to conservation of norm, this predicts a Hawking emission rate of

$$|\beta|^2 = \frac{1}{\exp\left(\frac{\pi}{a} (K_R^{ur} - K_L^u)\right) - 1}. \quad (4.6.5)$$

Eq. (4.6.5) is clearly very similar to a Planck spectrum of the form (4.4.1), and since thermal behaviour is essentially characterised by a  $1/\Omega$  pole near  $\Omega = 0$ , we expect that Eq. (4.6.5) will reduce to such a form in the limit of low frequency. Indeed, as shown in Appendix A, for small  $\Omega$  the wavevectors  $K_R^{ur}$  and  $K_L^u$  are approximately given by

$$K_R^{ur} \approx \frac{1}{1+U_R}\Omega, \quad K_L^u \approx \frac{1}{1+U_L}\Omega, \quad (4.6.6)$$

which means that

$$\frac{\pi}{a} (K_R^{ur} - K_L^u) \approx \frac{\pi}{a} \frac{(U_L - U_R)}{(1+U_R)(1+U_L)}\Omega. \quad (4.6.7)$$

Thus, Eq. (4.6.5) corresponds exactly to the Hawking prediction, with temperature given by Eq. (4.4.6), in the limit of low frequency. For higher frequencies, we expect deviations from thermality, and it remains to be seen whether Eq. (4.6.5) will correspond well with numerical results.

## 4.7. Numerical results

### 4.7.1. Central horizon

The typical example is one in which  $-1$  is the central value of the flow velocity, so that the event horizon occurs exactly at the centre of the variation. The asymptotic velocities  $U_R$  and  $U_L$  can be replaced by the single parameter  $h$ , the height of the step from  $-1$  to either of the asymptotic velocities. As we have seen from Eq. (4.4.6), the Hawking prediction gives a temperature

$$T_{\text{pred}} = \frac{ha}{2\pi}. \quad (4.7.1)$$

Figure 4.7 shows a variety of spectra, normalized according to Eq. (4.4.3) with the temperature given by Eq. (4.7.1). Figure 4.7(a) shows several spectra with the same

#### 4. Results for Acoustic Model

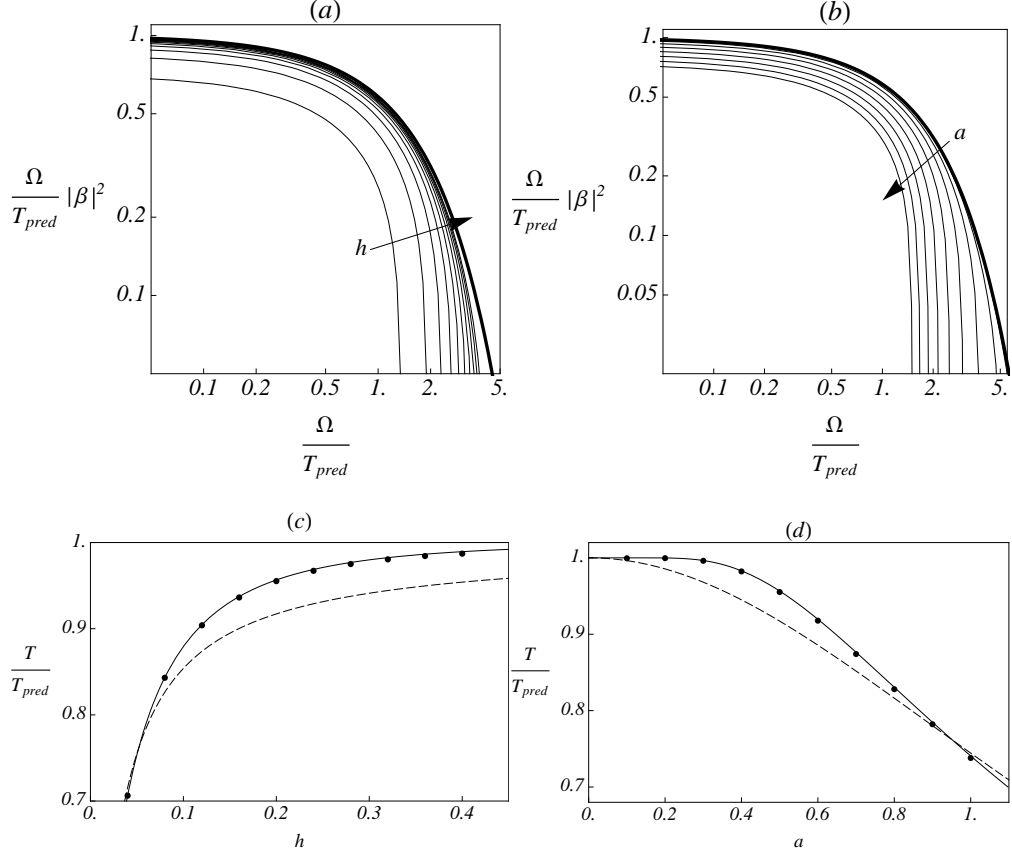


Figure 4.7.: HAWKING SPECTRA WITH A CENTRAL HORIZON, 1: In Figure (a), the parameter  $a$  is fixed at 0.5 while  $h$  is varied between 0.04 and 0.40; in Figure (b),  $h$  is fixed at 0.20 while  $a$  is varied between 0.1 and 1.0. The thick curve represents a thermal spectrum, and the arrows show the direction in which the relevant parameter increases. Figures (c) and (d) show  $T/T_{pred}$ , the low-frequency limit of the spectra in Figures (a) and (b), respectively. The functional form of Eq. (4.7.4) is shown as a dashed curve, while the solid curve corresponds to Eq. (4.7.5).

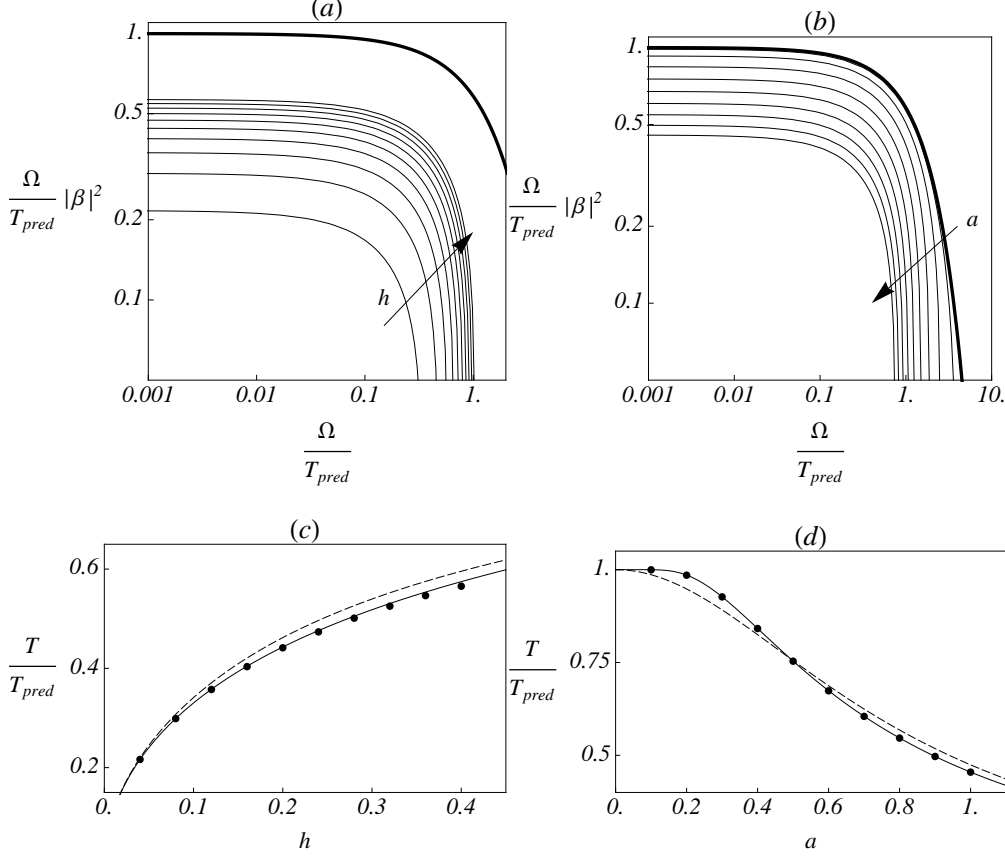


Figure 4.8.: HAWKING SPECTRA WITH A CENTRAL HORIZON, 2: In Figure (a), the parameter  $a$  is fixed at 2.0 while  $h$  is varied between 0.04 and 0.40; in Figure (b),  $h$  is fixed at 0.05 while  $a$  is varied between 0.1 and 1.0. The thick curve represents a thermal spectrum, and the arrows show the direction in which the relevant parameter increases. Figures (c) and (d) plot  $T/T_{pred}$ , the low-frequency limit of the spectra in Figures (a) and (b). The functional form given in Eq. (4.7.4) is plotted as a dashed line, while the solid line corresponds to Eq. (4.7.5).

#### 4. Results for Acoustic Model

value of  $a$  and different values of  $h$ ; Figure 4.7(b) shows spectra with the same value of  $h$  but various values of  $a$ . In each plot, a pure thermal spectrum is also shown.

These spectra (of Figs. 4.7(a) and (b)) all have a faster fall to zero than the thermal spectrum, as expected: they must go to zero at the maximum frequency  $\Omega_{\max}$ , while the thermal spectrum is non-zero for all frequencies. Also, the measured spectra all approach limiting values for low frequencies, indicating that the creation rate  $|\beta_\Omega|^2 / (2\pi)$  always has the  $\frac{1}{\Omega}$  pole that is characteristic of a thermal spectrum. However, since they do not all approach a limiting value of 1, it is clear that they do not all accord with the prediction of Eq. (4.7.1), which seems to be true only in the limit of high  $h$  and low  $a$ . (These trends have been noted previously [44].) Recalling Eq. (4.4.4), the limiting values of the spectra as  $\Omega \rightarrow 0$  are precisely the values of  $T/T_{\text{pred}}$ , where  $T$  is the true low-frequency temperature. Some spectra, then, have a value of  $T$  which is lower than  $T_{\text{pred}}$ . Again, this is to be expected: the Hawking prediction yields a temperature which can increase without bound, whereas we have seen that there is a limiting temperature as  $a \rightarrow \infty$  (given by Eq. (4.4.7)).

Figures 4.7(c) and (d) plot the values of  $T/T_{\text{pred}}$  for the spectra of (a) and (b), respectively. They also show two analytic, though heuristically derived, curves - one of which gives excellent agreement with the measured values. To find this, let us consider the dependence of  $T$  on  $a$ , i.e., we treat  $h$  as fixed. It is clear that, at low  $a$ , the temperature is given by  $T_{\text{pred}} = ha/(2\pi)$ , and is thus linear in  $a$ . The temperature increases monotonically with  $a$ , approaching the limiting value  $T_\infty$ , which is independent of  $a$ . There are many functional forms that would behave as such, but the hyperbolic tangent is a natural guess, given that the velocity profile has precisely this form. Even so, there are two possible guesses for the form of the temperature which behave in the required way:

$$T = T_\infty \tanh\left(\frac{ha}{2\pi T_\infty}\right), \quad \text{or} \quad T = \frac{ha}{2\pi} \tanh\left(\frac{2\pi T_\infty}{ha}\right). \quad (4.7.2)$$

Substituting in Eq. (4.4.7) the values  $U_R = -1 + h$  and  $U_L = -1 - h$ , we find

$$T_\infty = \frac{h^{3/2}}{(2-h)^{1/2}(2+h)}. \quad (4.7.3)$$

Plugging this into the above forms for the temperature and dividing by  $T_{\text{pred}} = ha/(2\pi)$ , the guessed temperature curves are

$$\frac{T}{T_{\text{pred}}} = \frac{2\pi h^{1/2}}{a(2-h)^{1/2}(2+h)} \tanh\left(\frac{a(2-h)^{1/2}(2+h)}{2\pi h^{1/2}}\right), \quad (4.7.4)$$

$$\text{or} \quad \frac{T}{T_{\text{pred}}} = \tanh\left(\frac{2\pi h^{1/2}}{a(2-h)^{1/2}(2+h)}\right). \quad (4.7.5)$$

As shown in Fig. 4.7, Eq. (4.7.5) agrees remarkably well with numerical results, over the entire parameter space. This is the first demonstration of such a universally valid expression for the low-frequency temperature.

More spectra are shown in Fig. 4.8, with fixed values of  $a = 2.0$  and  $h = 0.05$  chosen so as to increase the deviation from the thermal prediction of Eq. (4.7.1). The values of  $T/T_{\max}$  are also plotted, and once again it is found that Eq. (4.7.5) agrees very well with numerical results.

#### 4.7.2. Non-central horizon

We have seen that, when the central value of the velocity profile is equal to  $-1$ , then the ratio of the measured temperature to the predicted temperature,

$$\frac{T}{T_{\text{pred}}} = \tanh\left(\frac{T_{\infty}}{T_{\text{pred}}}\right).$$

It is reasonable to generalise this to the case of an arbitrary velocity profile, so long as it is equal to  $-1$  somewhere (for, if it is not, then the Hawking prediction of Eq. (4.4.5) is inapplicable). Plugging in the expressions for  $T_{\text{pred}}$  and  $T_{\infty}$  as given in Eqs. (4.4.6) and (4.4.7), respectively, then we find

$$\frac{T}{T_{\text{pred}}} = \tanh\left(\frac{\pi}{a} (1 - U_R^2)^{1/2} \frac{(U_L + U_R)}{(1 - U_R)(U_L - 1)}\right), \quad (4.7.6)$$

or

$$T = \frac{a}{\pi} \frac{(1 + U_R)(1 + U_L)}{(U_L - U_R)} \tanh\left(\frac{\pi}{a} (1 - U_R^2)^{1/2} \frac{(U_L + U_R)}{(1 - U_R)(U_L - 1)}\right). \quad (4.7.7)$$

Figure 4.9 plots the values of  $T/T_{\text{pred}}$  for various values of the parameters  $U_R$ ,  $U_L$  and  $a$ . The independent variable in the plot is taken to be the combination of these parameters that appears in the argument of the hyperbolic tangent function in Eqs. (4.7.6). This equation predicts that the resulting plot should be simply the hyperbolic tangent function; that is indeed found to be the case.

When the central value of  $U$  - hereafter referred to as  $U_m$  - is equal to  $-1$ , the deviation of the spectra from the thermal spectrum occurs as a result of the cut-off frequency  $\Omega_{\max}$ , so that they fall sharply to zero as this frequency is approached. However, when  $U_m$  is different from  $-1$ , the deviations from the thermal spectrum are much more significant. Figure 4.10 shows examples for different values of  $U_m$ ; the values of  $h$  and  $a$  are fixed at values such that  $T/T_{\text{pred}} \approx 1$ . The most striking difference occurs when  $U_m > -1$ , for then the observed spectrum is *greater* than the thermal spectrum (at the high-frequency end).

Also of note in Fig. 4.10 is how accurate the phase integral prediction of Eq. (4.6.5) is, clearly in accordance with the deviations just mentioned. This is the first demonstration of an analytic expression valid over the entire spectrum. The only significant deviation occurs very close to  $\Omega_{\max}$ , when again the measured spectrum falls off more sharply than the model predicts. It is also worth noting that the phase-integral approximation is only accurate when the low-frequency temperature agrees very well with the Hawking prediction, i.e., when  $T/T_{\text{pred}} \approx 1$ . Indeed, taking the low-frequency limit of Eq. (4.6.5) yields precisely the temperature of Eq. (4.4.6). It is not clear whether the phase integral approximation can be modified to accord with the modified temperature of Eq. (4.7.7).

#### 4. Results for Acoustic Model

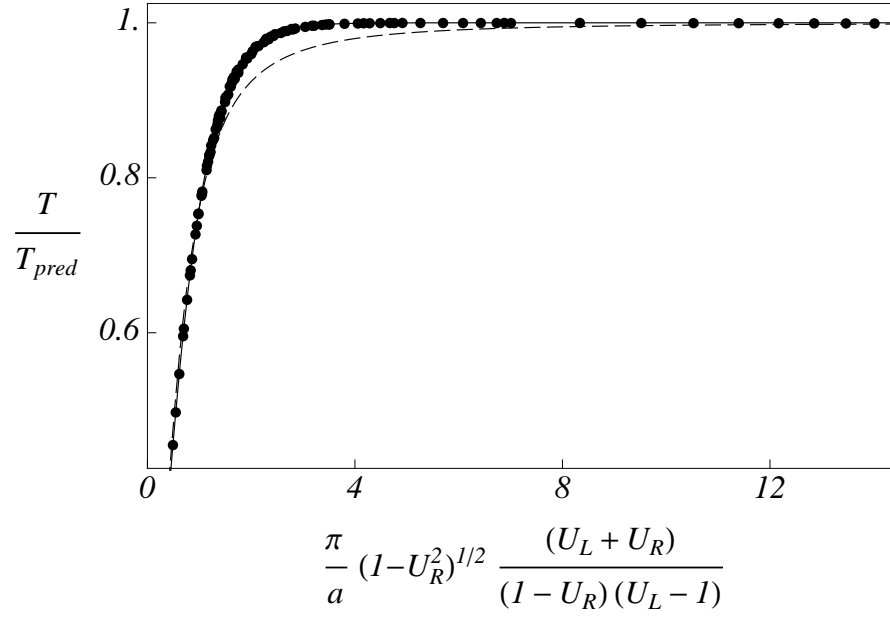


Figure 4.9.: LOW-FREQUENCY TEMPERATURE: This figure plots  $T/T_{pred}$ , or the low-frequency limit of  $\Omega |\beta|^2 / T_{pred}$ , for various values of  $U_R$ ,  $U_L$  and  $a$ . Writing the abscissa as simply  $x$ , the solid curve plots  $\tanh(x)$ , while the dashed curve plots  $x \tanh(1/x)$ , which is the generalised form of Eq. (4.7.4). The low-frequency temperature is thus seen to agree very well with Eq. (4.7.6).

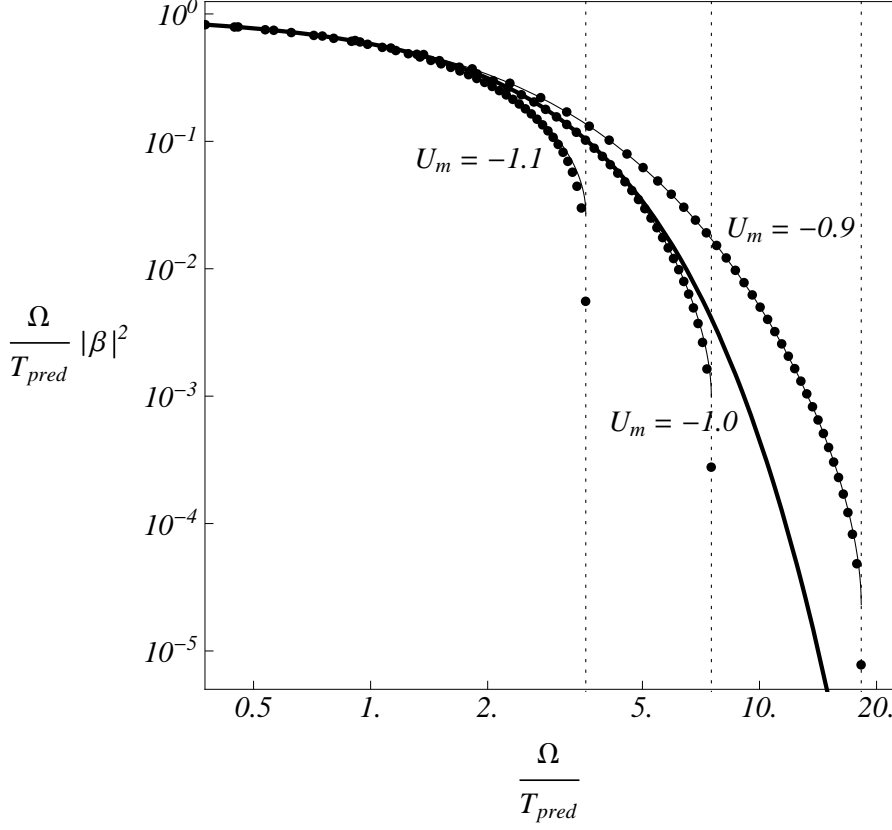


Figure 4.10.: HAWKING SPECTRA WITH NON-CENTRAL HORIZON: The thick curve represents a thermal spectrum, while the thinner curves are the spectra obtained from Eq. (4.6.5) with various values of  $U_m$ . (We have fixed  $h = 0.2$  and  $a = 0.2$ , so that the low-frequency temperature (4.7.7) agrees very well with Eq. (4.4.6).) The dots are data points obtained by solving for the spectra numerically. The dotted vertical lines show the positions of  $\Omega_{max}/T_{pred}$  for each curve.

### 4.7.3. No low-frequency horizon

What happens if there is no point at which  $U = -1$ ? Such a regime is never examined in the literature, for it does not correspond to a black hole in the dispersionless limit. The Hawking prediction of Eqs. (4.4.1) and (4.4.5) cannot be applied, so it might be imagined that the spectrum vanishes. However, we have already seen that the Hawking prediction does not always apply, the relation between the temperature and the derivative at the horizon being rather less straightforward; and, moreover, that the spectra are not purely thermal anyway, exhibiting large deviations from thermality when  $U_m > -1$ . (This would, of course, be the case if  $U_L$  were increased to be greater than  $-1$ .) Recalling the observation made in §2.6 that an event horizon is not a necessary ingredient for Hawking radiation to be possible, we conclude that there is no reason to suppose that the Hawking spectrum will vanish when  $U$  is everywhere greater than  $-1$  - except, perhaps, that it is likely to be far from thermal.

Recall that, in this case, there are two types of frequency, separated by a critical frequency  $\Omega_c$ : those frequencies above  $\Omega_c$  (and, of course, below  $\Omega_{\max}$ ) experience a group-velocity horizon, and are treated in the same way as before; frequencies below  $\Omega_c$ , however, do not have a group-velocity horizon, and can occur in pairs of  $u - ul$  or  $u - ur$  modes. (We continue to ignore the backward-travelling  $v$ -modes.) We must take account of both of these pairings, and their spectra will in general be different.

Figure 4.11 shows an example of such a spectrum, with  $U_R = -0.5$ ,  $U_L = -0.9$  and  $a = 0.1$ . It is clearly non-zero, and is also clearly non-thermal. The two possible channels for phonon creation give very different spectra, and, for the  $ur - u$  pair, there is a change of behaviour at the frequency  $\Omega_c$ , the spectrum reaching a maximum at this point and approaching zero at both zero frequency and  $\Omega_{\max}$ .

The numerically calculated spectra are also in good agreement with the phase-integral approximation, although this claim requires some further explanation. When  $\Omega_c < \Omega < \Omega_{\max}$ , so that we have a group-velocity horizon, the phase-integral approximation gives the same expression as Eq. (4.6.5),

$$|\beta_{\Omega}^{ur}|^2 \approx \exp \left( -\frac{\pi}{a} (K_R^{ur} - K_L^u) \right). \quad (4.7.8)$$

(These values are small enough that we needn't make the modification of Eq. (4.6.5).) When  $\Omega < \Omega_c$ , this requires some modification. The spectrum is calculated using the  $u$ -in mode, the creation rates given by the norms of the out-components for the  $ul$ - and  $ur$ -modes. The phase integral of Eq. (3.3.17) is then taken between the  $K^u$ -branch and either the  $K^{ur}$ - or  $K^{ul}$ -branch. Taking the  $ul - u$  pairing first: the imaginary part of  $X(K)$  is  $\pi/(2a)$  in the regions between the branches; however, on traversing the  $K^{ur}$ -branch,  $X(K)$  is not purely real but has an imaginary part of  $\pi/a$ . The total integral, then, has an imaginary part of  $\pi(K_L^{ul} - K_L^u + K_L^{ur} - K_R^{ur})/(2a)$ , and the predicted creation rate is

$$|\beta_{\Omega}^{ul}|^2 \approx \exp \left( -\frac{\pi}{a} (K_L^{ul} - K_L^u + K_L^{ur} - K_R^{ur}) \right). \quad (4.7.9)$$

The creation rate of the  $ur - u$  pairing would seem to have the same expression as in Eq. (4.7.8). However, numerics show that the spectrum becomes linear in  $\Omega$  as  $\Omega \rightarrow 0$ , a



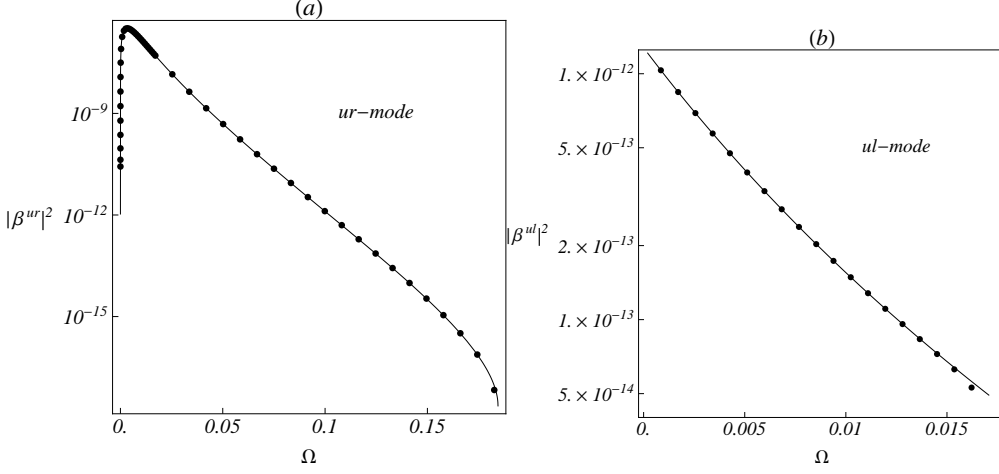


Figure 4.11.: HAWKING SPECTRUM WITH NO LOW-FREQUENCY HORIZON, 1: Here, we have taken  $U_R = -0.5$ ,  $U_L = -0.9$  and  $a = 0.1$ , so that  $U$  is nowhere equal to  $-1$ . Figure (a) shows the spectrum for the  $ur-u$  mode pairing, while Figure (b) corresponds to the  $ul-u$  mode pairing. The dots show the results of numerical calculations, while the curves plot the modified phase-integral predictions of Eqs. (4.7.8)-(4.7.10). Note that the  $ul-u$  pairing can only occur for  $\Omega < \Omega_c$ , while the  $ur-u$  pairing is possible right up to  $\Omega_{\max}$ . The two spectra approach zero at the upper limit of their frequency ranges, while the  $ur-u$  spectra has a maximum value at the frequency  $\Omega_c$ .

#### 4. Results for Acoustic Model

form not given by this exponential factor. It is found heuristically, using the fact that both  $K_R^{ur}$  and  $K_L^{ur}$  approach zero as  $\Omega \rightarrow 0$ , that the  $ur$ - $u$  spectrum conforms to the expression

$$|\beta_\Omega^{ur}|^2 \approx \exp\left(-\frac{\pi}{a}(K_R^{ur} - K_L^u)\right) - \exp\left(-\frac{\pi}{a}(K_L^{ur} - K_L^u)\right). \quad (4.7.10)$$

Although the discontinuous ( $a \rightarrow \infty$ ) velocity profile can be solved to show that  $|\beta_\Omega^{ur}|^2$  is indeed linear in  $\Omega$  at low frequencies, it is unclear why the spectrum should obey Eq. (4.7.10) so well. (This may require a more sophisticated phase-integral method, mentioned in §3.3, in which various solutions are linearly combined to give the required mode; the corresponding norms might then exhibit linear combination of various phase integrals, as suggested by Eq. (4.7.10).) Note that Eqs. (4.7.10) and (4.7.8) together indicate that the  $ur$ - $u$  spectrum reaches a maximum at  $\Omega_c$ , the boundary between the existence and non-existence of a group-velocity horizon.

However, we cannot expect the phase-integral approximation to hold universally, and indeed it does not. If the parameters are altered in such a way that invalidates the phase-integral approximation in the presence of a horizon - that is, if the steepness  $a$  is increased or the step height  $h = (U_R - U_L)/2$  is decreased - then the phase-integral approximation for the case of no low-frequency horizon also becomes less accurate. Figure 4.12 shows such spectra: the upper plots have the same value of  $a$  as Fig. 4.11, but the step height has been decreased to 0.05; the lower plots have the same asymptotic velocities as Fig. 4.11, but  $a$  has been increased to 0.4. It is perhaps worthy of note that the  $ul$ -mode spectrum deviates more from the phase-integral prediction than does the  $ur$ -mode spectrum.

#### 4.8. Concluding remarks

The question of whether Hawking radiation is robust with respect to dispersive effects can be answered affirmatively. Hawking radiation is still predicted once dispersion is introduced, though the resulting spectra are no longer purely thermal. When we have a low-frequency event horizon, the low-frequency end of the spectrum is thermal, with a temperature given by Eq. (4.7.7). This has been derived heuristically, though it agrees with Hawking's original result when the hyperbolic tangent is approximately 1. At higher frequencies, the spectrum deviates from thermality, though it is still well-approximated by the phase-integral prediction of Eq. (4.6.5).

We have also found that, when dispersion is included, Hawking radiation does not require the presence of a low-frequency event horizon, an observation that does not seem to have been appreciated before. Though  $U$  might nowhere equal  $-1$ , a spectrum of spontaneously created phonons is predicted, even for frequencies which do not experience a group-velocity horizon. These spectra are non-thermal, though they can be well-approximated by a modified phase-integral prediction, as given in Eqs. (4.7.8)-(4.7.10).

This raises the question of the precise origins of the created quanta. In the dispersionless case, which requires an event horizon for Hawking radiation, one can imagine the creation of a virtual pair at the event horizon, one on either side. The horizon prevents

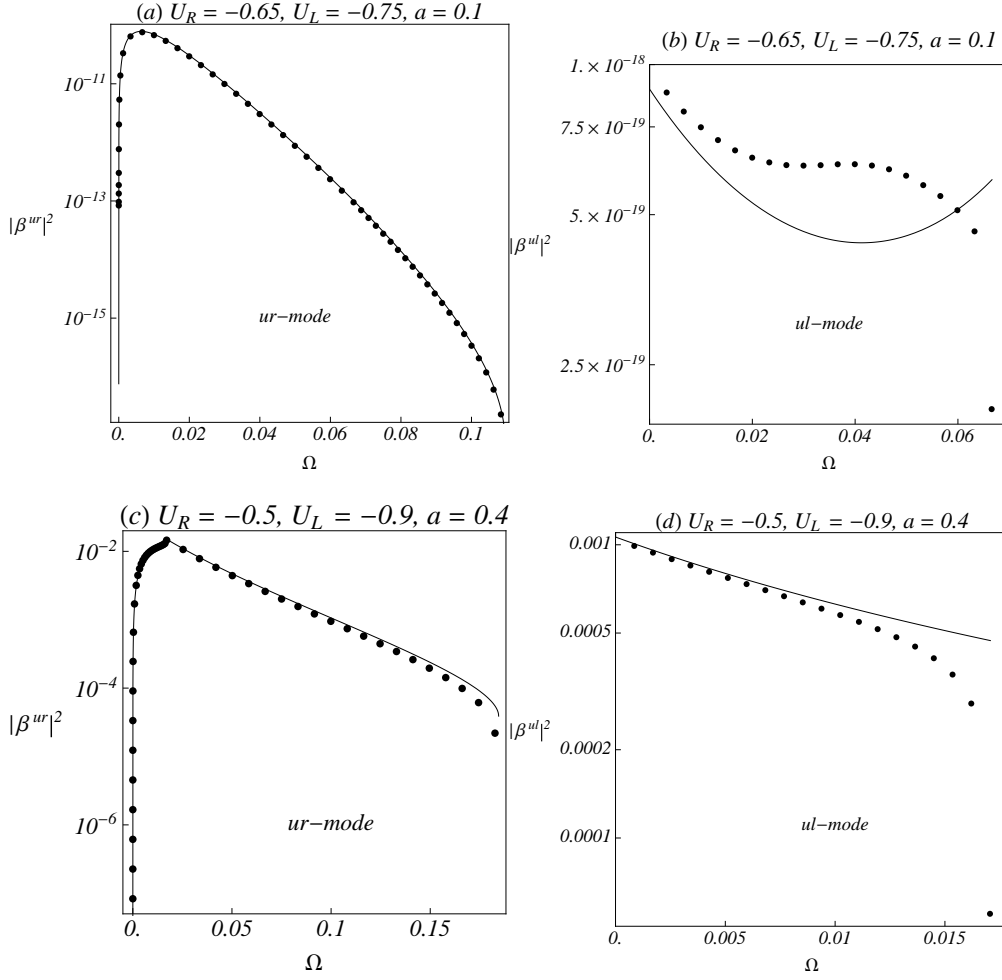


Figure 4.12.: HAWKING SPECTRA WITH NO LOW-FREQUENCY HORIZON, 2: Figures (a) and (b) show the  $ur$ - and  $ul$ -mode spectra for  $a = 0.1$ , as in Fig. 4.11, but with a decreased step height of 0.05; similarly, Figures (c) and (d) show the  $ur$ - and  $ul$ -mode spectra for  $U_R = -0.5$  and  $U_L = -0.9$ , as in Fig. 4.11, but with an increased steepness of  $a = 0.4$ .

#### 4. Results for Acoustic Model

them from recombining, so that they are rendered in reality. But when we have no event horizon - when the created quanta may actually be emitted in the same direction, like the  $u-ul$  pair - how are they produced? We might say that there is a *phase-velocity* horizon, for the created quanta, having oppositely signed (free-fall) frequencies, must have oppositely directed phase velocities. This, however, is not a well-defined concept, for the phase velocity  $\omega/k$  can never become zero if  $\omega$  is conserved. Moreover, if the existence of a phase-velocity horizon truly determined the Hawking spectrum, we would expect that a greater height in the velocity profile would increase the range of frequencies for which a phase-velocity horizon occurs; yet, an increase in the width of this part of the spectrum is not observed under an increase in the step height. The origin of the radiation thus remains a mystery.

Part III.

# Hawking Radiation in Optical Fibres



## 5. Nonlinear Fibre Optics

The fluid model is difficult to implement in practice. The velocity gradients and the Hawking temperatures they induce are typically so small (around 10 nK [23]) that a fluid with temperature close to absolute zero must be used. Thus, the proposed systems of Helium-3 [25, 26, 27, 28, 29] and Bose-Einstein condensate [19, 20, 21, 22] represent the most feasible means of observing spontaneous particle creation in fluids, but require sophisticated technology to do so.

From a practical viewpoint, light in moving media provides an attractive experimental setup for the observation of Hawking radiation. Light is the simplest of quantum objects, exhibiting quantum properties without the need for very low temperatures. Indeed, there is evidence that Hawking radiation has already been observed in the optical arena [60]. In the remainder of this thesis, we shall examine the simple one-dimensional system of light in optical fibres, a system routinely used in the laboratory setting, looking particularly at its capacity for event horizon analogies and the generation of Hawking radiation.

This chapter examines some of the essential physics of light in optical fibres. After reviewing the basic linear response in §5.1, in §5.2 we look at the lowest-order nonlinear response and some of its effects, culminating in the interaction of a soliton with a weak continuous probe wave. Finally, in §5.3, we introduce a coordinate frame in which this system resembles wave propagation in a dispersive moving medium, before concluding the chapter in §5.4.

### 5.1. Linear effects

Electromagnetic waves (such as light) are propagating disturbances of electric field  $\mathbf{E}$  and magnetic field  $\mathbf{H}$ , which are governed by Maxwell's equations [61]:

$$\nabla \times \mathbf{E} = -\frac{\partial \mathbf{B}}{\partial t}, \quad (5.1.1)$$

$$\nabla \times \mathbf{H} = \mathbf{J} + \frac{\partial \mathbf{D}}{\partial t}, \quad (5.1.2)$$

$$\nabla \cdot \mathbf{D} = \rho_f, \quad (5.1.3)$$

$$\nabla \cdot \mathbf{B} = 0, \quad (5.1.4)$$

where  $\mathbf{J}$  is the free current density,  $\rho_f$  is the free charge density, and  $\mathbf{B}$  and  $\mathbf{D}$  are related to  $\mathbf{E}$  and  $\mathbf{H}$  via the constitutive relations:

$$\mathbf{D} = \epsilon_0 \mathbf{E} + \mathbf{P}, \quad (5.1.5)$$

$$\mathbf{B} = \mu_0 \mathbf{H} + \mathbf{M}. \quad (5.1.6)$$

## 5. Nonlinear Fibre Optics

$\mathbf{P}$  and  $\mathbf{M}$  are the polarization and magnetization, respectively. Restricting our attention to optical fibres [62, 63], which are non-magnetic ( $\mathbf{M} = \mathbf{0}$ ), non-conducting ( $\mathbf{J} = \mathbf{0}$ ) and electrically neutral ( $\rho_f = 0$ ), we can substitute the constitutive relations into Maxwell's equations and eliminate  $\mathbf{D}$  and  $\mathbf{B}$ , yielding

$$\nabla \times \mathbf{E} = -\mu_0 \frac{\partial \mathbf{H}}{\partial t}, \quad (5.1.7)$$

$$\nabla \times \mathbf{H} = \epsilon_0 \frac{\partial \mathbf{E}}{\partial t} + \frac{\partial \mathbf{P}}{\partial t}, \quad (5.1.8)$$

$$\nabla \cdot \mathbf{E} = -\frac{1}{\epsilon_0} \nabla \cdot \mathbf{P}, \quad (5.1.9)$$

$$\nabla \cdot \mathbf{H} = 0. \quad (5.1.10)$$

$\mathbf{H}$  may be eliminated from these equations by taking the curl of Eq. (5.1.7) and substituting Eq. (5.1.8), resulting in the wave equation

$$\nabla \times (\nabla \times \mathbf{E}) = -\mu_0 \epsilon_0 \frac{\partial^2 \mathbf{E}}{\partial t^2} - \mu_0 \frac{\partial^2 \mathbf{P}}{\partial t^2}. \quad (5.1.11)$$

The product  $\mu_0 \epsilon_0 = 1/c^2$ , where  $c$  is the speed of light in vacuum; for vacuum, which contains no bound charges, cannot be polarized, and has  $\mathbf{P} = \mathbf{0}$ . Optical fibres, however, are made of dielectric material, so that  $\mathbf{P}$  is non-zero and must be accounted for.

In order to solve Eq. (5.1.11), we must determine the relationship between the polarization  $\mathbf{P}$  and the electric field  $\mathbf{E}$ . Since  $\mathbf{P}$  results from the response of bound charges within the medium to the electric field  $\mathbf{E}$ , and this response is unlikely to be instantaneous, our first guess at this relationship might be [63]

$$\mathbf{P} = \epsilon_0 \int_{-\infty}^t \chi(t-t') \mathbf{E}(t') dt'. \quad (5.1.12)$$

This describes the polarization as a linear response to the electric field, containing terms in only the first power of  $\mathbf{E}$ ; but, to incorporate the non-instantaneous nature of the response, it is built up of contributions from  $\mathbf{E}$  at all earlier times. The weight of the contribution from  $\mathbf{E}$  at time  $t$  before the measurement of  $\mathbf{P}$  is given by the response function,  $\chi(t)$ . Substituting in Eq. (5.1.11), the wave equation becomes

$$\nabla \times (\nabla \times \mathbf{E}) + \frac{1}{c^2} \frac{\partial^2}{\partial t^2} \left( \mathbf{E} + \int_{-\infty}^t \chi(t-t') \mathbf{E}(t') dt' \right) = 0. \quad (5.1.13)$$

This is more readily solved by taking the Fourier transform with respect to time [62, 63], which gives

$$\nabla \times (\nabla \times \tilde{\mathbf{E}}) - \frac{\omega^2}{c^2} (1 + \tilde{\chi}(\omega)) \tilde{\mathbf{E}} = 0, \quad (5.1.14)$$

where we have defined

$$\tilde{\mathbf{E}}(\omega, \mathbf{r}) = \int_{-\infty}^{+\infty} e^{i\omega t} \mathbf{E}(t, \mathbf{r}) dt \quad (5.1.15)$$



and

$$\tilde{\chi}(\omega) = \int_{-\infty}^{+\infty} e^{i\omega t} \chi(t) dt. \quad (5.1.16)$$

In regions where  $\tilde{\chi}(\omega)$  is independent of position, i.e., where the medium is homogeneous, Eq. (5.1.14) can be simplified. For, taking the Fourier transform with respect to time of Eq. (5.1.9), we find

$$\nabla \cdot \left( \tilde{\mathbf{E}} + \frac{1}{\epsilon_0} \tilde{\mathbf{P}} \right) = \nabla \cdot \left( (1 + \tilde{\chi}(\omega)) \tilde{\mathbf{E}} \right) = (1 + \tilde{\chi}(\omega)) \nabla \cdot \tilde{\mathbf{E}} = 0, \quad (5.1.17)$$

which implies

$$\nabla \cdot \tilde{\mathbf{E}} = 0. \quad (5.1.18)$$

We also use the vector identity

$$\nabla \times (\nabla \times \tilde{\mathbf{E}}) = \nabla (\nabla \cdot \tilde{\mathbf{E}}) - \nabla^2 \tilde{\mathbf{E}} = -\nabla^2 \tilde{\mathbf{E}}. \quad (5.1.19)$$

Substituting into Eq. (5.1.14), we find the Helmholtz equation:

$$\nabla^2 \tilde{\mathbf{E}} + \frac{\omega^2}{c^2} (1 + \tilde{\chi}(\omega)) \tilde{\mathbf{E}} = 0. \quad (5.1.20)$$

Eq. (5.1.20) describes wave propagation in media. We see that the effect of any particular medium on wave propagation depends mainly on the *linear susceptibility*  $\tilde{\chi}(\omega)$ , and is clearly frequency-dependent. We define the *permittivity*  $\epsilon(\omega) = (n(\omega) + i\alpha(\omega)/2\omega)^2 \equiv 1 + \tilde{\chi}(\omega)$ ; if the imaginary part of the susceptibility is small, as is often the case, then  $\epsilon(\omega)$  is approximately equal to  $n^2(\omega)$ .  $n(\omega)$  is the *refractive index*, and Eq. (5.1.20) can be written

$$\nabla^2 \tilde{\mathbf{E}} + \frac{\omega^2}{c^2} n^2(\omega) \tilde{\mathbf{E}} = 0, \quad (5.1.21)$$

whence it is clear that the refractive index describes a frequency-dependent wave speed: assuming a monochromatic wave, and comparing Eq. (5.1.21) with the vacuum case  $n(\omega) = 1$ , we see that the vacuum wave speed  $c$  is simply replaced by  $c/n(\omega)$ , and it admits plane wave solutions of the form  $\exp[-i\omega(t - n(\omega)z/c)]$ . So the refractive index describes the dispersion of the fibre. Looking retrospectively at Eqs. (5.1.12)-(5.1.14), we see that, in optical fibres, dispersion is a consequence of the non-instantaneous linear response of the material polarization to the electric field. It is therefore associated with a nonlocality in *time*; this should be compared to the acoustic case of Chapter 2, where the dispersion was assumed to arise from nonlocality in *space*.

Confining light to an optical fibre introduces further dispersive effects, for a fibre acts as a waveguide, forcing the waves to travel in a single direction. Using cylindrical coordinates  $\rho$ ,  $\phi$  and  $z$ , Eq. (5.1.21) becomes [62, 63]

$$\partial_\rho^2 \tilde{\mathbf{E}} + \frac{1}{\rho} \partial_\rho \tilde{\mathbf{E}} + \frac{1}{\rho^2} \partial_\phi^2 \tilde{\mathbf{E}} + \partial_z^2 \tilde{\mathbf{E}} + \frac{\omega^2}{c^2} n^2(\omega) \tilde{\mathbf{E}} = 0. \quad (5.1.22)$$

## 5. Nonlinear Fibre Optics

Focusing for clarity on the component  $\tilde{E}_z$  and separating the variables as follows,

$$\tilde{E}_z(\mathbf{r}, \omega) = A(\omega) R(\rho) \exp(im\phi) \exp(i\beta z), \quad (5.1.23)$$

we find that Eq. (5.1.22) is equivalent to the following differential equation for  $R(\rho)$ :

$$\partial_\rho^2 R + \frac{1}{\rho} \partial_\rho R + \left( \frac{\omega^2}{c^2} n^2(\omega) - \beta^2 - \frac{m^2}{\rho^2} \right) R = 0. \quad (5.1.24)$$

This is the equation for Bessel functions of order  $m$  [64]. In order that the solution for the radial dependence should be free of singularities within the fibre core and exponentially decreasing far from the fibre core, only a certain number of discrete solutions are allowed, each corresponding to a particular value of  $\beta$ . Under certain conditions (small core radius and small refractive index difference between core and cladding [63]), only a single value of  $\beta$  corresponds to a given frequency.

For every mode, there are in fact two orthogonal solutions. (When  $\beta$  is single-valued, these correspond approximately to polarization of the electric field along the  $x$ - or the  $y$ -axis [62].) Depending on the transverse structure of the fibre, these two orthogonal modes can have different values of  $\beta$ , so that both frequency *and* polarization can affect wave speed. This phenomenon is known as *birefringence*. The two polarizations are often denoted the *fast* and *slow* axes, depending on their relative speed: hence the slow axis has a higher refractive index than the fast axis.

Factoring out the transverse form of the guided modes (i.e., their  $\rho$ - and  $\phi$ -dependence), the wave equation (5.1.21) is reduced to the one-dimensional form [65]

$$\left( \partial_z^2 \tilde{E} + \beta^2(\omega) \tilde{E} \right) = 0, \quad (5.1.25)$$

and we may define a modified refractive index to satisfy

$$\beta(\omega) = \frac{n'(\omega)\omega}{c}. \quad (5.1.26)$$

$n'(\omega)$  differs from  $n(\omega)$  in Eq. (5.1.21) in that it includes the effects of waveguide dispersion, arising from the restriction of light propagation to a single spatial dimension. In what follows, we always assume a one-dimensional optical fibre, and for convenience we shall simply use  $n(\omega)$  to mean the modified refractive index defined in Eq. (5.1.26).

Eq. (5.1.25) may be transformed back to real space via the substitutions  $\tilde{E} \rightarrow E$  and  $\omega \rightarrow i\partial_t$ . At this point, however, it is convenient to return to Eq. (5.1.11), and to recall that we have only included the linear polarization in Eq. (5.1.25). Reintroducing the nonlinear part of the polarization  $P^{\text{NL}}$ , the full wave equation in real space becomes [65]

$$c^2 (\partial_z^2 + \beta^2(i\partial_t)) E = \frac{1}{\epsilon_0} \partial_t^2 P^{\text{NL}}. \quad (5.1.27)$$

The operator  $\beta^2(i\partial_t)$  is formed by inserting the operator  $i\partial_t$  into the Taylor expansion for  $\beta^2(\omega)$ , analogously to the operator  $F^2(-i\partial_x)$  in Eq. (2.1.4). When the polarization

is assumed linear and  $P^{\text{NL}} = 0$ , the general solution is simply a linear superposition of plane waves with frequency and propagation constant related by  $\beta(\omega)$ . These plane waves evolve independently of each other. When  $P^{\text{NL}}$  is non-zero, the various plane waves may couple to each other, resulting in frequency shifting and Hawking radiation [65].

## 5.2. Nonlinear effects

We have seen how the linear polarization induced in an optical fibre leads to dispersion and birefringence, which are frequency- and polarization-dependencies of the phase velocity of plane waves; or, equivalently, of the propagation constant  $\beta$ . Both of these effects are highly manipulable in photonic crystal fibres [63, 66], and can be made relatively strong. We shall now consider nonlinear effects in fibres.

### 5.2.1. Nonlinear polarization

Although Eq. (5.1.12) yields accurate predictions of wave propagation if the optical power is low, a more general form of the polarization can be written in the manner of a Taylor series, as follows:

$$\mathbf{P} = \mathbf{P}^{(1)} + \mathbf{P}^{(2)} + \mathbf{P}^{(3)} + \dots \quad (5.2.1)$$

where  $\mathbf{P}^{(n)}$  is of order  $n$  in the electric field:

$$P_i^{(n)} = \epsilon_0 \int_{-\infty}^t dt_1 \dots \int_{-\infty}^t dt_n \chi_{ij_1 j_2 \dots j_n}^{(n)}(t - t_1, \dots, t - t_n) E_{j_1}(t_1) \dots E_{j_n}(t_n) . \quad (5.2.2)$$

The  $n^{\text{th}}$ -order susceptibility  $\chi^{(n)}$  is a tensor of rank  $n + 1$ , and we adopt the convention that repeated indices ( $j_1, j_2$ , etc.) are summed over. Eq. (5.1.12) is a special case of Eqs. (5.2.1) and (5.2.2) in which it is assumed that only  $\chi^{(1)}$  is non-zero, and that  $\chi^{(1)}(t)$  is simply a function of time multiplied by the identity operator. This must be true in an isotropic medium, so  $\chi^{(1)}$  will continue to have this form. The next-highest order susceptibility,  $\chi^{(2)}$ , is found to be zero when the molecules of the dielectric are symmetric [63, 67]. This is true of silica; therefore, the lowest-order nonlinear effects are derived from  $\chi^{(3)}$  and the third-order polarization. This is generated from the nonlinear response of electronic vibrations in the fibre medium, and works on a timescale comparable to the transit time of light over the diameter of an atom [63]. We can, therefore, assume this nonlinear response to be instantaneous, and the time dependence of  $\chi^{(3)}$  to be simply the product of three delta functions:

$$\chi_{ij_1 j_2 j_3}^{(3)}(t - t_1, t - t_2, t - t_3) = \chi_{ij_1 j_2 j_3}^{(3)} \delta(t - t_1) \delta(t - t_2) \delta(t - t_3) . \quad (5.2.3)$$

We have seen that there are two orthogonal polarizations of the electric field, which we shall denote by  $E_{\pm}$ , where the subscripts  $+$  and  $-$  represent the fast and slow axes of the fibre, respectively. There will also be two corresponding nonlinear polarizations  $P_{\pm}$ , which, combining Eqs. (5.2.2) and (5.2.3), are related to  $E_{\pm}$  by

$$P_{\pm}^{\text{NL}} = \epsilon_0 \chi_{\pm j_1 j_2 j_3}^{(3)} E_{j_1} E_{j_2} E_{j_3} , \quad (5.2.4)$$

## 5. Nonlinear Fibre Optics

where  $j_1$ ,  $j_2$  and  $j_3$  are summed over  $+$  and  $-$ . Some physical considerations help to simplify Eq. (5.2.4). Firstly, note that  $P_{\pm}^{\text{NL}}$  cannot depend on odd powers of  $E_{\mp}$ : for, if it did, the direction of  $P_{\pm}^{\text{NL}}$  would be determined by the direction of  $E_{\mp}$ , in violation of isotropy. Secondly, and also a consequence of isotropy, we have the relation [63]

$$\chi_{\pm\pm\pm\pm}^{(3)} = \chi_{\pm\pm\mp\mp}^{(3)} + \chi_{\pm\mp\pm\mp}^{(3)} + \chi_{\pm\mp\mp\pm}^{(3)}. \quad (5.2.5)$$

Thus, Eq. (5.2.4) becomes

$$P_{\pm}^{\text{NL}} = \epsilon_0 \chi_{\pm\pm\pm\pm}^{(3)} (E_{\pm}^3 + E_{\mp}^2 E_{\pm}). \quad (5.2.6)$$

Simple though Eq. (5.2.6) may be, it is useful to modify it further. So far, we have taken  $E$  and  $P^{\text{NL}}$  to be real quantities; however, given their oscillatory nature, it is easier for the sake of calculation to replace them with complex quantities by making the substitutions

$$P_{\pm}^{\text{NL}} \rightarrow \frac{1}{2} (P_{\pm}^{\text{NL}} + P_{\pm}^{\text{NL}\star}), \quad (5.2.7)$$

$$E_{\pm} \rightarrow \frac{1}{2} (E_{\pm} + E_{\pm}^{\star}). \quad (5.2.8)$$

Then Eq. (5.2.6) becomes

$$P_{\pm}^{\text{NL}} = \frac{1}{4} \epsilon_0 \chi_{\pm\pm\pm\pm}^{(3)} (E_{\pm}^3 + 3 E_{\pm}^2 E_{\pm}^{\star} + E_{\mp}^2 E_{\pm} + E_{\mp}^2 E_{\pm}^{\star} + 2 E_{\pm} E_{\mp} E_{\mp}^{\star}). \quad (5.2.9)$$

Finally, we note that, in general, only that component of the polarization  $\mathbf{P}^{\text{NL}}$  which has a similar frequency to the electric field  $\mathbf{E}$  will have a significant effect on wave propagation. (Different frequency components require phase matching, which usually occurs only by design.) Taking  $E_{\pm}$  to have a positive frequency, only those terms of  $P_{\pm}^{\text{NL}}$  which include a complex conjugate can satisfy the frequency-matching condition. Finally, then, Eq. (5.2.9) becomes [65]

$$P_{\pm}^{\text{NL}} = \frac{3}{4} \epsilon_0 \chi_{\pm\pm\pm\pm}^{(3)} \left( |E_{\pm}|^2 E_{\pm} + \frac{2}{3} |E_{\mp}|^2 E_{\pm} + \frac{1}{3} E_{\mp}^2 E_{\pm}^{\star} \right). \quad (5.2.10)$$

Although Eq. (5.2.10) is wholly derived from the assumption of a third-order polarization, its various terms are associated with different qualitative effects. The first and second terms describe, respectively, the phenomena of *self-phase modulation* and *cross-phase modulation*; that is, they lead to phase shifts in the electric field as a result of either the nonlinear effect of a polarized field on itself, or of one polarized field on the orthogonally polarized field [63]. The third term describes *four-wave mixing* between the two polarizations [63].

The self-phase modulation term can be decomposed further. If the electric field is composed of two distinct frequency bands, it is useful to separate these components by writing

$$E_{\pm} = E_1 e^{i\beta_1 z - i\omega_1 t} + E_2 e^{i\beta_2 z - i\omega_2 t}, \quad (5.2.11)$$

where  $E_1$  and  $E_2$  are assumed to be slowly-varying compared with the plane waves they multiply. Then the first term of Eq. (5.2.10) becomes

$$|E_{\pm}|^2 E_{\pm} = \left(|E_1|^2 + 2|E_2|^2\right) E_1 e^{i\beta_1 z - i\omega_1 t} + \left(|E_2|^2 + 2|E_1|^2\right) E_2 e^{i\beta_2 z - i\omega_2 t}, \quad (5.2.12)$$

where we have neglected all terms that do not oscillate at  $\omega_1$  or  $\omega_2$  (and therefore require phase matching to have a significant effect). Thus, we see that, within a single polarization, we can separate the nonlinear effects of a certain frequency band on itself and on other frequency bands; these effects are also commonly referred to as self- and cross-phase modulation, where the descriptive terms are now in reference to the frequency rather than the direction of polarization.

### 5.2.2. Optical solitons

One of the most notable consequences of third-order polarization is the existence of stable localised solutions of the wave equation; that is, pulses whose shapes are not distorted during propagation through the fibre [63]. In these specific cases, the nonlinear effects contrive to cancel the linear (dispersive) effects, which acting alone would tend to stretch and smear the pulse. The possibility of stable pulses is useful in forming an analogy with a moving fluid: in the frame co-moving with a stable pulse (introduced in §5.3), the background is time-independent.

Let us derive these stable pulse solutions. Firstly, since we are considering a single electric field with well-defined frequency, the nonlinear polarization includes only the self-phase modulation term; that is,  $P^{\text{NL}} = \frac{3}{4}\epsilon_0\chi^{(3)}|E|^2 E$ . (The subscripts  $\pm$  have been omitted for clarity, though it should be remembered that  $\chi^{(3)}$  may be polarization-dependent.) Secondly, we assume the validity of the *slowly-varying envelope approximation*, i.e., we write the total electric field as the product of an envelope and a carrier wave,

$$E(z, t) = \mathcal{E}(z, t) \exp(i\beta_s z - i\omega_s t), \quad (5.2.13)$$

(where  $\beta_s \equiv \beta(\omega_s)$ ) and assume that the envelope varies on scales much longer than an optical cycle. Specifically, this amounts to the assumption of the validity of the following relations:

$$|\partial_z^2 \mathcal{E}| \ll |\beta_s \partial_z \mathcal{E}|, \quad |\partial_t^2 \mathcal{E}| \ll |\omega_s \partial_t \mathcal{E}|. \quad (5.2.14)$$

Under the slowly-varying envelope approximation, the two sides of the wave equation (5.1.27) can be well-approximated by terms containing only first-order derivatives:

$$c^2 (\partial_z^2 + \beta^2 (i\partial_t)) E \approx \exp(i\beta_s z - i\omega_s t) 2\beta_s c^2 (i\partial_z + \beta - \beta_s) \mathcal{E}, \quad (5.2.15)$$

$$\frac{1}{\epsilon_0} \partial_t^2 P^{\text{NL}} \approx -\exp(i\beta_s z - i\omega_s t) \frac{3}{4} i\chi^{(3)} \omega_s \mathcal{E} \left( -i\omega_s |\mathcal{E}|^2 + 3\partial_t |\mathcal{E}|^2 \right). \quad (5.2.16)$$

In Eq. (5.2.15), when the operator  $\beta$  acts on the envelope  $\mathcal{E}$  rather than the full electric field  $E$ , it should be remembered that it is the difference frequency  $\omega - \omega_s$  which is

## 5. Nonlinear Fibre Optics

replaced by the operator  $i\partial_t$ , and not  $\omega$  itself. Forming a second-order Taylor expansion of  $\beta$  at the pulse frequency  $\omega_s$ ,

$$\beta \approx \beta_s + \beta_{1,s}(\omega - \omega_s) + \frac{1}{2}\beta_{2,s}(\omega - \omega_s)^2, \quad (5.2.17)$$

we can write Eq. (5.2.15) in the form

$$c^2 (\partial_z^2 + \beta^2 (i\partial_t)) E \approx \exp(i\beta_s z - i\omega_s t) 2\beta_s c^2 \left( i\partial_z + i\beta_{1,s}\partial_t - \frac{1}{2}\beta_{2,s}\partial_t^2 \right) \mathcal{E}. \quad (5.2.18)$$

In Eq. (5.2.16), we assume that the intensity  $|\mathcal{E}|^2$  also varies slowly in comparison with the frequency  $\omega_s$ , so that we can neglect the derivative term. Making these approximations and setting the two sides of the wave equation equal, we obtain

$$i \left( \partial_t + \frac{1}{\beta_{1,s}} \partial_z \right) \mathcal{E} - \frac{\beta_{2,s}}{2\beta_{1,s}} \partial_t^2 \mathcal{E} + \frac{3}{8} \chi^{(3)} \frac{\omega_s^2}{c^2 \beta_s \beta_{1,s}} |\mathcal{E}|^2 \mathcal{E} = 0. \quad (5.2.19)$$

The combination of first-order derivatives in Eq. (5.2.19) strongly suggests the usefulness of the following coordinate transformation:

$$z' = z, \quad (5.2.20)$$

$$\tau = t - \beta_{1,s} z. \quad (5.2.21)$$

Since  $\beta_{1,s}$  is simply the inverse of the group velocity of the pulse, this is a transformation into a frame of reference that moves with the pulse; we shall have more to say about it later. The partial derivatives of the various coordinates are related as follows:

$$\partial_z = \partial_{z'} - \beta_{1,s} \partial_\tau, \quad (5.2.22)$$

$$\partial_t = \partial_\tau, \quad (5.2.23)$$

and substituting these in Eq. (5.2.19) yields

$$i\partial_{z'} \mathcal{E} - \frac{1}{2}\beta_{2,s}\partial_\tau^2 \mathcal{E} + \frac{3\chi^{(3)}\omega_s^2}{8c^2\beta_s} |\mathcal{E}|^2 \mathcal{E} = 0. \quad (5.2.24)$$

Eq. (5.2.24) is very similar in form to the Schrödinger equation; the only mathematical difference is that the “potential” depends on the squared magnitude of the “wavefunction”  $\mathcal{E}$ . (Of course, there is also the physical difference that space and time coordinates have been interchanged, a consequence of the transformation (5.2.20)-(5.2.21). We shall return to this point in §5.3.) For this reason, it is often referred to as the *nonlinear* Schrödinger equation. It describes the propagation of a pulse, taking into account dispersive effects via the  $\partial_\tau^2 \mathcal{E}$  term, and nonlinear effects via the  $|\mathcal{E}|^2 \mathcal{E}$  term. As has been stated, one of its most important properties is its admittance of stable solutions whose shapes do not change during their propagation, thus achieving a perfect balance between the dispersive and nonlinear effects. These solutions are only possible when  $\beta_{2,s} < 0$ , i.e., when the group velocity dispersion is anomalous. This makes intuitive sense, for the nonlinearity

cannot be negative, and so one sign of the dispersion should help to increase the nonlinear effects while the other should contrive to cancel it out.

The stable solution is [63, 68]

$$\mathcal{E} = \mathcal{E}_0 \operatorname{sech} \left( \frac{\tau}{T_s} \right) \exp \left( i \frac{|\beta_{2,s}| z'}{2T_s^2} \right) \quad (5.2.25)$$

$$= \mathcal{E}_0 \operatorname{sech} \left( \frac{t - \beta_{1,s} z}{T_s} \right) \exp \left( i \frac{|\beta_{2,s}| z}{2T_s^2} \right) \quad (5.2.26)$$

where

$$\mathcal{E}_0^2 = \frac{8c^2 \beta_s |\beta_{2,s}|}{3\chi^{(3)} \omega_s^2 T_s^2}. \quad (5.2.27)$$

A pulse of the form of Eq. (5.2.26) is called a *fundamental soliton* [63]. (Higher-order solitons exist, with shapes which are not constant but periodic in  $z$  [63, 68]. These, however, are not relevant to our discussions.) Note that, at a given frequency  $\omega_s$  (which must obey the condition  $\beta_{2,s} = \partial^2 \beta / \partial \omega^2 (\omega_s) < 0$ ), the fundamental solitons form a one-parameter family of solutions of the nonlinear Schrödinger equation. The parameter that characterises them is  $T_s$ , the “width” of the soliton. (For the intensity profile  $|\mathcal{E}|^2$ , the full-width half-maximum is approximately  $1.76 T_s$ ). Note that, as a consequence of its nonlinear nature, the peak intensity of the soliton is entirely determined by  $T_s$ , and becomes larger as  $T_s$  is made smaller. Thus, solitons vary between long, weak pulses and short, intense pulses.

### 5.2.3. Pulse and probe

For our purposes, we shall mostly be interested in cross-phase modulation. We shall consider two fields: one an optical pulse, which we usually take to be a fundamental soliton; the other a continuous-wave probe, whose intensity is much less than that of the pulse. These are well-separated in frequency, and we denote their central frequencies by  $\omega_s$  and  $\omega_p$ , respectively. The nonlinear effects acting between these two fields will be essentially unidirectional, with the pulse acting on the probe, since the low intensity of the latter means that, to a very good approximation, we can neglect any back-reaction on the pulse. From Eqs. (5.2.10) and (5.2.12), we find that the appropriate nonlinear polarization is

$$P^{\text{NL}} = \frac{r}{2} \epsilon_0 \chi^{(3)} |E_s|^2 E_p, \quad (5.2.28)$$

where

$$r = \begin{cases} 3 & \text{fields similarly polarized} \\ 1 & \text{fields orthogonally polarized} \end{cases}. \quad (5.2.29)$$

This nonlinear polarization is in the same direction as the probe field  $E_p$ . Substituting in the wave equation (5.1.27), we find

$$c^2 [\partial_z^2 + \beta^2 (i\partial_t)] E_p = \partial_t^2 (\chi E_p), \quad (5.2.30)$$

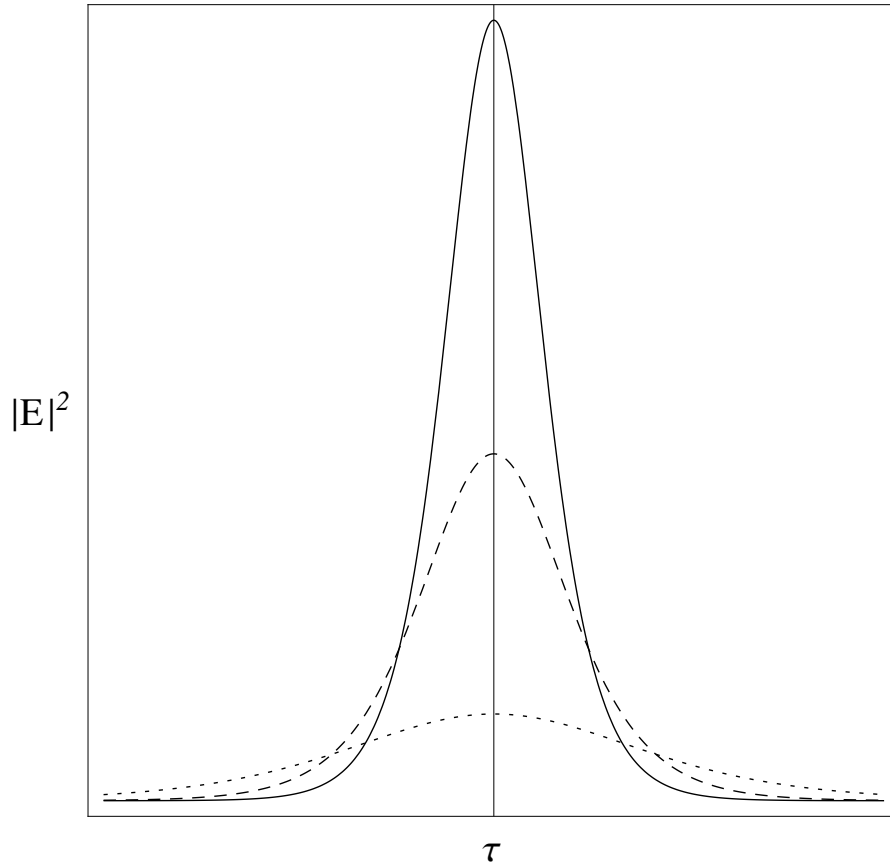


Figure 5.1.: OPTICAL SOLITONS: For a frequency at which  $\partial^2\beta/\partial\omega^2 < 0$ , the dispersive and nonlinear effects of wave propagation contrive to cancel each other out, and stable solutions called solitons are possible. Here, the optical intensity of several solitons is plotted; and, in accordance with Eq. (5.2.27), the peak power is proportional to  $1/T_s^2$ , where  $T_s$  is the soliton width.



where the nonlinear susceptibility  $\chi$  induced by the pulse is given by

$$\chi = \frac{r}{2} \chi^{(3)} |E_s|^2. \quad (5.2.31)$$

Since the propagation constant  $\beta = \omega n(\omega)/c$ , Eq. (5.2.30) can be written in the form

$$c^2 \partial_z^2 E_p - \partial_t^2 n^2 (i \partial_t) E_p - \partial_t^2 (\chi E_p) = 0, \quad (5.2.32)$$

whence we see that the influence of  $\chi$  on the probe is as a local change of refractive index,

$$n_{\text{eff}}^2 = n^2 + \chi. \quad (5.2.33)$$

This increase in refractive index is often referred to as the *Kerr effect*.

Let us briefly consider the implications of Eq. (5.2.33). The behaviour of waves is usually described by a refractive index profile, and where we restrict our attention to waves of relatively low intensity, the refractive index, while it depends on frequency, is constant along the fibre. Thus, a certain frequency will propagate with the same phase and group velocity at all times, and the complexity of propagation of a wavepacket is due to the fact that the phase and group velocities differ for different frequencies. This is the dispersion phenomenon, which is entirely described by the linear polarization, all higher-order polarizations being negligible.

With the introduction of a relatively intense pulse and the third-order polarization induced by it, a new phenomenon comes to light: while we can still describe the behaviour of waves by a refractive index profile, this profile now obtains a dependence on position (and time), the change being proportional to the intensity of the pulse and thus propagating along the fibre as the pulse does. (Recall that we have assumed an instantaneous third-order polarization; in reality the refractive index change will lag very slightly behind the pulse, but in most circumstances we can neglect this lag.) If a probe wave also propagates down the fibre, it will experience a transient increase in refractive index and, hence, a decrease in its phase velocity. Dispersion will also cause a small shift in the frequency of the wave. Usually, this transient effect will be almost negligible; but, if either the phase or group velocity of the probe is initially very close to the group velocity of the pulse, so that their relative speed is very small, the effect of the pulse may be very significant.

## 5.3. Co-moving frame

### 5.3.1. Coordinate transformation

Let us examine further the setup of an intense pulse propagating in an optical fibre, and its effect on weak probe waves. This is most easily done in a frame of reference in which the pulse is stationary. Such a frame is constructed via the following coordinate transformation:

$$\zeta = \frac{z}{u}, \quad (5.3.1)$$

$$\tau = t - \frac{z}{u}, \quad (5.3.2)$$

## 5. Nonlinear Fibre Optics

where  $u$  is the group velocity of the pulse; this transformation is illustrated in Figure 5.2. Note that this is essentially the same as the transformation made in Eqs. (5.2.20) and (5.2.21), the only difference being that, instead of keeping the propagation distance, we have now normalised it with respect to the velocity to get the propagation time. It is very similar to a Galilean transformation, differing in that the roles of space and time have been reversed. (This causes the counter-propagating  $v$ -modes to appear to travel backwards in time, as shown in Fig. 5.2.) It is clear that the pulse remains centered at  $\tau = 0$  and is independent of  $\zeta$ , so that the nonlinear susceptibility is simply a function of  $\tau$ :  $\chi = \chi(\tau)$ . Note that the transformation defined by Eqs. (5.3.1) and (5.3.2) is not a Lorentz transformation, an inequality made more pronounced by the fact that  $u$ , the speed of a pulse in an optical fibre, is comparable with  $c$ , the speed of light in vacuum. The coordinates  $\zeta$  and  $\tau$ , then, do not correspond to space and time coordinates in the co-moving frame. They do, however, define a perfectly valid (non-inertial) coordinate system; we can solve the wave equation in this coordinate system and invert the transformation to find the solution in the original laboratory frame.

The partial derivatives in the co-moving and the lab frame are related via

$$\partial_z = \frac{1}{u} (\partial_\zeta - \partial_\tau) , \quad (5.3.3)$$

$$\partial_t = \partial_\tau . \quad (5.3.4)$$

Substituting into the wave equation (5.2.30) for the probe/pulse system, we find

$$(\partial_\zeta - \partial_\tau)^2 E_p + u^2 \beta^2 (i \partial_\tau) E_p - \frac{u^2}{c^2} \partial_\tau^2 (\chi E_p) = 0 . \quad (5.3.5)$$

This is the desired wave equation for weak probe waves in the presence of an intense pulse. It is now clear why the roles of space and time have been switched from the usual Galilean transformation in Eqs. (5.3.1) and (5.3.2): this leaves the time derivative unchanged, and hence the operator  $\beta^2 (i \partial_t)$  maintains its simple form. (This should be compared with Eq. (2.1.4), where the dispersion operator contains derivatives with respect to space rather than time.)

It is more useful to express the optical wave equation in terms of the vector potential  $A_p$ , which is related to the electric and magnetic fields via

$$E_p = -\partial_t A_p , \quad B_p = \partial_z A_p , \quad (5.3.6)$$

for then Eq. (5.3.5) becomes

$$(\partial_\zeta - \partial_\tau)^2 A_p + u^2 \beta^2 (i \partial_\tau) A_p - \frac{u^2}{c^2} \partial_\tau (\chi \partial_\tau A_p) = 0 . \quad (5.3.7)$$

Although this difference may seem trivial, Eq. (5.3.7) is preferable to Eq. (5.3.5) because it can be derived from a relatively simple Lagrangian, analogous to that of Eq. (2.1.2) for the acoustic model. We defer discussion of this until §7.1.

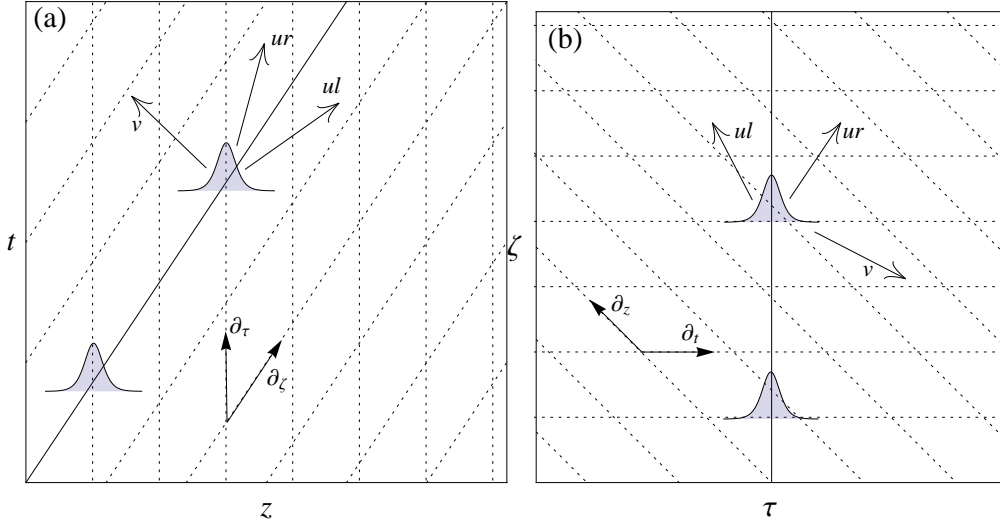


Figure 5.2.: CO-MOVING FRAME: The system of a pulse in an optical fibre, as seen from the lab frame in Figure (a), and from the co-moving frame in Figure (b); these are related via the coordinate transformation in Eqs. (5.2.20) and (5.2.21). Note the behaviour of waves in the two frames: the co-propagating  $u$ -modes are split between those moving faster or slower than the pulse, and these have different directions in the co-moving frame; the counter-propagating  $v$ -modes, travelling towards negative  $z$ , appear to move backwards in *time* in the co-moving frame. Also note the apparent flip between left and right: in the co-moving frame, points with a negative value of  $\tau$  (retarded time) are *further along the fibre* than the pulse.

### 5.3.2. Dispersion relation

The wave equation is generally solved by decomposing a solution into its plane wave components. It is useful, therefore, to know the dispersion relation in the co-moving frame, to see how these plane waves behave. First, we must define appropriate variables. In the usual laboratory frame, in which we have coordinates  $(z, t)$ , we also have wavenumber  $k$  and frequency  $\omega$ . These are defined as derivatives of the phase: we assume a solution of the form

$$A = \mathcal{A} \exp(i\varphi) \quad (5.3.8)$$

where  $\mathcal{A}$  and  $\varphi$  are real quantities.  $k$  and  $\omega$  are then defined as follows:

$$k = \partial_z \varphi, \quad \omega = -\partial_t \varphi. \quad (5.3.9)$$

In the co-moving frame defined by the coordinate transformation Eqs. (5.3.1) and (5.3.2), we have coordinates  $(\tau, \zeta)$ , both of which have dimensions of time. We define two frequencies,  $\omega$  and  $\omega'$ , as follows:

$$\omega = -\partial_\tau \varphi, \quad \omega' = -\partial_\zeta \varphi. \quad (5.3.10)$$

The definitions of Eqs. (5.3.9) and (5.3.10) are related via the transformation of the partial derivatives, Eqs. (5.3.3) and (5.3.4). Eq. (5.3.4) shows that the two definitions of  $\omega$  are equivalent, hence the use of the same variable. Eq. (5.3.3) yields the relation

$$k = \frac{1}{u} (\omega - \omega'), \quad \text{or} \quad \omega' = \omega - uk. \quad (5.3.11)$$

$\omega'$ , then, is simply the Doppler-shifted frequency measured in the co-moving frame. For this reason, we shall refer to it as the *co-moving* frequency; in contrast,  $\omega$  will be referred to as the *lab* frequency.

We saw in Eq. (5.2.33) that the nonlinearity  $\chi$  behaves as an increase in the square of the refractive index:  $n_{\text{eff}}^2 = n^2 + \chi$ . Assuming  $\chi$  is constant in both space and time, this can be incorporated into the dispersion relation. Defining

$$\beta_\chi(\omega) = \frac{n_{\text{eff}}(\omega)\omega}{c} \approx \frac{\omega}{c} \left( n(\omega) + \frac{\chi}{2n(\omega)} \right), \quad (5.3.12)$$

where the second step is valid if  $\chi \ll n^2(\omega)$ , then we have

$$k = \frac{1}{u} (\omega - \omega') = \pm \beta_\chi(\omega), \quad (5.3.13)$$

or, rearranging,

$$\begin{aligned} \omega' &= \omega \mp u\beta_\chi(\omega) \\ &= \omega \left( 1 \mp \frac{u}{c} n_{\text{eff}}(\omega) \right) \\ &\approx \omega \left( 1 \mp \frac{u}{c} \left( n(\omega) + \frac{\chi}{2n(\omega)} \right) \right). \end{aligned} \quad (5.3.14)$$

This is the dispersion relation in the co-moving frame. The effect of the nonlinearity is to alter the form of the dispersion profile  $\beta_\chi(\omega)$ ; it does not affect the velocity  $u$ , which is assumed constant. There are two branches of the dispersion relation, corresponding to probe waves which propagate either with (*co-propagating*, or *u-modes*) or against (*counter-propagating*, or *v-modes*) the pulse. We shall deal mainly with co-propagating waves, which take the plus sign in Eq. (5.3.13) and the minus sign in Eq. (5.3.14).

## 5.4. Conclusion and discussion

The interaction between electromagnetic waves and matter is entirely determined by the induced polarization,  $\mathbf{P}$ , of the matter. We have seen that the linear response determines the refractive index  $n(\omega)$ , but this is not sufficient to allow different wave components to interact. For this, we must introduce the nonlinear component of the polarization, the lowest order of which is the third order. We have seen that third-order polarization gives rise to several different effects, and we paid particular attention to the existence of optical solitons and the interaction of an intense pulse with a low-intensity probe wave. The coordinate transformation of Eqs. (5.3.1) and (5.3.2) defines a reference frame in which the pulse is stationary. The interaction of this pulse with a probe wave is described by a wave equation, Eq. (5.3.7), which in turn yields the dispersion relation of Eq. (5.3.14).

It is this dispersion relation that is most useful in pinning down the analogy with waves in moving fluids. Since it is independent of  $\zeta$ ,  $\omega'$  is a conserved quantity, much as  $\omega$  is conserved in the acoustic model.  $\omega'$  depends on both  $\omega$  and  $\chi$ , where  $\chi$  is in general  $\tau$ -dependent; in the acoustic model,  $\omega$  is a function of  $k$  and  $V$ , where  $V$  is in general  $x$ -dependent. The essential difference between the two models is the following: in the acoustic model, the inhomogeneity of wave speed is due to a change in the flow velocity, the dispersion profile remaining unchanged; in the optical model, the flow velocity is constant, and the change in wave speed is brought about by an effective change in the dispersion profile, and hence a change in the wave speed with respect to the medium. These behave differently when the effects on co-propagating and counter-propagating wave are compared: for an inhomogeneous flow velocity, the change in speed is in the same direction for both *u*- and *v*-modes; for an inhomogeneous dispersion profile, the change in speed is opposite in direction for *u*- and *v*-modes. But, for a single branch, the two situations are indistinguishable, the total wave velocity being the important quantity. We thus expect the interaction of co-propagating probe waves with a light pulse to exhibit the same features of horizons already demonstrated by the acoustic waves in a moving medium. In the next Chapter, we shall encounter frequency shifting, like that seen in wavepacket propagation simulations for acoustic waves, showing that group-velocity horizons can exist in optical fibres. In Chapter 7, we shall develop the theory of spontaneous photon creation in optical fibres, closely following the derivation given in Chapter 2 for the acoustic model.



## 6. Frequency Shifting in Optical Fibres

The existence of event horizons in optical fibres can be demonstrated by the classical effect of frequency shifting [65, 69], and it is to this phenomenon that we first direct our attention. We begin by expounding the black and white hole analogies, and using straightforward geometrical optics we explain why we expect these to be induced by a light pulse in an optical fibre. We then solve the full wave equation, and compare our theoretical predictions with experimental observations. There are some discrepancies. Another nonlinear effect - the *Raman effect* - is invoked in an attempt to explain these discrepancies, but ultimately it fails to do so.

The main analysis and results of this chapter are presented in Reference [69].

### 6.1. The fiber-optical analogy and geometrical optics

As discussed in Chapter 5, pulses in fibres simulate a non-trivial flow velocity profile that moves with respect to the medium. Through the Kerr effect, the pulse effectively increases the local refractive index of the fiber. Since the speed of light waves is determined by the refractive index, this behaves like a perturbation in the flow velocity of the medium. In the co-moving frame in which the pulse is stationary, the fiber appears as a moving medium, with constant background flow equal in magnitude - but opposite in direction - to the velocity of the pulse. A co-propagating wave attempts to move against this flow, and the decrease in velocity induced by interaction with the pulse can be described as a dip in the local flow velocity; that is, to complete the analogy with a moving fluid, the medium must be considered as moving faster (in the backward direction) in the vicinity of the pulse. If the incident wave already has a low speed in the co-moving frame, then it is possible that this dip forms an event horizon. In fact, if a horizon is formed at all, there must be a pair of horizons: a white hole at the pulse's trailing edge, where the medium's speed decreases in the direction of flow, and a black hole horizon at the leading edge, where the opposite occurs.

Suppose there is a frequency at which this pair of horizons is formed. Let a wavepacket at this frequency be incident on the pulse. How does this wavepacket behave? Numerical simulations show that it is reflected from the pulse with a different frequency, a process called *frequency shifting*. This is illustrated in Figure 6.1 - it is also analogous to the frequency shifting seen in Figure 3.1 - and can be understood conceptually as follows. Let us focus initially on the white hole horizon on the pulse's trailing edge. An incident wave, propagating against the flow of the medium, is slowed by the increase in flow velocity. The front of the wavepacket interacts with the pulse first, and will be slowed down before the back of the wavepacket; this results in a compression of its wavefronts, and an increase in its frequency. It might be considered that this continues indefinitely, the

## 6. Frequency Shifting in Optical Fibres

wavepacket becoming squashed at the horizon with ever-increasing frequency. Dispersion, however, limits this shifting, for an increase in frequency, as experienced by the incident wavepacket, is also accompanied by a decrease in speed with respect to the medium (assuming normal dispersion). At some point, the wave's speed becomes less than the flow velocity of the medium, and the wave is dragged back away from the horizon. The overall result is reflection of the wavepacket at a higher frequency: a white hole causes *blueshifting*.

A similar process can occur at the black hole horizon on the pulse's leading edge, but it is more difficult to describe in real time. Thankfully, the time-reversal symmetry of black holes and white holes can be invoked here: the process that occurs at the black hole horizon is simply the time-reverse of a corresponding process at the white hole horizon. If a certain frequency is blueshifted by the white hole horizon, then the resulting frequency will be shifted back to the original frequency by the black hole horizon. A black hole, then, causes *redshifting*.

The value of the frequency shift is easily determined, for the frequency shifting process must conform to the conservation of co-moving frequency,  $\omega'$ . This allows a diagrammatic interpretation of the process. Let us examine the dispersion relation, including the  $\tau$ -dependent change induced by the pulse, so that  $\beta$  becomes a function of both  $\omega$  and  $\tau$ :

$$\beta(\omega, \tau) = \frac{\omega}{c} (n(\omega) + \delta n(\omega, \tau)) . \quad (6.1.1)$$

(Recall that  $\delta n$  is approximately equal to  $\chi/2n$ .) The co-moving frequency is given by

$$\omega' = \omega - u\beta(\omega, \tau) = \omega \left( 1 - \frac{u}{c} (n(\omega) + \delta n(\omega, \tau)) \right) . \quad (6.1.2)$$

Assuming  $u/c$  and  $n(\omega)$  are given, the condition that  $\omega'$  is constant determines a family of contours in the  $\omega$ - $\delta n$  plane. An example is shown in Fig. 6.2. The incoming lab frequency  $\omega$  determines the value of  $\omega'$  ( $\delta n = 0$  far from the pulse), and hence on which of these contours the wave lies. During the interaction, it must always lie on this contour. Frequency shifting, which causes reflection in the co-moving frame, takes place in a frequency window around the frequency  $\omega_m$  at which the group velocity in the co-moving frame vanishes;  $\omega_m$  is the group-velocity-matching frequency which has the same group velocity as the pulse. Taylor expanding  $\beta(\omega)$  around this frequency, we have

$$\beta(\omega) = \beta_{0,m} + \beta_{1,m}(\omega - \omega_m) + \frac{1}{2}\beta_{2,m}(\omega - \omega_m)^2 \quad (6.1.3)$$

where  $\beta_{j,m} \equiv \partial^j \beta / \partial \omega^j (\omega_m)$ . Using the fact that  $\beta_1$  is the inverse of the group velocity, and so  $\beta_{1,m} = 1/u$ , plugging this into Eq. (6.1.2) gives

$$\omega' \approx \omega'_m - \frac{1}{2}\beta_{2,m}u(\omega - \omega_m)^2 - \frac{u}{c}\omega\delta n , \quad (6.1.4)$$

or

$$\delta n \approx \frac{c}{u} \frac{1}{\omega_m} \left[ \omega'_m - \omega' - \frac{1}{2}\beta_{2,m}u(\omega - \omega_m)^2 \right] , \quad (6.1.5)$$



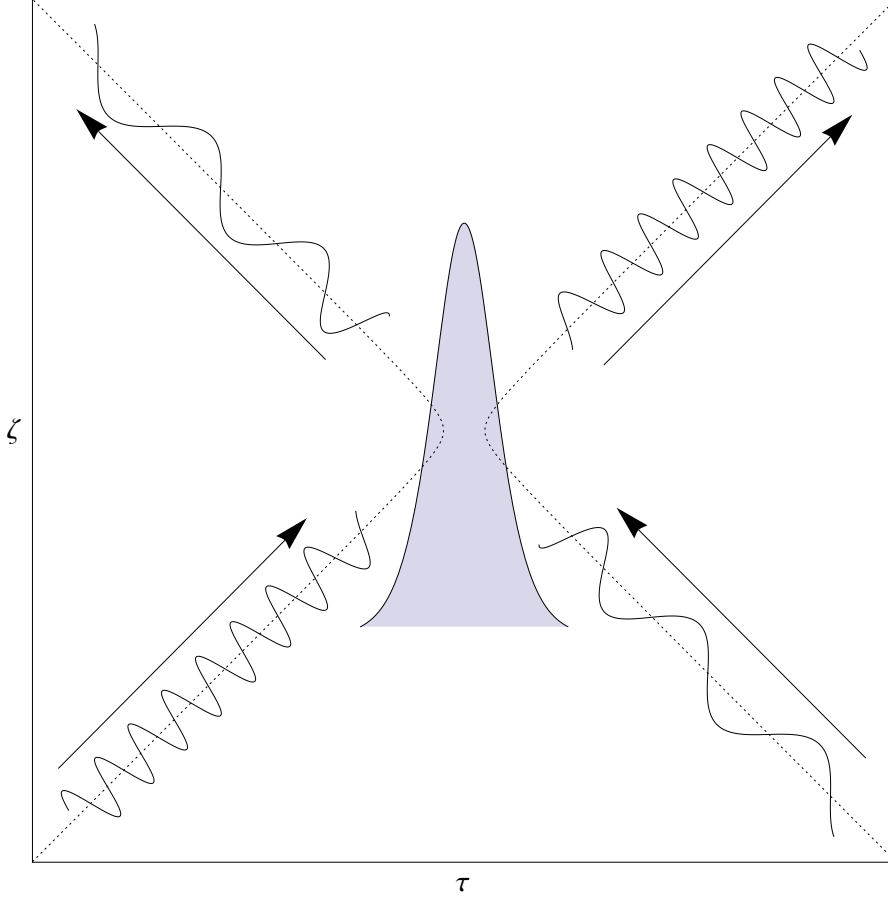


Figure 6.1.: FREQUENCY SHIFTING BY A PULSE: Nonlinear effects effectively increase the refractive index in the vicinity of the pulse. This causes a slight decrease in the phase velocity of incident waves, changing their wavelength; in turn, the dispersion of the fibre causes a corresponding change in the group velocity. For some frequencies, this results in a reflection from the pulse. The white hole horizon at the trailing edge of the pulse cause blueshifting, while the black hole horizon at the leading edge causes redshifting.

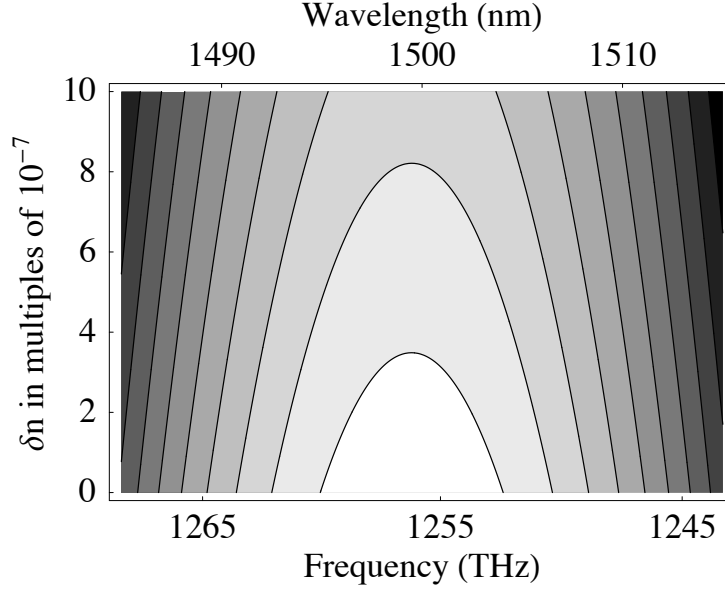


Figure 6.2.: FREQUENCY SHIFTING CONTOURS: Each contour corresponds to a single co-moving frequency,  $\omega'$ , in the  $\omega$ - $\delta n$  plane. As described by Eq. (6.1.5), these contours form parabolas centred at the group-velocity-matching frequency,  $\omega_m$ .

where  $\omega'_m \equiv \omega_m - u\beta_{0,m}$ . Around the group-velocity-matching frequency, the contours of constant  $\omega'$  form parabolas centred at  $\omega_m$ . When a wave first encounters the pulse, it moves to a higher value of  $\delta n$ , and its lab frequency  $\omega$  must also change accordingly. The end result depends on the maximum value of  $\delta n$ . It is seen from Eq. (6.1.5) that the height of the contour is  $(\omega'_m - \omega')c/u\omega_m$ . If this is greater than  $\delta n_{max}$ , then the wave cannot pass over the peak of the contour. It sees the pulse as a transient change in velocity, moving to a slightly different frequency while traversing it, then returning to its original frequency on clearing the pulse; it experiences no event horizon. On the other hand, if the height of the contour is *less* than  $\delta n_{max}$ , the situation is very different: now, the wave cannot pass over the peak of the *pulse*, and must pass over the peak of the contour instead. Thus it lands at the shifted frequency  $2\omega_m - \omega$  (the second zero of the parabola), whose group velocity is opposite to that of the incident frequency. The position of the event horizon is well-defined: it is that point at which the value of  $\delta n$  is equal to the height of the contour, and beyond which the wave cannot penetrate. What is more, the contour whose height is equal to  $\delta n_{max}$  marks the edge of the frequency window for which frequency shifting is possible: those frequencies enclosed within this contour will experience an event horizon and be frequency-shifted, while those outside of this contour will be able to pass through the pulse.

## 6.2. Wave solutions of the pulse-probe interaction

So far, we have used geometrical optics - in which waves travel on well-defined ray trajectories - to discuss the frequency shifting process. This led to the conclusion that a given wave will either pass through the pulse or be reflected from it at a shifted frequency. Real waves, however, are spatially extended, and cannot have well-defined values of both  $\omega$  and  $\tau$  as required by Eq. (6.1.2). Frequency shifting can be described more accurately by a full wave treatment of the optical field.

Firstly, let us define the difference frequencies

$$\bar{\omega} = \omega - \omega_m, \quad \bar{\omega}' = \omega' - \omega'_m,$$

so that the dispersion relation (not including any local perturbations due to the pulse) is simply

$$\bar{\omega}' = -\frac{1}{2}\beta_{2,m}u\bar{\omega}^2. \quad (6.2.1)$$

Defining the envelope  $\mathcal{A}$  such that the probe field  $A_p = \mathcal{A} \exp(-i\omega'_m\zeta - i\omega_m\tau)$ , the pulse-probe interaction is described by the wave equation [63]

$$-i\partial_\zeta \mathcal{A} + \frac{1}{2}\beta_{2,m}u\partial_\tau^2 \mathcal{A} = \frac{2}{3}r\gamma_m P \mathcal{A}, \quad (6.2.2)$$

where  $P$  is the optical power of the pulse,  $\gamma_m$  is the nonlinear coefficient at the group-velocity-matching frequency, and  $r$  is a dimensionless constant that depends on the relative polarization of the pulse and probe ( $r = 3$  for co-polarized,  $r = 1$  for cross-polarized). We have assumed that the intensity of the probe is very weak compared to that of the pulse, so that any back-reaction on the pulse and any self-interaction of the probe is negligible.

Assuming the pulse power  $P$  is independent of  $\zeta$ , Eq. (6.2.2) is equivalent in form to the time-dependent Schrödinger equation. Factoring out a  $\zeta$ -dependent phase,

$$\mathcal{A} = \psi_{\bar{\omega}} \exp(-i\bar{\omega}'\zeta), \quad (6.2.3)$$

leads to the time-independent form

$$-\frac{2}{\beta_{2,m}u}\bar{\omega}'\psi_{\bar{\omega}} = \bar{\omega}^2\psi_{\bar{\omega}} = -\partial_\tau^2\psi_{\bar{\omega}} + \frac{2r\gamma_m}{\beta_{2,m}}P\psi_{\bar{\omega}}, \quad (6.2.4)$$

where we used Eq. (6.2.1) to simplify the left-hand side.

If the pulse power  $P$  is truly independent of  $\zeta$ , then the pulse must be a fundamental soliton. Therefore, the optical power has the form

$$P(\tau) = \frac{|\beta_{2,s}|}{T_s^2\gamma_s} \text{sech}^2\left(\frac{\tau}{T_s}\right), \quad (6.2.5)$$

where  $T_s$  is the soliton width (full width at half maximum  $\approx 1.76 T_s$ ),  $\gamma_s$  is the nonlinear coefficient at the soliton frequency  $\omega_s$ , and  $\beta_{2,s} = \partial^2\beta/\partial\omega^2(\omega_s) < 0$  (since solitons can only exist in regions of anomalous dispersion). Eq. (6.2.4) now becomes

$$\bar{\omega}^2 T_s^2 \psi_{\bar{\omega}} = -T_s^2 \partial_\tau^2 \psi_{\bar{\omega}} + 2r \frac{\gamma_m}{\gamma_s} \frac{|\beta_{2,s}|}{\beta_{2,m}} \text{sech}^2\left(\frac{\tau}{T_s}\right) \psi_{\bar{\omega}}. \quad (6.2.6)$$

## 6. Frequency Shifting in Optical Fibres

This equation is exactly solvable (see Problem 4, §25 of Ref. [59]); the solution is

$$\psi_{\bar{\omega}} = \left( \frac{1}{4} (1 - \xi^2) \right)^{i\bar{\omega}T_s/2} {}_2F_1 \left[ i\bar{\omega}T_s - \sigma, i\bar{\omega}T_s + \sigma + 1; i\bar{\omega}T_s + 1; \frac{1}{2} (1 - \xi) \right], \quad (6.2.7)$$

where

$$\xi = \tanh \left( \frac{\tau}{T_s} \right)$$

and

$$\sigma = \frac{1}{2} \left( -1 + \sqrt{1 - 8r \frac{\gamma_m}{\gamma_s} \frac{|\beta_{2,s}|}{\beta_{2,m}}} \right). \quad (6.2.8)$$

${}_2F_1[a, b; c; z]$  is a hypergeometric function:

$${}_2F_1[a, b; c; z] = \sum_{n=0}^{\infty} \frac{(a)_n (b)_n}{(c)_n} \frac{z^n}{n!}, \quad (a)_n = a(a+1) \dots (a+n-1) = \frac{\Gamma(a+n)}{\Gamma(a)}.$$

Although Eq. (6.2.7) is exact, it is not especially helpful in this form. Its complicated nature makes it very difficult to use in calculations, and it is not obvious what the solution actually looks like. Fortunately, it is relatively easy to simplify it. Since the “potential” of Eq. (6.2.4) is proportional to the pulse power, it is non-zero only in a relatively short region; outside this region, the general solution is simply a sum of the plane waves  $\exp(-i\bar{\omega}\tau)$  and  $\exp(i\bar{\omega}\tau)$ . These are precisely the plane waves converted into each other by frequency shifting (they share the same value of  $\omega'$ , and are equidistant from the group-velocity-matching frequency  $\omega_m$ , which of course has a difference frequency  $\bar{\omega} = 0$ ). So, in the limit  $\tau \rightarrow \pm\infty$  (or  $\xi \rightarrow \pm 1$ ), the exact solution Eq. (6.2.7) should degenerate into sums of these plane waves. Indeed, the solution is normalized such that, as  $\tau \rightarrow \infty$ ,  $\psi_{\bar{\omega}} \rightarrow \exp(-i\bar{\omega}\tau)$ . In the other asymptotic region, as  $\tau \rightarrow -\infty$ , the form of  $\psi_{\bar{\omega}}$  is found to be

$$\psi_{\bar{\omega}} \rightarrow \frac{\Gamma(i\bar{\omega}T_s + 1) \Gamma(i\bar{\omega}T_s)}{\Gamma(i\bar{\omega}T_s + \sigma + 1) \Gamma(i\bar{\omega}T_s - \sigma)} \exp(-i\bar{\omega}\tau) + \frac{\Gamma(i\bar{\omega}T_s + 1) \Gamma(-i\bar{\omega}T_s)}{\Gamma(\sigma + 1) \Gamma(-\sigma)} \exp(i\bar{\omega}\tau).$$

Multiplying through by a constant, we can write the asymptotic form of the solution

$$\psi_{\bar{\omega}}(\tau) \rightarrow \begin{cases} \exp(-i\bar{\omega}\tau) + R_{\bar{\omega}} \exp(i\bar{\omega}\tau), & \tau \rightarrow -\infty \\ T_{\bar{\omega}} \exp(-i\bar{\omega}\tau), & \tau \rightarrow +\infty \end{cases}, \quad (6.2.9)$$

where we have defined

$$R_{\bar{\omega}} = \frac{\Gamma(-i\bar{\omega}T_s) \Gamma(i\bar{\omega}T_s + \sigma + 1) \Gamma(i\bar{\omega}T_s - \sigma)}{\Gamma(i\bar{\omega}T_s) \Gamma(\sigma + 1) \Gamma(-\sigma)} \quad (6.2.10)$$

and

$$T_{\bar{\omega}} = \frac{\Gamma(i\bar{\omega}T_s + \sigma + 1) \Gamma(i\bar{\omega}T_s - \sigma)}{\Gamma(i\bar{\omega}T_s + 1) \Gamma(i\bar{\omega}T_s)}. \quad (6.2.11)$$

## 6.2. Wave solutions of the pulse-probe interaction

Assuming for the moment that  $\bar{\omega}$  is positive - that is,  $\omega$  is greater than the group-velocity-matching frequency  $\omega_m$  - the asymptotic solutions of Eq. (6.2.9) describe a plane wave,  $\exp(-i\bar{\omega}\tau)$ , incident on the pulse from negative  $\tau$ . This implies, in the lab frame, that the wave of frequency  $\omega$  has a group velocity less than that of the pulse, and that the pulse is able to catch up with it. It interacts with the pulse's leading edge, where there may be a black hole event horizon. There is thus a reflected component,  $R_{\bar{\omega}} \exp(i\bar{\omega}\tau)$ , at a lower (redshifted) frequency and travelling back towards negative  $\tau$  (or with group velocity faster than that of the pulse in the lab frame). There is also a transmitted component,  $T_{\bar{\omega}} \exp(-i\bar{\omega}\tau)$ , at the original frequency and continuing on towards positive  $\tau$ , having managed to traverse the entire pulse. Unlike geometrical optics, in which a wave is either reflected or transmitted, the wave picture shows that these two effects are always present, albeit in varying degrees. The relative amounts of wave energy which are reflected or transmitted are given by the squared moduli  $|R_{\bar{\omega}}|^2$  and  $|T_{\bar{\omega}}|^2$ , with conservation of energy encoded in the identity  $|R_{\bar{\omega}}|^2 + |T_{\bar{\omega}}|^2 = 1$ . We find

$$|T_{\bar{\omega}}|^2 = \begin{cases} \sinh^2(\pi\bar{\omega}T_s) / \left[ \sinh^2(\pi\bar{\omega}T_s) + \cos^2\left(\frac{\pi}{2}\sqrt{1 - 8r\frac{\gamma_m}{\gamma_s}\frac{|\beta_{2,s}|}{\beta_{2,m}}}\right) \right], & 8r\frac{\gamma_m}{\gamma_s}\frac{|\beta_{2,s}|}{\beta_{2,m}} < 1 \\ \sinh^2(\pi\bar{\omega}T_s) / \left[ \sinh^2(\pi\bar{\omega}T_s) + \cosh^2\left(\frac{\pi}{2}\sqrt{8r\frac{\gamma_m}{\gamma_s}\frac{|\beta_{2,s}|}{\beta_{2,m}} - 1}\right) \right], & 8r\frac{\gamma_m}{\gamma_s}\frac{|\beta_{2,s}|}{\beta_{2,m}} > 1 \end{cases} \quad (6.2.12)$$

The reflection and transmission coefficients are plotted in Fig. 6.3. Note that we have total reflection at  $\bar{\omega} = 0$ , and that the amount of reflection decreases as we move away from the group-velocity-matching frequency. This is in accordance with our expectation that frequency shifting should occur most strongly for frequencies close to  $\omega_m$ , so that, in the co-moving frame, they are significantly slowed by the pulse.

We have seen that the solution Eq. (6.2.7) corresponds to redshifting at the black hole horizon when  $\bar{\omega}$  is positive. Blueshifting at the white hole horizon must also correspond to some solutions of Eq. (6.2.6), but these are not found simply by allowing  $\bar{\omega}$  to be negative. The reason is that the blueshifting process occurs at the trailing edge of the pulse, so that the incoming and reflected waves must be present for  $\tau \rightarrow +\infty$ , while only the transmitted wave should be present for  $\tau \rightarrow -\infty$ . The solution of Eq. (6.2.7) clearly does not share this basic property of the blueshifting process. Rather, we must make use of the reflection symmetry of the wave equation (6.2.6), i.e., its invariance under the transformation  $\tau \rightarrow -\tau$ . This means that, if  $\psi_{\bar{\omega}}(\tau)$  is a solution, then  $\psi_{\bar{\omega}}(-\tau)$  is also a solution. This transformation simply changes the sign of  $\xi$  in Eq. (6.2.7), while the asymptotic solutions become

$$\psi_{\bar{\omega}}(-\tau) \rightarrow \begin{cases} T_{\bar{\omega}} \exp(i\bar{\omega}\tau), & \tau \rightarrow -\infty \\ \exp(i\bar{\omega}\tau) + R_{\bar{\omega}} \exp(-i\bar{\omega}\tau), & \tau \rightarrow +\infty \end{cases}.$$

This corresponds precisely to blueshifting at the white hole horizon: the plane wave  $\exp(i\bar{\omega}\tau)$ , with frequency less than  $\omega_m$ , is incident from positive values of  $\tau$  (i.e., in the lab frame, it has a group velocity greater than that of the pulse, and catches up with it); this results in a reflected blueshifted wave,  $R_{\bar{\omega}} \exp(-i\bar{\omega}\tau)$ , which travels back toward positive  $\tau$ ; and a transmitted wave,  $T_{\bar{\omega}} \exp(i\bar{\omega}\tau)$ , a part of the original frequency

## 6. Frequency Shifting in Optical Fibres

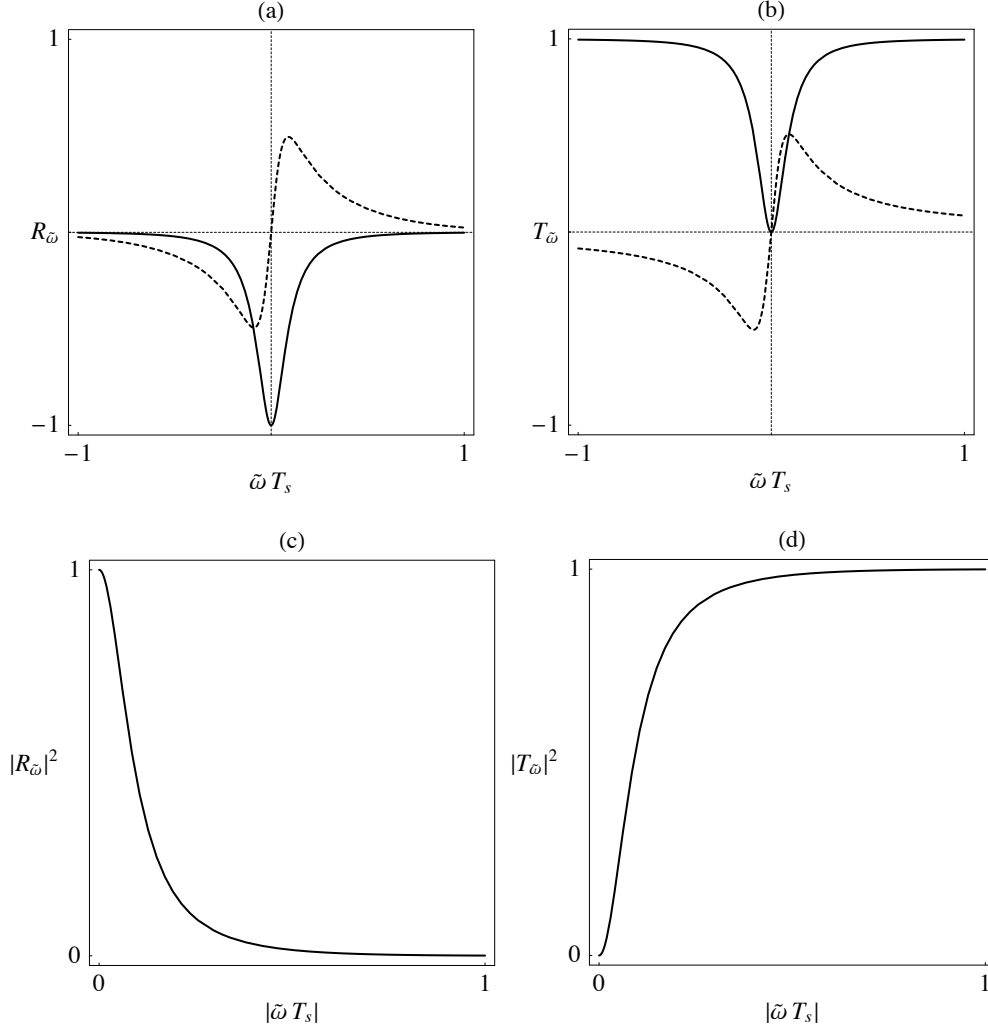


Figure 6.3.: REFLECTION AND TRANSMISSION AMPLITUDES: Figures (a) and (b) show the real (solid line) and imaginary (dotted line) parts of  $R_{\tilde{\omega}}$  and  $T_{\tilde{\omega}}$ , given by Eqs. (6.2.10) and (6.2.11). Figures (c) and (d) show the squared magnitudes  $|R_{\tilde{\omega}}|^2 = 1 - |T_{\tilde{\omega}}|^2$  and  $|T_{\tilde{\omega}}|^2$ , given by Eq. (6.2.12). Here, we have taken  $\sigma = -0.092$ , in accordance with experiment.

which has managed to traverse the whole pulse. Note that the reflection and transmission amplitudes are exactly the same as for the redshifting case.

### 6.3. General solution

A general solution of Eq. (6.2.2) can be expressed as a linear combination of eigenfunctions (those solutions with a specified value of  $\bar{\omega}'$ ). In order to form such an expression, the coefficients of the various eigenfunctions must be obtainable. This is possible through product integration if the eigenfunctions themselves are orthonormal. We first ensure that we have a complete, orthonormal set of eigenfunctions, and then we use them to form a general solution of the pulse-probe interaction.

The functions  $\psi_{\bar{\omega}}(\tau)$  and  $\psi_{\bar{\omega}}(-\tau)$  - where  $\bar{\omega}$  varies from zero to infinity - form a complete set of solutions of the wave equation (6.2.6). Those with different values of  $\bar{\omega}$  have different eigenvalues, and are therefore orthogonal. However,  $\psi_{\bar{\omega}}(\tau)$  has the same eigenvalue as  $\psi_{\bar{\omega}}(-\tau)$ ; these solutions are degenerate, and need not be orthogonal. In order to have a complete set of orthonormal solutions, we define the following sets of functions:

$$\begin{aligned}\psi_{\bar{\omega}}^+(\tau) &= \frac{1}{\sqrt{4\pi}} [\psi_{\bar{\omega}}(\tau) + \psi_{\bar{\omega}}(-\tau)] , \\ \psi_{\bar{\omega}}^-(\tau) &= \frac{1}{\sqrt{4\pi}} [\psi_{\bar{\omega}}(\tau) - \psi_{\bar{\omega}}(-\tau)] .\end{aligned}$$

$\psi_{\bar{\omega}}^+$  and  $\psi_{\bar{\omega}}^-$  are even and odd functions of  $\tau$ , respectively. Their product is therefore odd, and integrates to zero, so by virtue of their definitions  $\psi_{\bar{\omega}}^+$  and  $\psi_{\bar{\omega}}^-$  are orthogonal to each other. The overall factor of  $(4\pi)^{-1/2}$  ensures that they are *orthonormal*, i.e., that their products integrate to give  $\delta(\bar{\omega}_1 - \bar{\omega}_2)$ . Since the integral over any finite region must be finite, the contribution to the  $\delta$  function comes from integration over the asymptotic regions. Let us, then, write the asymptotic expressions explicitly:

$$\psi_{\bar{\omega}}^+(\tau) \rightarrow \frac{1}{\sqrt{4\pi}} \begin{cases} \exp(-i\bar{\omega}\tau) + (R_{\bar{\omega}} + T_{\bar{\omega}}) \exp(i\bar{\omega}\tau) , & \tau \rightarrow -\infty \\ \exp(i\bar{\omega}\tau) + (R_{\bar{\omega}} + T_{\bar{\omega}}) \exp(-i\bar{\omega}\tau) , & \tau \rightarrow +\infty \end{cases} , \quad (6.3.1)$$

$$\psi_{\bar{\omega}}^-(\tau) \rightarrow \frac{1}{\sqrt{4\pi}} \begin{cases} \exp(-i\bar{\omega}\tau) + (R_{\bar{\omega}} - T_{\bar{\omega}}) \exp(i\bar{\omega}\tau) , & \tau \rightarrow -\infty \\ -\exp(i\bar{\omega}\tau) - (R_{\bar{\omega}} - T_{\bar{\omega}}) \exp(-i\bar{\omega}\tau) , & \tau \rightarrow +\infty \end{cases} . \quad (6.3.2)$$

Then the product of  $\psi_{\bar{\omega}}^+$  with itself gives

$$\begin{aligned}\int_{-\infty}^{+\infty} [\psi_{\bar{\omega}_1}^+(\tau)]^* \psi_{\bar{\omega}_2}^+(\tau) d\tau &\approx \frac{1}{2\pi} \int_0^\infty [e^{-i\bar{\omega}_1\tau} + (R_{\bar{\omega}_1}^* + T_{\bar{\omega}_1}^*) e^{i\bar{\omega}_1\tau}] [e^{i\bar{\omega}_2\tau} + (R_{\bar{\omega}_2} + T_{\bar{\omega}_2}) e^{-i\bar{\omega}_2\tau}] d\tau \\ &= \frac{1}{2\pi} \int_0^\infty \left[ e^{-i(\bar{\omega}_1 - \bar{\omega}_2)\tau} + (R_{\bar{\omega}_1}^* + T_{\bar{\omega}_1}^*) e^{i(\bar{\omega}_1 + \bar{\omega}_2)\tau} \right. \\ &\quad \left. + (R_{\bar{\omega}_2} + T_{\bar{\omega}_2}) e^{-i(\bar{\omega}_1 + \bar{\omega}_2)\tau} + (R_{\bar{\omega}_1}^* + T_{\bar{\omega}_1}^*) (R_{\bar{\omega}_2} + T_{\bar{\omega}_2}) e^{i(\bar{\omega}_1 - \bar{\omega}_2)\tau} \right] d\tau \\ &= \frac{1}{2\pi} [\pi \delta(\bar{\omega}_1 - \bar{\omega}_2) + (R_{\bar{\omega}_1}^* + T_{\bar{\omega}_1}^*) (R_{\bar{\omega}_2} + T_{\bar{\omega}_2}) \pi \delta(\bar{\omega}_1 - \bar{\omega}_2)]\end{aligned}$$

## 6. Frequency Shifting in Optical Fibres

where, in the last line, we have included only terms in  $\delta(\bar{\omega}_1 - \bar{\omega}_2)$ , since the positivity of  $\bar{\omega}$  means that  $\delta(\bar{\omega}_1 + \bar{\omega}_2)$  is always equal to zero, and any finite contributions can be ignored on the grounds that the exact solution must be proportional to a  $\delta$  function (since it is a solution of the Schrödinger equation). The coefficient of the second term can be rewritten with  $\bar{\omega}_2$  set equal to  $\bar{\omega}_1$ :

$$|R_{\bar{\omega}_1} + T_{\bar{\omega}_1}|^2 = |R_{\bar{\omega}_1}|^2 + R_{\bar{\omega}_1}^* T_{\bar{\omega}_1} + R_{\bar{\omega}_1} T_{\bar{\omega}_1}^* + |T_{\bar{\omega}_1}|^2 .$$

Conservation of energy, as mentioned previously, implies  $|R_{\bar{\omega}_1}|^2 + |T_{\bar{\omega}_1}|^2 = 1$ . The product  $R_{\bar{\omega}_1}^* T_{\bar{\omega}_1}$  can be calculated directly from Eqs. (6.2.10) and (6.2.11):

$$\begin{aligned} R_{\bar{\omega}_1}^* T_{\bar{\omega}_1} &= \frac{\Gamma(i\bar{\omega}_1 T_s) \Gamma(-i\bar{\omega}_1 T_s + \sigma^* + 1) \Gamma(-i\bar{\omega}_1 T_s - \sigma^*) \Gamma(i\bar{\omega}_1 T_s + \sigma + 1) \Gamma(i\bar{\omega}_1 T_s - \sigma)}{\Gamma(-i\bar{\omega}_1 T_s) \Gamma(\sigma^* + 1) \Gamma(-\sigma^*) \Gamma(i\bar{\omega}_1 T_s + 1) \Gamma(i\bar{\omega}_1 T_s)} \\ &= \frac{1}{i\bar{\omega}_1 T_s} \frac{|\Gamma(i\bar{\omega}_1 T_s + \sigma + 1)|^2 |\Gamma(i\bar{\omega}_1 T_s - \sigma)|^2}{|\Gamma(i\bar{\omega}_1 T_s)|^2 \Gamma(\frac{1}{2} + (\sigma^* + \frac{1}{2})) \Gamma(\frac{1}{2} - (\sigma^* + \frac{1}{2}))} . \end{aligned}$$

Given the definition of  $\sigma$  in Eq. (6.2.8),  $\frac{1}{2} + (\sigma^* + \frac{1}{2})$  and  $\frac{1}{2} - (\sigma^* + \frac{1}{2})$  are either purely real or complex conjugates of each other.  $R_{\bar{\omega}_1}^* T_{\bar{\omega}_1}$ , then, is purely imaginary, and  $R_{\bar{\omega}_1}^* T_{\bar{\omega}_1} + R_{\bar{\omega}_1} T_{\bar{\omega}_1}^* = 0$ . Therefore,  $|R_{\bar{\omega}_1} + T_{\bar{\omega}_1}|^2 = 1$ , and we have

$$\int_{-\infty}^{+\infty} [\psi_{\bar{\omega}_1}^+(\tau)]^* \psi_{\bar{\omega}_2}^+(\tau) d\tau = \delta(\bar{\omega}_1 - \bar{\omega}_2) ,$$

as desired. An entirely analogous calculation shows that  $|R_{\bar{\omega}_1} - T_{\bar{\omega}_1}|^2 = 1$  and, consequently, that

$$\int_{-\infty}^{+\infty} [\psi_{\bar{\omega}_1}^-(\tau)]^* \psi_{\bar{\omega}_2}^-(\tau) d\tau = \delta(\bar{\omega}_1 - \bar{\omega}_2) .$$

The general solution of Eq. (6.2.2), where  $P(\tau)$  is given by Eq. (6.2.5), is

$$\mathcal{A}(\tau, \zeta) = \int_0^\infty \{c_+(\bar{\omega}) \psi_{\bar{\omega}}^+(\tau) + c_-(\bar{\omega}) \psi_{\bar{\omega}}^-(\tau)\} \exp\left(i\frac{1}{2}\beta_{2,m}u\zeta\bar{\omega}^2\right) d\bar{\omega} , \quad (6.3.3)$$

where we have replaced the phase factor that was removed in the transition from the time-dependent to the time-independent Schrödinger equation (see Eq. (6.2.3)). The coefficients  $c_+(\bar{\omega})$  and  $c_-(\bar{\omega})$  are arbitrary, but they are completely determined by the initial form of  $\mathcal{A}$ . The orthonormality condition on the eigenfunctions allows their calculation:

$$\begin{aligned} \int_{-\infty}^{+\infty} [\psi_{\bar{\omega}}^\pm(\tau)]^* \mathcal{A}(\tau, 0) d\tau &= \int_0^\infty \left\{ c_+(w) \int_{-\infty}^{+\infty} [\psi_{\bar{\omega}}^\pm(\tau)]^* \psi_w^+(\tau) d\tau \right. \\ &\quad \left. + c_-(w) \int_{-\infty}^{+\infty} [\psi_{\bar{\omega}}^\pm(\tau)]^* \psi_w^-(\tau) d\tau \right\} dw \\ &= \int_0^\infty c_\pm(w) \delta(\bar{\omega} - w) dw \\ &= c_\pm(\bar{\omega}) . \end{aligned} \quad (6.3.4)$$



## 6.4. Solution for a continuous wave

In experiment [65], a soliton is sent into the fiber alongside a continuous probe wave, whose frequency we denote  $\omega_p$  ( $\bar{\omega}_p = \omega_p - \omega_m$ ). The initial form of the probe wave,  $\mathcal{A}(\tau, 0)$ , is its value at the entrance to the fiber ( $z = 0$ ) as a function of time, since here  $\tau = t$ . Thus,

$$\mathcal{A}(\tau, 0) = \exp(-i\bar{\omega}_p\tau), \quad (6.4.1)$$

and the coefficients  $c_{\pm}(\bar{\omega})$  are just Fourier transforms of (complex conjugates of) eigenfunctions:

$$c_{\pm}(\bar{\omega}) = \left[ \tilde{\psi}_{\bar{\omega}}^{\pm}(\bar{\omega}_p) \right]^* \quad (6.4.2)$$

where we have defined

$$\tilde{\psi}_{\bar{\omega}}^{\pm}(\bar{w}) = \int_{-\infty}^{+\infty} \psi_{\bar{\omega}}^{\pm}(\tau) \exp(i\bar{w}\tau) d\tau. \quad (6.4.3)$$

Plugging Eq. (6.4.2) into Eq. (6.3.3), then taking its Fourier transform, we find:

$$\tilde{\mathcal{A}}(\bar{w}, \zeta) = \int_0^{\infty} \left\{ \left[ \tilde{\psi}_{\bar{\omega}}^{+}(\bar{\omega}_p) \right]^* \tilde{\psi}_{\bar{\omega}}^{+}(\bar{w}) + \left[ \tilde{\psi}_{\bar{\omega}}^{-}(\bar{\omega}_p) \right]^* \tilde{\psi}_{\bar{\omega}}^{-}(\bar{w}) \right\} \exp\left(i\frac{1}{2}\beta_{2,m}u\zeta\bar{\omega}^2\right) d\bar{\omega}. \quad (6.4.4)$$

These Fourier transforms can be calculated to a very good approximation if we perform the Fourier integration using the asymptotic forms of Eqs. (6.3.1) and (6.3.2). These give

$$\begin{aligned} \tilde{\psi}_{\bar{\omega}}^{+}(\bar{w}) \approx & \frac{1}{\sqrt{4\pi}} \left[ \pi(1 + R_{\bar{\omega}} + T_{\bar{\omega}}) (\delta(\bar{\omega} - \bar{w}) + \delta(\bar{\omega} + \bar{w})) \right. \\ & \left. + i(1 - R_{\bar{\omega}} - T_{\bar{\omega}}) \left( \frac{1}{\bar{\omega} - \bar{w}} + \frac{1}{\bar{\omega} + \bar{w}} \right) \right], \end{aligned} \quad (6.4.5)$$

$$\begin{aligned} \tilde{\psi}_{\bar{\omega}}^{-}(\bar{w}) \approx & \frac{1}{\sqrt{4\pi}} \left[ \pi(1 - R_{\bar{\omega}} + T_{\bar{\omega}}) (\delta(\bar{\omega} - \bar{w}) - \delta(\bar{\omega} + \bar{w})) \right. \\ & \left. + i(1 + R_{\bar{\omega}} - T_{\bar{\omega}}) \left( \frac{1}{\bar{\omega} - \bar{w}} - \frac{1}{\bar{\omega} + \bar{w}} \right) \right]. \end{aligned} \quad (6.4.6)$$

Plugging Eqs. (6.4.5) and (6.4.6) into Eq. (6.4.4), we find that we can write  $\tilde{\mathcal{A}}(\bar{w}, \zeta)$  as a sum of three distinct terms, corresponding to different terms of the integrand when Eqs. (6.4.5) and (6.4.6) are substituted in Eq. (6.4.4). The products of  $\delta$  functions with other  $\delta$  functions indicate the appearance of a  $\delta$  function in the result; cross terms of  $\delta$  functions with poles can be evaluated by simple substitution; and only terms involving products of poles remain to be integrated. Separating these terms explicitly,

$$\tilde{\mathcal{A}}(\bar{w}, \zeta) \approx C_{\delta}(\zeta) 2\pi \delta(\bar{w} - \bar{\omega}_p) + \tilde{\mathcal{A}}_{\text{cross}}(\bar{w}, \zeta) + \tilde{\mathcal{A}}_{\text{poles}}(\bar{w}, \zeta). \quad (6.4.7)$$

The  $\delta$  function arises because, far from the pulse, the initial probe wave evolves as if it were purely a continuous wave; in other words, the presence of the pulse affects only

## 6. Frequency Shifting in Optical Fibres

a finite portion of the probe wave. This term, then, is the same as would be expected if there were no pulse present at all. Since, in that case, plane waves have the form  $\exp(-i\bar{\omega}\tau + i\frac{1}{2}\beta_{2,m}u\zeta\bar{\omega}^2)$  (see Eq. (6.2.1)), we have

$$C_\delta(\zeta) = \exp\left(i\frac{1}{2}\beta_{2,m}u\zeta\bar{\omega}_p^2\right).$$

$\tilde{\mathcal{A}}_{\text{cross}}(\bar{w}, \zeta)$  is fairly straightforward to evaluate, although some care must be taken with regard to the signs of  $\bar{u}$  and  $\bar{\omega}_p$  since the integral is only half infinite. The result is

$$\tilde{\mathcal{A}}_{\text{cross}}(\bar{w}, \zeta) = \frac{f_{\text{cross}}(\bar{w}) - f_{\text{cross}}(\bar{\omega}_p)}{\bar{w} - \bar{\omega}_p} + \frac{f'_{\text{cross}}(\bar{w}) - f'_{\text{cross}}(-\bar{\omega}_p)}{\bar{w} + \bar{\omega}_p},$$

where we have defined

$$\begin{aligned} f_{\text{cross}}(\bar{w}) &= \text{Im}[T_{\bar{w}}] \exp\left(i\frac{1}{2}\beta_{2,m}u\zeta\bar{w}^2\right), \\ f'_{\text{cross}}(\bar{w}) &= \text{Im}[R_{\bar{w}}] \exp\left(i\frac{1}{2}\beta_{2,m}u\zeta\bar{w}^2\right). \end{aligned}$$

The remaining term,  $\tilde{\mathcal{A}}_{\text{poles}}(\bar{w}, \zeta)$ , can, after some manipulation, be brought to the simplified form

$$\tilde{\mathcal{A}}_{\text{poles}}(\bar{w}, \zeta) = \frac{f_{\text{poles}}(\bar{w}) - f_{\text{poles}}(\bar{\omega}_p)}{\bar{w} - \bar{\omega}_p} + \frac{f'_{\text{poles}}(\bar{w}) - f'_{\text{poles}}(-\bar{\omega}_p)}{\bar{w} + \bar{\omega}_p},$$

where we have defined

$$\begin{aligned} f_{\text{poles}}(\bar{w}) &= \frac{1}{\pi} \int_{-\infty}^{+\infty} \text{Re}[1 - T_{\bar{\omega}}] \frac{\exp\left(i\frac{1}{2}\beta_{2,m}u\zeta\bar{\omega}^2\right)}{\bar{\omega} - \bar{w}} d\bar{\omega}, \\ f'_{\text{poles}}(\bar{w}) &= \frac{1}{\pi} \int_{-\infty}^{+\infty} \text{Re}[-R_{\bar{\omega}}] \frac{\exp\left(i\frac{1}{2}\beta_{2,m}u\zeta\bar{\omega}^2\right)}{\bar{\omega} - \bar{w}} d\bar{\omega}. \end{aligned}$$

Combining these, we find a more illuminating form of the spectrum than Eq. (6.4.7); that is, we can write

$$\tilde{\mathcal{A}}(\bar{w}, \zeta) \approx \exp\left(i\frac{1}{2}\beta_{2,m}u\zeta\bar{\omega}_p^2\right) 2\pi \delta(\bar{w} - \bar{\omega}_p) + \frac{F(\bar{w}) - F(\bar{\omega}_p)}{\bar{w} - \bar{\omega}_p} + \frac{F'(\bar{w}) - F'(-\bar{\omega}_p)}{\bar{w} + \bar{\omega}_p}, \quad (6.4.8)$$

where we have defined

$$F(\bar{w}) = f_{\text{cross}}(\bar{w}) + f_{\text{poles}}(\bar{w}), \quad F'(\bar{w}) = f'_{\text{cross}}(\bar{w}) + f'_{\text{poles}}(\bar{w}). \quad (6.4.9)$$

Rather than splitting into three parts for mathematical convenience, as in Eq. (6.4.7), we see in Eq. (6.4.8) that the spectrum splits into three parts of physical significance: a  $\delta$  function at the input frequency  $\bar{\omega}_p$ , a shoulder surrounding this  $\delta$  function, and a peak at the shifted frequency  $-\bar{\omega}_p$ .

Figure 6.4 shows plots of the predicted spectrum of Eq. (6.4.8), together with experimentally observed frequency-shifting spectra.

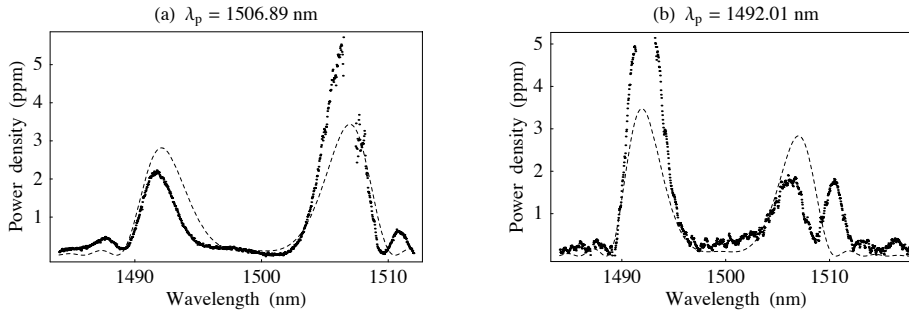


Figure 6.4.: FREQUENCY SHIFTING SPECTRA FOR A CONSTANT-VELOCITY PULSE: The group-velocity-matching wavelength is  $\lambda_m = 1499.47$  nm. Figure (a) shows a blueshifting spectrum, while Figure (b) is a redshifting spectrum. Data points represent experimental observations, while dashed curves are theoretical predictions (from Eq. (6.4.8)). The experimentally obtained spectra are normalized with respect to the probe power and are measured in parts per million (ppm). The heights of the theoretical curves were fitted using the least- $\chi^2$  method. (Data courtesy of Chris Kuklewicz and Friedrich König.)

## 6.5. The Raman effect

Despite the careful analysis given above, there is a discrepancy between the theoretical predictions it generates and the experimental results. Qualitatively, the appearance of the  $\delta$  function and the peaks at the initial and shifted frequencies has been explained. However, there is disagreement over the relative heights of these peaks, and there are noticeable differences with regard to the side-bands, which are relatively small according to theory but quite prominent in experiment.

A possible explanation for these discrepancies is our neglect of the Raman effect [63] in the previous calculation. Whereas the Kerr effect - which is responsible for the interaction between the pulse and the probe - is caused by the nonlinear response of the electrons of the fiber medium to the electric field, the Raman effect is caused by the nonlinear response of the nuclei (i.e., molecular vibrations) of the fibre medium. This nuclear response is much slower than the electronic response, and in silica takes place on a time scale of around 60 – 70 fs [70, 71, 72, 73]. For pulses much longer than this, the nuclear response is essentially instantaneous and cannot be distinguished from the electronic response, so that there is no discernible Raman effect. However, for pulses with lengths on the same order as this time scale, the nuclear response cannot be regarded as instantaneous, and new effects emerge. Energy is transferred to vibrational modes within the fiber, at the cost of energy of the pulse. This causes a gradual redshift of the pulse's carrier frequency; and, since the pulse is a soliton and exists in a region of anomalous dispersion, this redshift is accompanied by a decrease in its group velocity. As far as frequency shifting is concerned, this deceleration is the Raman effect's most important consequence. As

## 6. Frequency Shifting in Optical Fibres

we have seen, energy is shifted between frequencies that are equidistant from the group-velocity-matching frequency,  $\omega_m$ , but this depends crucially on the group velocity of the pulse. Since the dispersion at  $\omega_m$  is normal,  $\omega_m$  must increase as  $\omega_s$  decreases, and an incident probe wave will be reflected at a frequency which is continuously increasing.

To account for a decelerating pulse, the coordinate transformation that moves into a co-moving frame must be different from that which we have used. Suppose that, in the lab frame, the pulse propagates with velocity

$$u(z) = u_0 - \frac{az}{u_0}, \quad (6.5.1)$$

where  $a$  has units of acceleration. The time taken for the pulse to propagate a distance  $z$  is

$$T(z) = \int_0^z \frac{dz'}{u(z')} = \frac{1}{u_0} \int_0^z \frac{dz'}{1 - az'/u_0^2} \approx \frac{1}{u_0} \int_0^z \left(1 + \frac{az'}{u_0^2}\right) dz' = \frac{z}{u_0} + \frac{az^2}{2u_0^3}.$$

Note that this is valid only when  $|az/u_0^2| \ll 1$ ; this is true if the relative change in the velocity of the pulse is much less than unity. The co-moving frame - in which the pulse appears stationary - can be described by the coordinates

$$\tau = t - \frac{z}{u_0} - \frac{az^2}{2u_0^3}, \quad \zeta = \frac{z}{u_0}. \quad (6.5.2)$$

These coordinates reduce to those of a reference frame with uniform velocity  $u_0$  as  $a \rightarrow 0$ . Partial derivatives transform according to the chain rule:

$$\partial_z = \frac{1}{u_0} \left[ \partial_\zeta - \left(1 + \frac{a\zeta}{u_0}\right) \partial_\tau \right], \quad \partial_t = \partial_\tau. \quad (6.5.3)$$

Just as we define wavenumber and frequency in the lab frame as derivatives of the phase,

$$k = \frac{\partial\varphi}{\partial z}, \quad \omega = -\frac{\partial\varphi}{\partial t},$$

so we define two frequencies in the co-moving frame as derivatives of  $\tau$  and  $\zeta$ ,

$$\omega = -\frac{\partial\varphi}{\partial\tau}, \quad \omega' = -\frac{\partial\varphi}{\partial\zeta},$$

and these are related via the transformation of partial derivatives given above. As before, we find  $\omega$  is the same in both frames (hence the use of the same label). On the other hand,

$$\omega' = \omega - u_0 k + \frac{a\zeta}{u_0} \omega = \omega - u_0 \beta(\omega) + \frac{a\zeta}{u_0} \omega,$$

where, in the second step, we have imposed the condition that  $k$  be positive, and hence that all waves be forward-propagating. The only difference from the non-decelerating case is the appearance of a  $\zeta$ -dependent term.

To find the optical wave equation in the decelerating frame, we return to the full wave equation,

$$\partial_z^2 E + \beta^2 (i\partial_t) E = \frac{1}{\epsilon_0 c^2} \partial_t^2 P. \quad (6.5.4)$$

Since  $\partial_t = \partial_\tau$ , an identity that holds true even in the non-decelerating case, the terms  $\beta^2 (i\partial_t) E$  and  $\partial_t^2 P / (\epsilon_0 c^2)$  are unaltered from the previous analysis, while  $\partial_z^2 E$  is computed below. As before, we define the slowly-varying envelope  $\mathcal{E}$  such that

$$E = \mathcal{E} \exp(i\beta_m z - i\omega_m t) = \mathcal{E} \exp\left(-i\omega_m \tau - i(\omega_m - u_0 \beta_m) \zeta - i\omega_m \frac{a\zeta^2}{2u_0}\right),$$

where we have replaced the lab coordinates  $z$  and  $t$  with the new coordinates of the decelerating frame, as defined in Eq. (6.5.2). Then, from previous calculations, we have

$$\beta^2 (i\partial_t) E \approx \left[ \beta_m^2 \mathcal{E} + 2i\beta_m \frac{1}{u_0} \partial_\tau \mathcal{E} - \left( \beta_m \beta_{2,m} + \frac{1}{u_0^2} \right) \partial_\tau^2 \mathcal{E} \right] \exp(i\beta_m z - i\omega_m t) \quad (6.5.5)$$

$$\frac{1}{\epsilon_0 c^2} \partial_t^2 P \approx -2\kappa \frac{\omega_m^2}{c^2} I \mathcal{E} \exp(i\beta_m z - i\omega_m t). \quad (6.5.6)$$

For  $\partial_z^2 E$ , we substitute the partial derivatives given in Eq. (6.5.3):

$$\begin{aligned} \partial_z^2 E &= \frac{1}{u_0^2} \left[ \partial_\zeta - \left( 1 + \frac{a\zeta}{u_0} \right) \partial_\tau \right]^2 \mathcal{E} \exp\left(-i\omega_m \tau - i(\omega_m - u_0 \beta_m) \zeta - i\omega_m \frac{a\zeta^2}{2u_0}\right) \\ &= \frac{1}{u_0^2} \left[ \partial_\zeta - \left( 1 + \frac{a\zeta}{u_0} \right) \partial_\tau \right] \left[ \partial_\zeta \mathcal{E} - \left( 1 + \frac{a\zeta}{u_0} \right) \partial_\tau \mathcal{E} + iu_0 \beta_m \mathcal{E} \right] \\ &\quad \times \exp\left(-i\omega_m \tau - i(\omega_m - u_0 \beta_m) \zeta - i\omega_m \frac{a\zeta^2}{2u_0}\right) \\ &= \frac{1}{u_0^2} \left[ \partial_\zeta^2 \mathcal{E} - 2 \left( 1 + \frac{a\zeta}{u_0} \right) \partial_\zeta \partial_\tau \mathcal{E} + 2iu_0 \beta_m \partial_\zeta \mathcal{E} - \left( 2iu_0 \beta_m \left( 1 + \frac{a\zeta}{u_0} \right) + \frac{a}{u_0} \right) \partial_\tau \mathcal{E} \right. \\ &\quad \left. + \left( 1 + \frac{a\zeta}{u_0} \right)^2 \partial_\tau^2 \mathcal{E} - u_0^2 \beta_m^2 \mathcal{E} \right] \exp\left(-i\omega_m \tau - i(\omega_m - u_0 \beta_m) \zeta - i\omega_m \frac{a\zeta^2}{2u_0}\right) \\ &\approx \frac{1}{u_0^2} \left[ 2iu_0 \beta_m \partial_\zeta \mathcal{E} - \left( 2iu_0 \beta_m \left( 1 + \frac{a\zeta}{u_0} \right) + \frac{a}{u_0} \right) \partial_\tau \mathcal{E} + \left( 1 + \frac{a\zeta}{u_0} \right)^2 \partial_\tau^2 \mathcal{E} - u_0^2 \beta_m^2 \mathcal{E} \right] \\ &\quad \times \exp(i\beta_m z - i\omega_m t), \end{aligned} \quad (6.5.7)$$

where, in the last step, we used the slowly-varying envelope approximation to neglect the second-order derivatives  $\partial_\zeta^2 \mathcal{E}$  and  $\partial_\zeta \partial_\tau \mathcal{E}$ . Substituting Eqs. (6.5.5)-(6.5.7) into Eq. (6.5.4), we find the wave equation for the envelope  $\mathcal{E}$ :

$$i\partial_\zeta \mathcal{E} = \left( i\frac{a\zeta}{u_0} + \frac{a}{2\beta_m u_0^2} \right) \partial_\tau \mathcal{E} + \left( \frac{\beta_{2,m} u_0}{2} - \frac{a\zeta}{\beta_m u_0^2} \left( 1 + \frac{a\zeta}{2u_0} \right) \right) \partial_\tau^2 \mathcal{E} - 2\kappa \frac{\omega_m^2}{c^2} I \mathcal{E}.$$

It can be shown that the second term of each bracket is negligibly small in comparison to the first, so that this simplifies to

$$i\partial_\zeta \mathcal{E} = i\frac{a\zeta}{u_0} \partial_\tau \mathcal{E} + \frac{\beta_{2,m} u_0}{2} \partial_\tau^2 \mathcal{E} - 2\kappa \frac{\omega_m^2}{c^2} I \mathcal{E}. \quad (6.5.8)$$

## 6. Frequency Shifting in Optical Fibres

Let us make the substitution

$$\mathcal{E} = \psi \exp(-i\phi), \quad \phi = \frac{a\zeta\tau}{\beta_{2,m}u_0^2} + \frac{a^2\zeta^3}{6\beta_{2,m}u_0^3}. \quad (6.5.9)$$

Then Eq. (6.5.8) becomes

$$\begin{aligned} i \left( \partial_\zeta \psi - i \frac{a\tau}{\beta_{2,m}u_0^2} \psi - i \frac{a^2\zeta^2}{2\beta_{2,m}u_0^3} \psi \right) e^{-i\phi} &= i \frac{a\zeta}{u_0} \left( \partial_\tau \psi - i \frac{a\zeta}{\beta_{2,m}u_0^2} \psi \right) e^{-i\phi} \\ &+ \frac{\beta_{2,m}u_0}{2} \left( \partial_\tau^2 \psi - 2i \frac{a\zeta}{\beta_{2,m}u_0^2} \partial_\tau \psi - \frac{a^2\zeta^2}{\beta_{2,m}^2u_0^4} \psi \right) e^{-i\phi} - 2\kappa \frac{\omega_m^2}{c^2} I \psi e^{-i\phi}, \end{aligned}$$

and, rearranging, we have

$$-i\partial_\zeta \psi = -\frac{\beta_{2,m}u_0}{2} \partial_\tau^2 \psi + \left( \frac{a\tau}{\beta_{2,m}u_0^2} + 2\kappa \frac{\omega_m^2}{c^2} I \right) \psi. \quad (6.5.10)$$

If the pulse is a fundamental soliton, this becomes

$$-i\partial_\zeta \psi = -\frac{\beta_{2,m}u_0}{2} \partial_\tau^2 \psi + \left( \frac{a\tau}{\beta_{2,m}u_0^2} + ru_0 \frac{\gamma_m}{\gamma_s} \frac{|\beta_{2,s}|}{T_s^2} \operatorname{sech}^2 \left( \frac{\tau}{T_s} \right) \right) \psi. \quad (6.5.11)$$

As in the non-decelerating case, we have arrived at a wave equation equivalent in form to the time-dependent Schrödinger equation. The mathematical effect of the deceleration is now made apparent: the Schrödinger “potential” now includes not only the pulse intensity, but also a term linear in  $\tau$  and proportional to the magnitude of the deceleration.

## 6.6. Accelerated waves in the absence of a pulse

Given the typically short duration of the pulse, we are, as before, more interested in asymptotic solutions of Eq. (6.5.10) which hold in the limit  $\tau \rightarrow \pm\infty$ . In these regions, the intensity of the pulse is zero, and the wave equation is simply

$$-i\partial_\zeta \psi = -\frac{\beta_{2,m}u_0}{2} \partial_\tau^2 \psi + \frac{a\tau}{\beta_{2,m}u_0^2} \psi. \quad (6.6.1)$$

Factoring out a  $\zeta$ -dependent phase,

$$\psi = \psi_{\tau_0} \exp \left( i \frac{a\zeta\tau_0}{\beta_{2,m}u_0^2} \right), \quad (6.6.2)$$

where  $\tau_0$  is a free parameter (analogous to energy in the usual Schrödinger equation), the wave equation is transformed to the form of the time-independent Schrödinger equation,

$$-\frac{\beta_{2,m}u_0}{2} \partial_\tau^2 \psi + \frac{a(\tau - \tau_0)}{\beta_{2,m}u_0^2} \psi = 0. \quad (6.6.3)$$

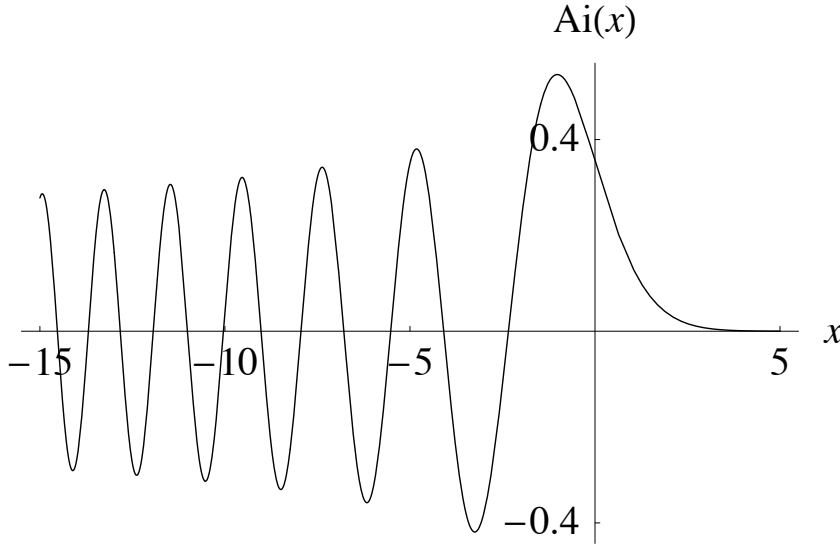


Figure 6.5.: THE AIRY FUNCTION:  $\text{Ai}(x)$  is exponentially decreasing for positive  $x$  and oscillatory for negative  $x$ .

This can be simplified further by defining the dimensionless variables

$$\theta = \frac{\tau}{\tau_1}, \quad \theta_0 = \frac{\tau_0}{\tau_1}, \quad (6.6.4)$$

where the characteristic time scale  $\tau_1$  is given by

$$\tau_1^3 = \frac{\beta_{2,m}^2 u_0^3}{2a}. \quad (6.6.5)$$

Then Eq. (6.6.3) becomes

$$\partial_\theta^2 \psi_{\theta_0} = (\theta - \theta_0) \psi_{\theta_0}. \quad (6.6.6)$$

This is the well-known Airy equation; its solutions are the Airy functions  $\text{Ai}(\theta - \theta_0)$  and  $\text{Bi}(\theta - \theta_0)$ . Since  $\text{Bi}(\theta - \theta_0)$  increases exponentially as  $\theta \rightarrow +\infty$ , in the absence of a pulse  $\text{Ai}(\theta - \theta_0)$  represents the only physical solution.

Let us pause to consider the meanings of the parameters  $\tau_0$  and  $\tau_1$ . Consider the Airy function  $\text{Ai}(\theta - \theta_0)$ , plotted in Fig. (6.5): for positive  $\theta - \theta_0$ , it decays exponentially; for negative  $\theta - \theta_0$ , its amplitude decays as  $(\theta_0 - \theta)^{-1/4}$ , while it oscillates with continuously increasing frequency  $\omega \propto (\theta_0 - \theta)^{1/2}$ .

$\tau_1$  is a wave scale; it determines the characteristic oscillation period of the envelope. As we would expect, these oscillations become more prominent for larger acceleration  $a$ , since  $\tau_1$  - and hence the oscillation period - decreases.

$\tau_0$  represents the “turning point” which marks the boundary between oscillatory behaviour and exponential decay; it is a point beyond which the wave barely penetrates. This boundedness of the wave is closely related to pulse trapping [74, 75, 76, 77], which

## 6. Frequency Shifting in Optical Fibres

was explained by Gorbach and Skryabin [78] using a linear “gravity-like” potential like that in Eq. (6.6.1).

The general solution of Eq. (6.6.1) is found by replacing the phase of Eq. (6.6.2) and forming a linear superposition of the eigenfunctions  $\psi_{\theta_0} = \text{Ai}(\theta - \theta_0)$ :

$$\psi(\theta, \zeta) = \int_{-\infty}^{+\infty} c(\theta_0) \text{Ai}(\theta - \theta_0) \exp\left(i \frac{a\zeta\tau_1}{\beta_{2,m}u_0^2} \theta_0\right) d\theta_0. \quad (6.6.7)$$

## 6.7. Including the pulse-probe interaction

Complete solutions of the pulse-probe interaction, where the pulse experiences a Raman deceleration, must obey Eq. (6.5.10). However, there is no analytic solution for a potential which includes both a linear term and the soliton ( $\text{sech}^2$ ) term. We require a further approximation in order to find analytic expressions for the eigenfunctions. We shall assume that the Raman deceleration can be neglected on time scales of the order of the soliton width  $T_s$ ; that is, we assume that there is a region outside, but close to, the pulse, in which the solutions found for a non-decelerating pulse (Eqs. (6.2.7) and (6.2.9)) are valid. (We can include the asymptotic solutions because these are valid wherever the pulse intensity is essentially zero.) The solutions here can be matched to Airy functions  $\text{Ai}(\theta - \theta_0)$  and  $\text{Bi}(\theta - \theta_0)$  in the asymptotic regions.

We have already made one important conclusion about the solutions in the decelerating case: due to the exponentially increasing behaviour of  $\text{Bi}(\theta - \theta_0)$ , the solution as  $\theta \rightarrow +\infty$  must contain  $\text{Ai}(\theta - \theta_0)$  exclusively. The pulse-probe interaction, then, must manifest itself through the appearance of a term including  $\text{Bi}(\theta - \theta_0)$  in the asymptotic region  $\theta \rightarrow -\infty$ . The general solution for  $\psi_{\theta_0}$  is then

$$\psi_{\theta_0}(\theta) = \mathcal{N}_{\theta_0} \begin{cases} c_{\theta_0}^A \text{Ai}(\theta - \theta_0) + c_{\theta_0}^B \text{Bi}(\theta - \theta_0), & \theta \rightarrow -\infty \\ \text{Ai}(\theta - \theta_0), & \theta \rightarrow +\infty \end{cases}, \quad (6.7.1)$$

where  $\mathcal{N}_{\theta_0}$  is a prefactor that ensures the eigenfunctions are normalized according to the condition

$$\int_{-\infty}^{+\infty} \psi_{\theta'_0}(\theta) \psi_{\theta_0}(\theta) d\theta = \delta(\theta_0 - \theta'_0). \quad (6.7.2)$$

At least for the exact solutions, it must be possible to choose  $\mathcal{N}_{\theta_0}$  such that this normalization condition holds, since they are simply solutions of the Schrödinger equation. The  $\delta$  function, however, is determined by the asymptotics of the integrand, so we may use the asymptotic forms of Eq. (6.7.1) to find  $\mathcal{N}_{\theta_0}$ . The integral over positive  $\theta$  involves the product of two Ai functions; since  $\text{Ai}(x)$  decays exponentially for positive  $x$  ( $\text{Ai}(x) \sim \exp(-2x^{3/2}/3)$  [79, 64]), this integral is finite, and cannot contribute to the  $\delta$  function. We are then left with the integral over negative  $\theta$ , where the Airy functions are oscillatory [79, 64]:

$$\begin{aligned} \text{Ai}(\theta - \theta_0) &\rightarrow \frac{1}{\sqrt{\pi}} (\theta_0 - \theta)^{-1/4} \sin\left(\frac{2}{3}(\theta_0 - \theta)^{3/2} + \frac{\pi}{4}\right) \\ &\rightarrow \frac{1}{\sqrt{\pi}} (-\theta)^{-1/4} \sin\left(\frac{2}{3}(-\theta)^{3/2} + \theta_0(-\theta)^{1/2} + \frac{\pi}{4}\right), \end{aligned}$$



### 6.7. Including the pulse-probe interaction

and similarly for  $\text{Bi}(\theta - \theta_0)$  with  $\sin$  replaced by  $\cos$ . The products  $\text{Ai}(\theta - \theta'_0) \text{Ai}(\theta - \theta_0)$  and  $\text{Bi}(\theta - \theta'_0) \text{Bi}(\theta - \theta_0)$  result in a cosine term whose argument is the difference of the arguments of the individual terms; more explicitly, we have

$$\begin{aligned} \int_{-\infty}^0 \text{Ai}(\theta - \theta'_0) \text{Ai}(\theta - \theta_0) d\theta &\approx \int_{-\infty}^0 \frac{1}{2\pi} (-\theta)^{1/2} \cos\left((\theta_0 - \theta'_0)(-\theta)^{1/2}\right) d\theta \\ &= \frac{1}{\pi} \int_0^{\infty} \cos((\theta_0 - \theta'_0)x) dx \\ &= \frac{1}{2\pi} \int_0^{\infty} (\exp(i(\theta_0 - \theta'_0)x) + \exp(-i(\theta_0 - \theta'_0)x)) dx \\ &\approx \delta(\theta_0 - \theta'_0), \end{aligned}$$

where, in the last line, we have included only the  $\delta$  function. This calculation also holds for the integral of  $\text{Bi}(\theta - \theta'_0) \text{Bi}(\theta - \theta_0)$ . For the mixed product  $\text{Ai}(\theta - \theta'_0) \text{Bi}(\theta - \theta_0)$ , the relevant term is a sine rather than a cosine, so we have

$$\begin{aligned} \int_{-\infty}^0 \text{Ai}(\theta - \theta'_0) \text{Bi}(\theta - \theta_0) d\theta &\approx \int_{-\infty}^0 \frac{1}{2\pi} (-\theta)^{1/2} \sin\left((\theta_0 - \theta'_0)(-\theta)^{1/2}\right) d\theta \\ &= \frac{1}{\pi} \int_0^{\infty} \sin((\theta_0 - \theta'_0)x) dx \\ &= \frac{1}{2i\pi} \int_0^{\infty} (\exp(i(\theta_0 - \theta'_0)x) - \exp(-i(\theta_0 - \theta'_0)x)) dx \\ &\approx 0. \end{aligned}$$

The last line includes only the  $\delta$  function term, which vanishes. Therefore, on substitution of Eq. (6.7.1) into Eq. (6.7.2), we find

$$\mathcal{N}_{\theta'_0} \mathcal{N}_{\theta_0} \left( c_{\theta'_0}^A c_{\theta_0}^A + c_{\theta'_0}^B c_{\theta_0}^B \right) \delta(\theta_0 - \theta'_0) = \delta(\theta_0 - \theta'_0),$$

which holds if the normalizing prefactor is defined to be

$$\mathcal{N}_{\theta_0} = \frac{1}{\sqrt{(c_{\theta_0}^A)^2 + (c_{\theta_0}^B)^2}}. \quad (6.7.3)$$

All that remains is to find the coefficients  $c_{\theta_0}^A$  and  $c_{\theta_0}^B$ . For this purpose, it is useful to distinguish three cases:  $\theta_0 \lesssim -1$ ,  $-1 \lesssim \theta_0 \lesssim 1$  and  $\theta_0 \gtrsim 1$ .

In the case  $\theta_0 \lesssim -1$ , the turning point is far on the negative side. We can argue, as before, that due to its exponentially increasing behaviour for positive argument,  $\text{Bi}(\theta - \theta_0)$  cannot appear here, and the solution is purely  $\text{Ai}(\theta - \theta_0)$ . In terms of the coefficients, this implies  $c_{\theta_0}^A = 1$  and  $c_{\theta_0}^B = 0$ . From the perspective of geometrical optics, the probe wave turns around before it has a chance to interact with the pulse, so the solution is essentially the same as if no pulse were present.

In the case  $-1 \lesssim \theta_0 \lesssim 1$ , the behaviour of the Airy functions near  $\theta = 0$  is not well-approximated by either of their asymptotic forms, so there are no approximations that

## 6. Frequency Shifting in Optical Fibres

can be made. Instead, we must directly solve Eq. (6.5.11), or, with the  $\zeta$ -dependent phase of Eq. (6.6.2) and the dimensionless variables defined in Eqs. (6.6.4) and (6.6.5), the following equation:

$$\partial_\theta^2 \psi_{\theta_0} = \left[ \theta - \theta_0 + 2r \frac{\gamma_m |\beta_{2,s}|}{\gamma_s \beta_{2,m}} \frac{\tau_1^2}{T_s^2} \operatorname{sech}^2 \left( \theta \frac{\tau_1}{T_s} \right) \right] \psi_{\theta_0}. \quad (6.7.4)$$

This is done by picking a point  $\theta_*$  situated well outside the soliton (typically,  $\theta_* \gtrsim 5T_s/\tau_1$ ), setting the value and first derivative of  $\psi_{\theta_0}$  at  $\theta_*$  to be  $\operatorname{Ai}(\theta_* - \theta_0)$  and  $\operatorname{Ai}'(\theta_* - \theta_0)$ , respectively, and solving Eq. (6.7.4) back to, say,  $-2\theta_*$ . The solution in the region between  $-2\theta_*$  and  $-\theta_*$  is then fitted to the linear combination  $c_{\theta_0}^A \operatorname{Ai}(\theta - \theta_0) + c_{\theta_0}^B \operatorname{Bi}(\theta - \theta_0)$ .

In the case  $\theta_0 \gtrsim 1$ , the turning point is far on the positive side, and the behaviour of the Airy functions near  $\theta = 0$  is oscillatory. We can write asymptotic expressions as previously, this time treating  $|\theta/\theta_0| \ll 1$ :

$$\begin{aligned} \operatorname{Ai}(\theta - \theta_0) &\approx \frac{1}{\sqrt{\pi}} (\theta_0 - \theta)^{-1/4} \sin \left( \frac{2}{3} (\theta_0 - \theta)^{3/2} + \frac{\pi}{4} \right) \\ &\approx \frac{1}{\sqrt{\pi}} \theta_0^{-1/4} \sin \left( \frac{2}{3} \theta_0^{3/2} - \theta_0^{1/2} \theta + \frac{\pi}{4} \right) \\ &= \frac{1}{\sqrt{\pi}} \theta_0^{-1/4} \frac{1}{2i} \left[ \exp \left( i \left( \frac{2}{3} \theta_0^{3/2} - \theta_0^{1/2} \theta + \frac{\pi}{4} \right) \right) \right. \\ &\quad \left. - \exp \left( -i \left( \frac{2}{3} \theta_0^{3/2} - \theta_0^{1/2} \theta + \frac{\pi}{4} \right) \right) \right], \end{aligned} \quad (6.7.5)$$

$$\begin{aligned} \operatorname{Bi}(\theta - \theta_0) &\approx \frac{1}{\sqrt{\pi}} (\theta_0 - \theta)^{-1/4} \cos \left( \frac{2}{3} (\theta_0 - \theta)^{3/2} + \frac{\pi}{4} \right) \\ &\approx \frac{1}{\sqrt{\pi}} \theta_0^{-1/4} \cos \left( \frac{2}{3} \theta_0^{3/2} - \theta_0^{1/2} \theta + \frac{\pi}{4} \right) \\ &= \frac{1}{\sqrt{\pi}} \theta_0^{-1/4} \frac{1}{2} \left[ \exp \left( i \left( \frac{2}{3} \theta_0^{3/2} - \theta_0^{1/2} \theta + \frac{\pi}{4} \right) \right) \right. \\ &\quad \left. + \exp \left( -i \left( \frac{2}{3} \theta_0^{3/2} - \theta_0^{1/2} \theta + \frac{\pi}{4} \right) \right) \right]. \end{aligned} \quad (6.7.6)$$

Combining these expressions leads to the expression for a plane wave in terms of Airy functions, valid near  $\theta = 0$ :

$$\exp(-i\theta_0^{1/2}\theta) \approx \sqrt{\pi} \theta_0^{1/4} \exp \left( -i \frac{2}{3} \theta_0^{3/2} \right) \left[ e^{i\pi/4} \operatorname{Ai}(\theta - \theta_0) + e^{-i\pi/4} \operatorname{Bi}(\theta - \theta_0) \right]. \quad (6.7.7)$$

$\exp(i\theta_0^{1/2}\theta)$  is, of course, given simply by the complex conjugate of this. We may now use the non-decelerating solutions of Eq. (6.2.9) to find the decelerating solutions. Starting from the fact that the solution for positive  $\theta$  must be  $\operatorname{Ai}(\theta - \theta_0)$  (we ignore the

normalization for now), we expand this using Eq. (6.7.5) above to find the form of the solution, for positive  $\theta$ , near the soliton:

$$\psi_{\theta_0} \sim \frac{1}{\sqrt{\pi}} \theta_0^{-1/4} \frac{1}{2i} \exp \left( i \left( \frac{2}{3} \theta_0^{3/2} + \frac{\pi}{4} \right) \right) \exp \left( -i \theta_0^{1/2} \theta \right) + \text{c.c.}$$

Eq. (6.2.9) transforms this into a solution, still near the soliton, but for *negative*  $\theta$ :

$$\psi_{\theta_0} \sim \frac{1}{\sqrt{\pi}} \theta_0^{-1/4} \frac{1}{2i} \exp \left( i \left( \frac{2}{3} \theta_0^{3/2} + \frac{\pi}{4} \right) \right) \frac{1}{T_{\theta_0^{1/2}/\tau_1}} \left[ \exp \left( -i \theta_0^{1/2} \theta \right) + R_{\theta_0^{1/2}/\tau_1} \exp \left( i \theta_0^{1/2} \theta \right) \right] + \text{c.c.},$$

where  $R_{\omega}$  and  $T_{\omega}$  are the reflection and transmission amplitudes defined in Eqs. (6.2.10) and (6.2.11). We may now use Eq. (6.7.7) and its complex conjugate to express this solution in terms of Airy functions, allowing it to hold for all negative  $\theta$ :

$$\begin{aligned} \psi_{\theta_0} &\sim \frac{1}{2T_{\theta_0^{1/2}/\tau_1}} \left[ \exp \left( i \frac{4}{3} \theta_0^{3/2} \right) R_{\theta_0^{1/2}/\tau_1} (\text{Bi}(\theta - \theta_0) - i \text{Ai}(\theta - \theta_0)) + \text{Ai}(\theta - \theta_0) - i \text{Bi}(\theta - \theta_0) \right] + \text{c.c.} \\ &= \text{Re} \left\{ \frac{1}{T_{\theta_0^{1/2}/\tau_1}} \left[ 1 - i \exp \left( i \frac{4}{3} \theta_0^{3/2} \right) R_{\theta_0^{1/2}/\tau_1} \right] \right\} \text{Ai}(\theta - \theta_0) \\ &\quad + \text{Im} \left\{ \frac{1}{T_{\theta_0^{1/2}/\tau_1}} \left[ 1 + i \exp \left( i \frac{4}{3} \theta_0^{3/2} \right) R_{\theta_0^{1/2}/\tau_1} \right] \right\} \text{Bi}(\theta - \theta_0). \end{aligned}$$

We can now read off the expressions for the coefficients  $c_{\theta_0}^A$  and  $c_{\theta_0}^B$ :

$$c_{\theta_0}^A = \text{Re} \left\{ \frac{1}{T_{\theta_0^{1/2}/\tau_1}} \left[ 1 - i \exp \left( i \frac{4}{3} \theta_0^{3/2} \right) R_{\theta_0^{1/2}/\tau_1} \right] \right\}, \quad (6.7.8)$$

$$c_{\theta_0}^B = \text{Im} \left\{ \frac{1}{T_{\theta_0^{1/2}/\tau_1}} \left[ 1 + i \exp \left( i \frac{4}{3} \theta_0^{3/2} \right) R_{\theta_0^{1/2}/\tau_1} \right] \right\}. \quad (6.7.9)$$

## 6.8. Solution in the decelerating case

Having derived the form of the eigenfunctions when a constant deceleration of the pulse is included, we now use these in the calculation of the spectrum due to frequency shifting. The general solution of Eq. (6.7.4) is a linear superposition of the eigenfunctions  $\psi_{\theta_0}$  with the  $\zeta$ -dependent phase of Eq. (6.6.2) replaced:

$$\psi(\theta, \zeta) = \int_{-\infty}^{+\infty} c(\theta_0) \psi_{\theta_0}(\theta) \exp \left( i \frac{a\zeta\tau_1}{\beta_{2,m}u_0^2} \theta_0 \right) d\theta_0. \quad (6.8.1)$$

## 6. Frequency Shifting in Optical Fibres

The coefficients  $c(\theta_0)$  are completely determined by the value of  $\psi$  at  $\zeta = 0$ ; for, using the orthonormality condition of Eq. (6.7.2), we have

$$\begin{aligned} \int_{-\infty}^{+\infty} \psi(\theta, 0) \psi_{\theta_0}(\theta) d\theta &= \int_{-\infty}^{+\infty} \int_{-\infty}^{+\infty} c(\theta'_0) \psi_{\theta'_0}(\theta) \psi_{\theta_0}(\theta) d\theta'_0 d\theta \\ &= \int_{-\infty}^{+\infty} c(\theta'_0) \delta(\theta_0 - \theta'_0) d\theta'_0 \\ &= c(\theta_0) . \end{aligned}$$

The general solution for the envelope  $\mathcal{E}$ , where the electric field  $E = \mathcal{E} \exp(i\beta_m z - i\omega_m t)$ , is found by replacing the phases extracted in Eq. (6.5.9):

$$\mathcal{E}(\theta, \zeta) = \exp\left(-i\frac{a\zeta\tau_1}{\beta_{2,m}u_0^2}\theta - i\frac{a^2\zeta^3}{6\beta_{2,m}u_0^3}\right) \psi(\theta, \zeta) . \quad (6.8.2)$$

As before, our initial wave is the value of the continuous-wave probe at the input of the fibre ( $\zeta = 0$ ); that is,

$$\psi(\theta, 0) = \exp(-i\bar{\omega}_p\tau_1\theta) , \quad (6.8.3)$$

where  $\bar{\omega}_p = \omega_p - \omega_m$ . The coefficients  $c(\theta_0)$ , then, are given by

$$\begin{aligned} c(\theta_0) &= \int_{-\infty}^{+\infty} \exp(-i\bar{\omega}_p\tau_1\theta) \psi_{\theta_0}(\theta) d\theta \\ &= \tilde{\psi}_{\theta_0}(-\bar{\omega}_p\tau_1) , \end{aligned}$$

where we have defined the Fourier-transformed eigenfunction

$$\tilde{\psi}_{\theta_0}(w) = \int_{-\infty}^{+\infty} \exp(iw\theta) \psi_{\theta_0}(\theta) d\theta . \quad (6.8.4)$$

The continuous wave of Eq. (6.8.3) therefore evolves according to

$$\psi(\theta, \zeta) = \int_{-\infty}^{+\infty} \tilde{\psi}_{\theta_0}(-\bar{\omega}_p\tau_1) \psi_{\theta_0}(\theta) \exp\left(i\frac{a\zeta\tau_1}{\beta_{2,m}u_0^2}\theta_0\right) d\theta_0 ,$$

and the probe envelope is given by

$$\mathcal{E}(\theta, \zeta) = \exp\left(-i\frac{a^2\zeta^3}{6\beta_{2,m}u_0^3}\right) \int_{-\infty}^{+\infty} \tilde{\psi}_{\theta_0}(-\bar{\omega}_p\tau_1) \psi_{\theta_0}(\theta) \exp\left(-i\frac{a\zeta\tau_1}{\beta_{2,m}u_0^2}(\theta - \theta_0)\right) d\theta_0 .$$

In order to find the power spectrum, which is the measured quantity in experiment, we must take the Fourier transform of the probe envelope, which gives

$$\tilde{\mathcal{E}}(w, \zeta) = \exp\left(-i\frac{a^2\zeta^3}{6\beta_{2,m}u_0^3}\right) \int_{-\infty}^{+\infty} \tilde{\psi}_{\theta_0}(-\bar{\omega}_p\tau_1) \tilde{\psi}_{\theta_0}\left(w - \frac{a\zeta\tau_1}{\beta_{2,m}u_0^2}\right) \exp\left(i\frac{a\zeta\tau_1}{\beta_{2,m}u_0^2}\theta_0\right) d\theta_0 . \quad (6.8.5)$$

This is not yet in a form suitable for numerical integration, because the spectrum contains a  $\delta$  function, for the same reason given in the non-decelerating case: a finite portion of the probe wave interacts with the pulse, while far from the pulse it evolves just as a continuous wave in the absence of a pulse. We therefore expect Eq. (6.8.5) to contain a term  $\delta(w - \bar{\omega}_p \tau_1)$ , and this must first be extracted in order to make the numerical integration stable. To this end, we introduce some further definitions. Consider the identity

$$\int_{-\infty}^{+\infty} \exp(iw\theta) \text{Ai}(\theta - \theta_0) d\theta = \exp\left(-i\frac{w^3}{3} + iw\theta_0\right) \quad (6.8.6)$$

as motivation for the following definitions:

$$\int_{-\infty}^0 \exp(iw\theta) \text{Ai}(\theta - \theta_0) d\theta = \exp\left(-i\frac{w^3}{3} + iw\theta_0\right) a_{\theta_0}(w), \quad (6.8.7)$$

$$\int_{-\infty}^0 \exp(iw\theta) \text{Bi}(\theta - \theta_0) d\theta = \exp\left(-i\frac{w^3}{3} + iw\theta_0\right) b_{\theta_0}(w). \quad (6.8.8)$$

Both  $a_{\theta_0}(w)$  and  $b_{\theta_0}(w)$  must approach zero as  $\theta_0 \rightarrow -\infty$ , while as  $\theta_0 \rightarrow +\infty$ ,  $a_{\theta_0}(w)$  approaches unity while  $b_{\theta_0}(w)$  diverges exponentially. Note that Eqs. (6.8.6) and (6.8.7) together imply the following:

$$\int_0^{+\infty} \exp(iw\theta) \text{Ai}(\theta - \theta_0) d\theta = \exp\left(-i\frac{w^3}{3} + iw\theta_0\right) [1 - a_{\theta_0}(w)]. \quad (6.8.9)$$

Substitution of Eqs. (6.8.7)-(6.8.9) in Eq. (6.8.4) gives, for the Fourier-transformed eigenfunction,

$$\tilde{\psi}_{\theta_0}(w) = \exp\left(-i\frac{w^3}{3} + iw\theta_0\right) \xi_{\theta_0}(w), \quad (6.8.10)$$

where we have defined

$$\xi_{\theta_0}(w) = \mathcal{N}_{\theta_0} [1 + (c_{\theta_0}^A - 1) a_{\theta_0}(w) + c_{\theta_0}^B b_{\theta_0}(w)]. \quad (6.8.11)$$

The function  $\xi_{\theta_0}(w)$  approaches unity both as  $\theta_0 \rightarrow -\infty$  and as  $\theta_0 \rightarrow +\infty$ . It is this asymptotic behaviour that generates the  $\delta$  function. Plugging Eq. (6.8.10) into Eq. (6.8.5), we have

$$\begin{aligned} \tilde{\mathcal{E}}(w, \zeta) &= \exp\left(-i\frac{a^2\zeta^3}{6\beta_{2,m}u_0^3} + i\frac{1}{3}(\bar{\omega}_p\tau_1)^3 - i\frac{1}{3}\left(w - \frac{a\zeta\tau_1}{\beta_{2,m}u_0^2}\right)^3\right) \\ &\quad \int_{-\infty}^{+\infty} \exp(i(w - \bar{\omega}_p\tau_1)\theta_0) \xi_{\theta_0}(-\bar{\omega}_p\tau_1) \xi_{\theta_0}\left(w - \frac{a\zeta\tau_1}{\beta_{2,m}u_0^2}\right) d\theta_0 \\ &= \exp\left(-i\frac{a^2\zeta^3}{6\beta_{2,m}u_0^3} + i\frac{1}{3}(\bar{\omega}_p\tau_1)^3 - i\frac{1}{3}\left(w - \frac{a\zeta\tau_1}{\beta_{2,m}u_0^2}\right)^3\right) \\ &\quad \left\{ 2\pi \delta(w - \bar{\omega}_p\tau_1) \right. \\ &\quad \left. + \int_{-\infty}^{+\infty} \exp(i(w - \bar{\omega}_p\tau_1)\theta_0) \left[ \xi_{\theta_0}(-\bar{\omega}_p\tau_1) \xi_{\theta_0}\left(w - \frac{a\zeta\tau_1}{\beta_{2,m}u_0^2}\right) - 1 \right] d\theta_0 \right\} \quad (6.8.12) \end{aligned}$$

## 6.9. Comparison with experimental results

In order to take the Raman deceleration into account, we must have some idea of its value, or, equivalently, of the value of  $\tau_1$ . This can be estimated from measurable quantities as follows. Dispersion is normally measured via the group-velocity dispersion  $D = \partial^2\beta/\partial\omega\partial\lambda$ , or, since  $\partial\beta/\partial\omega$  is simply the inverse of the group velocity,  $D = \partial(1/v_g)/\partial\lambda$ . If the wavelength shift of the soliton,  $\Delta\lambda_s$ , is measured, then we have

$$\frac{1}{v_f} - \frac{1}{v_i} \approx D_s \Delta\lambda_s, \quad (6.9.1)$$

where  $v_i$  and  $v_f$  are the initial and final values of the soliton's group velocity, and  $D_s$  is the value of  $D$  at the soliton wavelength. Then

$$v_f - v_i = v_f v_i \left( \frac{v_f - v_i}{v_f v_i} \right) = v_f v_i \left( \frac{1}{v_i} - \frac{1}{v_f} \right) \approx -u_0^2 D_s \Delta\lambda_s, \quad (6.9.2)$$

where  $u_0$  is the initial velocity of the soliton, and we have assumed that its fractional change over the course of the fibre is much less than unity. According to Eq. (6.5.1), we have  $v_f - v_i = -aL/u_0$ , where  $L$  is the length of the fibre. Therefore,

$$\frac{a}{u_0^3} \approx \frac{D_s \Delta\lambda_s}{L}. \quad (6.9.3)$$

Plugging this into the definition of  $\tau_1$  (Eq. (6.6.5)), and using the identity  $\beta_2 = \partial^2\beta/\partial\omega^2 = -(\lambda^2/2\pi c) D$ , we find

$$\tau_1 \approx \left( \frac{D_m^2 \lambda_m^4 L}{8\pi^2 c^2 D_s \Delta\lambda_s} \right)^{1/3}. \quad (6.9.4)$$

In our experimental setup, this gives  $\tau_1 \approx 650$  fs.

The above derivation of the value of  $\tau_1$  took an experimentally observed value of the soliton wavelength shift,  $\Delta\lambda_s$ . We may also reinforce the conclusion by using an analytic expression for this shift (as given in Reference [63]):

$$\Delta\omega_s = \omega_f - \omega_i = -\frac{8T_R |\beta_{2,s}| L}{15T_s^4} = -\frac{4T_R \lambda_s^2 D_s L}{15\pi c T_s^4}, \quad (6.9.5)$$

where  $T_s$  is the soliton width (as appears in Eq. (6.2.5)) and  $T_R$  is a Raman parameter that is found to be around 3 fs in silica. The change in wavelength is therefore

$$\Delta\lambda_s \approx \frac{\partial\lambda}{\partial\omega} \Delta\omega_s = -\frac{\lambda_s^2}{2\pi c} \Delta\omega_s = \frac{2T_R \lambda_s^4 D_s L}{15\pi^2 c^2 T_0^4}. \quad (6.9.6)$$

Plugging this into Eq. (6.9.4), we find

$$\tau_1 \approx \left( \frac{15\lambda_m^4 D_m^2 T_s}{16\lambda_s^4 D_s^2 T_R} \right)^{1/3} T_s. \quad (6.9.7)$$

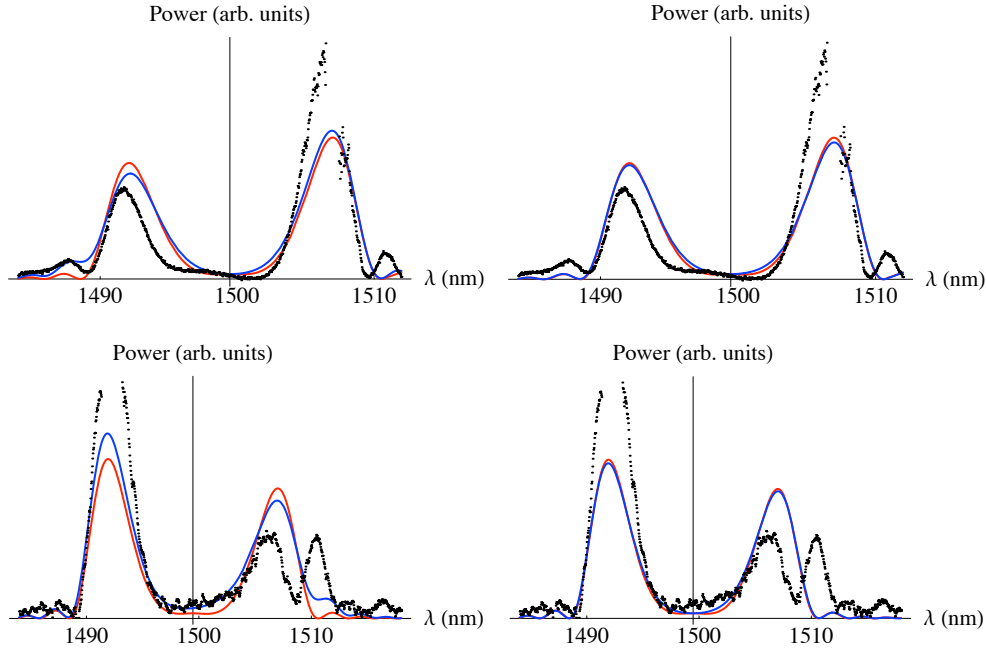


Figure 6.6.: FREQUENCY SHIFTING SPECTRA INCLUDING RAMAN DECELERATION: The dots are experimental data, while the curves are theoretical predictions, without (dashed line) and with (solid line) the Raman effect. The experimentally obtained spectra are normalized with respect to the probe power and are measured in parts per million (ppm). The heights of the theoretical curves were fitted using the least- $\chi^2$  method. (Data courtesy of Chris Kuklewicz and Friedrich König.)

## 6. Frequency Shifting in Optical Fibres

Again, we find  $\tau_1 \approx 650$  fs.

Figure 6.6 shows plots of the theoretical predictions for the spectra - both without (Eq. (6.4.8)) and with (Eq. (6.8.12)) the Raman effect - and the experimentally observed spectra. We see that, if  $\tau_1$  is taken to be 650 fs as deduced above, then the Raman deceleration of the soliton has very little effect: the spectra are almost the same as those calculated when the soliton propagates at a constant speed. Plots are also shown when  $\tau_1$  takes a value of 325 fs, for it is only at around this value that the Raman effect makes appreciable differences to the frequency-shifting spectra. Since  $a \propto \tau_1^{-3}$ , this corresponds to a deceleration - and a wavelength shift - higher than the deduced values by a factor of 8. It thus appears that the discrepancies between theory and experiment are *not* due to the Raman effect.

## 6.10. Conclusion and discussion

The Kerr interaction between pulse and probe does, indeed, induce the equivalent of a group-velocity horizon for some probe frequencies. Frequency shifting occurs, and has been experimentally observed. The theoretical prediction varies negligibly when the Raman effect is taken into account - the Raman deceleration must be increased by an order of magnitude before it has any noticeable effect. However, a discrepancy between theory and experiment remains, and is as yet unresolved.



## 7. The Fibre-Optical Model for Hawking Radiation

The previous chapter has shown that pulses in optical fibres do exhibit features of black- and white-hole horizons, and that the effects of these horizons are experimentally detectable. This raises expectations that Hawking radiation might also be among these features. In this chapter, we present an analysis almost exactly analogous to that of Chapter 2, but using instead the probe/pulse system described in §§5.2 and 5.3. This shall lead us to conclude that Hawking radiation is indeed possible in this system.

### 7.1. Action and scalar product

We begin, as before, with an action integral:

$$S = \int \int d\tau d\zeta u L(A, \partial_\zeta A, \partial_\tau A, \partial_\tau^2 A, \dots) . \quad (7.1.1)$$

The Lagrangian for electromagnetic fields is given by [80]

$$\begin{aligned} L &= \frac{1}{2}\epsilon_0 (n^2|E|^2 - c^2|B|^2) \\ &= \frac{1}{2}\epsilon_0 (n^2|\partial_t A|^2 - c^2|\partial_z A|^2) . \end{aligned} \quad (7.1.2)$$

The refractive index depends on both the dispersion of the fibre and, as we have seen (see Eq. (5.2.33)), on the nonlinearity induced by a pulse. Given that the dispersion is normally described via the propagation constant  $\beta = n\omega/c$ , the Lagrangian is naturally modified to include the dispersive and nonlinear effects as follows:

$$\begin{aligned} L &= \frac{1}{2}\epsilon_0 [c^2|\beta(i\partial_t)A|^2 + \chi|\partial_t A|^2 - c^2|\partial_z A|^2] \\ &= \frac{1}{2}\epsilon_0 \left[ c^2|\beta(i\partial_\tau)A|^2 + \chi|\partial_\tau A|^2 - \frac{c^2}{u^2}|(\partial_\zeta - \partial_\tau)A|^2 \right] , \end{aligned} \quad (7.1.3)$$

where, in the second line, we have transformed to the coordinates  $\tau$  and  $\zeta$  via the transformation of Eqs. (5.3.3) and (5.3.4). Then, plugging into the Euler-Lagrange equation (2.1.3) (with appropriate re-labelling), we find the wave equation

$$\frac{c^2}{u^2}(\partial_\zeta - \partial_\tau)^2 A + c^2\beta^2(i\partial_\tau)A - \partial_\tau(\chi\partial_\tau A) = 0 . \quad (7.1.4)$$

## 7. The Fibre-Optical Model for Hawking Radiation

In the case where the fibre is dispersionless, with a refractive index  $n$  that is independent of frequency, the Lagrangian reduces to

$$L = \frac{1}{2}\epsilon_0 \left[ (n^2 + \chi) |\partial_\tau A|^2 - \frac{c^2}{u^2} |(\partial_\zeta - \partial_\tau) A|^2 \right], \quad (7.1.5)$$

and we see that the effect of the nonlinearity  $\chi$  is to increase the refractive index in accordance with Eq. (5.2.33). Unfortunately, Eq. (7.1.5) cannot be written in the form for a massless scalar field, i.e., there is no metric such that  $L = \frac{1}{2}\sqrt{-g}g^{\mu\nu}\partial_\mu A^*\partial_\nu A$ . For, in order to find such a metric, we must multiply Eq. (7.1.5) by a factor of  $u/c/\sqrt{n^2 + \chi}$ , and since  $\chi$  is  $\tau$ -dependent, this alters the wave equation. However, we can gain some insight by continuing down this road, the following results being exact if  $\chi$  is constant. The resulting Lagrangian corresponds to a massless scalar field in a spacetime with metric

$$ds^2 = \frac{u^2}{c^2} (n^2 + \chi) d\zeta^2 - (d\tau + d\zeta)^2. \quad (7.1.6)$$

Comparing with the general form of Eq. (1.1.7), we see that Eq. (7.1.6) describes a moving medium in which the flow velocity is constant ( $V = -1$ ), but the velocity of null trajectories (i.e., the velocity of waves) with respect to the medium has the  $\tau$ -dependent value  $\frac{u^2}{c^2}(n^2 + \chi)$ . This is in accordance with the discussion in §5.4: the pulse affects not the velocity of the fibre, but of the waves with respect to the fibre. An event horizon is established wherever  $\chi = c^2/u^2 - n^2$ , and the Hawking temperature is given, as in Eq. (1.7.3), by the derivative of the wave velocity at the horizon:

$$T = \frac{1}{2\pi} \frac{d}{d\tau} \left[ \frac{u}{c} \sqrt{n^2 + \chi} - 1 \right]_{\chi=c^2/u^2-n^2} = \frac{1}{4\pi} \frac{u^2}{c^2} \chi'(\tau_h). \quad (7.1.7)$$

This is inexact, but we shall see in §9.4 that, if  $\chi = c^2/u^2 - n^2$  at some point and the variation in  $\chi$  is small, the resulting Hawking temperature does indeed agree with Eq. (7.1.7).

Returning to the exact Lagrangian of Eq. (7.1.3), we remark that, like its acoustic counterpart (see §2.1), it is invariant with respect to both translation in  $\zeta$  (“time” translation) and phase rotation of  $A$ . The former leads to the existence of stationary modes, discussed in the next section; the latter leads to conservation of the scalar product

$$\begin{aligned} (A_1, A_2) &= i\epsilon_0 \frac{c^2}{u^2} \int d\tau [A_1^* (\partial_\zeta - \partial_\tau) A_2 - A_2 (\partial_\zeta - \partial_\tau) A_1^*] \\ &= i \int d\tau [A_2 \pi_1^* - A_1^* \pi_2], \end{aligned} \quad (7.1.8)$$

where  $\pi$  is the canonical momentum,

$$\pi = \frac{\partial L}{\partial (\partial_\zeta A^*)} = -\epsilon_0 \frac{c^2}{u^2} (\partial_\zeta - \partial_\tau) A. \quad (7.1.9)$$

In regions where  $\chi$  is constant in  $\tau$ , the formula for the scalar product can be written in a more instructive form. We separate the branches of the dispersion relation into those

## 7.2. Decomposition into modes

with positive and negative lab frame wavenumbers, i.e., we define the two branches via the dispersion relations  $(\omega - \omega')/u = |\beta_\chi(\omega)|$  and  $(\omega - \omega')/u = -|\beta_\chi(\omega)|$ , or

$$\omega' = \omega \mp u |\beta_\chi(\omega)|, \quad (7.1.10)$$

where  $\beta_\chi(\omega) = \beta(\omega) \sqrt{1 + \chi/n^2(\omega)}$ . (Note that the *minus* sign in Eq. (7.1.10) corresponds to a *positive* lab-frame wavenumber, and vice versa.) Any solution of the optical wave equation can be expressed as a sum of two Fourier integrals, covering the two branches of the dispersion relation:

$$A(\tau, \zeta) = \frac{1}{2\pi} \int_{-\infty}^{+\infty} \tilde{A}^{(+)}(\omega) e^{-i\omega\tau - i(\omega - u|\beta_\chi(\omega)|)\zeta} d\omega \\ + \frac{1}{2\pi} \int_{-\infty}^{+\infty} \tilde{A}^{(-)}(\omega) e^{-i\omega\tau - i(\omega + u|\beta_\chi(\omega)|)\zeta} d\omega. \quad (7.1.11)$$

The canonical momentum, defined in Eq. (7.1.9), is

$$\pi(\tau, \zeta) = \frac{-i \epsilon_0 c^2}{2\pi u} \int_{-\infty}^{+\infty} |\beta_\chi(\omega)| \tilde{A}^{(+)}(\omega) e^{-i\omega\tau - i(\omega - u|\beta_\chi(\omega)|)\zeta} d\omega \\ + \frac{i \epsilon_0 c^2}{2\pi u} \int_{-\infty}^{+\infty} |\beta_\chi(\omega)| \tilde{A}^{(-)}(\omega) e^{-i\omega\tau - i(\omega + u|\beta_\chi(\omega)|)\zeta} d\omega. \quad (7.1.12)$$

Then, applying Eq. (7.1.8) for the scalar product, we find

$$(A_1, A_2) = \frac{1}{\pi} \frac{\epsilon_0 c^2}{u} \int_{-\infty}^{+\infty} |\beta_\chi(\omega)| \left\{ \tilde{A}_1^{(+)*}(\omega) \tilde{A}_2^{(+)}(\omega) - \tilde{A}_1^{(-)*}(\omega) \tilde{A}_2^{(-)}(\omega) \right\} d\omega. \quad (7.1.13)$$

In the case of the norm of a wave - the scalar product of the wave with itself - this becomes

$$(A, A) = \frac{1}{\pi} \frac{\epsilon_0 c^2}{u} \int_{-\infty}^{+\infty} |\beta_\chi(\omega)| \left\{ \left| \tilde{A}^{(+)}(\omega) \right|^2 - \left| \tilde{A}^{(-)}(\omega) \right|^2 \right\} d\omega. \quad (7.1.14)$$

This is completely analogous to the acoustic case, where we also found (see §2.2) that the norm was determined by the difference of the squared magnitudes of the Fourier components corresponding to the two different branches of the dispersion relation. That these contribute to the norm with different signs means that it is possible to increase the norm of each separately while maintaining the value of the overall norm; this corresponds to pair creation. Our switching of the roles of space and time has caused the integration to be over  $\omega$  (rather than  $k$ ), and the factor multiplying the Fourier components is the lab-frame wavenumber (rather than the free-fall frequency).

## 7.2. Decomposition into modes

Just as for the acoustic field, we can express the general optical field  $A(\tau, \zeta)$  as a linear superposition of orthonormal modes. For now, we shall continue to assume that  $\chi$  is

## 7. The Fibre-Optical Model for Hawking Radiation

constant in  $\tau$  (this condition is relaxed in §7.3). We first note that the branches of the dispersion relation characterised by the sign of the norm are related via complex conjugation:

$$e^{-i\omega\tau - i(\omega - |\beta_\chi(\omega)|)\zeta} = \left[ e^{-i(-\omega)\tau - i(-\omega + |\beta_\chi(-\omega)|)\zeta} \right]^*.$$

We therefore define  $\omega' = \omega - u |\beta_\chi(\omega)|$  (taking the norm to be positive) and include the complex conjugates of the resulting plane waves, forming a complete set of solutions. The normalized plane wave solutions are defined as

$$A_\omega(\tau, \zeta) = \sqrt{\frac{u}{4\pi\epsilon_0 c^2 |\beta_\chi(\omega)|}} e^{-i\omega\tau - i(\omega - u |\beta_\chi(\omega)|)\zeta}. \quad (7.2.1)$$

Given this definition, the scalar products between modes are given by

$$(A_{\omega_1}, A_{\omega_2}) = - (A_{\omega_1}^*, A_{\omega_2}^*) = \delta(\omega_1 - \omega_2), \quad (A_{\omega_1}, A_{\omega_2}^*) = (A_{\omega_1}^*, A_{\omega_2}) = 0. \quad (7.2.2)$$

If we transform back to the lab coordinates  $z$  and  $t$  (using Eqs. (5.3.1) and (5.3.2)), the phase of the mode  $A_\omega$  transforms as

$$\begin{aligned} \varphi = -\omega\tau - (\omega - u |\beta_\chi(\omega)|)\zeta &= -\omega \left( t - \frac{z}{u} \right) - (\omega - u |\beta_\chi(\omega)|) \frac{z}{u} \\ &= |\beta_\chi(\omega)| z - \omega t, \end{aligned}$$

so positive-norm modes are those that

- if  $\omega > 0$ , propagate along the fiber in the forward (co-propagating) direction, i.e., they are  $u$ -modes;
- if  $\omega < 0$ , propagate along the fiber in the backward (counter-propagating) direction, i.e., they are  $v$ -modes.

For negative-norm modes, the sign in front of  $|\beta_\chi(\omega)|$  is changed, and the reverse is true.

It would do well to re-emphasise that  $\omega$  is the frequency *as measured in the laboratory*, and it is generally *not* conserved. It should not be confused with the frequency  $\omega$  as defined in the context of the acoustic model, which is a genuine Killing frequency. Rather, the co-moving frequency  $\omega'$  is a Killing frequency here, while  $\omega$  is analogous to the wavevector  $k$  in the acoustic model. So that statement that  $v$ -modes with  $\omega < 0$  have positive norm, despite first appearances, is actually in accordance with the similar statement made in §2.3.

Expressing the total optical field  $A$  as a sum over the individual modes, and constraining  $A$  to be real since it describes a physical quantity, we have

$$A(\tau, \zeta) = \int_{-\infty}^{+\infty} \{a(\omega) A_\omega(\tau, \zeta) + a^*(\omega) A_\omega^*(\tau, \zeta)\} d\omega, \quad (7.2.3)$$

with canonical momentum

$$\pi(\tau, \zeta) = -i \frac{\epsilon_0 c^2}{u} \int_{-\infty}^{+\infty} |\beta_\chi(\omega)| \{a(\omega) A_\omega(\tau, \zeta) - a^*(\omega) A_\omega^*(\tau, \zeta)\} d\omega, \quad (7.2.4)$$

### 7.3. Transforming to the $\omega'$ -representation

where the coefficient functions can be expressed very simply using the orthonormality conditions of Eqs. (7.2.2):

$$a(\omega) = (A_\omega, A), \quad a^*(\omega) = -(A_\omega^*, A). \quad (7.2.5)$$

The optical field is readily quantized: the real-valued quantities  $A$  and  $\pi$  are promoted to the Hermitian operators  $\hat{A}$  and  $\hat{\pi}$ , and the coefficients  $a(\omega)$  and  $a^*(\omega)$  to the Hermitian conjugate operators  $\hat{a}_\omega$  and  $\hat{a}_\omega^\dagger$ :

$$\hat{A}(\tau, \zeta) = \int_{-\infty}^{+\infty} \left\{ \hat{a}_\omega A_\omega(\tau, \zeta) + \hat{a}_\omega^\dagger A_\omega^*(\tau, \zeta) \right\} d\omega, \quad (7.2.6)$$

$$\hat{\pi}(\tau, \zeta) = -i \frac{\epsilon_0 c^2}{u} \int_{-\infty}^{+\infty} |\beta_\chi(\omega)| \left\{ \hat{a}_\omega A_\omega(\tau, \zeta) - \hat{a}_\omega^\dagger A_\omega^*(\tau, \zeta) \right\} d\omega. \quad (7.2.7)$$

Imposing the equal time (i.e., equal propagation time,  $\zeta$ ) commutation relation

$$[\hat{A}(\tau_1, \zeta), \hat{\pi}(\tau_2, \zeta)] = i \delta(\tau_1 - \tau_2), \quad (7.2.8)$$

we find that  $\hat{a}_\omega$  and  $\hat{a}_\omega^\dagger$  satisfy the Bose commutation relations

$$[\hat{a}_{\omega_1}, \hat{a}_{\omega_2}^\dagger] = \delta(\omega_1 - \omega_2), \quad [\hat{a}_{\omega_1}, \hat{a}_{\omega_2}] = [\hat{a}_{\omega_1}^\dagger, \hat{a}_{\omega_2}^\dagger] = 0. \quad (7.2.9)$$

### 7.3. Transforming to the $\omega'$ -representation

Eqs. (7.2.6)-(7.2.9) describe the field in the  $\omega$ -representation, i.e., the variable used to specify the various field modes is the lab frequency  $\omega$ . This is fine when  $\chi$  is constant. However, if  $\chi$  is a function of  $\tau$ , then  $\omega$  is not conserved, and the field modes defined above are only valid in regions where  $\chi$  is approximately constant. Even then, these modes do not evolve independently, but can be transformed into each other by the inhomogeneous nonlinearity profile. To express the field in terms of modes which do evolve independently, we must use a representation based on the conserved co-moving frequency  $\omega'$ . (This is analogous to the transformation from the  $k$ - to the  $\omega$ -representation performed in §2.4.)

#### 7.3.1. Constant $\chi$

We begin by assuming a constant value of  $\chi$ . The dispersion relation is given by the positive-norm branch of Eq. (7.1.10),

$$\omega - \omega' = u |\beta_\chi(\omega)| = \frac{u}{c} |\omega| n(\omega) \sqrt{1 + \frac{\chi}{n^2(\omega)}}, \quad (7.3.1)$$

and the possible values of  $\omega$  corresponding to a single value of  $\omega'$  are found by plotting these two functions and noting their points of intersection, as illustrated in Figure 7.1.

Since the function  $\omega(\omega')$  is multi-valued, the transformation from an integral over  $\omega$  to an integral over  $\omega'$  must be split into several terms, each of which covers a branch over which  $\omega(\omega')$  is single-valued. An examination of Fig. 7.1 shows that there are four such branches:

## 7. The Fibre-Optical Model for Hawking Radiation

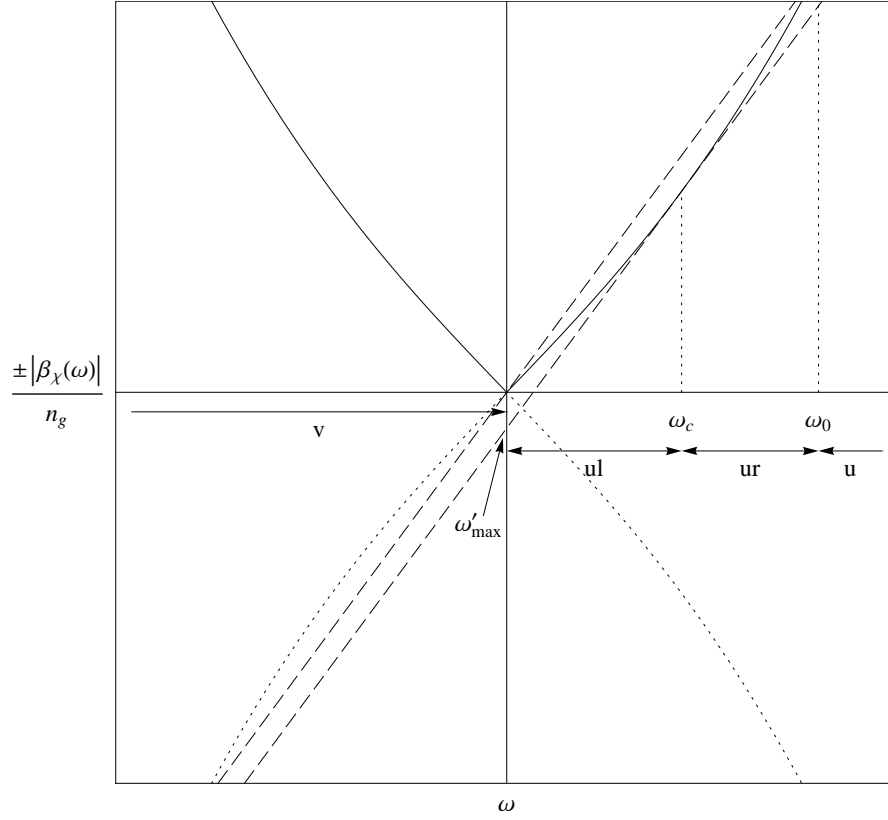


Figure 7.1.: SOLUTIONS OF FIBRE-OPTICAL DISPERSION RELATION: For given values of  $\chi$  and  $\omega'$ , the possible lab frequencies  $\omega$  are the points of intersection of the straight line  $\omega - \omega'$  and the dispersion curve  $\pm u |\beta_\chi(\omega)|$ . If  $\chi < c^2/u^2 - 1$ , the real  $\omega$ -axis splits into the four branches  $v$ ,  $ul$ ,  $ur$  and  $u$ ; these are delimited by  $\omega' = 0$  and  $\omega' = \omega'_{\max}$ , whose corresponding curves are plotted here as dashed lines. If  $\omega' > 0$ , there are two positive-norm solutions, which lie on the  $v$ - and  $u$ -branches; if  $-\omega'_{\max} < \omega' < 0$ , there are still two positive-norm solutions, but they lie on the  $ul$ - and  $ur$ -branches.

### 7.3. Transforming to the $\omega'$ -representation

- $-\infty < \omega < 0$ , which covers all plane waves that are backward-propagating in the lab frame; this is the  $v$ -branch;
- $0 < \omega < \omega_c$ , where  $\omega_c$  has the most negative value of the co-moving frequency, which we shall call  $-\omega'_{\max}$ ; these waves are forward-propagating and have a negative-directed (left-moving) group velocity in the co-moving frame, and thus make up the  $ul$ -branch;
- $\omega_c < \omega < \omega_0$ , where  $\omega_0$  has zero co-moving frequency; these forward-propagating waves have a positive-directed (right-moving) group velocity in the co-moving frame, and make up the  $ur$ -branch;
- $\omega_0 < \omega < \infty$ , which covers the remainder of the waves that are forward-propagating in the lab frame; this is the remaining  $u$ -branch.

The integral over all  $\omega$  is a sum of the integrals over each of these branches:

$$\int_{-\infty}^0 \hat{a}_\omega A_\omega(\tau, \zeta) d\omega = \int_0^\infty \hat{a}_{\omega^v(\omega')} A_{\omega^v(\omega')}(\tau, \zeta) \left| \frac{d\omega^v}{d\omega'} \right| d\omega' = \int_0^\infty \hat{a}_{\omega'}^v A_{\omega'}^v(\tau) e^{-i\omega'\zeta} d\omega', \quad (7.3.2)$$

$$\int_0^{\omega_c} \hat{a}_\omega A_\omega(\tau, \zeta) d\omega = \int_{-\omega'_{\max}}^0 \hat{a}_{\omega^{ul}(\omega')} A_{\omega^{ul}(\omega')}(\tau, \zeta) \left| \frac{d\omega^{ul}}{d\omega'} \right| d\omega' = \int_{-\omega'_{\max}}^0 \hat{a}_{\omega'}^{ul} A_{\omega'}^{ul}(\tau) e^{-i\omega'\zeta} d\omega', \quad (7.3.3)$$

$$\int_{\omega_c}^{\omega_0} \hat{a}_\omega A_\omega(\tau, \zeta) d\omega = \int_{-\omega'_{\max}}^0 \hat{a}_{\omega^{ur}(\omega')} A_{\omega^{ur}(\omega')}(\tau, \zeta) \left| \frac{d\omega^{ur}}{d\omega'} \right| d\omega' = \int_{-\omega'_{\max}}^0 \hat{a}_{\omega'}^{ur} A_{\omega'}^{ur}(\tau) e^{-i\omega'\zeta} d\omega', \quad (7.3.4)$$

$$\int_{\omega_0}^\infty \hat{a}_\omega A_\omega(\tau, \zeta) d\omega = \int_0^\infty \hat{a}_{\omega^u(\omega')} A_{\omega^u(\omega')}(\tau, \zeta) \left| \frac{d\omega^u}{d\omega'} \right| d\omega' = \int_0^\infty \hat{a}_{\omega'}^u A_{\omega'}^u(\tau) e^{-i\omega'\zeta} d\omega', \quad (7.3.5)$$

where we have defined

$$\hat{a}_{\omega'}^v = \sqrt{\left| \frac{d\omega^v}{d\omega'} \right|} \hat{a}_{\omega^v(\omega')}, \quad A_{\omega'}^v(\tau) e^{-i\omega'\zeta} = \sqrt{\left| \frac{d\omega^v}{d\omega'} \right|} A_{\omega^v(\omega')}(\tau, \zeta), \quad (7.3.6)$$

and similarly for the other branches. These definitions ensure that the newly-defined modes are orthonormal with respect to the co-moving frequency  $\omega'$ ,

$$\begin{aligned} \left( A_{\omega'_1}^v(\tau) e^{-i\omega'_1\zeta}, A_{\omega'_2}^v(\tau) e^{-i\omega'_2\zeta} \right) &= \left| \frac{d\omega^v}{d\omega'} \right| \left( A_{\omega^v(\omega'_1)}(\tau, \zeta), A_{\omega^v(\omega'_2)}(\tau, \zeta) \right) \\ &= \left| \frac{d\omega^v}{d\omega'} \right| \delta(\omega^v(\omega'_1) - \omega^v(\omega'_2)) \\ &= \delta(\omega'_1 - \omega'_2), \end{aligned} \quad (7.3.7)$$

## 7. The Fibre-Optical Model for Hawking Radiation

while the operators obey commutation relations that are now defined with respect to  $\omega'$ ,

$$\begin{aligned} \left[ \hat{a}_{\omega'_1}^v, \hat{a}_{\omega'_2}^{v\dagger} \right] &= \left| \frac{d\omega^v}{d\omega'} \right| \left[ \hat{a}_{\omega^v(\omega'_1)}, \hat{a}_{\omega^v(\omega'_2)}^\dagger \right] \\ &= \left| \frac{d\omega^v}{d\omega'} \right| \delta(\omega^v(\omega'_1) - \omega^v(\omega'_2)) \\ &= \delta(\omega'_1 - \omega'_2) . \end{aligned} \quad (7.3.8)$$

Similar relations hold for the other branches.

Replacing the Hermitian conjugates, the total optical field is given by

$$\begin{aligned} \hat{A}(\tau, \zeta) &= \int_0^\infty \left\{ (\hat{a}_{\omega'}^v A_{\omega'}^v(\tau) + \hat{a}_{\omega'}^u A_{\omega'}^u(\tau)) e^{-i\omega'\zeta} + \left( (\hat{a}_{\omega'}^v)^\dagger [A_{\omega'}^v(\tau)]^* + (\hat{a}_{\omega'}^u)^\dagger [A_{\omega'}^u(\tau)]^* \right) e^{i\omega'\zeta} \right\} d\omega' \\ &+ \int_{-\omega'_{max}}^0 \left\{ \left( \hat{a}_{\omega'}^{ul} A_{\omega'}^{ul}(\tau) + \hat{a}_{\omega'}^{ur} A_{\omega'}^{ur}(\tau) \right) e^{-i\omega'\zeta} + \left( (\hat{a}_{\omega'}^{ul})^\dagger [A_{\omega'}^{ul}(\tau)]^* + (\hat{a}_{\omega'}^{ur})^\dagger [A_{\omega'}^{ur}(\tau)]^* \right) e^{i\omega'\zeta} \right\} d\omega' . \end{aligned} \quad (7.3.9)$$

A mode with negative  $\omega'$  is the Hermitian conjugate of a mode with positive  $\omega'$ , and vice versa. Since any modes with the same co-moving frequency can be mixed, our final task is to rewrite the optical field operator such that all modes with the same  $\omega'$  are grouped together, and each value of  $\omega'$  appears only once. As discussed in §2.4, this amounts to rewriting the second term above - an integral over negative frequencies - as an integral over positive frequencies:

$$\begin{aligned} &\int_{-\omega'_{max}}^0 \left\{ \left( \hat{a}_{\omega'}^{ul} A_{\omega'}^{ul}(\tau) + \hat{a}_{\omega'}^{ur} A_{\omega'}^{ur}(\tau) \right) e^{-i\omega'\zeta} + \left( (\hat{a}_{\omega'}^{ul})^\dagger [A_{\omega'}^{ul}(\tau)]^* + (\hat{a}_{\omega'}^{ur})^\dagger [A_{\omega'}^{ur}(\tau)]^* \right) e^{i\omega'\zeta} \right\} d\omega' \\ &= \int_0^{\omega'_{max}} \left\{ \left( \hat{a}_{-\omega'}^{ul} A_{-\omega'}^{ul}(\tau) + \hat{a}_{-\omega'}^{ur} A_{-\omega'}^{ur}(\tau) \right) e^{i\omega'\zeta} \right. \\ &\quad \left. + \left( (\hat{a}_{-\omega'}^{ul})^\dagger [A_{-\omega'}^{ul}(\tau)]^* + (\hat{a}_{-\omega'}^{ur})^\dagger [A_{-\omega'}^{ur}(\tau)]^* \right) e^{-i\omega'\zeta} \right\} d\omega' . \end{aligned} \quad (7.3.10)$$

Finally, the optical field operator can be expressed in the simple form

$$\hat{A}(\tau, \zeta) = \int_0^\infty \left\{ \hat{A}_{\omega'}(\tau) e^{-i\omega'\zeta} + \hat{A}_{\omega'}^\dagger(\tau) e^{i\omega'\zeta} \right\} d\omega' , \quad (7.3.11)$$

where we have defined

$$\hat{A}_{\omega'}(\tau) = \begin{cases} \hat{a}_{\omega'}^v A_{\omega'}^v(\tau) + \hat{a}_{\omega'}^u A_{\omega'}^u(\tau) + (\hat{a}_{-\omega'}^{ul})^\dagger [A_{-\omega'}^{ul}(\tau)]^* + (\hat{a}_{-\omega'}^{ur})^\dagger [A_{-\omega'}^{ur}(\tau)]^* , & \omega' < \omega'_{max} \\ \hat{a}_{\omega'}^v A_{\omega'}^v(\tau) + \hat{a}_{\omega'}^u A_{\omega'}^u(\tau) , & \omega' > \omega'_{max} \end{cases} . \quad (7.3.12)$$

Just as in the acoustic case, the mixing of positive- and negative-norm modes corresponds to a mixing of annihilation and creation operators. This mixing, however, is still purely incidental if  $\chi$  is independent of  $\tau$ , for then  $\omega$  is separately conserved.



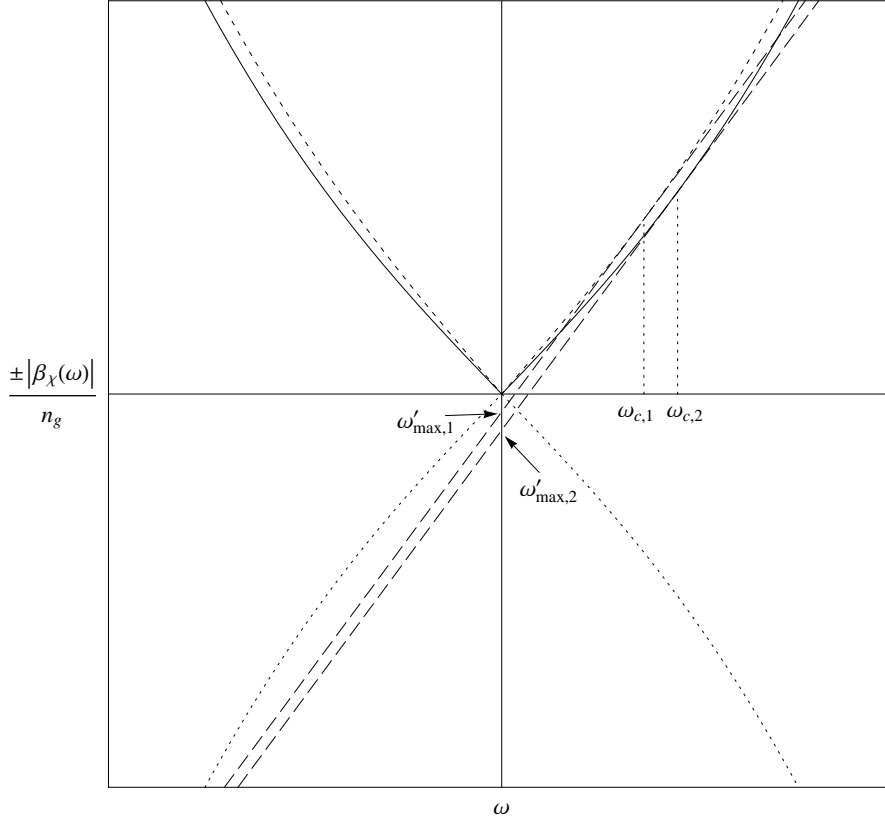


Figure 7.2.: EFFECT OF NONLINEARITY ON SOLUTIONS OF DISPERSION RELATION:

Varying  $\chi$  varies the dispersion profile  $\beta_\chi(\omega)$ , so having different asymptotic values of  $\chi$  results in different asymptotic values of  $\omega'_{\max}$ . Those values of  $\omega'$  that lie between these two values experience a group-velocity horizon.

### 7.3.2. Nonconstant $\chi$

Now let  $\chi$  be a nonconstant function of  $\tau$ . As usual, we assume that  $\chi$  approaches limiting asymptotic values as  $\tau \rightarrow \pm\infty$ ; in practice, since light pulses are localised, these asymptotic values will both be zero, but we needn't make this assumption. Since  $\omega$  is no longer conserved, the description of the field in the  $\omega'$ -representation given by Eqs. (7.3.11) and (7.3.12) is now its natural form. The assignment of branch labels ( $v, u, ul, ur$ ) follows the example set by the acoustic model in §2.4: we specify two types of modes, labelled in- and out-modes, which are characterised either by a single incident frequency scattered into many outgoing frequencies, or many incident frequencies scattered into a single outgoing frequency; the branch label applies to this single incident or outgoing frequency. For a graphical illustration, refer back to Fig. 2.6.

Another difference arises if the asymptotic values of  $\chi$  are distinct. Then the dispersion relation on the right-hand side of Eq. (7.3.1) is slightly different in each asymptotic

## 7. The Fibre-Optical Model for Hawking Radiation

region; in particular,  $\omega'_{max}$  differs, as shown in Figure 7.2. Let us label these different values as  $\omega'_{max,1}$  and  $\omega'_{max,2}$ , with  $\omega'_{max,2} > \omega'_{max,1}$ . Then there are three distinct cases:

- $0 < \omega' < \omega'_{max,1}$ : Both values of  $\chi$  have four real solutions for  $\omega$ , and these solutions vary smoothly as  $\chi$  varies. The mode is decomposed according to the first line of Eq. (7.3.12).
- $\omega'_{max,1} < \omega' < \omega'_{max,2}$ : One value of  $\chi$  has four real solutions for  $\omega$ , while the other has only two. The two that exist for both values of  $\chi$  correspond to the  $v$ - and  $u$ - branches, and these vary smoothly as  $\chi$  is varied. The other two solutions correspond to the  $ur$ - and  $ul$ -branches, and these exist only for one asymptotic value of  $\chi$ . As  $\chi$  varies, these solutions merge, becoming complex conjugates in the other asymptotic region; they thus experience a group-velocity horizon, and, as discussed in §2.4, are combined into a single branch, which will be labelled the  $url$ -branch. The field mode is decomposed similarly to the first line of Eq. (2.4.16).
- $\omega' > \omega'_{max,2}$ : Each value of  $\chi$  has only two real solutions for  $\omega$ , which vary smoothly as  $\chi$  varies. These correspond to the  $v$ - and  $u$ -branches, and the mode is expanded in accordance with the second line of Eq. (7.3.12).

To summarise, the total field remains in the form of Eq. (7.3.11), and the individual modes are now decomposed as follows:

$$\hat{A}_{\omega'}(\tau) = \begin{cases} \hat{a}_{\omega'}^v A_{\omega'}^v(\tau) + \hat{a}_{\omega'}^u A_{\omega'}^u(\tau) + (\hat{a}_{-\omega'}^{ul})^\dagger [A_{-\omega'}^{ul}(\tau)]^* + (\hat{a}_{-\omega'}^{ur})^\dagger [A_{-\omega'}^{ur}(\tau)]^* , & 0 < \omega' < \omega'_{max,1} \\ \hat{a}_{\omega'}^v A_{\omega'}^v(\tau) + \hat{a}_{\omega'}^u A_{\omega'}^u(\tau) + (\hat{a}_{-\omega'}^{url})^\dagger [A_{-\omega'}^{url}(\tau)]^* , & \omega'_{max,1} < \omega' < \omega'_{max,2} \\ \hat{a}_{\omega'}^v A_{\omega'}^v(\tau) + \hat{a}_{\omega'}^u A_{\omega'}^u(\tau) . & \omega' > \omega'_{max,2} \end{cases} .$$

The modes appearing in this decomposition may be in- or out-modes, each of these forming a complete orthonormal set. (Again, see §2.4.) Therefore, we have, for  $0 < \omega' < \omega'_{max,1}$ , the identity

$$\begin{aligned} \hat{A}_{\omega'}(\tau) &= \hat{a}_{\omega'}^{v,in} A_{\omega'}^{v,in}(\tau) + \hat{a}_{\omega'}^{u,in} A_{\omega'}^{u,in}(\tau) + (\hat{a}_{-\omega'}^{ur,in})^\dagger [A_{-\omega'}^{ur,in}(\tau)]^* + (\hat{a}_{-\omega'}^{ul,in})^\dagger [A_{-\omega'}^{ul,in}(\tau)]^* \\ &= \hat{a}_{\omega'}^{v,out} A_{\omega'}^{v,out}(\tau) + \hat{a}_{\omega'}^{u,out} A_{\omega'}^{u,out}(\tau) + (\hat{a}_{-\omega'}^{ur,out})^\dagger [A_{-\omega'}^{ur,out}(\tau)]^* + (\hat{a}_{-\omega'}^{ul,out})^\dagger [A_{-\omega'}^{ul,out}(\tau)]^* , \end{aligned} \quad (7.3.13)$$

with similar identities for other values of  $\omega'$ .

Since typically  $\omega'_{max,1}$  and  $\omega'_{max,2}$  are very close in value, we shall assume in what follows  $0 < \omega' < \omega'_{max,1}$ , so that there is no group-velocity horizon; for  $\omega'_{max,1} < \omega' < \omega'_{max,2}$ , the analysis is akin to that of §2.4. Completeness of the modes ensures that we can express

### 7.3. Transforming to the $\omega'$ -representation

one type of mode as a linear combination of the other, so we may write

$$\begin{aligned} A_{\omega'}^{v,\text{in}}(\tau) &= C_{\omega'}^{v,v} A_{\omega'}^{v,\text{out}}(\tau) + C_{\omega'}^{v,u} A_{\omega'}^{u,\text{out}}(\tau) + C_{\omega'}^{v,ur} [A_{-\omega'}^{ur,\text{out}}(\tau)]^* + C_{\omega'}^{v,ul} [A_{-\omega'}^{ul,\text{out}}(\tau)]^*, \\ A_{\omega'}^{u,\text{in}}(\tau) &= C_{\omega'}^{u,v} A_{\omega'}^{v,\text{out}}(\tau) + C_{\omega'}^{u,u} A_{\omega'}^{u,\text{out}}(\tau) + C_{\omega'}^{u,ur} [A_{-\omega'}^{ur,\text{out}}(\tau)]^* + C_{\omega'}^{u,ul} [A_{-\omega'}^{ul,\text{out}}(\tau)]^*, \\ [A_{-\omega'}^{ur,\text{in}}(\tau)]^* &= C_{\omega'}^{ur,v} A_{\omega'}^{v,\text{out}}(\tau) + C_{\omega'}^{ur,u} A_{\omega'}^{u,\text{out}}(\tau) + C_{\omega'}^{ur,ur} [A_{-\omega'}^{ur,\text{out}}(\tau)]^* + C_{\omega'}^{ur,ul} [A_{-\omega'}^{ul,\text{out}}(\tau)]^*, \\ [A_{-\omega'}^{ul,\text{in}}(\tau)]^* &= C_{\omega'}^{ul,v} A_{\omega'}^{v,\text{out}}(\tau) + C_{\omega'}^{ul,u} A_{\omega'}^{u,\text{out}}(\tau) + C_{\omega'}^{ul,ur} [A_{-\omega'}^{ur,\text{out}}(\tau)]^* + C_{\omega'}^{ul,ul} [A_{-\omega'}^{ul,\text{out}}(\tau)]^*. \end{aligned}$$

The coefficients are equal to scalar products between modes, e.g.,  $C_{\omega'}^{v,v} = (A_{\omega'}^{v,\text{out}}, A_{\omega'}^{v,\text{in}})$  and  $C_{\omega'}^{v,ur} = -([A_{-\omega'}^{ur,\text{out}}]^*, A_{\omega'}^{v,\text{in}})$ . Applying the identity  $(A_2, A_1) = (A_1, A_2)^*$  - which follows from the definition of the scalar product in Eq. (7.1.8) - we can express the out-modes as combinations of in-modes using the same coefficients:

$$\begin{aligned} A_{\omega'}^{v,\text{out}}(\tau) &= (C_{\omega'}^{v,v})^* A_{\omega'}^{v,\text{in}}(\tau) + (C_{\omega'}^{u,v})^* A_{\omega'}^{u,\text{in}}(\tau) - (C_{\omega'}^{v,ur})^* [A_{-\omega'}^{ur,\text{in}}(\tau)]^* - (C_{\omega'}^{v,ul})^* [A_{-\omega'}^{ul,\text{in}}(\tau)]^*, \\ A_{\omega'}^{u,\text{out}}(\tau) &= (C_{\omega'}^{v,u})^* A_{\omega'}^{v,\text{in}}(\tau) + (C_{\omega'}^{u,u})^* A_{\omega'}^{u,\text{in}}(\tau) - (C_{\omega'}^{u,ur})^* [A_{-\omega'}^{ur,\text{in}}(\tau)]^* - (C_{\omega'}^{u,ul})^* [A_{-\omega'}^{ul,\text{in}}(\tau)]^*, \\ [A_{-\omega'}^{ur,\text{out}}(\tau)]^* &= - (C_{\omega'}^{v,ur})^* A_{\omega'}^{v,\text{in}}(\tau) - (C_{\omega'}^{u,ur})^* A_{\omega'}^{u,\text{in}}(\tau) + (C_{\omega'}^{ur,ur})^* [A_{-\omega'}^{ur,\text{in}}(\tau)]^* \\ &\quad + (C_{\omega'}^{ul,ur})^* [A_{-\omega'}^{ul,\text{in}}(\tau)]^*, \\ [A_{-\omega'}^{ul,\text{out}}(\tau)]^* &= - (C_{\omega'}^{v,ul})^* A_{\omega'}^{v,\text{in}}(\tau) - (C_{\omega'}^{u,ul})^* A_{\omega'}^{u,\text{in}}(\tau) + (C_{\omega'}^{ur,ul})^* [A_{-\omega'}^{ur,\text{in}}(\tau)]^* \\ &\quad + (C_{\omega'}^{ul,ul})^* [A_{-\omega'}^{ul,\text{in}}(\tau)]^*. \end{aligned}$$

Substitution in Eq. (7.3.13) gives the corresponding transformation of the annihilation and creation operators:

$$\begin{aligned} \hat{a}_{\omega'}^{v,\text{out}} &= C_{\omega'}^{v,v} \hat{a}_{\omega'}^{v,\text{in}} + C_{\omega'}^{u,v} \hat{a}_{\omega'}^{u,\text{in}} + C_{\omega'}^{v,ur} (\hat{a}_{-\omega'}^{ur,\text{in}})^\dagger + C_{\omega'}^{v,ul} (\hat{a}_{-\omega'}^{ul,\text{in}})^\dagger, \\ \hat{a}_{\omega'}^{u,\text{out}} &= C_{\omega'}^{v,u} \hat{a}_{\omega'}^{v,\text{in}} + C_{\omega'}^{u,u} \hat{a}_{\omega'}^{u,\text{in}} + C_{\omega'}^{u,ur} (\hat{a}_{-\omega'}^{ur,\text{in}})^\dagger + C_{\omega'}^{u,ul} (\hat{a}_{-\omega'}^{ul,\text{in}})^\dagger, \\ (\hat{a}_{-\omega'}^{ur,\text{out}})^\dagger &= C_{\omega'}^{v,ur} \hat{a}_{\omega'}^{v,\text{in}} + C_{\omega'}^{u,ur} \hat{a}_{\omega'}^{u,\text{in}} + C_{\omega'}^{ur,ur} (\hat{a}_{-\omega'}^{ur,\text{in}})^\dagger + C_{\omega'}^{ul,ur} (\hat{a}_{-\omega'}^{ul,\text{in}})^\dagger, \\ (\hat{a}_{-\omega'}^{ul,\text{out}})^\dagger &= C_{\omega'}^{v,ul} \hat{a}_{\omega'}^{v,\text{in}} + C_{\omega'}^{u,ul} \hat{a}_{\omega'}^{u,\text{in}} + C_{\omega'}^{ur,ul} (\hat{a}_{-\omega'}^{ur,\text{in}})^\dagger + C_{\omega'}^{ul,ul} (\hat{a}_{-\omega'}^{ul,\text{in}})^\dagger. \end{aligned}$$

Similarly, the inverse transformation is found:

$$\begin{aligned} \hat{a}_{\omega'}^{v,\text{in}} &= (C_{\omega'}^{v,v})^* \hat{a}_{\omega'}^{v,\text{out}} + (C_{\omega'}^{v,u})^* \hat{a}_{\omega'}^{u,\text{out}} - (C_{\omega'}^{v,ur})^* (\hat{a}_{-\omega'}^{ur,\text{out}})^\dagger - (C_{\omega'}^{v,ul})^* (\hat{a}_{-\omega'}^{ul,\text{out}})^\dagger, \\ \hat{a}_{\omega'}^{u,\text{in}} &= (C_{\omega'}^{u,v})^* \hat{a}_{\omega'}^{v,\text{out}} + (C_{\omega'}^{u,u})^* \hat{a}_{\omega'}^{u,\text{out}} - (C_{\omega'}^{u,ur})^* (\hat{a}_{-\omega'}^{ur,\text{out}})^\dagger - (C_{\omega'}^{u,ul})^* (\hat{a}_{-\omega'}^{ul,\text{out}})^\dagger, \\ (\hat{a}_{-\omega'}^{ur,\text{in}})^\dagger &= - (C_{\omega'}^{v,ur})^* \hat{a}_{\omega'}^{v,\text{out}} - (C_{\omega'}^{u,ur})^* \hat{a}_{\omega'}^{u,\text{out}} + (C_{\omega'}^{ur,ur})^* (\hat{a}_{-\omega'}^{ur,\text{out}})^\dagger + (C_{\omega'}^{ur,ul})^* (\hat{a}_{-\omega'}^{ul,\text{out}})^\dagger, \\ (\hat{a}_{-\omega'}^{ul,\text{in}})^\dagger &= - (C_{\omega'}^{v,ul})^* \hat{a}_{\omega'}^{v,\text{out}} - (C_{\omega'}^{u,ul})^* \hat{a}_{\omega'}^{u,\text{out}} + (C_{\omega'}^{ul,ur})^* (\hat{a}_{-\omega'}^{ur,\text{out}})^\dagger + (C_{\omega'}^{ul,ul})^* (\hat{a}_{-\omega'}^{ul,\text{out}})^\dagger. \end{aligned}$$

## 7. The Fibre-Optical Model for Hawking Radiation

As in the acoustic case, this is where the significance of mixing between positive- and negative-norm modes becomes manifest: a single operator corresponding to an in- or out-mode, when written in terms of those operators for the other type of mode, can contain both annihilation and creation operators.

### 7.4. Spontaneous creation of photons

Assuming that the quantum state is the in-vacuum,  $|0_{\text{in}}\rangle$ , which contains no incoming particles and is annihilated by all in-mode annihilation operators, i.e.,

$$\hat{a}_{\omega'}^{v,\text{in}} |0_{\text{in}}\rangle = \hat{a}_{\omega'}^{u,\text{in}} |0_{\text{in}}\rangle = \hat{a}_{-\omega'}^{ur,\text{in}} |0_{\text{in}}\rangle = \hat{a}_{-\omega'}^{ul,\text{in}} |0_{\text{in}}\rangle = 0, \quad (7.4.1)$$

we find that the mixing of different types of operator still allows the presence of outgoing particles. For example, the expectation number for the outgoing  $u$ -mode is

$$\begin{aligned} \langle 0_{\text{in}} | \left( \hat{a}_{\omega'_1}^{u,\text{out}} \right)^\dagger \hat{a}_{\omega'_2}^{u,\text{out}} | 0_{\text{in}} \rangle &= \langle 0_{\text{in}} | \left\{ \left( C_{\omega'_1}^{ur,u} \right)^* \hat{a}_{-\omega'_1}^{ur,\text{in}} + \left( C_{\omega'_1}^{ul,u} \right)^* \hat{a}_{-\omega'_1}^{ul,\text{in}} \right\} \\ &\quad \times \left\{ C_{\omega'_2}^{ur,u} \left( \hat{a}_{-\omega'_2}^{ur,\text{in}} \right)^\dagger + C_{\omega'_2}^{ul,u} \left( \hat{a}_{-\omega'_2}^{ul,\text{in}} \right)^\dagger \right\} | 0_{\text{in}} \rangle \\ &= \langle 0_{\text{in}} | \left\{ \left( C_{\omega'_1}^{ur,u} \right)^* C_{\omega'_2}^{ur,u} \hat{a}_{-\omega'_1}^{ur,\text{in}} \left( \hat{a}_{-\omega'_2}^{ur,\text{in}} \right)^\dagger + \left( C_{\omega'_1}^{ul,u} \right)^* C_{\omega'_2}^{ul,u} \hat{a}_{-\omega'_1}^{ul,\text{in}} \left( \hat{a}_{-\omega'_2}^{ul,\text{in}} \right)^\dagger \right\} | 0_{\text{in}} \rangle \\ &= \langle 0_{\text{in}} | \left\{ \left( C_{\omega'_1}^{ur,u} \right)^* C_{\omega'_2}^{ur,u} \left( \delta(\omega'_1 - \omega'_2) + \left( \hat{a}_{-\omega'_2}^{ur,\text{in}} \right)^\dagger \hat{a}_{-\omega'_1}^{ur,\text{in}} \right) \right. \\ &\quad \left. + \left( C_{\omega'_1}^{ul,u} \right)^* C_{\omega'_2}^{ul,u} \left( \delta(\omega'_1 - \omega'_2) + \left( \hat{a}_{-\omega'_2}^{ul,\text{in}} \right)^\dagger \hat{a}_{-\omega'_1}^{ul,\text{in}} \right) \right\} | 0_{\text{in}} \rangle \\ &= \left( \left| C_{\omega'_1}^{ur,u} \right|^2 + \left| C_{\omega'_1}^{ul,u} \right|^2 \right) \delta(\omega'_1 - \omega'_2), \end{aligned} \quad (7.4.2)$$

where the normalization of the state  $|0_{\text{in}}\rangle$  and the commutator of Eq. (7.3.8) were used. Similar expressions hold for the expectation values of the other modes:

$$\langle 0_{\text{in}} | \left( \hat{a}_{\omega'_1}^{v,\text{out}} \right)^\dagger \hat{a}_{\omega'_2}^{v,\text{out}} | 0_{\text{in}} \rangle = \left( \left| C_{\omega'_1}^{ur,v} \right|^2 + \left| C_{\omega'_1}^{ul,v} \right|^2 \right) \delta(\omega'_1 - \omega'_2), \quad (7.4.3)$$

$$\langle 0_{\text{in}} | \left( \hat{a}_{\omega'_1}^{ur,\text{out}} \right)^\dagger \hat{a}_{\omega'_2}^{ur,\text{out}} | 0_{\text{in}} \rangle = \left( \left| C_{\omega'_1}^{v,ur} \right|^2 + \left| C_{\omega'_1}^{u,ur} \right|^2 \right) \delta(\omega'_1 - \omega'_2), \quad (7.4.4)$$

$$\langle 0_{\text{in}} | \left( \hat{a}_{\omega'_1}^{ul,\text{out}} \right)^\dagger \hat{a}_{\omega'_2}^{ul,\text{out}} | 0_{\text{in}} \rangle = \left( \left| C_{\omega'_1}^{v,ul} \right|^2 + \left| C_{\omega'_1}^{u,ul} \right|^2 \right) \delta(\omega'_1 - \omega'_2), \quad (7.4.5)$$

and also for those modes with co-moving frequency such that  $\omega'_{\text{max},1} < \omega' < \omega'_{\text{max},2}$ :

$$\langle 0_{\text{in}} | \left( \hat{a}_{\omega'_1}^{v,\text{out}} \right)^\dagger \hat{a}_{\omega'_2}^{v,\text{out}} | 0_{\text{in}} \rangle = \left| C_{\omega'_1}^{url,v} \right|^2 \delta(\omega'_1 - \omega'_2), \quad (7.4.6)$$

$$\langle 0_{\text{in}} | \left( \hat{a}_{\omega'_1}^{u,\text{out}} \right)^\dagger \hat{a}_{\omega'_2}^{u,\text{out}} | 0_{\text{in}} \rangle = \left| C_{\omega'_1}^{url,u} \right|^2 \delta(\omega'_1 - \omega'_2), \quad (7.4.7)$$

$$\langle 0_{\text{in}} | \left( \hat{a}_{\omega'_1}^{url,\text{out}} \right)^\dagger \hat{a}_{\omega'_2}^{url,\text{out}} | 0_{\text{in}} \rangle = \left( \left| C_{\omega'_1}^{ur,rl,v} \right|^2 + \left| C_{\omega'_1}^{ur,rl,u} \right|^2 \right) \delta(\omega'_1 - \omega'_2). \quad (7.4.8)$$

However, for those modes with co-moving frequency  $\omega' > \omega'_{\max,2}$ , there is no mixing of positive- and negative-norm modes and hence no particle creation.

The  $\delta$  functions appearing in the expectation values above are due to the continuous nature of the stationary modes into which the optical field is decomposed. Arguments entirely analogous to those given in §2.5 show that the expectation values should be interpreted, upon division by  $2\pi$ , as spectral flux densities:

$$\frac{d^2 N}{d\zeta d\omega'} = \frac{1}{2\pi} |\beta_{\omega'}|^2, \quad (7.4.9)$$

where  $|\beta_{\omega'}|^2$  is the factor multiplying the delta functions in the expectation values above. However, this is defined in the co-moving frame, and requires some modification to be turned into a more useful quantity, defined with respect to the lab frame. Instead of the variables  $\zeta$  and  $\omega'$ , we would like a spectral flux density in terms of  $t$  and  $\omega$ . Firstly, it should be noted that Eq. (7.4.9) refers to a single pulse; in practice, a stream of pulses are coupled into the fibre with repetition rate  $\nu_{\text{rep}}$ . So, in order to find the number of photons emitted per unit time, we first find the number of photons emitted per pulse, and multiply by  $\nu_{\text{rep}}$ . The number of photons per pulse is found by integrating with respect to  $\zeta$  over the entire length of the fibre, and assuming that the pulse is a soliton so that it remains stationary in the co-moving frame, so amounts to multiplying by  $L/u$ , where  $L$  is the length of the fibre and  $u$  is the group velocity of the pulse. Therefore, Eq. (7.4.9) becomes

$$\frac{d^2 N}{dt d\omega'} = \frac{1}{2\pi} \frac{L \nu_{\text{rep}}}{u} |\beta_{\omega'}|^2, \quad (7.4.10)$$

or, multiplying by  $|d\omega'/d\omega|$  to effect the transformation from variable  $\omega'$  to  $\omega$ ,

$$\frac{d^2 N}{dt d\omega} = \frac{1}{2\pi} \frac{L \nu_{\text{rep}}}{u} \left| \frac{d\omega'}{d\omega} \right| |\beta_{\omega'}|^2. \quad (7.4.11)$$

Taking the values from the experiment in Chapter 6,  $L = 1.5$  m,  $\nu_{\text{rep}} = 80$  MHz and  $u = c/n_g$  where  $n_g \approx 1.5$ , we find that  $L \nu_{\text{rep}}/u \approx 0.6$ ; loosening these restrictions slightly, we can say that the transformation from the co-moving frame to the lab frame roughly preserves the order of magnitude of the spectral flux density. However, it should be borne in mind that the actual value depends on the factor  $L \nu_{\text{rep}}/u$ . Of the quantities appearing there, the most important is  $L$ , for in the derivation we assumed that the pulse maintains its shape throughout the fibre. However, if instead we make use of self-steepening mechanisms, so that the pulse shape changes with its propagation, then  $L$  should be replaced by an effective length  $L_{\text{eff}}$ , over which the pulse emits photons most efficiently.

## 7.5. Concluding remarks

Having quantized the optical probe field in the presence of a strong pulse, we have shown, as in the acoustic case, that there are two natural sets of modes into which the field may

## *7. The Fibre-Optical Model for Hawking Radiation*

be decomposed: in-modes and out-modes. These sets define two vacuum states, and it is found that, due to the mixing of modes of positive and negative norm, these vacuum states are not equal. Thus, in the in-vacuum, which has no incoming photons, there are outgoing photons, which are emitted spontaneously by the pulse.

## 8. Methods of Fibre-Optical Model

Having developed the theoretical foundations of our fibre-optical model of the event horizon, we come now to the methods employed to calculate the expected spectrum of Hawking radiation. These bear many similarities to the methods of Chapter 3 used in the acoustic model. As there, we examine an FDTD algorithm for wavepacket propagation; an ordinary differential equation solver and algebraic technique for finding steady-state solutions; and an analytic method derived from linearization of the nonlinearity profile.

### 8.1. Wavepacket propagation

When discussing methods for solving the acoustic case in §3.1, we began by following in the spirit of Unruh [18], calculating negative-frequency contributions by solving for the propagation of a wavepacket directly using an FDTD (Finite Difference Time Domain) algorithm. The starting point is, of course, the fibre-optical wave equation (7.1.4), which can be decomposed into two PDEs of the first order in  $\zeta$  using (a quantity proportional to) the canonical momentum  $\pi$  of Eq. (7.1.9):

$$\partial_{\zeta} A - \partial_{\tau} A = \Pi, \quad (8.1.1)$$

$$\partial_{\zeta} \Pi - \partial_{\tau} \Pi = -u^2 \beta^2 (i \partial_{\tau}) A + \frac{u^2}{c^2} (\partial_{\tau} \chi) \partial_{\tau} A + \frac{u^2}{c^2} \chi \partial_{\tau}^2 A. \quad (8.1.2)$$

Notice that Eq. (8.1.2) contains a term in  $\partial_{\tau}^2 A$ , and is therefore not purely first-order. The operation of  $\beta^2$  on  $A$  is analogous to that of  $F^2$  on  $\phi$  in the acoustic model: if  $\tilde{A}(\omega)$  is the Fourier transform of  $A$  with respect to  $\tau$ ,

$$\tilde{A}(\omega) = \int_{-\infty}^{+\infty} e^{i\omega\tau} A(\tau) d\tau, \quad (8.1.3)$$

then the operation of  $\beta^2$  on  $A$  is given by

$$\beta^2 (i \partial_{\tau}) A(\tau) = \frac{1}{2\pi} \int_{-\infty}^{+\infty} \beta^2(\omega) e^{-i\omega\tau} \tilde{A}(\omega) d\omega. \quad (8.1.4)$$

The Fourier transform is implemented numerically using the FFT (Fast Fourier Transform) algorithm.

As in §3.1, we convert Eqs. (8.1.1) and (8.1.2) into finite difference equations by discretizing the  $\zeta$ - and  $\tau$ -axes into grids, with separations  $\Delta_{\zeta}$  and  $\Delta_{\tau}$  respectively. We also allow the grids representing values of  $A$  and  $\Pi$  to be offset by  $\Delta_{\zeta}/2$ . Then Eqs.

## 8. Methods of Fibre-Optical Model

(8.1.1) and (8.1.2) become

$$\begin{aligned} & \frac{A_{m+1,i} - A_{m,i}}{\Delta_\zeta} - \frac{1}{2} \left[ \frac{A_{m,i+1} - A_{m,i-1}}{2\Delta_\tau} + \frac{A_{m+1,i+1} - A_{m+1,i-1}}{2\Delta_\tau} \right] = \Pi_{m,i}, \\ & \frac{\Pi_{m+1,i} - \Pi_{m,i}}{\Delta_\zeta} - \frac{1}{2} \left[ \frac{\Pi_{m,i+1} - \Pi_{m,i-1}}{2\Delta_\tau} + \frac{\Pi_{m+1,i+1} - \Pi_{m+1,i-1}}{2\Delta_\tau} \right] \\ & = -u^2 [\beta^2 (i\partial_\tau)]_{m+1,i} + \frac{u^2}{c^2} [\partial_\tau \chi]_i \frac{A_{m+1,i+1} - A_{m+1,i-1}}{2\Delta_\tau} + \frac{u^2}{c^2} \chi_i \frac{A_{m+1,i+1} - 2A_{m+1,i} + A_{m+1,i-1}}{\Delta_\tau^2}. \end{aligned}$$

Rearranging, we have

$$A_{m+1,i} - \frac{\Delta_\zeta}{4\Delta_\tau} (A_{m+1,i+1} - A_{m+1,i-1}) = A_{m,i} + \frac{\Delta_\zeta}{4\Delta_\tau} (A_{m,i+1} - A_{m,i-1}) + \Delta_\zeta \Pi_{m,i}, \quad (8.1.5)$$

$$\begin{aligned} & \Pi_{m+1,i} - \frac{\Delta_\zeta}{4\Delta_\tau} (\Pi_{m+1,i+1} - \Pi_{m+1,i-1}) = \Pi_{m,i} + \frac{\Delta_\zeta}{4\Delta_\tau} (\Pi_{m,i+1} - \Pi_{m,i-1}) - \Delta_\zeta u^2 [\beta^2 (i\partial_\tau) A]_{m+1,i} \\ & + \frac{\Delta_\zeta}{2\Delta_\tau} \frac{u^2}{c^2} [\partial_\tau \chi]_i (A_{m+1,i+1} - A_{m+1,i-1}) + \frac{\Delta_\zeta}{\Delta_\tau^2} \frac{u^2}{c^2} \chi_i (A_{m+1,i+1} - 2A_{m+1,i} + A_{m+1,i-1}), \end{aligned} \quad (8.1.6)$$

or, in matrix form,

$$\begin{bmatrix} 1 & -a & & & a \\ & \ddots & & & \\ & & \ddots & & \\ & & & a & 1 & -a \\ & & & & \ddots & \\ -a & & & & & a & 1 \end{bmatrix} \begin{bmatrix} A_{m+1,1} \\ \vdots \\ \vdots \\ A_{m+1,i} \\ \vdots \\ \vdots \\ A_{m+1,n} \end{bmatrix} = \begin{bmatrix} b_{m,1} \\ \vdots \\ \vdots \\ b_{m,i} \\ \vdots \\ \vdots \\ b_{m,n} \end{bmatrix}, \quad (8.1.7)$$

$$\begin{bmatrix} 1 & -a & & & a \\ & \ddots & & & \\ & & \ddots & & \\ & & & a & 1 & -a \\ & & & & \ddots & \\ -a & & & & & a & 1 \end{bmatrix} \begin{bmatrix} \Pi_{m+1,1} \\ \vdots \\ \vdots \\ \Pi_{m+1,i} \\ \vdots \\ \vdots \\ \Pi_{m+1,n} \end{bmatrix} = \begin{bmatrix} c_{m,1} \\ \vdots \\ \vdots \\ c_{m,i} \\ \vdots \\ \vdots \\ c_{m,n} \end{bmatrix}, \quad (8.1.8)$$

where we have assumed periodic boundary conditions, identifying  $i = n + 1$  with  $i = 1$



and  $i = 0$  with  $i = n$ , and where we have defined

$$a = \frac{\Delta_\zeta}{4\Delta_\tau}, \quad (8.1.9)$$

$$b_{m,i} = A_{m,i} + \frac{\Delta_\zeta}{4\Delta_\tau} (A_{m,i+1} - A_{m,i-1}) + \Delta_\zeta \Pi_{m,i}, \quad (8.1.10)$$

$$\begin{aligned} c_{m,i} = & \Pi_{m,i} + \frac{\Delta_\zeta}{4\Delta_\tau} (\Pi_{m,i+1} - \Pi_{m,i-1}) - \Delta_\zeta u^2 [\beta^2 (i\partial_\tau) A]_{m+1,i} + \frac{\Delta_\zeta}{2\Delta_\tau} \frac{u^2}{c^2} [\partial_\tau \chi]_i (A_{m+1,i+1} - A_{m+1,i-1}) \\ & + \frac{\Delta_\zeta}{\Delta_\tau^2} \frac{u^2}{c^2} \chi_i (A_{m+1,i+1} - 2A_{m+1,i} + A_{m+1,i-1}). \end{aligned} \quad (8.1.11)$$

The solution follows as before. The vector  $\chi_i$  is assumed fixed in  $\zeta$  (hence its independence of  $m$ ), and determines the nonlinearity profile;  $[\partial_\tau \chi]_i$  is its  $\tau$ -derivative, and can be stored as a separate vector for convenience. Given the vectors  $A_m$  and  $\Pi_m$ , we can calculate  $b_m$  and solve Eq. (8.1.7) for  $A_{m+1}$ , using the algorithm for cyclic equations from Ref. [58]; then, given the vectors  $\Pi_m$  and  $A_{m+1}$ , we can calculate  $c_m$  and solve Eq. (8.1.8) for  $\Pi_{m+1}$ . The only remaining unknowns are the initial values  $A_1$  and  $\Pi_1$ , which are related via the Fourier Transform as in Eq. (3.1.9) and a half-step finite difference equation similar to Eq. (3.1.10).

The FDTD algorithm does not run so smoothly for the optical model as for the acoustic model. One problem is with the dispersion profile, which naturally increases with frequency, in principle without bound. Allowing such an unbounded form for  $\beta(\omega)$  can make the algorithm unstable; however, this problem is easily solved by applying an appropriate cut-off frequency, beyond which  $\beta$  is set to zero. A less tractable problem is that the degree of backscattering, or scattering from  $u$ -modes into  $v$ -modes, is greater in the optical model than in the acoustic model. Although the amount of backscattering in terms of norm is still small, the amplitude of the wave, which is proportional to  $\beta(\omega)^{-1/2}$ , is fairly large, since the  $v$ -modes occur at very low frequencies. This makes the above FDTD algorithm of limited value, especially visually, since this unphysical low-frequency mode quickly fills up the domain.

## 8.2. Steady-state solution

In practice, the spectrum of Hawking radiation is found by finding steady-state solutions for various values of  $\omega'$ , and finding their negative-norm components. The general nonlinearity profile is solved in an entirely analogous fashion to the acoustic model (see §3.2), and will be discussed only briefly. For the special case of a nonlinearity profile which is constant apart from step discontinuities, the method is again analogous to the acoustic model, but the resulting equations are slightly different and will be discussed in full.

### 8.2.1. General nonlinearity profile

Assuming a stationary solution of the form

## 8. Methods of Fibre-Optical Model

$$A(\zeta, \tau) = A_{\omega'}(\tau) e^{-i\omega'\zeta},$$

the optical wave equation (7.1.4) is transformed into the ordinary differential equation

$$-\omega'^2 A_{\omega'} + 2i\omega' \partial_\tau A_{\omega'} + \partial_\tau^2 A_{\omega'} + u^2 \beta^2(i\partial_\tau) A_{\omega'} - \frac{u^2}{c^2} \partial_\tau (\chi(\tau) \partial_\tau A_{\omega'}) = 0. \quad (8.2.1)$$

The order of this equation is the same as the order of  $\beta^2(\omega)$ . Assuming a constant value of  $\chi$  and taking the Fourier transform via the substitutions  $A_{\omega'}(\tau) \rightarrow \tilde{A}_{\omega'}(\omega)$  and  $\partial_\tau \rightarrow -i\omega$ , Eq. (8.2.1) becomes

$$\left\{ -(\omega' - \omega)^2 + u^2 \beta^2(\omega) + \frac{u^2}{c^2} \chi \omega^2 \right\} \tilde{A}_{\omega'} = 0,$$

and again we find the dispersion relation of Eqs. (5.3.12)-(5.3.14),

$$(\omega' - \omega)^2 = u^2 \beta^2(\omega) + \frac{u^2}{c^2} \chi \omega^2 = u^2 \beta_\chi^2(\omega). \quad (8.2.2)$$

If  $\chi$  approaches asymptotic values for  $\tau \rightarrow \pm\infty$ , then it can be approximated as constant in the asymptotic regions, and the dispersion relation of Eq. (8.2.2) will apply. The general solution in each asymptotic region is a sum of plane waves with frequencies determined by the dispersion relation, and the plane wave coefficients in each region are related via a scattering matrix as in Eq. (3.2.4). (Refer to Fig. 3.2 for an illustration.) The in- or out-mode that is to be solved determines which coefficients to set to zero, and the remaining coefficients are solved via linear algebra. The modes are normalized in the  $\omega'$ -representation according to Eqs. (7.2.1) and (7.3.6):

$$A_{\omega'}(\tau) = \sqrt{\frac{u}{4\pi\epsilon_0 c^2 |\beta_\chi(\omega)| |\partial\omega'/\partial\omega|}} e^{-i\omega\tau - i\omega'\zeta}. \quad (8.2.3)$$

Therefore, if we have the plane wave coefficients, the norm of a particular plane wave in relation to the single ingoing or outgoing wave is

$$\frac{(A_{\omega',\omega}, A_{\omega',\omega})}{(A_{\omega',\omega_{\text{in/out}}}, A_{\omega',\omega_{\text{in/out}}})} = \frac{\text{sgn}(\omega - \omega') |\beta_\chi(\omega)| |\partial\omega'/\partial\omega(\omega)| |C_{\omega',\omega}|^2}{\text{sgn}(\omega_{\text{in/out}} - \omega') |\beta_\chi(\omega_{\text{in/out}})| |\partial\omega'/\partial\omega(\omega_{\text{in/out}})| |C_{\omega',\omega_{\text{in/out}}}|^2}. \quad (8.2.4)$$

### 8.2.2. Discontinuous nonlinearity profile

Eq. (8.2.1) may be solved analytically in the special case where  $\chi$  is constant everywhere except at discrete points. This might correspond, for example, to a square pulse, whose intensity is constant in a certain region and zero elsewhere. It is of course an idealised case, formed by taking the limit as the derivative of  $\chi$  increases without bound.

We proceed exactly as in §3.2. We assume that  $\beta^2(\omega)$  is a polynomial of order  $2n$ ,

$$\beta^2(\omega) = \sum_{j=1}^n b_j \omega^{2j},$$

which would result in  $2n$  solutions of the dispersion relation. In any region of constant  $\chi$ , the solution is specified by the  $2n$  coefficients of the possible plane waves; if there are  $r$  regions, or  $r - 1$  points of discontinuity, there are  $2nr$  coefficients in total. However, there can only be  $2n$  linearly independent solutions, which means there must be  $2n(r - 1)$  conditions on these coefficients, or  $2n$  conditions for each point of discontinuity. These relate the limiting values of  $A_{\omega'}$  and its first  $2n - 1$  derivatives on each side of these points.

Expanding the last term of Eq. (8.2.1), and replacing the operator  $\beta^2(i\partial_\tau)$  with its polynomial expansion, we have

$$\begin{aligned} -\omega'^2 A_{\omega'} + 2i\omega' \partial_\tau A_{\omega'} + \partial_\tau^2 A_{\omega'} + \frac{u^2}{c^2} \chi'(\tau) \partial_\tau A_{\omega'} + \frac{u^2}{c^2} \chi(\tau) \partial_\tau^2 A_{\omega'} \\ + u^2 \sum_{j=1}^n (-1)^j b_j \partial_\tau^{2j} A_{\omega'} = 0. \end{aligned} \quad (8.2.5)$$

We see that the steady-state equation contains  $\chi$  and its first derivative  $\chi'$  only, and is therefore *almost* equivalent to the acoustic case, which contains the flow velocity  $V$  and its first derivative  $V'$  only. (The difference here is that  $\chi$  and  $\chi'$  are not multiplied, and the discontinuities in the derivatives of  $A_{\omega'}$  can have at most a  $1/\delta$  dependence, in contrast to the  $1/\delta^2$  dependence in the acoustic model.) We note that a discontinuity in  $\chi$  must be accompanied by a delta function in  $\chi'$ , and that these can only be cancelled by a discontinuity in  $\partial_\tau^{2n-1} A_{\omega'}$  accompanied by a delta function in  $\partial_\tau^{2n} A_{\omega'}$ . All other quantities must be continuous. Therefore, the first  $2n - 1$  of the  $2n$  conditions to be imposed at a point of discontinuity are the continuity of  $A_{\omega'}$  and its first  $2n - 2$  derivatives; the final condition involves imposing the correct discontinuity on  $\partial_\tau^{2n-1} A_{\omega'}$ .

Proceeding as in the acoustic case, we imagine a nonlinearity profile that varies linearly over a region of length  $\delta$  between two constant- $\chi$  regions, and is therefore continuous in  $\chi$  but discontinuous in  $\chi'$ ; the case of discontinuous  $\chi$  is found by taking the limit  $\delta \rightarrow 0$ . (See Fig. 3.4, replacing  $V$  with  $\chi$ .) A discontinuity in  $\chi'$  at the point  $\tau = \tau_\star$  must be accompanied by a corresponding discontinuity in  $\partial_\tau^{2n} A_{\omega'}$  at  $\tau_\star$ , so that Eq. (8.2.5) is always satisfied. We have

$$\lim_{\tau \rightarrow \tau_\star^-} \left[ \frac{u^2}{c^2} \chi' \partial_\tau A_{\omega'} - u^2 (-1)^n b_n \partial_\tau^{2n} A_{\omega'} \right] = \lim_{\tau \rightarrow \tau_\star^+} \left[ \frac{u^2}{c^2} \chi' \partial_\tau A_{\omega'} - u^2 (-1)^n b_n \partial_\tau^{2n} A_{\omega'} \right],$$

or, defining  $\Delta\chi' \equiv \lim_{\tau \rightarrow \tau_\star^+} \chi' - \lim_{\tau \rightarrow \tau_\star^-} \chi'$  and similarly for  $\Delta(\partial_\tau^{2n} A_{\omega'})$ ,

$$\begin{aligned} \Delta(\partial_\tau^{2n} A_{\omega'}) &= \frac{(-1)^n}{b_n c^2} (\partial_\tau A_{\omega'}) \Delta\chi' \\ &= \frac{(-1)^n}{b_n c^2} (\partial_\tau A_{\omega'}) \frac{(\chi_2 - \chi_1)}{\delta}, \end{aligned} \quad (8.2.6)$$

## 8. Methods of Fibre-Optical Model

where  $\partial_\tau A_{\omega'}$  is to be evaluated at  $\tau = \tau_*$  (this is continuous, so there is no ambiguity).

To find the change in  $\partial_\tau^{2n-1} A_{\omega'}$  over the change in  $\chi$ , we use the Taylor expansion

$$\begin{aligned} \partial_\tau^{2n-1} A_{\omega'}|_{\tau=\tau_*+h} - \partial_\tau^{2n-1} A_{\omega'}|_{\tau=\tau_*} &= \partial_\tau^{2n} A_{\omega'}|_{\tau \rightarrow \tau_*^+} \delta + \frac{1}{2} \partial_\tau^{2n+1} A_{\omega'}|_{\tau \rightarrow \tau_*^+} \delta^2 + \dots \\ &= \partial_\tau^{2n} A_{\omega'}|_{\tau \rightarrow \tau_*^-} \delta + \frac{1}{2} \partial_\tau^{2n+1} A_{\omega'}|_{\tau \rightarrow \tau_*^-} \delta^2 + \dots \\ &\quad + \Delta (\partial_\tau^{2n} A_{\omega'}) \delta + \frac{1}{2} \Delta (\partial_\tau^{2n+1} A_{\omega'}) \delta^2 + \dots \end{aligned}$$

Letting  $h \rightarrow 0$ , the only non-vanishing term is  $\Delta (\partial_\tau^{2n} A_{\omega'}) \delta$ , and we find that the discontinuity in  $\partial_\tau^{2n-1} A_{\omega'}$  is

$$\Delta (\partial_\tau^{2n-1} A_{\omega'}) = \frac{(-1)^n}{b_n c^2} (\partial_\tau A_{\omega'}) (\chi_2 - \chi_1). \quad (8.2.7)$$

This is the final condition to be imposed at each point of discontinuity. We are thus left with  $2n$  degrees of freedom, corresponding to the  $2n$ -dimensional space of solutions, for which we have the bases of  $2n$  in-modes or  $2n$  out-modes.

### 8.3. Linearized intensity profile

Using an approach very similar to that used in §3.3, we may derive an analytic expression for the creation rate. The essential assumption is that the creation process occurs in a very narrow region around the horizon, and therefore that we may approximate the intensity profile as a linear one - just as, in the acoustic case, we approximated the velocity profile as linear.

Assume a steady-state solution  $A_{\omega'}$ , which satisfies Eq. (8.2.1). Let the nonlinearity  $\chi(\tau)$  take the form

$$\chi(\tau) = \chi_h - \alpha\tau. \quad (8.3.1)$$

The optical wave equation now becomes first-order in  $\tau$ . Making the substitutions  $A_{\omega'}(\tau) \rightarrow \tilde{A}_{\omega'}(\omega)$ ,  $\tau \rightarrow -i\partial_\omega$  and  $\partial_\tau \rightarrow -i\omega$ , we find a first-order differential equation for the Fourier transform:

$$-(\omega' - \omega)^2 \tilde{A}_{\omega'} + u^2 \beta^2(\omega) \tilde{A}_{\omega'} + \frac{u^2}{c^2} \chi_h \omega^2 \tilde{A}_{\omega'} - i \frac{u^2}{c^2} \alpha \omega \tilde{A}_{\omega'} + i \frac{u^2}{c^2} \alpha \partial_\omega (\omega^2 \tilde{A}_{\omega'}) = 0. \quad (8.3.2)$$

Rearranging, this becomes

$$\partial_\omega (\omega^2 \tilde{A}_{\omega'}) = \left\{ \frac{1}{\omega} + \frac{i}{\alpha} \left[ \chi_h + c^2 \frac{\beta^2(\omega)}{\omega^2} - \frac{c^2}{u^2} \left( 1 - \frac{\omega'}{\omega} \right)^2 \right] \right\} \omega^2 \tilde{A}_{\omega'}. \quad (8.3.3)$$

The solution is found to be

$$\omega^2 \tilde{A}_{\omega'} = C \exp \left( \log \omega + \frac{i}{\alpha} \int^\omega \left[ \chi_h + c^2 \frac{\beta^2(\bar{\omega})}{\bar{\omega}^2} - \frac{c^2}{u^2} \left( 1 - \frac{\omega'}{\bar{\omega}} \right)^2 \right] d\bar{\omega} \right) \quad (8.3.4)$$

or

$$\tilde{A}_{\omega'} = \frac{C}{\omega} \exp \left( \frac{i}{\alpha} \int^{\omega} \left[ \chi_h + c^2 \frac{\beta^2(\bar{\omega})}{\bar{\omega}^2} - \frac{c^2}{u^2} \left( 1 - \frac{\omega'}{\bar{\omega}} \right)^2 \right] d\bar{\omega} \right), \quad (8.3.5)$$

where  $C$  is an arbitrary constant. This solution for the Fourier transform is exact if  $\chi(\tau)$  is exactly linear. This differs from the acoustic case, where the WKB approximation was invoked to provide an approximate solution for the Fourier transform.

In real space, the solution is given by the inverse Fourier transform,

$$\begin{aligned} A_{\omega'}(\tau) &= \int_{-\infty}^{+\infty} \tilde{A}_{\omega'}(\omega) \exp(-i\omega\tau) d\omega \\ &= \int_{-\infty}^{+\infty} \frac{C}{\omega} \exp(i\varphi(\omega)) d\omega \end{aligned} \quad (8.3.6)$$

where we have defined

$$\begin{aligned} \varphi(\omega) &= \frac{1}{\alpha} \int^{\omega} \left[ \chi_h - \alpha\tau + c^2 \frac{\beta^2(\bar{\omega})}{\bar{\omega}^2} - \frac{c^2}{u^2} \left( 1 - \frac{\omega'}{\bar{\omega}} \right)^2 \right] d\bar{\omega} \\ &= \frac{1}{\alpha} \int^{\omega} \left[ \chi(\tau) + c^2 \frac{\beta^2(\bar{\omega})}{\bar{\omega}^2} - \frac{c^2}{u^2} \left( 1 - \frac{\omega'}{\bar{\omega}} \right)^2 \right] d\bar{\omega}. \end{aligned} \quad (8.3.7)$$

As before, this is easily solved using the method of stationary phase: the main contributions to the integral come from near those points where  $\varphi'(\omega) = 0$ , where we approximate the integral as Gaussian. The stationary points  $\omega_j$  are easily found, for they satisfy

$$\varphi'(\omega_j) = \frac{1}{\alpha} \left[ \chi(\tau) + c^2 \frac{\beta^2(\omega_j)}{\omega_j^2} - \frac{c^2}{u^2} \left( 1 - \frac{\omega'}{\omega_j} \right)^2 \right] = 0,$$

or, rearranging,

$$(\omega_j - \omega')^2 = u^2 \beta^2(\omega_j) + \frac{u^2}{c^2} \chi(\tau) \omega_j^2. \quad (8.3.8)$$

That is, the stationary points are exactly those values of  $\omega$  that solve the dispersion relation, with  $\chi$  given by its value at  $\tau$ . Around these points, the phase  $\varphi(\omega)$  can be approximated as quadratic in  $\omega$ , and for this we need the second derivative of  $\varphi(\omega)$ :

$$\varphi''(\omega) = \frac{1}{\alpha} \frac{c^2 \left( \omega^2 (2\beta(\omega) \beta'(\omega) - 2(\omega - \omega')/u^2) - 2\omega (\beta^2(\omega) - (\omega - \omega')^2/u^2) \right)}{\omega^4}.$$

If  $\omega$  solves the dispersion relation of Eq. (8.3.8), then clearly

$$\frac{c^2}{u^2} \left( u^2 \beta^2(\omega) - (\omega - \omega')^2 \right) = -\chi(\tau) \omega^2.$$

Differentiating, we have

$$\frac{c^2}{u^2} \left( u^2 2\beta(\omega) \beta'(\omega) - 2(\omega - \omega') \left( 1 - \frac{\partial \omega'}{\partial \omega} \right) \right) = -\chi(\tau) 2\omega,$$

## 8. Methods of Fibre-Optical Model

or, rearranging,

$$\frac{c^2}{u^2} (2u^2 \beta(\omega) \beta'(\omega) - 2(\omega - \omega')) = -2 \frac{c^2}{u^2} (\omega - \omega') \frac{\partial \omega'}{\partial \omega} - 2\chi(\tau) \omega.$$

Substituting into the expression for  $\varphi''(\omega)$  above, we find the much simpler expression

$$\begin{aligned} \varphi''(\omega_j) &= \frac{1}{\alpha \omega_j^4} \left( -2 \frac{c^2}{u^2} \omega_j^2 (\omega_j - \omega') \frac{\partial \omega'}{\partial \omega} (\omega_j) - 2\chi(\tau) \omega_j^3 + 2\chi(\tau) \omega_j^3 \right) \\ &= \frac{2}{\alpha} \frac{c^2}{u^2} \frac{1}{\omega_j^2} (\omega_j - \omega') v_g(\omega_j), \end{aligned} \quad (8.3.9)$$

where  $v_g(\omega) = -\partial \omega' / \partial \omega$  is the group velocity in the co-moving frame. Around the frequency  $\omega_j$ , then,  $\varphi(\omega)$  can be approximated by

$$\begin{aligned} \varphi(\omega) &\approx \varphi(\omega_j) + \frac{1}{2} \varphi''(\omega_j) (\omega - \omega_j)^2 \\ &= \varphi(\omega_j) + \frac{1}{\alpha} \frac{c^2}{u^2} \frac{1}{\omega_j^2} (\omega_j - \omega') v_g(\omega_j) (\omega - \omega_j)^2. \end{aligned} \quad (8.3.10)$$

The integral in Eq. (8.3.6) can now be approximated as

$$\begin{aligned} A_{\omega'}(\tau) &\approx \sum_j \frac{C}{\omega_j} \int_{-\infty}^{+\infty} \exp \left( i\varphi(\omega_j) + \frac{i}{\alpha} \frac{c^2}{u^2} \frac{1}{\omega_j^2} (\omega_j - \omega') v_g(\omega_j) (\omega - \omega_j)^2 \right) d\omega \\ &= C \sum_j \frac{1}{\omega_j} \exp(i\varphi(\omega_j)) \sqrt{\pi |\alpha| \omega_j^2 \frac{u^2}{c^2} \frac{1}{|(\omega_j - \omega') v_g(\omega_j)|}} \exp \left( i \frac{\pi}{4} \text{sgn} [(\omega_j - \omega') v_g(\omega_j)] \right) \\ &= C \sqrt{\pi |\alpha|} \frac{u}{c} \sum_j \frac{\text{sgn} [\omega_j]}{\sqrt{|(\omega_j - \omega') v_g(\omega_j)|}} \exp \left( i \frac{\pi}{4} \text{sgn} [(\omega_j - \omega') v_g(\omega_j)] + i\varphi(\omega_j) \right). \end{aligned}$$

Note that the factor  $|(\omega_j - \omega') v_g(\omega_j)|^{-1/2}$  is precisely that factor needed to normalize the plane wave of frequency  $\omega_j$ . It seems reasonable that the remaining exponential term,  $\exp(i\varphi(\omega_j))$ , becomes just such a plane wave in the asymptotic region, where  $\chi$  becomes constant. Let us examine this term; from Eq. (8.3.7),

$$\varphi(\omega_j) = \frac{1}{\alpha} \int^{\omega_j} \left[ \chi_h - \alpha\tau + \frac{c^2}{u^2} \frac{u^2 \beta^2(\omega) - (\omega - \omega')^2}{\omega^2} \right] d\omega, \quad (8.3.11)$$

valid when  $\chi(\tau) = \chi_h - \alpha\tau$ . However, if we plug this form of  $\chi(\tau)$  into the dispersion relation Eq. (8.3.8), we find that we can express  $\tau$  as a function of  $\omega$ :

$$\tau(\omega) = \frac{1}{\alpha} \left[ \chi_h + \frac{c^2}{u^2} \frac{u^2 \beta^2(\omega) - (\omega - \omega')^2}{\omega^2} \right]. \quad (8.3.12)$$

The phase  $\varphi(\omega_j)$ , then, is simply given by

$$\varphi(\omega_j) = -\omega_j \tau + \int^{\omega_j} \tau(\omega) d\omega, \quad (8.3.13)$$

and we generalize the result by allowing  $\tau(\omega)$  to take an arbitrary form.

In the form of an integral over  $\omega$ , the simple nature of the phase is obscured; for, differentiating with respect to  $\tau$ , and bearing in mind that  $\omega_j$  itself is a function of  $\tau$ , we find  $d\varphi/d\tau = -\omega_j$ . Therefore,  $\varphi$  can also be written

$$\varphi = - \int^{\tau} \omega_j(\tau') d\tau'. \quad (8.3.14)$$

Clearly, in the asymptotic regions,  $\varphi \rightarrow -\omega_j \tau$ , and the solution becomes a sum over the normalized modes. The only way, in this approximation, that different modes can have different amplitudes is if  $\varphi(\omega)$  has an imaginary part. The norm, then, of one frequency  $\omega_1$  relative to another  $\omega_2$  is

$$\frac{(A_{\omega',\omega_1}, A_{\omega',\omega_1})}{(A_{\omega',\omega_2}, A_{\omega',\omega_2})} \approx \frac{\text{sgn}(\omega_1 - \omega')}{\text{sgn}(\omega_2 - \omega')} \exp(-2 \text{Im}\{J\}), \quad J = \int_{\omega_2}^{\omega_1} \tau(\bar{\omega}) d\bar{\omega}. \quad (8.3.15)$$

In particular, for photon creation, the relative weight between the Bogoliubov coefficients is

$$\left| \frac{\beta}{\alpha} \right|^2 = \exp \left( -2 \text{Im} \left[ \int_{\omega_\alpha}^{\omega_\beta} \tau(\bar{\omega}) d\bar{\omega} \right] \right). \quad (8.3.16)$$

## 8.4. Summary

The methods described in this chapter are entirely analogous to those developed in the context of the acoustic model. They are:

- an FDTD algorithm, for solving wavepacket propagation;
- numerical integration to find stationary modes; and
- an analytic approximation for a linearized intensity profile.

Of these, as before, numerical integration of stationary modes is the most convenient for calculating the Hawking spectra, while the analytic approximation is useful in pointing the way towards a better analytic expression.





## 9. Results for the Fibre-Optical Model

We come now to the presentation of the results obtained from solutions to the fibre-optical wave equation. This is the first such presentation for the fibre-optical model, although the main results - both old and new - of Chapter 4 in the context of the acoustic model are replicated here. However, when using realistic profiles for the pulse-induced nonlinearity, we find ourselves in a new regime which not only contains no low-frequency horizon, but whose spectrum is dominated by a frequencies which experience no group-velocity horizon. The qualitative results in this regime are rather different; in particular, we shall see that the width of the spectrum remains constant in  $h$ , the height of the nonlinearity, but that its value is proportional to  $h^2$ .

### 9.1. Dispersion relation

The dispersion is treated as subluminal, so that  $\beta'(\omega)$  increases with  $\omega$ . (Recall that  $\beta(\omega)$  is the wavenumber as a function of frequency; it is essentially the inverse of the function  $F(k)$  that was used in the acoustic model. Subluminal dispersion, then, is expressed as a decrease in  $F'(k)$  with  $k$  or an increase in  $\beta'(\omega)$  with  $\omega$ .) As before, the simplest deviation from the dispersionless case is the introduction of a quartic term in  $\beta^2(\omega)$ :

$$\beta^2(\omega) = \frac{\omega^2}{c^2} \left( 1 + \frac{\omega^2}{\omega_d^2} \right). \quad (9.1.1)$$

This is the first form of the dispersion relation we shall use. It cannot, of course, capture all the details of any realistic dispersion relation; indeed, it is characterised by a single parameter,  $\omega_d$ , which determines the scale at which deviations from the dispersionless case first become appreciable. We could, if we wished, more closely approximate a certain dispersion profile by adding higher even powers of  $\omega$ ; but such adjustments increase the complexity of the calculations - the order of the differential equation is increased, and usually some of the possible frequencies are complex, which can affect the accuracy of the numerics - and do not return their worth with significantly different results. Therefore, we shall not consider them.

It is convenient to express  $\beta$  not in terms of  $\omega_d$ , but of the lab frequency with zero co-moving frequency, which we shall call  $\omega_0$ . This is defined via the relation

$$\omega'(\omega_0) = \omega_0 - \frac{u}{c} \omega_0 \sqrt{1 + \frac{\omega_0^2}{\omega_d^2}} = 0 \implies \omega_0^2 = \omega_d^2 \left( \frac{c^2}{u^2} - 1 \right).$$

## 9. Results for the Fibre-Optical Model

Eq. (9.1.1) may now be written:

$$\beta^2(\omega) = \frac{\omega^2}{c^2} \left( 1 + \left( \frac{c^2}{u^2} - 1 \right) \frac{\omega^2}{\omega_0^2} \right). \quad (9.1.2)$$

However, even leaving the dispersion relation in this quartic form, there is still some room for manoeuvre. We shall be especially interested in the behaviour of high frequencies, around the frequency  $\omega_0$ . To find a form of  $\beta$  which models the dispersion around this frequency well, we wish both that  $\omega'$  vanish there and that the derivative  $d\omega'/d\omega$  is equal to a specified value (which may then be measured). Let  $\xi = -d\omega'/d\omega|_{\omega=\omega_0}$ . Matching these two conditions requires two variable parameters for  $\beta$ , but Eq. (9.1.1) has only one: the parameter  $\omega_d$ . This is because we have chosen  $\beta$  such that the phase velocity approaches  $c$  for low frequencies. If we require a better match at high frequencies, we must sacrifice this low-frequency condition. (There should be no qualms about doing this, for realistic fibres have a non-trivial refractive index as  $\omega \rightarrow 0$ , so the dispersionless limit is unrealistic anyway.) Doing so, we may write  $\beta^2$  in the more general form

$$\beta^2(\omega) = \frac{\omega^2}{c^2} (b_1 + b_2\omega^2),$$

then apply the conditions we want satisfied:

$$\begin{aligned} \omega'(\omega_0) &= \omega_0 - \frac{u}{c} \omega_0 \sqrt{b_1 + b_2\omega_0^2} = 0, \\ \frac{d\omega'}{d\omega}(\omega_0) &= 1 - \frac{u}{c} \frac{b_1 + 2\omega_0^2}{\sqrt{b_1 + b_2\omega_0^2}} = -\xi. \end{aligned}$$

These are easily solved to give

$$b_1 = \frac{c^2}{u^2} (1 - \xi), \quad b_2 = \frac{c^2}{u^2} \frac{\xi}{\omega_0^2}.$$

Finally, we have

$$\beta^2(\omega) = \frac{\omega^2}{u^2} \left( 1 - \xi + \xi \frac{\omega^2}{\omega_0^2} \right). \quad (9.1.3)$$

Comparing Eqs. (9.1.2) and (9.1.3), we see that the second can be made equal to the first via the substitution  $\xi \rightarrow 1 - u^2/c^2$ . Therefore, in what follows, we shall use the dispersion relation in Eq. (9.1.3) exclusively, and without loss of generality. For the purpose of comparison with the acoustic model, we shall include the case where  $n \rightarrow 1$  as  $\omega \rightarrow 0$ , bearing in mind that this is unrealistic. We shall also look at a more realistic model, whose value of  $\xi$  is determined by the high-frequency dispersion, near  $\omega_0$ , of a real fibre. Therefore, the two cases we shall examine are:

- $\xi \approx 0.56$  gives  $\beta^2(\omega) \rightarrow \frac{\omega}{c}$  at low frequencies (near  $\omega = 0$ ); and
- $\xi \approx 0.036$  gives a more realistic  $\beta^2(\omega)$  at high frequencies (near  $\omega = \omega_0$ ).

Let us also note that a purely subluminal dispersion relation, like those given above, is incompatible with the alleged existence of optical solitons in the fibre: as noted in §5.2, solitons are only possible in regions where  $\partial^2\beta/\partial\omega^2 < 0$ , which is clearly not the case for the above forms of  $\beta$ . However, the purpose of the soliton - if, indeed, the pulse is a soliton - is to provide the nonlinear change in refractive index; its frequency is irrelevant for the purposes of the mode conversion. It is the dispersion at the modes that are scattered into each other which is relevant for calculating the Hawking spectrum. Even then, as already noted, the quartic dispersion cannot be expected to apply to all frequencies, being only the simplest analytic deviation from the dispersionless case.

## 9.2. Intensity profile

The simplest intensity profile, by direct analogy with the acoustic model, is the hyperbolic tangent,

$$\chi(\tau) = \frac{1}{2}(\chi_R + \chi_L) + \frac{1}{2}(\chi_R - \chi_L) \tanh(\alpha\tau), \quad (9.2.1)$$

which varies monotonically between two asymptotic values:  $\chi_L$  on the left ( $\tau \rightarrow -\infty$ ) and  $\chi_R$  on the right ( $\tau \rightarrow +\infty$ ). Another possibility is the hyperbolic secant profile that would be associated with a fundamental soliton:

$$\chi(\tau) = \chi_0 \operatorname{sech}^2\left(\frac{\tau}{T_0}\right). \quad (9.2.2)$$

Although Eq. (9.2.2) describes an intensity profile which is exact for a fundamental soliton, and in that sense more realistic than Eq. (9.2.1), there are instances when this relationship might change. In particular, the phenomenon of self-steepening perturbs a soliton in such a way that its trailing edge becomes much steeper than its leading edge. Since radiation rates are strongly dependent on the steepness of the change in intensity, this single steep edge dominates the process, so that Eq. (9.2.1) becomes more physically relevant than Eq. (9.2.2), whose leading and trailing edges are equally steep.

## 9.3. Normalizing the wave equation

We now transform the optical wave equation into a form with as few parameters as possible. Beginning with the general fiber-optical wave equation (5.3.7),

$$\frac{c^2}{u^2}(\partial_\zeta - \partial_\tau)^2 A + c^2\beta^2(i\partial_\tau)A - \partial_\tau(\chi\partial_\tau A) = 0, \quad (9.3.1)$$

we substitute the quartic form of  $\beta(\omega)$  given in Eq. (9.1.3) to get

$$\frac{c^2}{u^2}(\partial_\zeta - \partial_\tau)^2 A - \frac{c^2}{u^2}(1 - \xi)\partial_\tau^2 A + \frac{c^2}{u^2}\frac{\xi}{\omega_0^2}\partial_\tau^4 A - \partial_\tau(\chi\partial_\tau A) = 0. \quad (9.3.2)$$

Transforming to dimensionless variables  $T = \omega_0\tau$  and  $Z = \omega_0\zeta$ , this becomes

$$\partial_Z^2 A - 2\partial_Z\partial_TA + \xi(\partial_T^2 A + \partial_T^4 A) - \partial_T\left(\frac{u^2}{c^2}\chi\partial_TA\right) = 0, \quad (9.3.3)$$

## 9. Results for the Fibre-Optical Model

or

$$(\partial_Z - \partial_T)^2 A + B^2 (i\partial_T) A - \partial_T (X \partial_T A) = 0, \quad \text{where } B^2(\Omega) = (1 - \xi)\Omega^2 + \xi\Omega^4$$

$$\text{and } X(T) = \frac{u^2}{c^2} \chi(T). \quad (9.3.4)$$

If  $\chi$  takes the hyperbolic tangent form of Eq. (9.2.1), then  $X$  may be written

$$X(T) = \frac{1}{2} (X_R + X_L) + \frac{1}{2} (X_R - X_L) \tanh(aT),$$

and we see that the normalized optical wave equation contains four parameters:

- $X_R$  and  $X_L$ , the asymptotic values of the intensity-dependent nonlinearity;
- $a = \alpha/\omega_0$ , a parameter that combines the steepness of the intensity profile with the strength of the dispersion; and
- $\xi$ , which determines the group velocity in the co-moving frame, or, in the lab frame, the speed of the pulse relative to the frequency regime in which we are interested.

### 9.4. Predicted behaviour for a low-frequency event horizon

In the absence of dispersion, the wave equation (9.3.1) takes the form

$$n_g^2 \partial_\zeta^2 A - 2n_g^2 \partial_\zeta \partial_\tau A - (\partial_\tau \chi) \partial_\tau A - (\chi - (n_g^2 - 1)) \partial_\tau^2 A = 0, \quad (9.4.1)$$

where  $n_g = c/u$  is the group index at the pulse frequency. It is clear that there is an event horizon for all frequencies at  $\chi = n_g^2 - 1$ ; this is equivalent to the point  $U = -1$  in the acoustic case. Even in the dispersive case, if such a point exists then all forward-propagating, positive-norm frequencies experience a group-velocity horizon. We expect the emission of Hawking radiation, which is thermal at low frequencies.

What is the low-frequency temperature of the emitted radiation? In the non-dispersive acoustic case, by direct analogy with gravitational black holes, the temperature was found to be proportional to the derivative of the velocity profile at the horizon. It was then found, by both numerical simulations and analytic approximations, that this form of the temperature does not change if the slope is small and the dispersion weak. Since the mathematical analogy between the optical model and the acoustic model is not exact, it is not so clear what form the low-frequency temperature should take, although it should be approximately proportional to the derivative of  $\chi$  at the event horizon. Instead, let us make use of the fact that linearizing the velocity profile in the vicinity of the horizon led in the acoustic model to an expression for the temperature that is valid in the low-slope, weak-dispersion regime. We also have such an expression for the optical model: according to Eq. (8.3.16), the predicted Hawking creation rate is given by

$$\left| \frac{\beta_{\Omega'}}{\alpha_{\Omega'}} \right|^2 = \exp(-2 \operatorname{Im} \{J\}) \quad (9.4.2)$$

#### 9.4. Predicted behaviour for a low-frequency event horizon

where

$$J = \int_{\Omega_L^{ul}}^{\Omega_L^u} T(\Omega) d\Omega. \quad (9.4.3)$$

This requires that  $T$  be given as a function of  $\Omega$ , which is done in the same way as for the acoustic case; the result is

$$T(\Omega) = \frac{1}{a} \operatorname{arctanh} \left[ \frac{2}{\chi_R - \chi_L} \left\{ \frac{n_g^2 (\Omega - \Omega')^2 - B^2(\Omega)}{\Omega^2} - \frac{1}{2} (\chi_R + \chi_L) \right\} \right]. \quad (9.4.4)$$

Restricting our attention to real values of  $\Omega$ , the only contribution to  $\operatorname{Im}\{J\}$  comes from those values of  $\Omega$  that do not correspond to real values of  $T$ . For these frequencies,  $T(\Omega) = i\pi/(2a)$ , up to an integer multiple of  $i\pi/a$ . Therefore,

$$\left| \frac{\beta_{\Omega'}}{\alpha_{\Omega'}} \right|^2 = \exp \left( -\frac{\pi}{a} (\Omega_L^{ul} - \Omega_R^u) \right), \quad (9.4.5)$$

where  $\Omega_L^{ul}$  and  $\Omega_R^u$  are frequencies in the asymptotic regions, and mark the extremities of the real branches of  $T(\Omega)$ . (We ignore the counter-propagating  $v$ -modes, whose contribution to the phase integral is negligible.) Using the relation  $|\alpha_{\Omega'}|^2 - |\beta_{\Omega'}|^2 = 1$ , this becomes the thermal-like spectrum

$$|\beta_{\Omega'}|^2 = \frac{1}{\exp \left( \frac{\pi}{a} (\Omega_L^{ul} - \Omega_R^u) \right) - 1}. \quad (9.4.6)$$

To first order in  $\Omega'$  we find

$$\Omega_L^{ul} = \frac{n_g}{n_g - \sqrt{\chi_L + 1}} \Omega', \quad \Omega_R^u = -\frac{n_g}{\sqrt{\chi_R + 1} - n_g} \Omega',$$

so that

$$\Omega_L^{ul} - \Omega_R^u = \frac{n_g (\sqrt{\chi_R + 1} - \sqrt{\chi_L + 1})}{(n_g - \sqrt{\chi_L + 1}) (\sqrt{\chi_R + 1} - n_g)} \Omega'.$$

For low co-moving frequencies, then, we have

$$|\beta_{\Omega'}|^2 = \frac{1}{\exp(\Omega'/T_{\text{pred}}) - 1}$$

where the predicted temperature  $T_{\text{pred}}$  is given by

$$T_{\text{pred}} = \frac{a (n_g - \sqrt{\chi_L + 1}) (\sqrt{\chi_R + 1} - n_g)}{\pi n_g (\sqrt{\chi_R + 1} - \sqrt{\chi_L + 1})}. \quad (9.4.7)$$

Analogous with Eq. (4.4.3) for the acoustic model, we define a rescaled energy spectrum

$$f_{\Omega'} = \frac{\Omega'}{T_{\text{pred}}} |\beta_{\Omega'}|^2, \quad (9.4.8)$$

## 9. Results for the Fibre-Optical Model

so that, if the spectrum is thermal at low frequencies with temperature  $T$ , then

$$f_{\Omega'} \rightarrow \frac{T}{T_{\text{pred}}} \quad \text{as} \quad \Omega' \rightarrow 0. \quad (9.4.9)$$

To see how this is related to the slope of the nonlinearity, let us find  $\chi'(T_h)$ , where  $\chi(T_h) = n_g^2 - 1$ . We have

$$n_g^2 - 1 = \frac{1}{2}(\chi_R + \chi_L) + \frac{1}{2}(\chi_R - \chi_L) \tanh(aT_h),$$

and so

$$\tanh(aT_h) = \frac{2(n_g^2 - 1) - (\chi_R + \chi_L)}{(\chi_R - \chi_L)} = -\frac{(\chi_R + 1 - n_g^2) - (n_g^2 - 1 - \chi_L)}{(\chi_R + 1 - n_g^2) + (n_g^2 - 1 - \chi_L)}.$$

The derivative is given by

$$\begin{aligned} \chi'(T_h) &= \frac{a}{2}(\chi_R - \chi_L)(1 - \tanh^2(aT_h)) \\ &= \frac{a}{2}(\chi_R - \chi_L) \frac{((\chi_R + 1 - n_g^2) + (n_g^2 - 1 - \chi_L))^2 - ((\chi_R + 1 - n_g^2) - (n_g^2 - 1 - \chi_L))^2}{((\chi_R + 1 - n_g^2) + (n_g^2 - 1 - \chi_L))^2} \\ &= \frac{a}{2} \frac{2(\chi_R + 1 - n_g^2)2(n_g^2 - 1 - \chi_L)}{(\chi_R - \chi_L)} \\ &= 2a \frac{(\sqrt{\chi_R + 1} - n_g)(n_g - \sqrt{\chi_L + 1})(\sqrt{\chi_R + 1} + n_g)(n_g + \sqrt{\chi_L + 1})}{(\sqrt{\chi_R + 1} - \sqrt{\chi_L + 1})(\sqrt{\chi_R + 1} + \sqrt{\chi_L + 1})}. \end{aligned}$$

The temperature of Eq. (9.4.7), then, is related to the derivative at the horizon by

$$T_{\text{pred}} = \frac{\chi'(T_h)}{2\pi n_g} \frac{(\sqrt{\chi_R + 1} + \sqrt{\chi_L + 1})}{(\sqrt{\chi_R + 1} + n_g)(n_g + \sqrt{\chi_L + 1})}. \quad (9.4.10)$$

If  $\chi_R$  and  $\chi_L$  are close to the horizon, i.e., if  $\chi_R \approx \chi_L \approx n_g^2 - 1$ , this reduces to the simple formula

$$T_{\text{pred}} \approx \frac{\chi'(T_h)}{4\pi n_g^2}. \quad (9.4.11)$$

This prediction agrees with that of Eq. (7.1.7), which was derived from the approximate description of the pulse/probe system as a spacetime geometry.

Eq. (9.4.10) suggests that the temperature increases without bound as the derivative of the nonlinearity does. However, we have seen that, in the presence of dispersion, the solutions of the wave equation are well-behaved in the limit  $a \rightarrow \infty$ . Eqs. (9.4.7) and (9.4.10) are valid only in the low- $a$  limit; in the high- $a$  limit, the temperature is determined by solving the discontinuous nonlinearity profile. Therefore, as  $a$  increases, the temperature becomes independent of  $a$  by approaching a limit. This limiting case is solved in Appendix B; the resulting low-frequency temperature is

$$T_\infty = (n_g^2 - 1 - \chi_L)^{1/2} \frac{\sqrt{1 + \chi_L}(\chi_R + 1 - n_g^2)(n_g - \sqrt{1 + \chi_L})}{n_g(\chi_R - \chi_L)(n_g + \sqrt{1 + \chi_L})}. \quad (9.4.12)$$

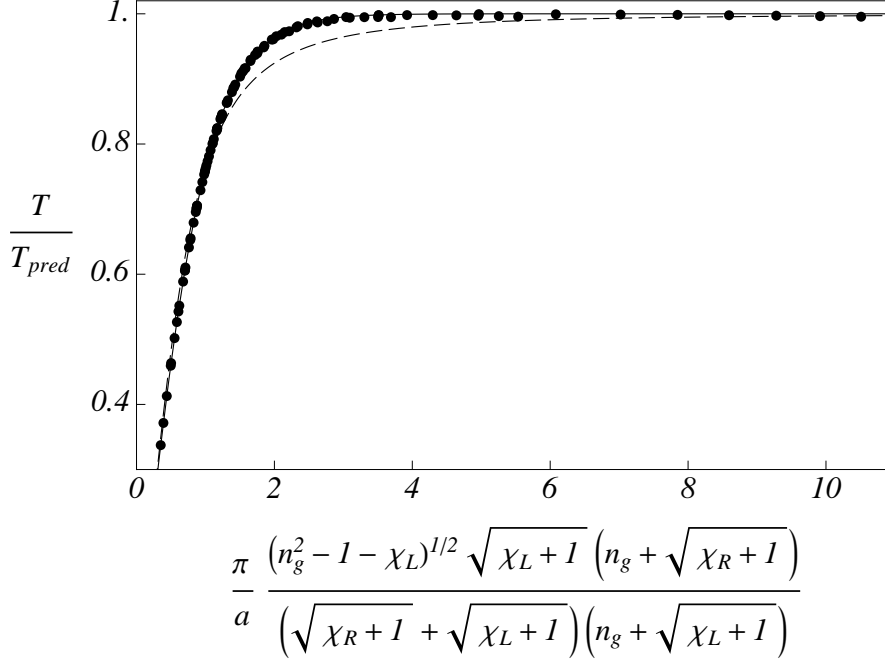


Figure 9.1.: LOW-FREQUENCY TEMPERATURE: This plots the limiting low- $\Omega'$  temperature, or  $\Omega' |\beta|^2 / T_{\text{pred}}$ , for various values of  $\chi_L$ ,  $\chi_R$  and  $a$ . Writing the abscissa simply as  $x$ , the solid line plots  $\tanh(x)$ , while the dashed line plots  $x \tanh(1/x)$ .

Comparing Eqs. (9.4.7) and (9.4.12), we find that the low- $a$  and high- $a$  forms of the temperature agree if we take

$$a = \pi (n_g^2 - 1 - \chi_L)^{1/2} \frac{\sqrt{1 + \chi_L} (\sqrt{1 + \chi_R} + n_g)}{(\sqrt{1 + \chi_R} + \sqrt{1 + \chi_L}) (n_g + \sqrt{1 + \chi_L})},$$

and it is expected that the transition from one regime to the other occurs when  $a$  is comparable to this value.

## 9.5. Numerical results

### 9.5.1. With a low-frequency horizon

We begin, as in the acoustic case, with the case where an event horizon for low frequencies is present. In the optical case, this occurs at  $\chi = n_g^2 - 1$ .

We have seen in Eq. (9.4.7) that the low-frequency temperature is predicted to be proportional to  $a$  when  $a$  is sufficiently small; we have also seen, in Eq. (9.4.12), that this temperature approaches a limiting value as  $a \rightarrow \infty$ . This is exactly as was found in the acoustic model, where we were able to fit the resulting temperatures to a hyperbolic tangent curve (see Fig. 4.9). Since the nonlinearity profile we use here is also a hyperbolic

## 9. Results for the Fibre-Optical Model

tangent, it is natural to guess that the temperature assumes a similar form. We have already seen, in §4.7, that there are two possibilities:

$$\frac{T}{T_{\text{pred}}} = \frac{T_{\infty}}{T_{\text{pred}}} \tanh\left(\frac{T_{\text{pred}}}{T_{\infty}}\right), \quad \text{or} \quad \frac{T}{T_{\text{pred}}} = \tanh\left(\frac{T_{\infty}}{T_{\text{pred}}}\right). \quad (9.5.1)$$

Both of these are plotted in Figure 9.1, along with results of the optical case with various values of the parameters  $\chi_L$ ,  $\chi_R$  and  $a$ . Once again, we find that the second of Eqs. (9.5.1) agrees remarkably well with the numerical results, clearly much more so than the first equation. Substituting Eqs. (9.4.7) and (9.4.12), we have

$$T = \frac{a(n_g - \sqrt{1 + \chi_L})(\sqrt{1 + \chi_R} - n_g)}{\pi n_g(\sqrt{1 + \chi_R} - \sqrt{1 + \chi_L})} \tanh\left(\frac{\pi(n_g^2 - 1 - \chi_L)^{1/2} \sqrt{1 + \chi_L}(\sqrt{1 + \chi_R} + n_g)}{a(\sqrt{1 + \chi_R} + \sqrt{1 + \chi_L})(n_g + \sqrt{1 + \chi_L})}\right). \quad (9.5.2)$$

It is also found that, if the parameters  $\chi_L$ ,  $\chi_R$  and  $a$  are chosen such that  $T/T_{\text{pred}} \approx 1$ , then the resulting spectra agree very well with the phase integral prediction of Eq. (9.4.6). Figure 9.2 shows several such spectra, together with the predicted spectra and a purely thermal spectrum. Again we find, as in the acoustic case, that the resulting spectrum is closest to thermal when the horizon - the point where  $\chi = n_g^2 - 1$  - is at the midpoint of the variation. Strikingly, if the middle value  $\chi_m = (\chi_L + \chi_R)/2$  is decreased, so that the event horizon is moved towards the far side of the variation, then the high-frequency end of the spectrum is enhanced in comparison to thermality.

### 9.5.2. With realistic values of $\chi$

Thermal emission from a horizon where  $\chi = n_g^2 - 1$ , though interesting and useful in constructing the analogy between the fibre-optical model and the more conventional acoustic model, is very difficult to set up in practice. A typical group index in glass is  $n_g \simeq 1.5$ , so that this horizon occurs at  $\chi \simeq 1.25$ . However, for femtosecond pulses, the peak value of  $\chi$  is typically less than  $10^{-3}$ . Can we still expect the emission of a measurable Hawking spectrum for such modest values of  $\chi$ ?

In a real fibre, of course,  $\chi = 0$  everywhere except in the vicinity of the light pulse. This is realisable mathematically if we assume a fundamental soliton, so that  $\chi$  is of the form

$$\chi(T) = h \operatorname{sech}^2(0.65 a T), \quad (9.5.3)$$

where  $h$  and  $a$  are parameters determining the height and width, respectively, of the soliton. However, self-steepening [63] perturbs the pulse such that its trailing edge is much steeper than its leading edge, so that the trailing edge dominates (see Figure 9.3). In this case, we can focus solely on the trailing edge of the pulse by using the hyperbolic tangent profile and setting  $\chi_R = 0$  and  $\chi_L = h$ :

$$\chi(T) = \frac{h}{2} (1 - \tanh(a T)). \quad (9.5.4)$$

Again,  $h$  determines the height of the profile, while  $a$  determines the “width” or length of the transition region. In both Eqs. (9.5.3) and (9.5.4), the length of the transition region,



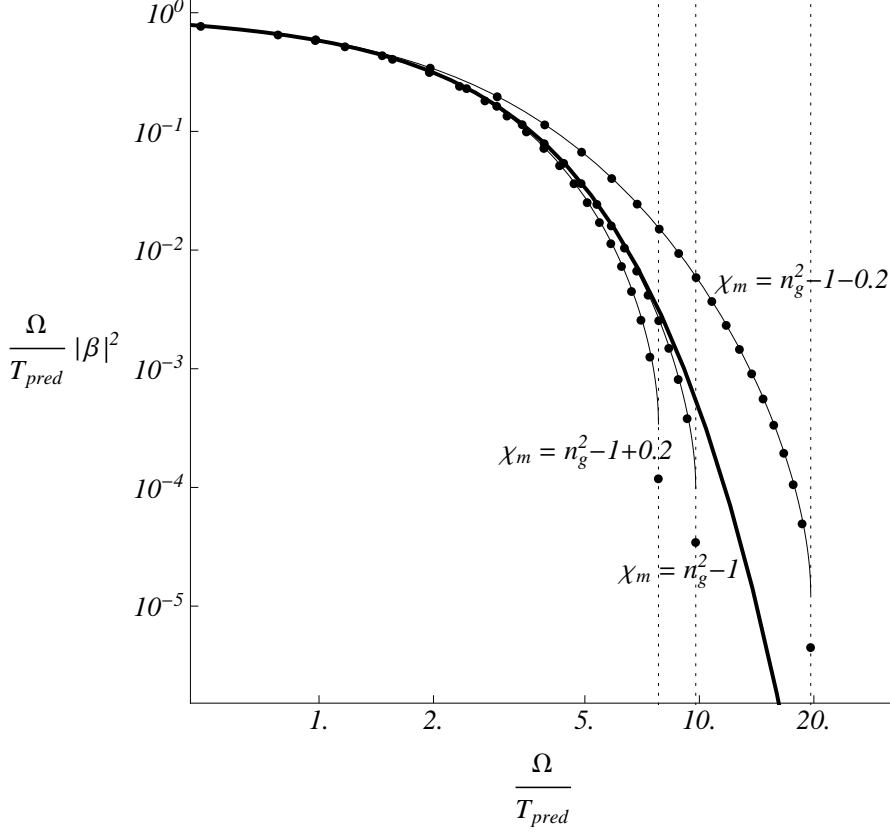


Figure 9.2.: HAWKING SPECTRA WITH A LOW-FREQUENCY HORIZON: The nonlinearity profile is such that  $\chi = n_g^2 - 1$  at some point. The dots plot the numerical results, the thin black curves plot the predictions of Eq. (9.4.6), and the thick curve shows the thermal spectrum. We have taken  $n_g = 1.6$ , and fixed  $\chi_L = n_g^2 - 1 - 0.6$  and  $a = 0.2$ . These values ensure that  $T/T_{\text{pred}} \approx 1$ , and since  $T/T_{\text{pred}}$  has a very weak dependence on  $\chi_R$ , we can vary the latter to achieve various values of  $\chi_m = (\chi_L + \chi_R)/2$ .

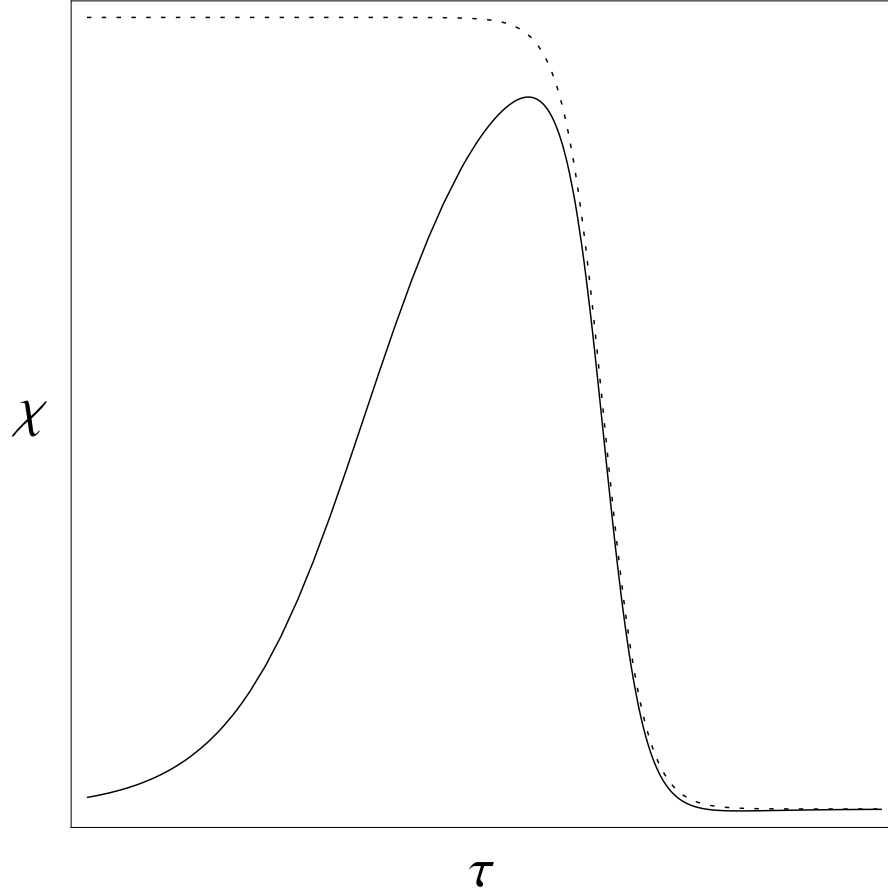


Figure 9.3.: SELF-STEEPENING OF A PULSE: Higher-order nonlinear effects cause the optical intensity to become concentrated near the trailing edge of the pulse. Since steepness is the main ingredient of Hawking radiation, we may approximate this as a single horizon with a hyperbolic tangent profile, as represented by the dotted curve.

where  $\chi$  varies between 0 and  $h$ , is given approximately by  $2/a$ ; due to the normalization of §9.3,  $a = 1/\pi \approx 0.3$  means that the transition occurs over about one cycle of the frequency  $\omega_0$ , a steepness in intensity which is achievable using few-cycle pulses [81, 82]. (This correspondence between the two profiles explains the appearance of the factor of 0.65 in Eq. (9.5.3).) It should be borne in mind that the soliton form of Eq. (9.5.3) has two such variations, one increasing and one decreasing.

Although the evolution of a pulse undergoing self-steepening is complicated, it is clear that the asymptotic values of  $\chi$  are always zero. This is clearly not the case for Eq. (9.5.4), where  $\chi \rightarrow h$  as  $T \rightarrow -\infty$ . We can compensate for this by adding another term

to  $\chi$  as follows:

$$\begin{aligned}\chi(T) &= \frac{h}{2} ((1 - \tanh(aT)) - (1 - \tanh(a'(T + T')))) \\ &= \frac{h}{2} (\tanh(a'(T + T')) - \tanh(aT)) ,\end{aligned}\tag{9.5.5}$$

where  $a' < a$  and  $T' > 0$ . This supplies a drop in  $\chi$  from  $h$  to zero as we approach negative  $T$ , and the low value of  $a'$  ensures that the steepness of this leading edge is less than the steepness of the trailing edge, still characterised by  $a$ . The main purpose of this form of  $\chi$  is to examine the effects of setting both asymptotic values of  $\chi$  to zero, and hence to check the validity of the results obtained using the form of Eq. (9.5.4).

Figures 9.4 and 9.5 show some results obtained using these more reasonable values of  $\chi$ . These compare both the use of the soliton (Eq. (9.5.3)) and hyperbolic tangent (Eq. (9.5.4)) forms of the nonlinearity, and the use of the different values of  $\xi$  given in §9.1, which correspond to  $n \rightarrow 1$  at low frequencies ( $\xi = 0.56$ ) and the more realistic case which is accurate near  $\Omega = 1$  ( $\xi = 0.036$ ). In Fig. 9.4,  $a$  is fixed while spectra for different values of  $h$  are plotted; in Fig. 9.5,  $h$  is fixed while  $a$  is varied.

There are several points to note about these results:

- There is no  $1/\Omega$  singularity at low frequencies, so the spectra are not thermal even in the low-frequency regime.
- There is a sharp, narrow peak near the maximum lab frequency, whose co-moving frequency is  $\Omega'_{\max}$ . At the same time, there is a sharp, narrow dip at the group-velocity-matched frequency, whose co-moving frequency is also  $\Omega'_{\max}$ . This is because, while the photon creation rate increases at these co-moving frequencies, they are spread over a relatively large frequency band in the lab frame.
- The hyperbolic tangent nonlinearity profile creates a sharp peak on the high-frequency side of the sharp dip. This is smoothed out if a soliton-type nonlinearity is used.
- The soliton profile gives lower spectra than the hyperbolic tangent profile for low values of  $a$ , but climbs to higher spectra for higher values of  $a$ .
- Setting the parameter  $\xi$  to 0.036 gives a higher creation rate than is obtained when  $\xi = 0.56$ .
- For the most part, the spectra are very nearly proportional to  $h^2$ . The only regions where this proportionality does not hold are where the co-moving frequency is at its maximum, i.e., near the group-velocity-matching frequency and its negative-norm counterpart. This makes sense: as  $h$  increases, so the range of frequencies which experience a group-velocity horizon (the *capture range*) widens, and the peak and dip at these frequencies will also widen.

## 9. Results for the Fibre-Optical Model

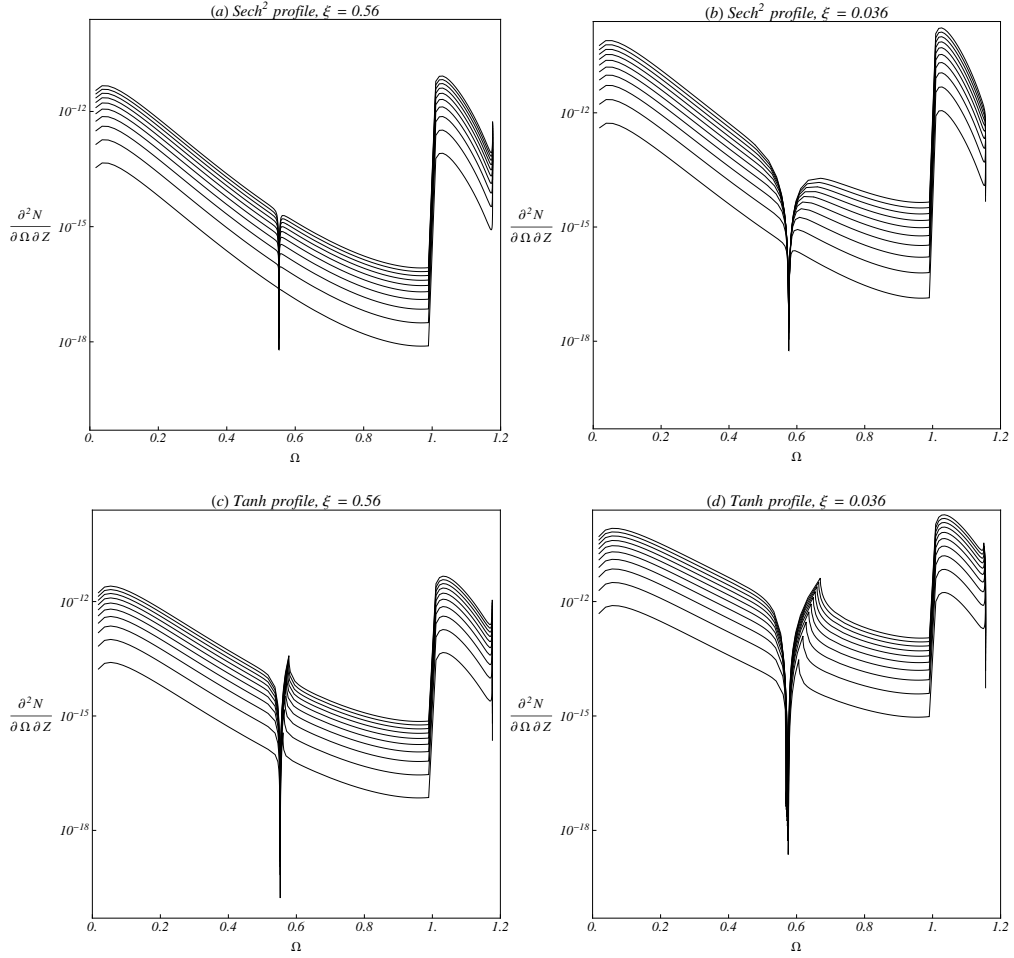


Figure 9.4.: HAWKING SPECTRA FOR REALISTIC VALUES OF  $\chi$ , 1: These plot photon flux spectra as functions of the lab frequency. All plots use the same logarithmic scale for the creation rate, and a linear scale for the (dimensionless) frequency  $\Omega = \omega/\omega_0$ . The top plots, Figs. (a) and (b), are obtained using a soliton-type nonlinearity, given in Eq. (9.5.3); the bottom plots, Figs. (c) and (d), are for the hyperbolic tangent profile of Eq. (9.5.4). In the left-hand plots (a) and (c),  $n \rightarrow 1$  at low frequencies and  $\xi = 0.56$  in Eqs. (9.3.3) and (9.3.4); in the right-hand plots (b) and (d), the dispersion is matched to a realistic fibre near  $\omega_0$  ( $\Omega = 1$ ), and  $\xi = 0.036$ . Throughout,  $a = 0.3$  while  $h$  varies between  $10^{-4}$  and  $10^{-3}$ .

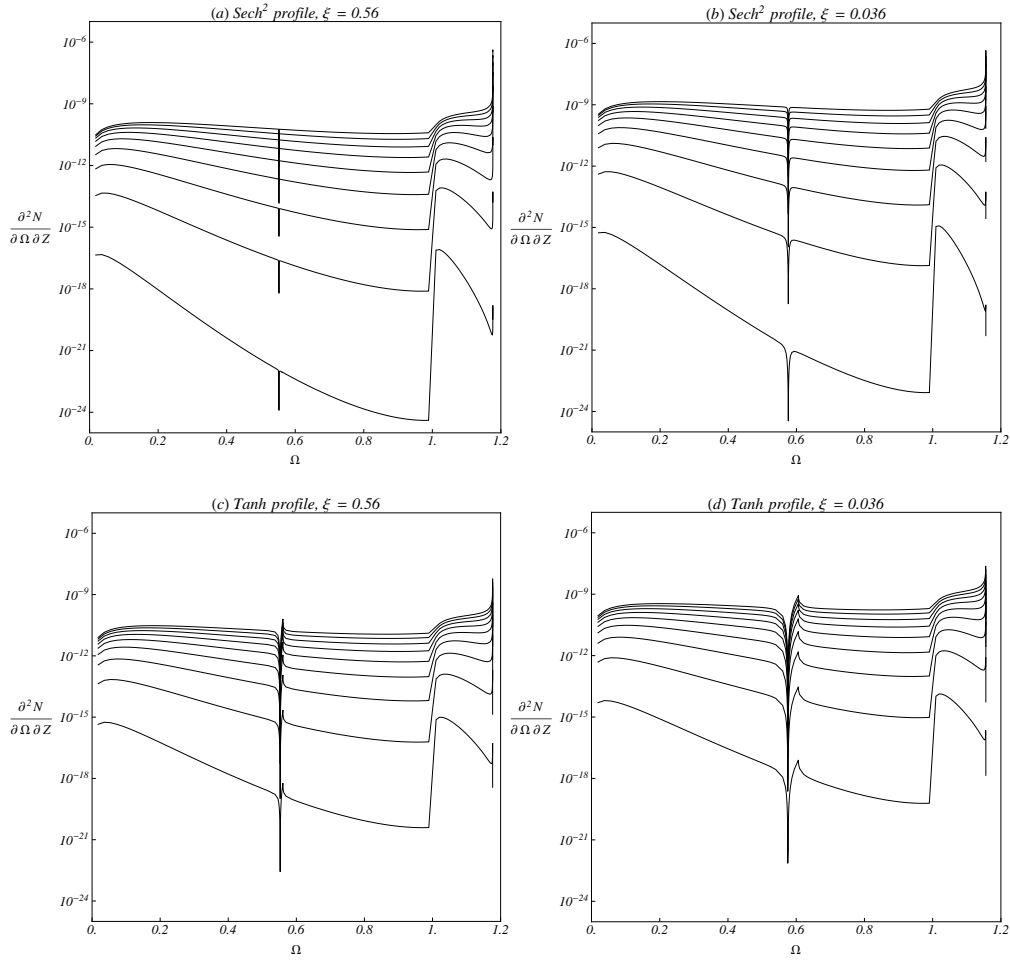


Figure 9.5.: HAWKING SPECTRA FOR REALISTIC VALUES OF  $\chi$ , 2: These plot photon flux spectra as functions of the lab frequency. The plots are arranged similarly to Figure 9.4. The only difference is that, here,  $h = 10^{-4}$  while  $a$  varies between 0.2 and 1.0.

## 9. Results for the Fibre-Optical Model

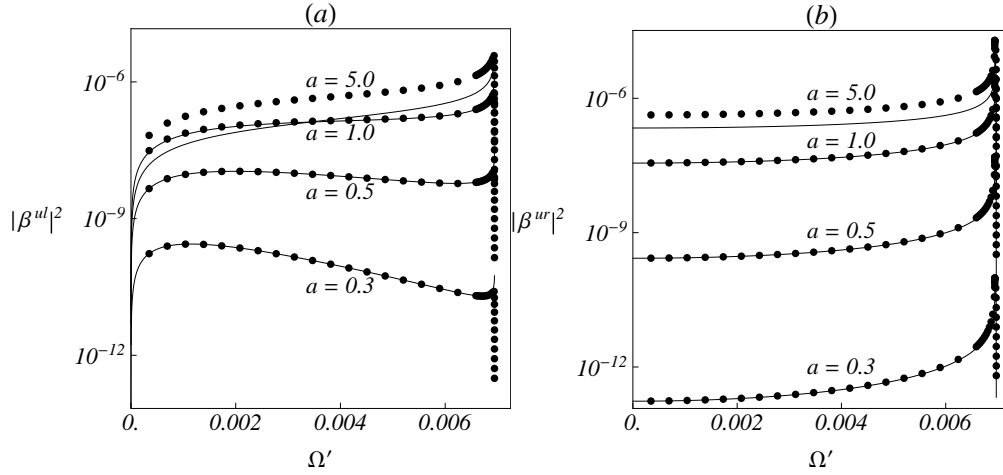


Figure 9.6.: HAWKING SPECTRA AND THE PHASE-INTEGRAL APPROXIMATION: These show numerically calculated Hawking spectra (dots) as functions of the co-moving frequency (*not* the lab frequency, for the sake of convenience). The purpose is to compare this with the modified phase-integral predictions of Eqs. (9.5.6)-(9.5.8) (curves), with which there is seen to be excellent agreement for  $a \lesssim 1$ . Throughout,  $h = 10^{-4}$ .

- For large  $a$  the spectra approach limiting curves, as expected. For low  $a$ , they are highly sensitive to its value. If the change in  $\chi$  takes place over more than about one cycle of the frequency  $\omega_0$ , then it is by far the *low* co-moving frequencies that dominate the spectra, reaching heights greater than the narrow peak at the maximum frequency. What is more, the coupling between the low-frequency  $ul$ -modes and the high-frequency  $u$ -modes vastly outweighs the coupling between the  $ur$ - and  $u$ -modes. As  $a$  increases, however, the whole spectrum increases exponentially and the low-frequency peak is smoothed out.

The asymmetric hyperbolic tangent profile produces Hawking spectra very similar to those for the pure hyperbolic tangent. The main difference lies in the region around the group-velocity-matching frequency: the sharp peak on the high-frequency side is smoothed, but unlike for the soliton profile, this peak clearly still exists.

It should be borne in mind that the calculated spectra, which are photon flux densities according to Eq. (7.4.9), are dimensionless quantities. In order to yield a measurable quantity, we must replace the factor of  $\omega_0$  that was factored out in §9.3. Typically,  $\omega_0$  lies in the ultraviolet regime at about 300 nm or  $6 \times 10^{15}$  Hz. Integrated over the range of  $\Omega$ , a constant value of  $10^{-15}$  for  $\partial^2 N / \partial \Omega \partial Z$  corresponds roughly to one emitted photon per second. This must then be modified by the factor  $L\nu_{\text{rep}}/u$  appearing in Eq. (7.4.11), which takes account of repeated pulses and propagation length. This can vary from about unity for a soliton in a metre-long fibre down to about  $10^{-3}$  for short pulses or effective propagation lengths. So Figure 9.4, where the intensity change occurs over

a single cycle of the frequency  $\omega_0$  and the height of the nonlinearity is on the order of  $10^{-3}$ , yields results ranging from less than a photon per minute to thousands of photons per second.

Remarkably, these spectra are still fairly well-approximated by analytic expressions analogous to those found in the acoustic model. As was the case there, some modification is required: it is found that, rather than simply a single exponential, the spectrum is formed from a linear combination of exponentials. For instance, when we have a group-velocity horizon (which occurs in the tail of the  $ur$ - $u$  spectrum, near  $\Omega'_{\max}$ ), the spectrum is not given by Eq. (9.4.5) but is much better approximated by

$$|\beta^{ur}|^2 \approx \exp\left(-\frac{\pi}{a}\left(\Omega_R^{ul} - \Omega_L^u\right)\right) - \exp\left(-\frac{\pi}{a}\left(\Omega_R^{ur} - \Omega_L^u\right)\right) \\ - \exp\left(-\frac{\pi}{a}\left(\Omega_R^{ul} - \Omega_R^u\right)\right) + \exp\left(-\frac{\pi}{a}\left(\Omega_R^{ur} - \Omega_R^u\right)\right). \quad (9.5.6)$$

Similarly, we find, when there is no group-velocity horizon, that the  $ul$ - $u$  and  $ur$ - $u$  spectra are approximately given by the following:

$$|\beta^{ul}|^2 \approx \exp\left(-\frac{\pi}{a}\left(\Omega_R^{ul} - \Omega_L^u\right)\right) - \exp\left(-\frac{\pi}{a}\left(\Omega_L^{ul} - \Omega_L^u\right)\right) \\ - \exp\left(-\frac{\pi}{a}\left(\Omega_R^{ul} - \Omega_R^u\right)\right) + \exp\left(-\frac{\pi}{a}\left(\Omega_L^{ul} - \Omega_R^u\right)\right), \quad (9.5.7)$$

$$|\beta^{ur}|^2 \approx \exp\left(-\frac{\pi}{a}\left(\Omega_L^{ul} - \Omega_R^u\right)\right) \left\{ \exp\left(-\frac{\pi}{a}\left(\Omega_L^{ur} - \Omega_L^u\right)\right) - \exp\left(-\frac{\pi}{a}\left(\Omega_R^{ur} - \Omega_L^u\right)\right) \right. \\ \left. - \exp\left(-\frac{\pi}{a}\left(\Omega_L^{ur} - \Omega_R^u\right)\right) + \exp\left(-\frac{\pi}{a}\left(\Omega_R^{ur} - \Omega_R^u\right)\right) \right\}. \quad (9.5.8)$$

These expressions are compared with numerical results in Figure 9.6. Note that agreement is good for lower values of  $a$  ( $\lesssim 1$ ), but not for higher values, where the linearization of  $\chi$  performed in §8.3 becomes invalid and the spectrum approaches that obtained from a discontinuous nonlinearity profile.

## 9.6. Concluding remarks

We have found, perhaps surprisingly, that Hawking radiation is not only predicted by the optical model, but it is also subject to the same observations made in the context of the acoustic model. When an event horizon is present, the spectrum is thermal at low frequencies, and the temperature is given by Eq. (9.5.2) - a direct analogy of Eq. (4.7.7) found for the acoustic case. The spectra deviate from thermality at higher frequencies, but are well-approximated by the phase-integral approximation. When there is no low-frequency horizon - the more realistic case - the spectra are no longer thermal but are well-approximated by a modified version of the phase-integral approximation which linearly combines different values of the phase integral; these are given in Eqs. (9.5.6)-(9.5.8). In particular, with small values of the step size  $h$ , the spectra (or those parts of the spectra not subject to a group-velocity horizon) are proportional to  $h^2$ .

## 9. Results for the Fibre-Optical Model

While these results look promising, it is worth examining a serious criticism of the optical model. This has to do with the validity of the low-frequency *ul*-modes, and is the subject of the next chapter.



## 10. The Low-Frequency Problem

In solving the complete optical wave equation, we have seen in Chapter 9 that, upon quantization of the optical field, spontaneous creation of photon pairs of vastly different frequencies occurs. Numerical simulations robustly conclude that the dominant pairing is between the very high frequencies of the  $u$ -mode and the very low frequencies of the  $ul$ -mode. This poses a problem unique to the optical model, to do with the strength of the nonlinear coupling between probe light and the pulse. In the acoustic model, the spontaneous creation of phonon pairs with wavenumbers of different orders of magnitude is perfectly plausible, provided the dispersion relation is valid in both regimes. These wavenumbers, however different, will “see” the same flow velocity profile, which is externally fixed - a property of the medium rather than the waves. In the optical model, the refractive index change induced by a pulse can be written as  $\delta n = 2n_2 I$  [63]. (The factor of 2 appears because the pulse and probe are assumed to have different frequencies, so that they interact through cross-phase modulation; see Eq. (5.2.12).)  $I$  is the intensity of the pulse, and can be considered as externally fixed since it is independent of the probe waves.  $n_2$ , however, is a frequency-dependent quantity:  $n_2 = n_2(\omega)$ , where  $\omega$  is the frequency of the probe. Frequencies of a similar order of magnitude - such as the  $u$ - and  $ur$ -modes around the point where  $\omega' = 0$  - will have similar values of  $n_2$ , and the refractive index change can be assumed identical for such frequencies. This assumption is invalid for frequencies of different orders of magnitude. Indeed, there should be virtually no nonlinear coupling at very low frequencies - precisely those frequencies which, as seen in Fig. 9.4, turn out to dominate the Hawking radiation!

How can we modify our model in order to suppress the low frequencies, leaving the  $u$ - and  $ur$ -modes as the dominant Hawking pairs?

### 10.1. Frequency-dependent $\chi$

A first modification is to introduce an explicit frequency-dependence into the form of  $\chi$ .

#### 10.1.1. Quadratic dependence on $\omega$

We assume that  $\chi$  can be written as the product

$$\chi(\omega, \tau) = \kappa(\omega) \chi(\tau), \quad (10.1.1)$$

so that the frequency  $\omega$  “sees” the nonlinearity profile  $\kappa(\omega) \chi(\tau)$ .  $\chi(\tau)$  is assumed to be the valid form of the nonlinearity when  $\omega$  is near  $\omega_0$ , the frequency with vanishing co-moving frequency; therefore,  $\kappa(\omega_0) = 1$ . To make the nonlinearity vanish at low

## 10. The Low-Frequency Problem

frequencies, we take  $\kappa(0) = 0$ . Since the frequencies  $\omega$  and  $-\omega$  must “see” identical nonlinearities,  $\kappa(\omega)$  must be an even function, and hence we find that the simplest form of  $\kappa$  is

$$\kappa(\omega) = \frac{\omega^2}{\omega_0^2}. \quad (10.1.2)$$

This is a highly artificial construction, but it should help to eliminate the unrealistic frequencies and give some indication of what the Hawking spectrum might look like in practice.

To implement Eqs. (10.1.1) and (10.1.2), we replace  $\omega$  by the operator  $i\partial_\tau$  and substitute into the optical wave equation. However, the arrangement of the two new differential operators must be chosen with care. This is done in such a way that the scalar product of Eq. (7.1.8) remains constant with respect to  $\zeta$ ; upon the taking of this derivative, and the substitution of the wave equation in the resulting integrand, we may use integration by parts to obtain cancelling terms only when the derivative operators  $i\partial_\tau$  are placed symmetrically around  $\chi$ . Therefore, the new wave equation is

$$n_g^2 (\partial_\zeta - \partial_\tau)^2 A + c^2 \beta^2 (i\partial_\tau) A + \frac{1}{\omega_0^2} \partial_\tau^2 (\chi \partial_\tau^2 A) = 0. \quad (10.1.3)$$

Plugging in the quartic form of the dispersion in Eq. (9.1.3) and normalizing the wave equation according to Eq. (9.3.3), this becomes

$$\partial_Z^2 A - 2\partial_Z \partial_T A + \xi (\partial_T^2 A + \partial_T^4 A) + \partial_T^2 (X \partial_T^2 A) = 0. \quad (10.1.4)$$

### 10.1.2. Results

Eq. (10.1.4) can be solved numerically as before. We assume a hyperbolic tangent nonlinearity profile:

$$X(T) = \frac{h}{2} (1 - \tanh(aT)). \quad (10.1.5)$$

We also assume that the contributions from the  $v$ -mode are negligible, so that the  $u$ -mode pairs only with the  $ul$ - and  $ur$ -modes. Then, we may use the method of §8.2 to numerically solve for the  $u$ -in mode, and the norms of the  $ul$ - and  $ur$ -out modes are interpreted as the spectral amplitudes  $|\beta^{ul}|^2$  and  $|\beta^{ur}|^2$ ; the spectrum of the  $u$ -mode is  $|\beta^u|^2 = |\beta^{ul}|^2 + |\beta^{ur}|^2$ .

Figure 10.1 shows some spectra obtained with this model. We see that the contribution from the low-frequency modes has indeed been greatly diminished, although there is still a significant contribution from the  $ul$ -mode when the frequency is not too close to zero. Other than this reduction, the spectra are almost identical with their counterparts when  $\chi$  is independent of frequency, and if  $a$  is low then the low-frequency component of the radiation remains the dominant one.

Also worthy of note is that the analytic expressions of Eqs. (9.5.6)-(9.5.8), which were previously found to be in good agreement with numerics, remain valid here. The plots are compared in Figure 10.2.

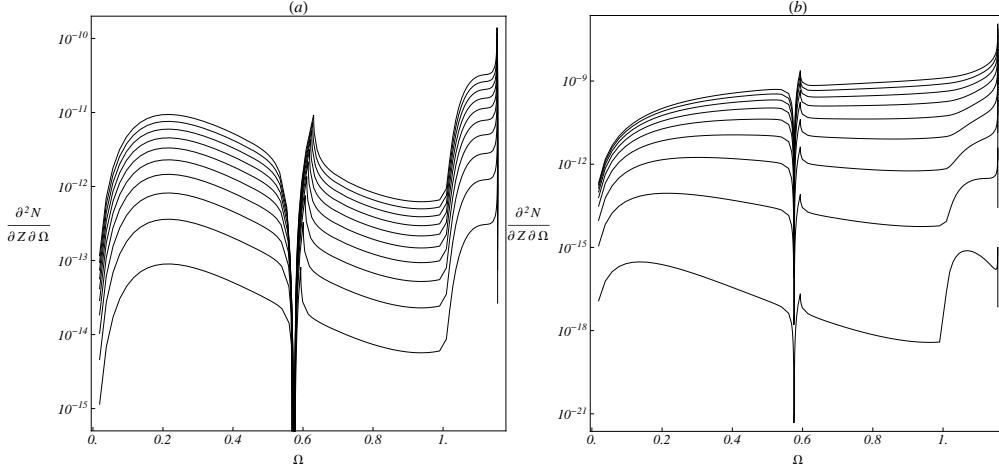


Figure 10.1.: HAWKING SPECTRA WITH FREQUENCY-DEPENDENT  $\chi$ : The spectral flux density is plotted on a logarithmic scale against the (normalized) lab frequency on a linear scale.  $\chi$  has the quadratic frequency dependence of Eq. (10.1.2) and the hyperbolic tangent spatial dependence of Eq. (10.1.5). In Figure (a),  $a$  is fixed at 0.3 while  $h$  varies between  $10^{-4}$  and  $10^{-3}$ ; in Figure (b),  $h = 10^{-4}$  while  $a$  varies between 0.2 and 1.0. In both plots,  $\xi = 0.036$ , the more realistic value.

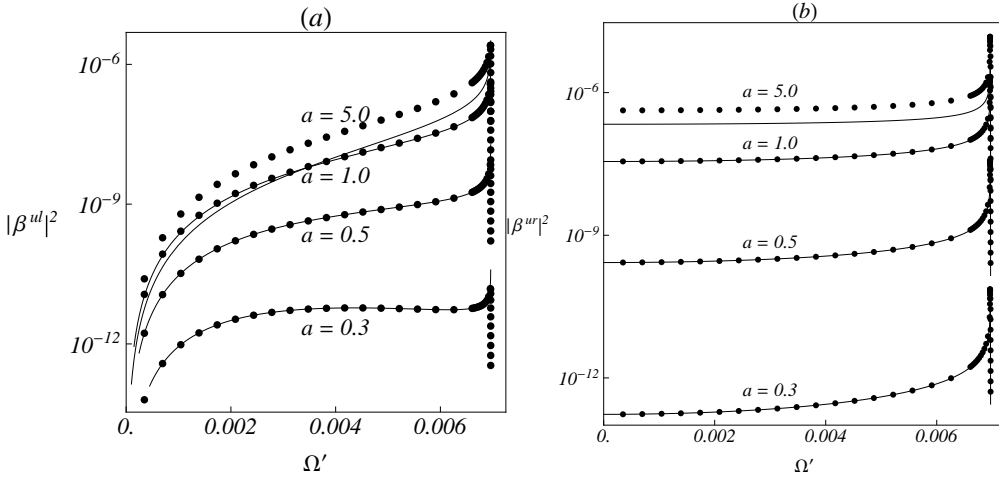


Figure 10.2.: HAWKING SPECTRA AND PHASE-INTEGRAL APPROXIMATION: The dots plot the numerically calculated spectra as functions of the normalized co-moving frequency, Figure (a) showing the spectra of the  $ul$ - $u$  pair whilst Figure (b) shows the spectra of the  $ur$ - $u$  pair. The curves plot the modified phase-integral predictions of Eqs. (9.5.6)-(9.5.8), and, as before, they are in excellent agreement for  $a \lesssim 1$ .

## 10.2. Reduction to two solutions

Discarding the low-frequency solutions of the dispersion relation (i.e., the  $v$ - and  $ul$ -modes), we are left with only two solutions: the  $u$ - and  $ur$ -modes, lying on either side of the frequency  $\omega_0$  whose co-moving frequency vanishes. Although we attempted, in the previous section, to suppress the low-frequency modes, we found that they tend to remain the dominant component of the radiation. We would like to find a way to eliminate them entirely, such that the high-frequency modes are really the only solutions, to check the robustness of the Hawking spectrum with respect to the presence or absence of the low-frequency modes.

There is, however, an immediate problem: the full optical wave equation has exactly two solutions in the absence of dispersion. Introducing dispersion - and giving the wavenumber  $\beta$  a more complicated dependence on  $\omega$  than mere proportionality - serves to increase the number of solutions. Therefore, we cannot reduce the number of solutions sufficiently using the full wave equation. Instead, we may formulate a “half” wave equation that describes purely forward-propagating waves. This is not easily derived from the optical wave equation (7.1.4), but an analogous equation is derived from the acoustic wave equation (2.1.4), which is factorizable into forward- and backward-propagating components. Our first task, then, is to alter the optical wave equation slightly so that it can be cast in the same form as the acoustic wave equation.

### 10.2.1. Analogy between acoustic and optical wave equations

The acoustic wave equation, fully expanded and in as general a form as possible, is

$$\partial_t^2 \phi + 2V \partial_t \partial_x \phi + (\partial_x V) \partial_t \phi + 2V (\partial_x V) \partial_x \phi + V^2 \partial_x^2 \phi + F^2 (-i \partial_x) \phi = 0. \quad (10.2.1)$$

Similarly for the optical wave equation:

$$\partial_\zeta^2 A - 2\partial_\zeta \partial_\tau A - \frac{1}{n_g^2} (\partial_\tau \chi) \partial_\tau A + \left(1 - \frac{1}{n_g^2} \chi\right) \partial_\tau^2 A + \frac{c^2}{n_g^2} \beta^2 (i \partial_\tau) A = 0, \quad (10.2.2)$$

where  $n_g = c/u$  is the group index of the pulse. It is clear that  $\phi$  and  $A$ ,  $t$  and  $\zeta$ , and  $x$  and  $\tau$  are pairs of analogous quantities. The terms  $F^2 (-i \partial_x) \phi$  and  $\frac{c^2}{n_g^2} \beta^2 (i \partial_\tau) A$  are also analogous. (The sign of the differential operator is irrelevant since both  $F^2(k)$  and  $\beta^2(\omega)$  are even functions of their arguments.) Also, the low-frequency wave velocity, usually denoted  $c$  in the acoustic model, corresponds to  $1/n_g$  in the optical model. The term  $V^2 \partial_x^2 \phi$  is clearly analogous to the term  $(1 - \chi/n_g^2) \partial_\tau^2 A$ , so that the flow velocity  $V$  - which, we recall, is usually taken to be negative - corresponds, in the optical model, to  $-(1 - \chi/n_g^2)^{1/2} \approx -1 + \chi/(2n_g^2)$ . To first order in  $\chi$ , then, the term  $2V (\partial_x V) \partial_x \phi$  corresponds to the term  $-(\partial_\tau \chi) \partial_\tau A/n_g^2$ . The terms  $2V \partial_t \partial_x \phi + (\partial_x V) \partial_t \phi$  would, to first order in  $\chi$ , correspond to  $-2\partial_\zeta \partial_\tau A + \chi \partial_\zeta \partial_\tau A/n_g^2 + (\partial_\tau \chi) \partial_\zeta A/(2n_g^2)$ . Neglecting the latter two terms, the correspondence between the acoustic and optical wave equations is complete. We conclude that, if we may neglect the terms  $\chi \partial_\zeta \partial_\tau A/n_g^2 + (\partial_\tau \chi) \partial_\zeta A/(2n_g^2)$ ,

then we may write the optical wave equation as

$$(\partial_\zeta + \partial_\tau X) (\partial_\zeta + X \partial_\tau) A + \frac{c^2}{n_g^2} \beta^2 (i \partial_\tau) A = 0, \quad (10.2.3)$$

where we have defined

$$X(\tau) = -1 + \frac{1}{2n_g^2} \chi(\tau). \quad (10.2.4)$$

Substituting the differential operators  $\partial_\zeta$  and  $\partial_\tau$  for  $-i\omega'$  and  $-i\omega$ , respectively, Eq. (10.2.3) becomes

$$(\omega' + \omega X) (\omega' + X\omega) A = \frac{c^2}{n_g^2} \beta^2(\omega) A. \quad (10.2.5)$$

### 10.2.2. “Half” wave equation

When  $X$  is constant, the wave equation can be Fourier transformed to give the dispersion relation

$$(\omega' + X\omega)^2 = \frac{c^2}{n_g^2} \beta^2(\omega) \implies \omega' = -X\omega \pm \frac{c}{n_g} \beta(\omega). \quad (10.2.6)$$

In the absence of pulses, or far away from them,  $\chi = 0$ , so from Eq. (10.2.4) we have  $X = -1$  and Eq. (10.2.6) becomes  $\omega' = \omega \pm c\beta(\omega)/n_g$ , where the minus sign corresponds to forward-propagating waves. Singling out the forward-propagating waves can be achieved by replacing Eq. (10.2.5) with its “square root”:

$$(\omega' + X\omega) A = -\frac{c}{n_g} \beta(\omega) A, \quad (10.2.7)$$

or, replacing the differential operators,

$$(\partial_\zeta + X \partial_\tau) A = i \frac{c}{n_g} \beta(i \partial_\tau) A. \quad (10.2.8)$$

When  $X$  is not constant in  $\tau$ , Eq. (10.2.8) does not give an exact solution of Eq. (10.2.3), and the norm is no longer conserved. However, the differences from the full wave equation might be small enough so that Eq. (10.2.8) can still give meaningful results.

### 10.2.3. Dispersion relation

The only remaining task to be done before using the “half” wave equation is to specify the form of  $\beta(\omega)$  that gives only two solutions. This can be derived quite simply as follows. When  $X$  is constant, the dispersion relation is  $\omega' + X\omega = -c\beta(\omega)/n_g$ . In order to have only two solutions for  $\omega$ , this equation must be quadratic in  $\omega$ , and since it already contains  $\omega$  to the powers of 0 and 1, it follows that  $\beta(\omega)$  must contain either a term in  $\omega^2$  or a term in  $\omega^{-1}$  (possibly alongside terms in  $\omega^0$  and  $\omega^1$ ). Since  $\beta(\omega)$  must be an odd function, it follows that its general form is

$$\frac{c}{n_g} \beta(\omega) = c_1 \omega + c_{-1} \omega^{-1}. \quad (10.2.9)$$

## 10. The Low-Frequency Problem

In the absence of pulses, or far away from them, the dispersion relation becomes

$$\omega' = (1 - c_1) \omega - c_{-1} \omega^{-1}. \quad (10.2.10)$$

Another requirement is that the co-moving frequency  $\omega'$  should vanish at the frequency  $\omega_0$ :

$$0 = (1 - c_1) \omega_0 - c_{-1} \omega_0^{-1} \implies c_{-1} = (1 - c_1) \omega_0^2.$$

Eq. (10.2.9) can now be written

$$\frac{c}{n_g} \beta(\omega) = c_1 \omega + (1 - c_1) \frac{\omega_0^2}{\omega}. \quad (10.2.11)$$

How is  $c_1$  to be interpreted? Since the dispersion relation should be most accurate near  $\omega = \omega_0$ , it is related to the parameter  $\xi \equiv -d\omega'/d\omega|_{\omega=\omega_0}$ . Substituting for  $c_{-1}$  in Eq. (10.2.10), we have

$$\omega' = (1 - c_1) \left( \omega - \frac{\omega_0^2}{\omega} \right), \quad (10.2.12)$$

and, therefore,

$$\frac{d\omega'}{d\omega} = (1 - c_1) \left( 1 + \frac{\omega_0^2}{\omega^2} \right). \quad (10.2.13)$$

When  $\omega = \omega_0$ , this gives  $-\xi = d\omega'/d\omega|_{\omega=\omega_0} = 2(1 - c_1)$ . Substituting in Eqs. (10.2.11) and (10.2.12), we finally have

$$\frac{c}{n_g} \beta(\omega) = \left( 1 + \frac{\xi}{2} \right) \omega - \frac{\xi \omega_0^2}{2 \omega}, \quad (10.2.14)$$

$$\omega' = -\frac{\xi}{2} \left( \omega - \frac{\omega_0^2}{\omega} \right). \quad (10.2.15)$$

The artificiality of this dispersion model yields some peculiar properties. One of these has to do with the signs of first- and second-order dispersion (i.e., the first and second derivatives of  $\beta(\omega)$ ). First-order dispersion is equal to the reciprocal of the lab-frame group velocity [63]. Usually, this is positive: in the lab frame, the phase and group velocities almost always point in the same direction. This corresponds, in the above model, to a positive value of  $\xi$ , for

$$\frac{c}{n_g} \beta'(\omega) = 1 + \frac{\xi}{2} \left( 1 + \frac{\omega_0^2}{\omega^2} \right).$$

The second-order dispersion is also usually positive, but there can exist regimes in which it is negative. (Solitons, for example, can exist only in regions with negative second-order dispersion, as mentioned in §5.2.) In our case, both first- and second-order dispersion are positive in the high-frequency regime. However, the second-order dispersion is given by

$$\frac{c}{n_g} \beta''(\omega) = -\xi \frac{\omega_0^2}{\omega^3}.$$

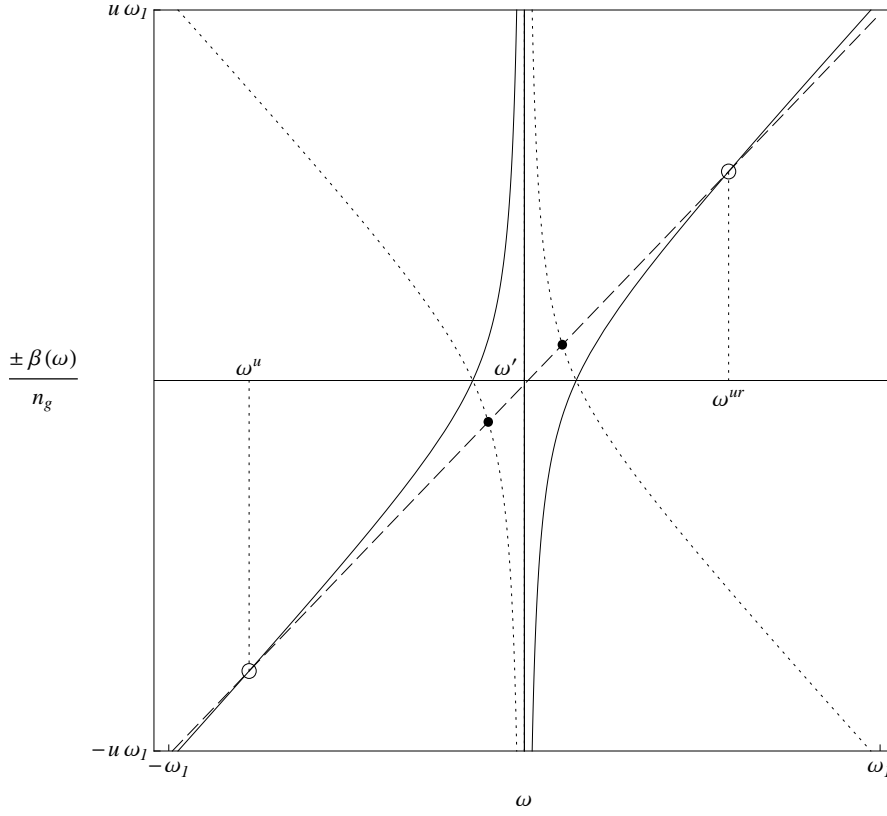


Figure 10.3.: TWO-SOLUTION DISPERSION WITH POSITIVE  $\xi$ : The solutions of the dispersion relation are the points of intersection between  $u\beta(\omega)$ , given by Eq. (10.2.14), and the line  $\omega - \omega'$ . The solid and dotted curves refer to co- and counter-propagating solutions (not positive- and negative-norm solutions, as in previous examples). For the “half” wave equation (10.2.8), only the solid curve applies. Note that the full wave equation would always have four real solutions.

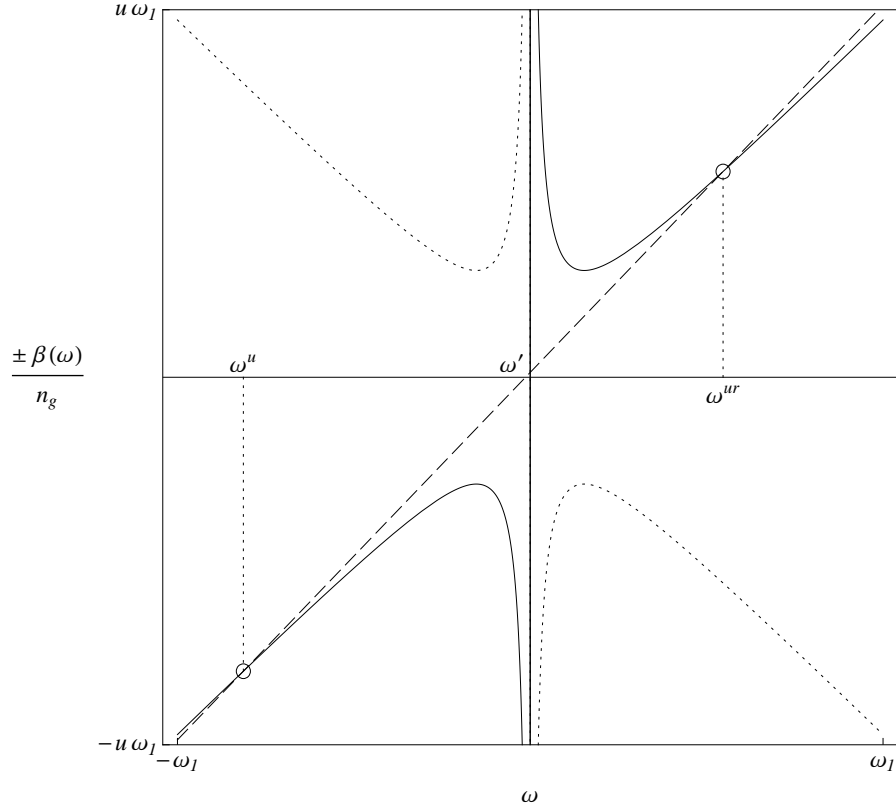


Figure 10.4.: TWO-SOLUTION DISPERSION WITH NEGATIVE  $\xi$ : The possible solutions of the dispersion relation are the points where  $u\beta(\omega)$ , where  $\beta(\omega)$  is given by Eq. (10.2.14), and the line  $\omega - \omega'$  intersect. The solid and dotted curves refer to the forward- and backward-propagating solutions (*not*, as in previous examples, the positive- and negative-norm solutions, which correspond directly to the sign of  $\omega - \omega'$ ). For the “half” wave equation (10.2.8), only the solid curve applies, and there are only the two solutions, corresponding to the  $u$ - and  $ur$ -modes of quartic dispersion (see Fig. 7.1). If  $\omega'$  is not too large, even the full wave equation has only two real solutions.



Although in reality both are positive, the dispersion model we have selected forces first- and second-order dispersion to have opposite signs. Figures 10.3 and 10.4 show the dispersion relations corresponding to positive and negative  $\xi$ , respectively. We may still use this model, so long as we recognise that it is only for the sake of verification that it is being used, and is by no means accurate, especially far from the frequency  $\omega_0$ .

#### 10.2.4. Numerical results

Some spectra obtained with the dispersion model of Eq. (10.2.14) are plotted in Fig. 10.5. Since this model applies only to frequencies near  $\omega_0$ , we have taken  $|\xi| = 0.036$  in accordance with §9.1. Due to the ambiguity in the sign of  $\xi$  noted above, we have plotted the results for both positive and negative  $\xi$ ; note that the change in sign makes little difference to the results.

One striking feature of the spectra is their width: they are very broad, reaching frequencies much higher than that obtained by previous spectra. This is because the dispersion model of Eqs. (10.2.14) and (10.2.15) does not have a group-velocity horizon for forward-propagating waves, and therefore has no cut-off frequency. However, the resulting spectra behave in a similar way to our previous results as the parameters  $h$  and  $a$  are varied. The spectra are almost exactly proportional to  $h^2$ , and since there is no group-velocity horizon, there is no exception to this rule. Somewhat counter-intuitively, it is  $a$ , not  $h$ , which determines the width of the spectra, and for lower values of  $a$  the height increases exponentially with  $a$ . As  $a$  increases further, we find that the spectrum tends to a limiting curve, as expected.

Comparing the results directly with those for quartic dispersion (see Figure 10.6), we see that, around the frequency  $\Omega = 1$  ( $\omega = \omega_0$ ), the spectra are of roughly the same order of magnitude. This concordance is seen more clearly if we simply remove the  $ul$ -contribution to the  $u$ -modes in the case of quartic dispersion, focusing solely on the coupling between the  $ur$ - and the  $u$ -modes. That this order of magnitude is reproduced even approximately when the low-frequency modes are rendered impossible shows that they have little influence on the  $ur$ - $u$  coupling. It would seem that, even if we must take account of them to solve the wave equation, we are justified in simply ignoring their contribution to the creation rate.

Again, we may strive for an analytic expression describing the Hawking spectra, and for this we may turn to the results of previous models for inspiration. It is found, for low values of  $a$ , that the spectra are well-approximated by the formula

$$|\beta_{\Omega'}|^2 \approx \exp\left(-\frac{\pi}{a}(\Omega_R^{ur} - \Omega_R^u)\right) - \exp\left(-\frac{\pi}{a}(\Omega_L^{ur} - \Omega_R^u)\right) \\ - \exp\left(-\frac{\pi}{a}(\Omega_R^{ur} - \Omega_L^u)\right) + \exp\left(-\frac{\pi}{a}(\Omega_L^{ur} - \Omega_L^u)\right). \quad (10.2.16)$$

Several spectra, together with curves given by Eq. (10.2.16), are plotted in Fig. 10.7.

## 10. The Low-Frequency Problem

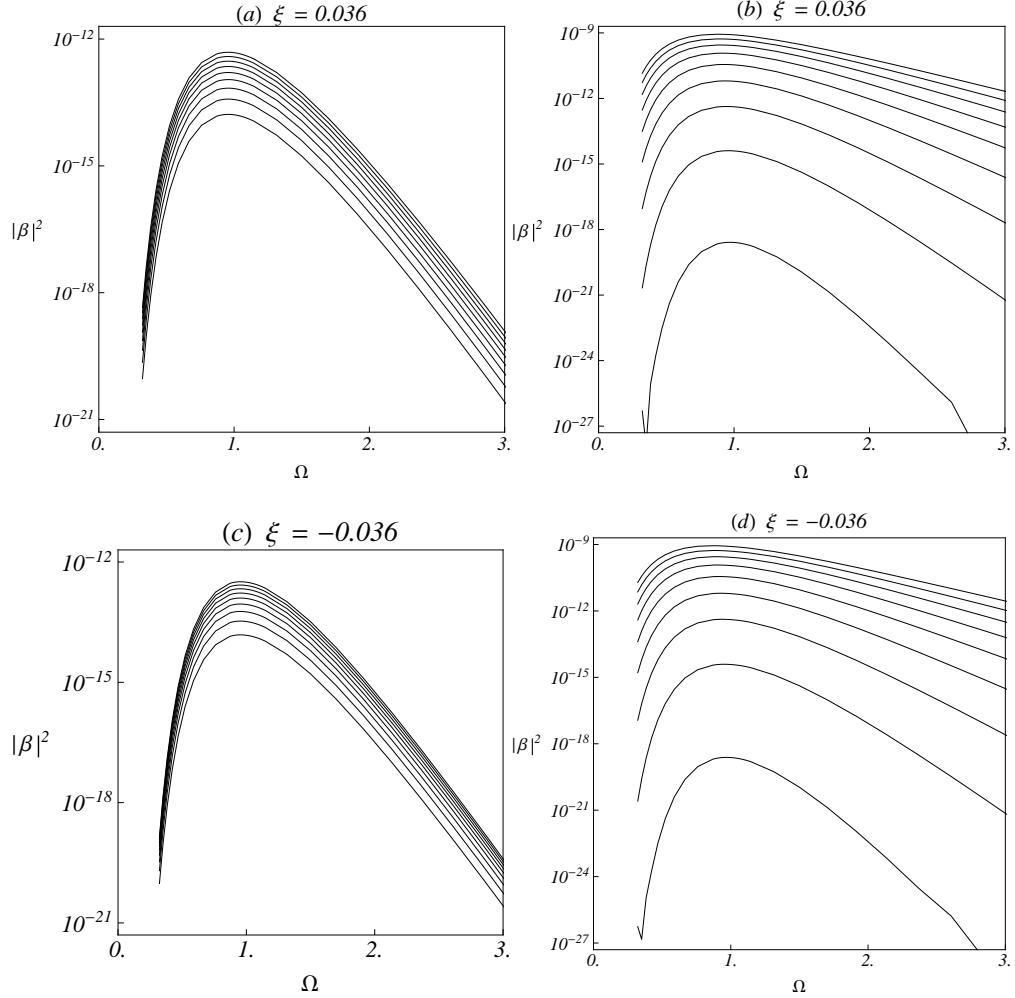


Figure 10.5.: HAWKING SPECTRA WITH TWO-SOLUTION DISPERSION: These plot numerically calculated spectra for the dispersion model of Eq. (10.2.14). In Figures (a) and (b),  $\xi = 0.036$ , while in Figures (c) and (d),  $\xi = -0.036$ . In Figs. (a) and (c),  $a$  is fixed at 0.3 while  $h$  varies between  $10^{-4}$  and  $10^{-3}$ ; in (b) and (d),  $h$  is fixed at  $10^{-4}$  while  $a$  varies between 0.2 and 1.0. Notice that the plots change very little when the sign of  $\xi$  is changed.

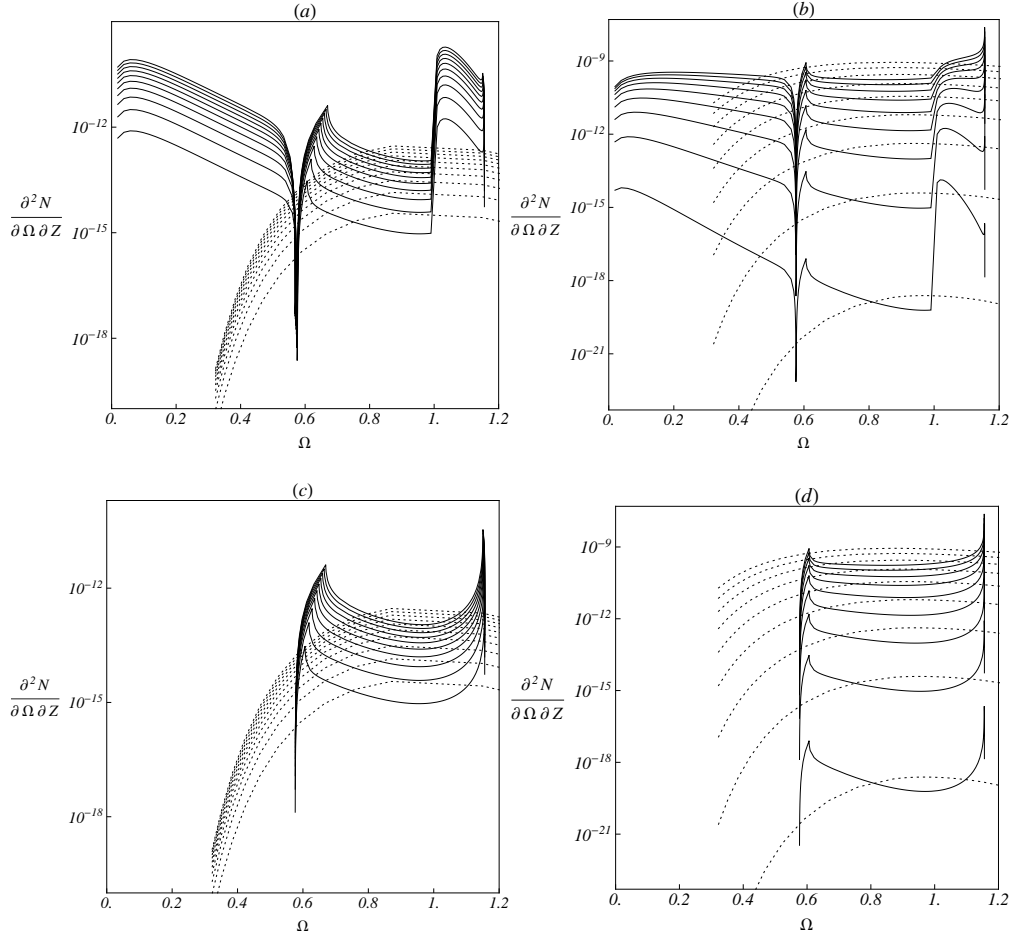


Figure 10.6.: COMPARING TWO-SOLUTION WITH QUARTIC DISPERSION: The two-solution spectra of Figure 10.5 are shown here as dotted curves, while the quartic-dispersion spectra of Figures 9.4(d) and 9.5(d) are shown as solid curves. Figures (a) and (b) show the full spectra, with  $h$  varying between  $10^{-4}$  and  $10^{-3}$  in (a), and  $a$  varying between 0.2 and 1.0 in (b). Figures (c) and (d) show the same curves, but omitting the  $ul-u$  pair contribution to the quartic-dispersion spectra.

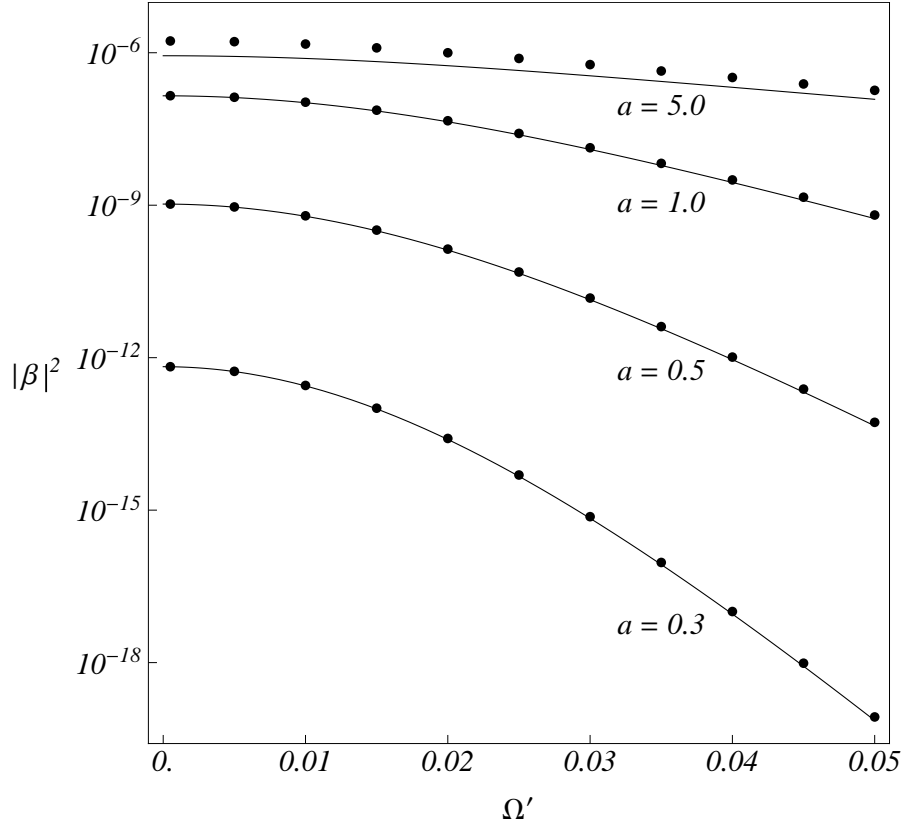


Figure 10.7.: TWO-SOLUTION DISPERSION AND PHASE-INTEGRAL APPROXIMATION: Numerically calculated spectra are shown as dots, while the curves plot the analytic expression of Eq. (10.2.16). We have taken  $h = 10^{-4}$  and  $\xi = -0.036$ , while  $a$  varies between 0.3 and 5.0. Note that, as previously, there is very good agreement for  $a \lesssim 1$ .

### 10.3. Concluding remarks

The most important result of this chapter is the observation that, upon suppression of the low-frequency *ul*-modes, the spectra of the *ur*-modes are to a large extent preserved. Thus, while many of the spectra of Chapter 9 - particularly those for low values of  $a$  - are dominated by *ul*-modes, we are justified in simply ignoring these, focusing instead only on the *ur-u* pair. This may be weaker, but it is non-zero, and it may be very significant for higher values of  $a$ . The Hawking spectrum, though diminished, survives.



Part IV.

Appendices





## A. Low-Frequency Temperature in Acoustic Model

In this appendix, we derive the result of Eq. (4.4.7), which gives the low-frequency Hawking temperature in the limit of a discontinuous flow velocity profile with subluminal quartic dispersion; the normalized dispersion relation is

$$f^2(K) = K^2 - K^4 \quad (\text{A.0.1})$$

and the flow velocity profile is

$$U(X) = U_L \theta(-X) + U_R \theta(X) , \quad (\text{A.0.2})$$

where  $U_L < -1$  and  $-1 < U_R < 0$ . This velocity profile is shown in Figure 4.2, and corresponds to a black hole horizon.

The mode to be calculated is the  $K^{ur}$ -out mode, illustrated in Figure A.1. Since we neglect the coupling to  $v$ -modes, the only pair produced is  $u - url$ , and since we have a black hole horizon,  $K^{ur}$  must be the outgoing wavevector. The creation rate is determined by the norm of the ingoing  $K^u$  wavevector.

Given the values of  $K$ , the coefficients are found by imposing continuity of  $\phi$ ,  $\partial_X \phi$  and  $\partial_X^2 \phi$ , and the condition of Eq. (3.2.14) for  $\partial_X^3 \phi$ , at  $X = 0$ . Eq. (3.2.14) gives

$$\Delta(\partial_X^3 \phi) = -(i\Omega\phi - (U_R + U_L)\partial_X \phi)(U_R - U_L) . \quad (\text{A.0.3})$$

$\phi$  is expressed as a sum of the plane wave solutions in each region:

$$\phi = \begin{cases} e^{iK^c X} , & X < 0 \\ a^v e^{iK^v X} + a^{ur} e^{iK^{ur} X} + a^{ul} e^{iK^{ul} X} + a^u e^{iK^u X} , & X > 0 \end{cases} . \quad (\text{A.0.4})$$

The conditions given above can then be expressed in matrix form as follows:

$$\begin{bmatrix} 1 & 1 & 1 & 1 \\ K^v & K^{ur} & K^{ul} & K^u \\ (K^v)^2 & (K^{ur})^2 & (K^{ul})^2 & (K^u)^2 \\ (K^v)^3 & (K^{ur})^3 & (K^{ul})^3 & (K^u)^3 \end{bmatrix} \begin{bmatrix} a^v \\ a^{ur} \\ a^{ul} \\ a^u \end{bmatrix} = \begin{bmatrix} 1 & \\ K^c & \\ (K^c)^2 & \\ (K^c)^3 + (U_R - U_L)(\Omega - K^c(U_R + U_L)) & \end{bmatrix} . \quad (\text{A.0.5})$$

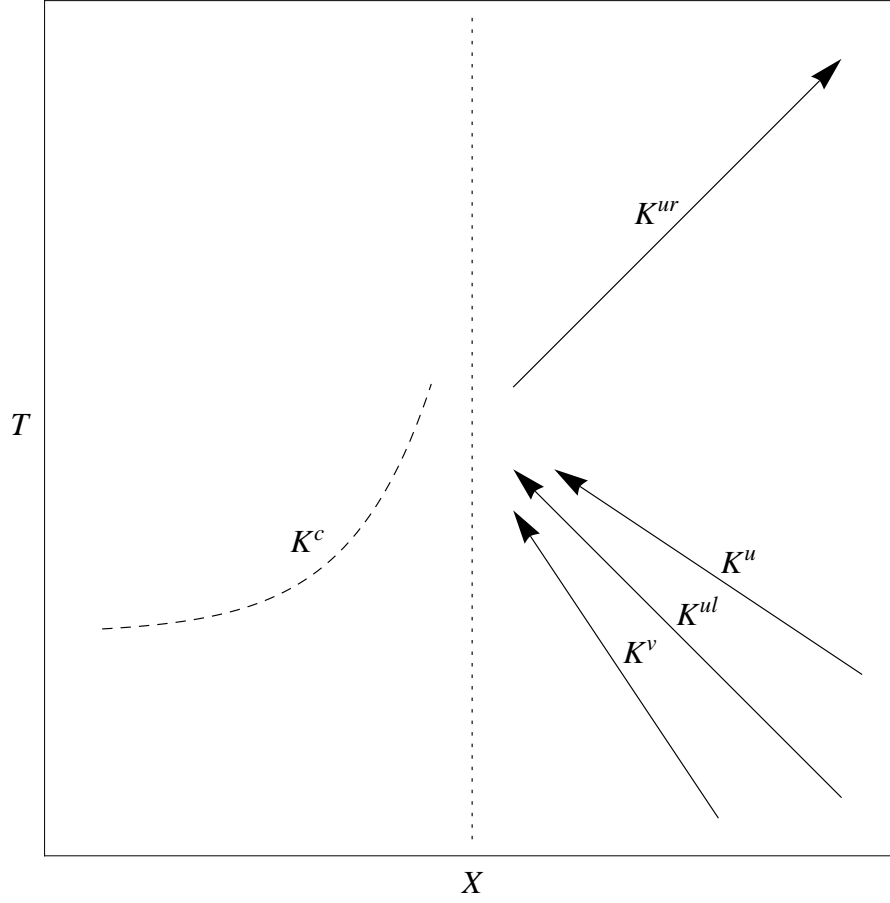


Figure A.1.: SPACE-TIME DIAGRAM OF THE  $K^{ur}$ -OUT MODE: This has a single decaying exponential on the left-hand side, and is the same mode that is found by numerical integration when the steepness is not assumed infinite.

The solution to this linear equation is

$$\begin{bmatrix} a^v \\ a^{ur} \\ a^{ul} \\ a^u \end{bmatrix} = \begin{bmatrix} \frac{(K^{ur}-K^c)(K^{ul}-K^c)(K^u-K^c)-(U_R-U_L)(\Omega-K^c(U_R+U_L))}{(K^{ur}-K^v)(K^{ul}-K^v)(K^u-K^v)} \\ \frac{(K^v-K^c)(K^{ul}-K^c)(K^u-K^c)-(U_R-U_L)(\Omega-K^c(U_R+U_L))}{(K^v-K^{ur})(K^{ul}-K^{ur})(K^u-K^{ur})} \\ \frac{(K^v-K^c)(K^{ur}-K^c)(K^u-K^c)-(U_R-U_L)(\Omega-K^c(U_R+U_L))}{(K^v-K^{ul})(K^{ur}-K^{ul})(K^u-K^{ul})} \\ \frac{(K^v-K^c)(K^{ur}-K^c)(K^{ul}-K^c)-(U_R-U_L)(\Omega-K^c(U_R+U_L))}{(K^v-K^u)(K^{ur}-K^u)(K^{ul}-K^u)} \end{bmatrix}. \quad (\text{A.0.6})$$

In accordance with Eq. (3.2.6), the relative negative-norm component is

$$|\beta_\Omega|^2 = \frac{|f(K^u)| |v_g(K^u)| |a^u|^2}{|f(K^{ur})| |v_g(K^{ur})| |a^{ur}|^2}. \quad (\text{A.0.7})$$

At low frequencies, we should have  $|\beta_\Omega|^2 \approx T_\infty/\Omega$ , where  $T_\infty$  is the temperature of the radiation. (The subscript indicates that this is the limiting temperature as the steepness of the velocity profile becomes infinite.) Our task now, then, is to express the quantities in Eq. (A.0.7) to lowest order in  $\Omega$ . This requires expressions for the five possible values of  $K$  -  $K^v$ ,  $K^{ur}$ ,  $K^{ul}$ ,  $K^u$  and  $K^c$  - to lowest order in  $\Omega$ .

For a constant flow velocity  $U$ , the solutions for  $K$  satisfy the dispersion relation

$$f^2(K) = K^2 - K^4 = (\Omega - UK)^2,$$

or, rearranging,

$$K^4 + (U^2 - 1)K^2 - 2U\Omega K + \Omega^2 = 0. \quad (\text{A.0.8})$$

Expressing  $K$  as a Taylor series in  $\Omega$ ,

$$K = c_0 + c_1\Omega + c_2\Omega^2 + \dots,$$

and plugging this series into Eq. (A.0.8), we find

$$\begin{aligned} c_0^2(c_0^2 + U^2 - 1) + c_0(2c_1(2c_0^2 + U^2 - 1) - 2U)\Omega \\ + (2c_0^2(3c_1^2 + 2c_0c_2) + (c_1^2 + 2c_0c_2)(U^2 - 1) - 2Uc_1 + 1)\Omega^2 + \dots = 0. \end{aligned}$$

For the series on the left of this equation to be identically zero requires that the coefficient of each power of  $\Omega$  is equal to zero:

$$c_0^2(c_0^2 + U^2 - 1) = 0, \quad (\text{A.0.9})$$

$$c_0(2c_1(2c_0^2 + U^2 - 1) - 2U) = 0, \quad (\text{A.0.10})$$

$$(2c_0^2(3c_1^2 + 2c_0c_2) + (c_1^2 + 2c_0c_2)(U^2 - 1) - 2Uc_1 + 1) = 0, \quad (\text{A.0.11})$$

and so on. From Eq. (A.0.9), we find that either  $c_0 = 0$  or  $c_0 = \pm(1 - U^2)^{1/2}$ . (If  $|U| > 1$ , then  $c_0 = \pm i(U^2 - 1)^{1/2}$ .) If  $c_0 = 0$ , Eq. (A.0.10) tells us nothing new, and so we must fall on Eq. (A.0.11); this reduces to

$$c_1^2(U^2 - 1) - 2Uc_1 + 1 = 0,$$

### A. Low-Frequency Temperature in Acoustic Model

a quadratic equation easily solved for  $c_1$ :

$$c_1 = \frac{1}{2(U^2 - 1)} \left( 2U \pm \sqrt{4U^2 - 4(U^2 - 1)} \right) = \frac{U \pm 1}{U^2 - 1} = \frac{1}{U \mp 1}.$$

On the other hand, if  $c_0^2 = 1 - U^2$  (and  $U^2 \neq 1$ ), then Eq. (A.0.10) reduces to

$$c_1 (1 - U^2) - U = 0 \implies c_1 = \frac{U}{1 - U^2}.$$

To first order in  $\Omega$ , then, we have

$$K^v \approx -\frac{1}{1 - U_R} \Omega, \quad (\text{A.0.12})$$

$$K^{ur} \approx \frac{1}{1 + U_R} \Omega, \quad (\text{A.0.13})$$

$$K^{ul} \approx (1 - U_R^2)^{1/2} + \frac{U_R}{1 - U_R^2} \Omega, \quad (\text{A.0.14})$$

$$K^u \approx -(1 - U_R^2)^{1/2} + \frac{U_R}{1 - U_R^2} \Omega, \quad (\text{A.0.15})$$

$$K^c \approx -i (U_L^2 - 1)^{1/2} - \frac{U_L}{U_L^2 - 1} \Omega. \quad (\text{A.0.16})$$

Note that, in Eq. (A.0.16), we have taken the imaginary part of  $K^c$  as negative in order to make it a decreasing exponential for negative  $X$ .

From Eq. (A.0.6), we see that

$$\begin{aligned} \frac{a^u}{a^{ur}} = & -\frac{(K^v - K^{ur})(K^{ul} - K^{ur})}{(K^v - K^u)(K^{ul} - K^u)} \\ & \times \frac{(K^v - K^c)(K^{ur} - K^c)(K^{ul} - K^c) - (U_R - U_L)(\Omega - K^c(U_R + U_L))}{(K^v - K^c)(K^{ul} - K^c)(K^u - K^c) - (U_R - U_L)(\Omega - K^c(U_R + U_L))} \end{aligned}$$

Plugging in the expansions of Eqs. (A.0.12)-(A.0.16), we find that, to lowest order,  $a^u/a^{ur}$  is a constant,

$$\frac{a^u}{a^{ur}} \approx -\frac{(U_L^2 - 1)^{1/2} \left( (U_L^2 - 1)^{1/2} - i(1 - U_R^2)^{1/2} \right)}{(1 - U_R)(1 - U_L)(U_R - U_L)},$$

and, therefore,

$$\left| \frac{a^u}{a^{ur}} \right|^2 \approx \frac{(U_L^2 - 1)((U_L^2 - 1) + (1 - U_R^2))}{(1 - U_R)^2(1 - U_L)^2(U_R - U_L)^2} = \frac{(1 + U_L)(U_R + U_L)}{(1 - U_R)^2(1 - U_L)(U_R - U_L)}. \quad (\text{A.0.17})$$

We must multiply this by  $(|f(K^u)| |v_g(K^u)|) / (|f(K^{ur})| |v_g(K^{ur})|)$ . Now,  $f(K) = K(1 - K^2)^{1/2} = \Omega - U_R K$  and  $v_g(K) = U_R + f'(K) = U_R + (1 - 2K^2) / (1 - K^2)^{1/2}$ . Therefore,

$$f(K) v_g(K) = U_R(\Omega - U_R K) + K(1 - 2K^2) = U_R \Omega + (1 - U_R^2) K - 2K^3,$$

and so

$$\frac{f(K^u) v_g(K^u)}{f(K^{ur}) v_g(K^{ur})} = \frac{U_R \Omega + (1 - U_R^2) K^u - 2(K^u)^3}{U_R \Omega + (1 - U_R^2) K^{ur} - 2(K^{ur})^3}.$$

Pluggin in the expansions of Eqs. (A.0.13) and (A.0.15), we find that, to lowest order,

$$\frac{f(K^u) v_g(K^u)}{f(K^{ur}) v_g(K^{ur})} \approx \frac{(1 - U_R^2)^{3/2}}{\Omega}. \quad (\text{A.0.18})$$

Combining Eqs. (A.0.17) and (A.0.18),

$$|\beta_\Omega|^2 \approx (1 - U_R^2)^{1/2} \frac{(1 + U_R)(1 + U_L)(U_R + U_L)}{(1 - U_R)(1 - U_L)(U_R - U_L)} \frac{1}{\Omega}, \quad (\text{A.0.19})$$

whence we may read off the low-frequency temperature, in accordance with Eq. (4.4.7):

$$T_\infty = (1 - U_R^2)^{1/2} \frac{(1 + U_R)(1 + U_L)(U_R + U_L)}{(1 - U_R)(1 - U_L)(U_R - U_L)}. \quad (\text{A.0.20})$$



## B. Low-Frequency Temperature in Optical Model

We now perform an analogous derivation for the optical model. We assume a discontinuous nonlinearity profile with quartic subluminal dispersion; the normalized dispersion relation is given by

$$B^2(\Omega) = \Omega^2 + \Omega^4 \quad (\text{B.0.1})$$

and the nonlinearity profile by

$$\chi(T) = \chi_L \theta(-T) + \chi_R \theta(T). \quad (\text{B.0.2})$$

The mode to be solved is the  $\Omega^{ul}$ -out mode, shown in Figure B.1, which has a single decreasing exponential for positive  $T$ . Ignoring the  $v$ -mode contribution, the only possible pairing is  $u - url$ , and since we have a black hole horizon,  $\Omega^{ul}$  is an outgoing frequency. The creation rate is found via the norm of the ingoing negative-norm wave with frequency  $\Omega^u$ .

Given the solutions  $\Omega$  of the dispersion relation, the coefficients of the various plane waves are found by imposing the conditions that  $A$ ,  $\partial_T A$  and  $\partial_T^2 A$  be continuous at  $T = 0$ , and that  $\partial_T^3 A$  has a discontinuity given by Eq. (8.2.7):

$$\Delta(\partial_T^3 A) = (\chi_R - \chi_L) \partial_T A. \quad (\text{B.0.3})$$

$A$  is expressed as a sum of the possible plane waves in each region:

$$A(T) = \begin{cases} a^v e^{-i\Omega^v T} + a^{ul} e^{-i\Omega^{ul} T} + a^{ur} e^{-i\Omega^{ur} T} + a^u e^{-i\Omega^u T}, & T < 0 \\ e^{-i\Omega^c T}, & T > 0 \end{cases}. \quad (\text{B.0.4})$$

The conditions at  $T = 0$  can be expressed in matrix form as follows:

$$\begin{bmatrix} 1 & 1 & 1 & 1 \\ \Omega^v & \Omega^{ul} & \Omega^{ur} & \Omega^u \\ (\Omega^v)^2 & (\Omega^{ul})^2 & (\Omega^{ur})^2 & (\Omega^u)^2 \\ (\Omega^v)^3 & (\Omega^{ul})^3 & (\Omega^{ur})^3 & (\Omega^u)^3 \end{bmatrix} \begin{bmatrix} a^v \\ a^{ul} \\ a^{ur} \\ a^u \end{bmatrix} = \begin{bmatrix} 1 \\ \Omega^c \\ (\Omega^c)^2 \\ (\Omega^c)^3 + \Omega^c(\chi_R - \chi_L) \end{bmatrix}. \quad (\text{B.0.5})$$

This has the solution

$$\begin{bmatrix} a^v \\ a^{ul} \\ a^{ur} \\ a^u \end{bmatrix} = \begin{bmatrix} \frac{(\Omega^{ul} - \Omega^c)(\Omega^{ur} - \Omega^c)(\Omega^u - \Omega^c) - \Omega^c(\chi_R - \chi_L)}{(\Omega^{ul} - \Omega^v)(\Omega^{ur} - \Omega^v)(\Omega^u - \Omega^v)} \\ \frac{(\Omega^v - \Omega^c)(\Omega^{ur} - \Omega^c)(\Omega^u - \Omega^c) - \Omega^c(\chi_R - \chi_L)}{(\Omega^v - \Omega^{ul})(\Omega^{ur} - \Omega^{ul})(\Omega^u - \Omega^{ul})} \\ \frac{(\Omega^v - \Omega^c)(\Omega^{ul} - \Omega^c)(\Omega^u - \Omega^c) - \Omega^c(\chi_R - \chi_L)}{(\Omega^v - \Omega^{ur})(\Omega^{ul} - \Omega^{ur})(\Omega^u - \Omega^{ur})} \\ \frac{(\Omega^v - \Omega^c)(\Omega^{ul} - \Omega^c)(\Omega^{ur} - \Omega^c) - \Omega^c(\chi_R - \chi_L)}{(\Omega^v - \Omega^u)(\Omega^{ul} - \Omega^u)(\Omega^{ur} - \Omega^u)} \end{bmatrix}. \quad (\text{B.0.6})$$

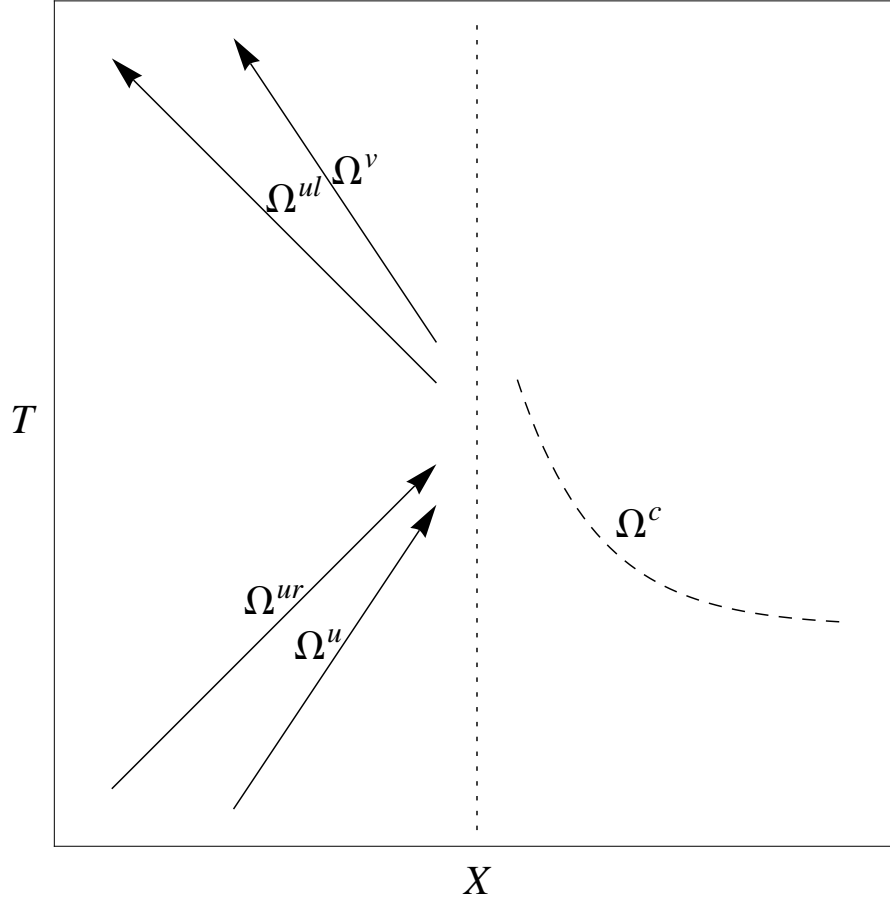


Figure B.1.: SPACE-TIME DIAGRAM OF THE  $\Omega^{ul}$ -OUT MODE: This has a single decreasing exponential on the right-hand side, and is also the mode found by numerical integration when the steepness of the nonlinearity is not assumed infinite. (Note that the  $v$ -mode is actually ingoing, as was pointed out in Figure 5.2.)



The Bogoliubov coefficient that describes particle creation is given by

$$|\beta_{\Omega'}|^2 = \frac{|B(\Omega^u)| |v_g(\Omega^u)| |a^u|^2}{|B(\Omega^{ul})| |v_g(\Omega^{ul})| |a^{ul}|^2}.$$

At low co-moving frequencies  $\Omega'$ , this should be given approximately by  $T_\infty/\Omega'$ , where  $T_\infty$  is the low-frequency temperature. (Again, the subscript indicates that the steepness of the nonlinearity profile has become infinite.) To find this, we need to express the quantities involved - namely, the frequencies  $\Omega^v$ ,  $\Omega^{ul}$ ,  $\Omega^{ur}$ ,  $\Omega^u$  and  $\Omega^c$  - to lowest order in  $\Omega'$ .

For a given co-moving frequency  $\Omega'$  and constant nonlinearity  $\chi$ , the possible lab frequencies satisfy the dispersion relation

$$n_g^2 (\Omega' - \Omega)^2 = B^2(\Omega) + \chi \Omega^2 = (1 + \chi) \Omega^2 + \Omega^4,$$

or, rearranging,

$$\Omega^4 - (n_g^2 - 1 - \chi) \Omega^2 + 2n_g^2 \Omega' \Omega - n_g^2 (\Omega')^2 = 0. \quad (\text{B.0.7})$$

We express  $\Omega$  as a Taylor series in  $\Omega'$ ,

$$\Omega = c_0 + c_1 \Omega' + c_2 (\Omega')^2 + \dots,$$

and plugging into Eq. (B.0.7) we find

$$\begin{aligned} c_0^2 (c_0^2 - (n_g^2 - 1 - \chi)) + 2c_0 (c_1 (2c_0^2 - (n_g^2 - 1 - \chi)) + n_g^2) \Omega \\ + (2c_0^2 (2c_0 c_2 + 3c_1^2) - (2c_0 c_2 + c_1^2) (n_g^2 - 1 - \chi) + 2n_g^2 c_1 - n_g^2) \Omega^2 + \dots = 0. \end{aligned}$$

For this to be identically zero, the coefficient of each power of  $\Omega$  must be equal to zero. Therefore, we have

$$c_0^2 (c_0^2 - (n_g^2 - 1 - \chi)) = 0, \quad (\text{B.0.8})$$

$$2c_0 (c_1 (2c_0^2 - (n_g^2 - 1 - \chi)) + n_g^2) = 0, \quad (\text{B.0.9})$$

$$(2c_0^2 (2c_0 c_2 + 3c_1^2) - (2c_0 c_2 + c_1^2) (n_g^2 - 1 - \chi) + 2n_g^2 c_1 - n_g^2) = 0, \quad (\text{B.0.10})$$

and so on. From Eq. (B.0.8), we find  $c_0 = 0$  or  $c_0 = \pm (n_g^2 - 1 - \chi)^{1/2}$ . (If  $\chi > n_g^2 - 1$ , then  $c_0 = \pm i (\chi + 1 - n_g^2)^{1/2}$ .) If  $c_0 = 0$ , then Eq. (B.0.9) is trivial, and Eq. (B.0.10) becomes

$$(n_g^2 - 1 - \chi) c_1^2 - 2n_g^2 c_1 + n_g^2 = 0.$$

This is easily solved to give

$$c_1 = \frac{1}{2(n_g^2 - 1 - \chi)} \left( 2n_g^2 \pm \sqrt{4n_g^4 - 4n_g^2 (n_g^2 - 1 - \chi)} \right) = \frac{n_g (n_g \pm \sqrt{1 + \chi})}{n_g^2 - 1 - \chi} = \frac{n_g}{n_g \mp \sqrt{1 + \chi}}.$$

On the other hand, if  $c_0^2 = n_g^2 - 1 - \chi$ , then Eq. (B.0.9) becomes

$$c_1 (n_g^2 - 1 - \chi) + n_g^2 = 0 \implies c_1 = -\frac{n_g^2}{n_g^2 - 1 - \chi}.$$

## B. Low-Frequency Temperature in Optical Model

Therefore, to first order in  $\Omega'$ , we have

$$\Omega^v \approx \frac{n_g}{n_g + \sqrt{1 + \chi_L}} \Omega', \quad (\text{B.0.11})$$

$$\Omega^{ul} \approx \frac{n_g}{n_g - \sqrt{1 + \chi_L}} \Omega', \quad (\text{B.0.12})$$

$$\Omega^{ur} \approx (n_g^2 - 1 - \chi_L)^{1/2} - \frac{n_g^2}{n_g^2 - 1 - \chi_L} \Omega', \quad (\text{B.0.13})$$

$$\Omega^u \approx -(n_g^2 - 1 - \chi_L)^{1/2} - \frac{n_g^2}{n_g^2 - 1 - \chi_L} \Omega', \quad (\text{B.0.14})$$

$$\Omega^c \approx -i(\chi_R + 1 - n_g^2)^{1/2} + \frac{n_g^2}{\chi_R + 1 - n_g^2} \Omega'. \quad (\text{B.0.15})$$

As before, we have given  $\Omega^c$  a negative imaginary part so that it represents a decreasing exponential.

From Eq. (B.0.6) we find

$$\frac{a^u}{a^{ul}} = -\frac{(\Omega^v - \Omega^{ul})(\Omega^{ur} - \Omega^{ul})}{(\Omega^v - \Omega^u)(\Omega^{ur} - \Omega^u)} \cdot \frac{(\Omega^v - \Omega^c)(\Omega^{ul} - \Omega^c)(\Omega^{ur} - \Omega^c) - \Omega^c(\chi_R - \chi_L)}{(\Omega^v - \Omega^c)(\Omega^{ur} - \Omega^c)(\Omega^u - \Omega^c) - \Omega^c(\chi_R - \chi_L)},$$

and, substituting Eqs. (B.0.11)-(B.0.15) in this expression, we find that, to lowest order,  $a^u/a^{ul}$  has the constant value

$$\frac{a^u}{a^{ul}} \approx -\frac{\sqrt{1 + \chi_L}(\chi_R + 1 - n_g^2)^{1/2}}{(\chi_R - \chi_L)(n_g + \sqrt{1 + \chi_L})} \left\{ (\chi_R + 1 - n_g^2)^{1/2} - i(n_g^2 - 1 - \chi_L)^{1/2} \right\};$$

therefore,

$$\begin{aligned} \left| \frac{a^u}{a^{ul}} \right|^2 &\approx \frac{(1 + \chi_L)(\chi_R + 1 - n_g^2)}{(\chi_R - \chi_L)^2(n_g + \sqrt{1 + \chi_L})^2} \left\{ (\chi_R + 1 - n_g^2) + (n_g^2 - 1 - \chi_L) \right\} \\ &= \frac{(1 + \chi_L)(\chi_R + 1 - n_g^2)}{(\chi_R - \chi_L)(n_g + \sqrt{1 + \chi_L})^2}. \end{aligned} \quad (\text{B.0.16})$$

We now turn to the factor  $(|B(\Omega^u)| |v_g(\Omega^u)|) / (|B(\Omega^{ul})| |v_g(\Omega^{ul})|)$ . Using  $B(\Omega) = \Omega\sqrt{1 + \chi + \Omega^2} = n_g(\Omega - \Omega')$  and  $v_g(\Omega) = -1 + B'(\Omega)/n_g = -1 + (1 + \chi + 2\Omega^2)/\sqrt{1 + \chi + \Omega^2}/n_g$ , we have

$$n_g B(\Omega) v_g(\Omega) = -n_g^2(\Omega - \Omega') + \Omega(1 + \chi + 2\Omega^2) = n_g^2 \Omega' - (n_g^2 - 1 - \chi)\Omega + 2\Omega^3,$$

and so

$$\frac{B(\Omega^u) v_g(\Omega^u)}{B(\Omega^{ul}) v_g(\Omega^{ul})} = \frac{n_g^2 \Omega' - (n_g^2 - 1 - \chi_L) \Omega^u + 2(\Omega^u)^3}{n_g^2 \Omega' - (n_g^2 - 1 - \chi_L) \Omega^{ul} + 2(\Omega^{ul})^3}.$$

Substituting the first-order Taylor expansions of Eqs. (B.0.12) and (B.0.14), we find, to lowest order,

$$\frac{B(\Omega^u) v_g(\Omega^u)}{B(\Omega^{ul}) v_g(\Omega^{ul})} \approx \frac{(n_g^2 - 1 - \chi_L)^{3/2}}{n_g \sqrt{1 + \chi_L}} \frac{1}{\Omega'}. \quad (\text{B.0.17})$$

Combining Eqs. (B.0.16) and (B.0.17), we find

$$|\beta_{\Omega'}|^2 \approx (n_g^2 - 1 - \chi_L)^{1/2} \frac{\sqrt{1 + \chi_L} (\chi_R + 1 - n_g^2) (n_g - \sqrt{1 + \chi_L})}{n_g (\chi_R - \chi_L) (n_g + \sqrt{1 + \chi_L})} \frac{1}{\Omega'}, \quad (\text{B.0.18})$$

from which we read off the temperature

$$T_\infty = (n_g^2 - 1 - \chi_L)^{1/2} \frac{\sqrt{1 + \chi_L} (\chi_R + 1 - n_g^2) (n_g - \sqrt{1 + \chi_L})}{n_g (\chi_R - \chi_L) (n_g + \sqrt{1 + \chi_L})}. \quad (\text{B.0.19})$$



# Bibliography

- [1] Hawking, S. W. (1974) Black hole explosions? *Nature*, **248**, 30–31.
- [2] Hawking, S. (1975) Particle creation by black holes. *Communications in Mathematical Physics*, **43**, 199–220, 10.1007/BF02345020.
- [3] Bekenstein, J. D. (1973) Black holes and entropy. *Phys. Rev. D*, **7**, 2333–2346.
- [4] Bekenstein, J. D. (1974) Generalized second law of thermodynamics in black-hole physics. *Phys. Rev. D*, **9**, 3292–3300.
- [5] Hartle, J. B. and Hawking, S. W. (1976) Path-integral derivation of black-hole radiance. *Phys. Rev. D*, **13**, 2188–2203.
- [6] Unruh, W. G. (1976) Notes on black-hole evaporation. *Phys. Rev. D*, **14**, 870–892.
- [7] Damour, T. and Ruffini, R. (1976) Black-hole evaporation in the klein-sauter-heisenberg-euler formalism. *Phys. Rev. D*, **14**, 332.
- [8] Sanchez, N. (1978) Absorption and emission spectra of a schwarzschild black hole. *Phys. Rev. D*, **18**, 1030.
- [9] Fredenhagen, K. and Haag, R. (1990) On the derivation of hawking radiation associated with the formation of a black hole. *Commun. Math. Phys.*, **127**, 273.
- [10] Parikh, M. K. and Wilczek, F. (2000) Hawking radiation as tunneling. *Phys. Rev. Lett.*, **85**, 5042.
- [11] 'tHooft, G. (1985) On the quantum structure of a black hole. *Nucl. Phys. B*, **256**, 727.
- [12] Jacobson, T. (1991) Black-hole evaporation and ultrashort distances. *Phys. Rev. D*, **44**, 1731–1739.
- [13] Brout, R., Massar, S., Parentani, R., and Spindel, P. (1995) A primer for black hole quantum physics. *Physics Reports*, **260**, 329–446.
- [14] Novello, M., Visser, M., and Volovik, G. (2002) *Artificial Black Holes*. World Scientific, Singapore.
- [15] Schützhold, R. and Unruh, W. (2007) *Quantum Analogues: From Phase Transitions to Black Holes and Cosmology*. Berlin: Springer.

## Bibliography

- [16] Unruh, W. G. (1981) Experimental black-hole evaporation? *Phys. Rev. Lett.*, **46**, 1351–1353.
- [17] Visser, M. (1993) Acoustic propagation in fluids: an unexpected example of lorentzian geometry. *arXiv:gr-qc/9311028*.
- [18] Unruh, W. G. (1995) Sonic analogue of black holes and the effects of high frequencies on black hole evaporation. *Phys. Rev. D*, **51**, 2827–2838.
- [19] Garay, L. J., Anglin, J. R., Cirac, J. I., and Zoller, P. (2000) Sonic analog of gravitational black holes in bose-einstein condensates. *Phys. Rev. Lett.*, **85**, 4643–4647.
- [20] Garay, L. J., Anglin, J. R., Cirac, J. I., and Zoller, P. (2001) Sonic black holes in dilute bose-einstein condensates. *Phys. Rev. A*, **63**, 023611.
- [21] Barceló, C., Liberati, S., and Visser, M. (2001) Towards the observation of hawking radiation in bose-einstein condensates. *arXiv:gr-qc/0110036*.
- [22] Barceló, C., Liberati, S., and Visser, M. (2001) Analogue gravity from bose-einstein condensates. *Class. Quantum Grav.*, **18**, 1137–1156.
- [23] Giovanazzi, S., Farrell, C., Kiss, T., and Leonhardt, U. (2004) Conditions for one-dimensional supersonic flow of quantum gases. *Phys. Rev. A*, **70**, 063602.
- [24] Giovanazzi, S. (2005) Hawking radiation in sonic black holes. *Phys. Rev. Lett.*, **94**, 061302.
- [25] Jacobson, T. A. and Volovik, G. E. (1998) Event horizons and ergoregions in  $^3\text{He}$ . *Phys. Rev. D*, **58**, 064021.
- [26] Volovik, G. E. (1999) Simulation of a panlevé-gullstrand black hole in a thin  $^3\text{He-A}$  film. *JETP Lett.*, **69**, 705.
- [27] Fischer, U. R. and Volovik, G. E. (2001) Thermal quasi-equilibrium states across landau horizons in the effective gravity of superfluids. *Int. J. Mod. Phys.*, **10**, 57–88.
- [28] Volovik, G. (2001) Superfluid analogies of cosmological phenomena. *Physics Reports*, **351**, 195 – 348.
- [29] Volovik, G. E. (2003) *The Universe in a Helium Droplet*. Clarendon Press, Oxford.
- [30] Schützhold, R. and Unruh, W. G. (2002) Gravity wave analogues of black holes. *Phys. Rev. D*, **66**, 044019.
- [31] Rousseaux, G., Mathis, C., Maïssa, P., Philbin, T. G., and Leonhardt, U. (2008) Observation of negative-frequency waves in a water tank: a classical analogue to the hawking effect? *New J. Phys.*, **10**, 053015.
- [32] Rousseaux, G., Maïssa, P., Mathis, C., Philbin, T. G., and Leonhardt, U. (2010) Horizon effects with surface waves on moving water. *New J. Phys.*, **12**, 095018.

- [33] Reznik, B. (1997) Origin of the thermal radiation in a solid-state analog of a black-hole. *arXiv:gr-qc/9703076*.
- [34] Leonhardt, U. and Piwnicki, P. (1999) Optics of nonuniformly moving media. *Phys. Rev. A*, **60**, 4301–4312.
- [35] Leonhardt, U. and Piwnicki, P. (2000) Relativistic effects of light in moving media with extremely low group velocity. *Phys. Rev. Lett.*, **84**, 822–825.
- [36] Leonhardt, U. (2002) A laboratory analogue of the event horizon using slow light in an atomic medium. *Nature*, **415**, 406.
- [37] Jacobson, T. (1996) On the origin of the outgoing black hole modes. *Phys. Rev. D*, **53**, 7082–7088.
- [38] Brout, R., Massar, S., Parentani, R., and Spindel, P. (1995) Hawking radiation without trans-planckian frequencies. *Phys. Rev. D*, **52**, 4559–4568.
- [39] Corley, S. and Jacobson, T. (1996) Hawking spectrum and high frequency dispersion. *Phys. Rev. D*, **54**, 1568–1586.
- [40] Corley, S. (1997) Particle creation via high frequency dispersion. *Phys. Rev. D*, **55**, 6155–6161.
- [41] Corley, S. (1998) Computing the spectrum of black hole radiation in the presence of high frequency dispersion: An analytical approach. *Phys. Rev. D*, **57**, 6280–6291.
- [42] Recati, A., Pavloff, N., and Carusotto, I. (2009) Bogoliubov theory of acoustic hawking radiation in bose-einstein condensates. *Phys. Rev. A*, **80**, 043603.
- [43] Jacobson, T. and Mattingly, D. (1999) Hawking radiation on a falling lattice. *Phys. Rev. D*, **61**, 024017.
- [44] Macher, J. and Parentani, R. (2009) Black/white hole radiation from dispersive theories. *Phys. Rev. D*, **79**, 124008.
- [45] Carusotto, I., Fagnocchi, S., Recati, A., Balbinot, R., and Fabbri, A. (2008) Numerical observation of hawking radiation from acoustic black holes in atomic bose-einstein condensates. *New J. Phys.*, **10**, 103001.
- [46] Himemoto, Y. and Tanaka, T. (2000) Generalization of the model of hawking radiation with modified high frequency dispersion relation. *Phys. Rev. D*, **61**, 064004.
- [47] Saida, H. and Sakagami, M. (2000) Black hole radiation with high frequency dispersion. *Phys. Rev. D*, **61**, 084023.
- [48] Unruh, W. G. and Schützhold, R. (2005) Universality of the hawking effect. *Phys. Rev. D*, **71**, 024028.

## Bibliography

- [49] Schützhold, R. and Unruh, W. G. (2008) Origin of the particles in black hole evaporation. *Phys. Rev. D*, **78**, 041504.
- [50] Misner, C. W., Thorne, K. S., and Wheeler, J. A. (1973) *Gravitation*. W. H. Freeman.
- [51] Painlevé, P. (1921) La mécanique classique et la théorie de la relativité. *C. R. Acad. Sci. (Paris)*, **173**, 677.
- [52] Gullstrand, A. (1922) Allgemeine lösung des statischen einkörperproblems in der einsteinschen gravitationstheorie. *Arkiv. Mat. Astron. Fys.*, **16**, 1–15.
- [53] Lemaître, G. (1933) *Ann. Soc. Sci. Brux.*, **A53**, 51–85.
- [54] Jacobson, T. (1999) Trans-planckian redshifts and the substance of the space-time river. *Progress of Theoretical Physics Supplement*, **136**, 1–17.
- [55] Hamilton, A. J. S. and Lisle, J. P. (2008) The river model of black holes. *American Journal of Physics*, **76**, 519–532.
- [56] Birrell, N. D. and Davies, P. C. W. (1982) *Quantum Fields in Curved Space*. Cambridge University Press.
- [57] Hawking, S. W. (1976) Breakdown of predictability in gravitational collapse. *Phys. Rev. D*, **14**, 2460.
- [58] Press, W. H., Teukolsky, S., Vetterling, W., and Flannery, B. (1992) *Numerical Recipes in Fortran*. Cambridge University Press.
- [59] Landau, L. D. and Lifshitz, E. M. (1977) *Quantum Mechanics (Non-relativistic theory)*. Butterworth-Heinemann.
- [60] Belgiorno, F., Cacciatori, S. L., Clerici, M., Gorini, V., Ortenzi, G., Rizzi, L., Rubino, E., Sala, V. G., and Faccio, D. (2010) Hawking radiation from ultrashort laser pulse filaments. *Phys. Rev. Lett.*, **105**, 203901.
- [61] Jackson, J. D. (1962) *Classical Electrodynamics*. John Wiley and Sons, Inc.
- [62] Okoshi, T. (1982) *Optical Fibers*. Academic Press.
- [63] Agrawal, G. P. (2007) *Nonlinear Fiber Optics*. Academic Press.
- [64] Abramowitz, M. and Stegun, I. (1964) *Handbook of Mathematical Functions with Formulas, Graphs and Mathematical Tables*. Dover.
- [65] Philbin, T. G., Kuklewicz, C., Robertson, S., Hill, S., König, F., and Leonhardt, U. (2008) Fiber-optical analogue of the event horizon. *Science*, **319**, 1367–1370.
- [66] Russell, P. (2003) Photonic crystal fibers. *Science*, **299**, 358–362.



- [67] Loudon, R. (2000) *The Quantum Theory of Light*. Oxford University Press.
- [68] Zakharov, V. E. and Shabat, A. B. (1972) *Sov. Phys. JETP*, **34**, 62.
- [69] Robertson, S. and Leonhardt, U. (2010) Frequency shifting at fiber-optical event horizons: The effect of raman deceleration. *Phys. Rev. A*, **81**, 063835.
- [70] Stolen, R. H., Gordon, J. P., Tomlinson, W. J., and Haus, H. A. (1989) Raman response function of silica-core fibers. *J. Opt. Soc. Am. B*, **6**, 1159–1166.
- [71] Blow, K. J. and Wood, D. (1989) Theoretical description of transient stimulated raman scattering in optical fibers. *IEEE Journal of Quantum Electronics*, **25**, 2665–2673.
- [72] Hollenbeck, D. and Cantrell, C. D. (2002) Multiple-vibrational-mode model for fiber-optic raman gain spectrum and response function. *J. Opt. Soc. Am. B*, **19**, 2886–2892.
- [73] Lin, Q. and Agrawal, G. P. (2006) Raman response function for silica fibers. *Opt. Lett.*, **31**, 3086–3088.
- [74] Nishizawa, N. and Goto, T. (2002) Characteristics of pulse trapping by ultrashort soliton pulse in optical fibers across zerodispersion wavelength. *Opt. Express*, **10**, 1151–1160.
- [75] Nishizawa, N. and Goto, T. (2002) Pulse trapping by ultrashort soliton pulses in optical fibers across zero-dispersion wavelength. *Opt. Lett.*, **27**, 152–154.
- [76] Nishizawa, N. and Goto, T. (2003) Ultrafast all optical switching by use of pulse trapping across zero-dispersion wavelength. *Opt. Express*, **11**, 359–365.
- [77] Hill, S., Kuklewicz, C. E., Leonhardt, U., and König, F. (2009) Evolution of light trapped by a soliton in a microstructured fiber. *Opt. Express*, **17**, 13588–13600.
- [78] Gorbach, A. V. and Skryabin, D. V. (2007) Light trapping in gravity-like potentials and expansion of supercontinuum spectra in photonic-crystal fibres. *Nature Photonics*, **1**, 653–657.
- [79] Vallée, O. and Soares, M. (2004) *Airy Functions and Applications to Physics*. Imperial College Press.
- [80] Landau, L. D. and Lifshitz, E. M. (1975) *The Classical Theory of Fields*. Pergamon, Oxford.
- [81] Kärtner, F. X. (2004) *Few-Cycle Laser Pulse Generation and Its Applications*. Springer, Berlin.
- [82] Brabec, T. and Krausz, F. (2000) Intense few-cycle laser fields: Frontiers of nonlinear optics. *Rev. Mod. Phys.*, **72**, 545–591.